POLITECNICO DI MILANO
ENERGY DEPARTMENT
DOCTORAL PROGRAMME IN ELECTRICAL ENGINEERING, XXXII-CYCLE

REAL-TIME PMU-BASED POWER SYSTEM INERTIA MONITORING CONSIDERING DYNAMIC EQUIVALENTS

Doctoral Dissertation of:
Guido Rossetto Moraes

Supervisor:
Prof. Alberto Berizzi

Tutor:
Prof. Cristian Bovo

The Chair of the Doctoral Program:
Prof. Gabriele D'Antona

2019 - XXXII

"We have this history of impossible solutions to insoluble problems"
Will Eisner

Acknowledgements

First of all I would like to thank my supervisor, Prof. Alberto Berizzi. My sincere gratitude for giving me the opportunity and for supporting me during the development of this thesis. Thanks for all the guidance and teachings. Very important was also the contribution of Prof. D'Antona, not only for the support given as coordinator of the PhD program, but also for the technical discussions that helped me on several parts of my research.

I would like to thank also the professors that accepted to review this thesis and accepted to take part on the evaluation board. Many thanks also to the professors of the department of Energy that participated in one way or another in the evaluation procedures of my doctorate.

In these three years, I counted with the collaboration of many colleagues which I need to thank. Prof. Grillo, Davide, Fabio and Manuel, it was a pleasure to work with you. I need to thank also the engineers from Terna SpA, for all the support given and the valuable discussions during the project.

Special thanks to my friend Roberto Salgado, my former supervisor in Brazil, that has deeply inspired me to continue my studies and has recommended me to PoliMi. Sincere thanks to Prof. Simões, who also expressed his support to my studies abroad.

My warm thanks to all the friends I have made at PoliMi. First to Claudio, Ilena, Lam and Mina for opening the doors of the office and integrating me to the group, and for the years of friendship across borders and countries, thank you so much. Special thanks also for Luca, Khaled and Alberto Carboni, friends from the same PhD cycle with whom I could face many of the challenges together. My sincere thanks to Alessandro, Valentin and Andrea, always available for work but also for spending free time together. I would like to thank Gabriel, brazilian friend who I had the pleasure to meet during his visiting period at PoliMi. I would like to thank also Matteo, Emanuele and Alberto Bolzoni, and all the other friends with whom I've shared these days at the university, thanks for everything. My heartfelt thanks to Marina, Silvia and Alfredo, not only for the friendship, but for being there when I needed. I will never forget, thank you so much.

Thanks to Caio, Murillo and Carla, friends from Brazil whom I had the pleasure to have as flatmates for a while. Also to my friends at my country of origin, which supported my decision to study abroad and came to meet me every time I was back in town, thank you. Many thanks to my friends that shared the same decision and came to do their PhD in Europe. We have shared the same dreams, we have faced

the same challenges. Staying in contact has made everything easier. Warm thanks to Toma and Anna, for all the visits, all the hours of conversation and all the kind support.

All my gratitude to my family. My parents, Raffaella and Sergio, for supporting me in every possible way. Stela, for supporting my decision and sharing all these days which I spent abroad, far in distance but close in heart. My grandparents, not only for all the love, but for giving me these roots that made me half brazilian and half italian.

Thank you all, for making me feel at home both in Italy and in Brazil.

Abstract

Nowadays, the energy portfolio is changing to include more Renewable Energy Sources (RES) in a search for mitigating the impact on the environment. However, the increasing penetration of RES in power systems has been bringing many challenges for Transmission System Operators (TSOs). RES-based generators are mainly connected to the grid by means of converters, that decouple the dynamics of prime movers from the bulk power system. Hence, these units do not contribute directly to the equivalent inertia of the system, and among the main consequences, larger and longer frequency excursions follows power imbalances on the grid. For that reason, estimating inertia in real-time is becoming indispensable for the overall security assessment of the system.

This thesis aims at investigating inertia estimation with the use of data coming from Phasor Measurement Units (PMUs), devices capable of acquiring measurements from the grid and providing phasors synchronized by Global Positioning System (GPS) in real-time at high sampling rates. The topic has been explored in the literature in the last few years, with many methods and solutions to estimate inertia from the terminals of single generators. However, monitoring individually each generating unit is a strong assumption taking into consideration the size of power systems and current high cost of PMUs. Hence, estimating equivalent inertias based on the data provided by few PMUs spread on the system becomes an interesting practical research topic.

The methodology used in this thesis consists in approaching some of the many challenges that a TSO may face on estimating inertia, divided according to different topics. Starting from the consideration that generators are monitored individually, to the case where areas are monitored at boundary buses, different methods were studied and novel methods and strategies are proposed to estimate inertia in some typical situations. Different types of perturbations were considered, including loss of generation, load steps, Renewable Energy Sources (RES) integration, and also inertia estimation under normal load variations.

To test the methods, experiments with 5 different test-systems were performed, with different levels of complexity. The experiments were divided in 13 different studies, where simulations were handled using MATLAB and PowerFactory to acquire the equivalent data that PMUs could provide, and the methods were applied subsequently.

Keywords: Inertia estimation, Phasor Measurement Units, dynamic equivalents.

Estratto

Al giorno d'oggi, il mix energetico sta cambiando per includere più fonti di energia rinnovabile (FER) al fine di mitigare l'impatto sull'ambiente. Tuttavia, la crescente penetrazione delle FER nei sistemi di generazione ha comportato molte sfide per i gestori dei sistemi di trasmissione (TSO). I generatori basati su FER sono principalmente collegati alla rete mediante convertitori, che disaccoppiano la dinamica del motore primo dalla rete. Pertanto, queste unità non contribuiscono direttamente all'inerzia equivalente del sistema e, tra le principali conseguenze, le escursioni di frequenza a seguito di squilibri di potenza sulla rete diventano più intense, e pericolose. Per tale motivo, la stima dell'inerzia in tempo reale sta diventando indispensabile per la valutazione complessiva della sicurezza del sistema.

Lo scopo di questa tesi è quello di studiare la possibilità di stimare l'inerzia con l'uso di dati provenienti dalle Phasor Measurement Units (PMUs), dispositivi in grado di acquisire misurazioni dalla rete e fornire fasori sincronizzati dal Global Positioning System (GPS) in tempo reale con alte frequenze di campionamento, ogni 20 ms. Il tema è stato studiato nella letteratura degli ultimi anni, e presenta molti metodi e soluzioni per stimare l'inerzia dei singoli generatori. Tuttavia, il monitoraggio individuale di ciascuna unità di generazione è un'ipotesi forte quando si tiene conto delle dimensioni dei sistemi di trasmissione reali e degli attuali costi delle PMU. Pertanto, stimare l'inerzia equivalente sulla base dei dati forniti da alcune PMU diffuse sul sistema diventa un tema di ricerca rilevante.

La metodologia utilizzata in questa tesi consiste nell'approcciare alcune delle molte sfide che un TSO si trova ad affrontare per stimare l'inerzia, suddivise in argomenti differenti. A partire dall'ipotesi che i generatori siano monitorati individualmente, fino al caso in cui le aree sono monitorate sulle sbarre di confine, sono stati studiati diversi metodi e sono stati proposti nuovi approcci e strategie per stimare l'inerzia delle aree in alcune condizioni tipiche. Sono stati considerati diversi tipi di perturbazione, tra cui perdita di generazione, gradino di carico, integrazione di FER e anche stima dell'inerzia in condizione di normali variazioni di carico.

Per validare i metodi, sono stati condotti esperimenti con 5 diversi casi studio, con diversi livelli di complessità. Gli esperimenti sono stati suddivisi in 13 diversi studi, in cui le simulazioni sono state condotte utilizzando MATLAB e PowerFactory per acquisire i dati equivalenti a quelli forniti dalle PMU

e i metodi sono stati applicati in sequenza.

Parole chiave: stima dell'Inerzia, Phasor Measurement Units, equivalenti dinamici.

Contents

List of Figures

List of Tables

List of Abbreviations

RES: Renewable Energy Source
PV: Photovoltaic
WP: Wind Power
TSO: Transmission System Operator
DSO: Distribution System Operator
SCADA: Supervisory Control and Data Acquisition
WAMS: Widea Area Monitoring Systems
PMU: Phasor Measurement Unit
SG: Synchoronous Generator
LS: Least-Squares
KF: Kalman Filter
EKF: Extended Kalman Filter
UFLS: Under Frequency Load Shedding
RoCoF: Rate of Change of Frequency
COI: Center of Inertia
AC: Alternate Current
DC: Direct Current
SCIG: Squirrel Cage Induction Generator
DFIG: Doubly-Fed Induction Generator
DDSG: Direct Drive Synchronous Generator
UKF: Unscented Kalman Filter
IME: Inter-Area Model Estimation
MEM: Model Estimation Methods
AGC: Automatic Generation Control
PFC: Primary Frequency Control
SFC: Secondary Frequency Control
GPS: Global Positioning System
PDC: Phasor Data Concentrator
PSS: Power System Stabilizer
AVR: Automatic Voltage Regulators
HVDC: High-Voltage DC

CHAPTER 1

Introduction

Mitigating climate change is one of the main challenges of modern society. In the electrical sector, three issues contribute to reduce carbon emissions: the use of energy provided by Renewable Energy Sources (RES), the search of energy efficiency and the electrification of heat and transport applications, which may provide 90% of the necessary reductions by the year 2050, [1]. Consequently, the energy generation portfolio has been changing: the penetration of RES is increasing in detriment of fossil fuel-based units year by year.

The transition for a greener energy mix requires the deployment of new units, supported by global policies and efforts. From 2009, the total amount of renewables increased from 1.136GW to 2.350GW worldwide, more than doubling the capacity in almost one decade, [2]. In 2016, nearly 62% of new units connected to the networks were renewables, accounting an estimated of 30% power generating capacity in the world [3]. During 2018, the growth in renewable generation capacity was 171GW, which represents 7.9% of increase with respect to the previous year.

Among renewable generation, Hydroelectrics still account for the largest share, about 50% of the total global capacity. Wind and Photovoltaic (PV) power units account together for 44%, while other types of units account only for 6%, [2]. However, this situation has been changing, since Wind Power (WP) and PV units have been growing worldwide much more than the others (accounting for 84% of all new capacity installed in the year of 2018), as Figure 1.1 shows. The reason behind the bigger increase of WP and PV units is that the environmental impact of these plants is smaller in comparison to the others, specially Hydroelectrics. The latter requires flooding large areas, affects the fauna and flora of the place and sometimes lead to resettling the local population.

In a long term view, renewable capacity is expanding in increasing amounts, from 20GW per year

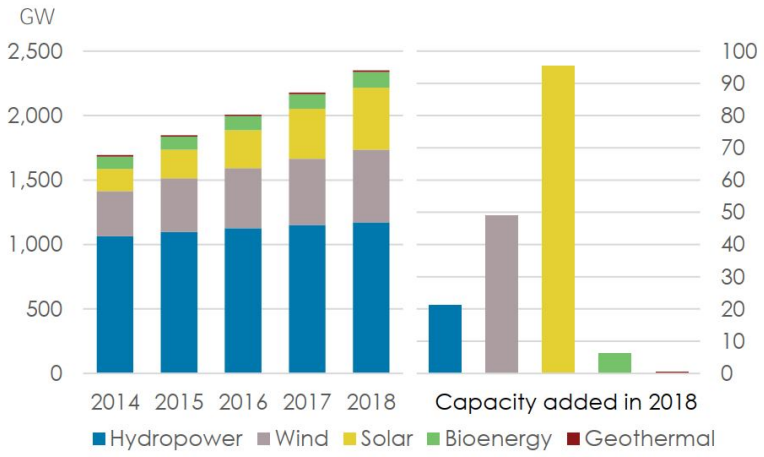

Figure 1.1: *Renewables capacity growth worldwide, [2]*

two decades ago to 160GW per year in the last years. At the same time, non-renewable capacity is still expanding, but with an oscillating behaviour that averages 115GW per year, being surpassed by the rate of renewable expansion in the last four years, as depicted in Figure 1.2. The expectation of RES growth is to meet 30% of global power demand by 2023, excluding hydro share, for the countries that committed to phase out traditional fossil fuel generation [4] and [5].

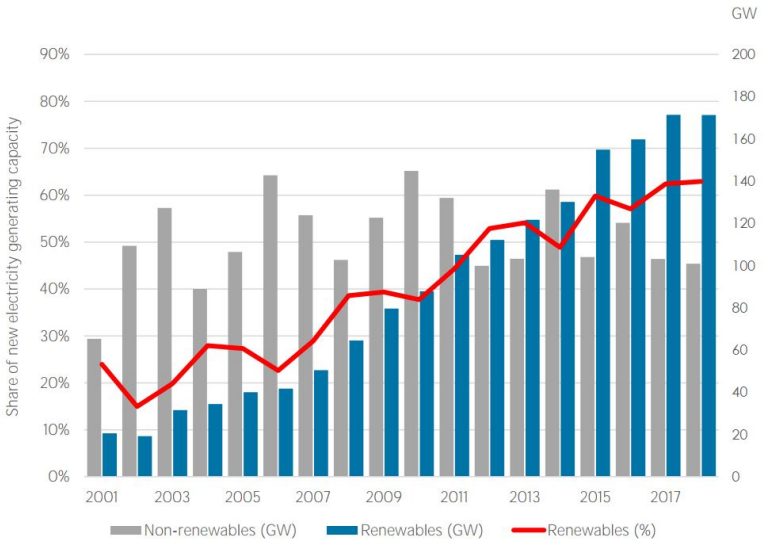

Figure 1.2: *Capacity transition, [2]*

With the growth in the installed capacity, many countries are already operating often with high level of RES-based energy generation. Denmark, perhaps the most prominent country on operating with high percentage of renewables, reportedly produced 43.6% of their whole electricity consumption in 2017 with the use of wind turbines [6]. At the day this sentence is being written (23/08/2019), WP generation produced almost 85% of the total load of the country for a short period of time early in the morning. At midday, WP generation accounted for 2071MW, and with a high contribution of PV (491MW), reached

60% of the of total load consumption of 4265MW at that moment. The remaining power was provided by Combined Heat and Power units and by importing from other countries. Partial details can be seen in Figure 1.3, while the full data can be seen in Figure A.1 of Appendix A.

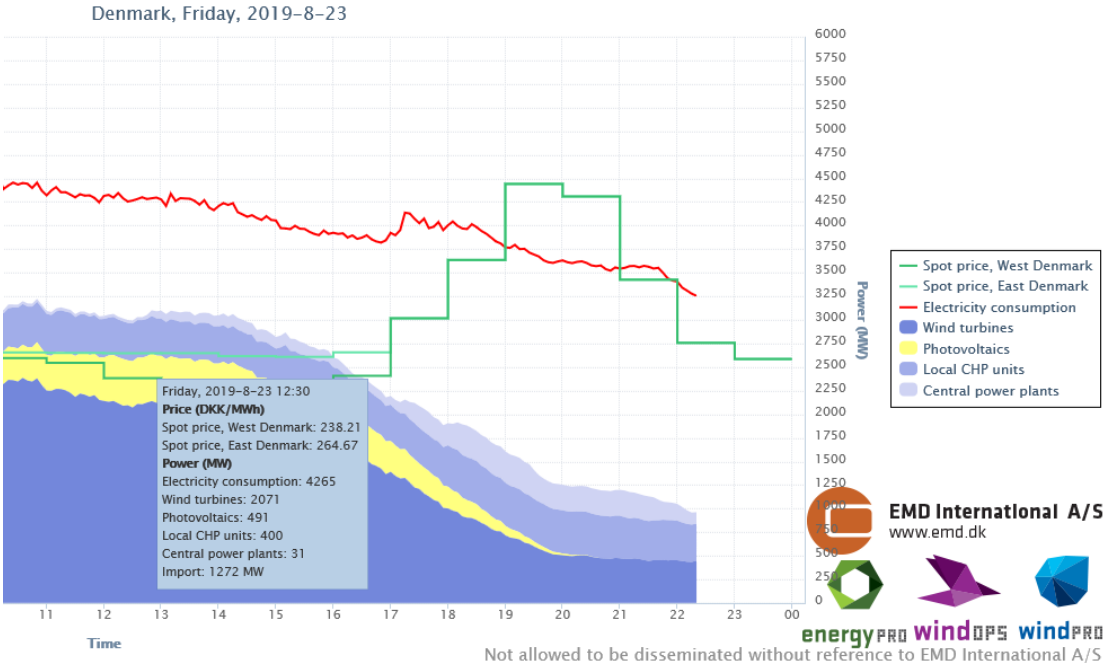

Figure 1.3: *Power generated at midday, Denmark, 23/08/2019, [7]*

In other countries, the percentage of WP in the generation portfolio is not yet so high but the amount of energy generated is already very significant. During the same week (18/08/2019-23/08/2019), WP generation often accounted for more than 30% of the power generated in Great Britain, as reported in [8] and depicted in Figure 1.4.

In Italy, the PV generation instead, is very representative. Also today (23/08/2019) at midday, PV generated 7.53GWh, about 18% of the total energy consumed (41.69GWh) at that moment, as Figure 1.5 presents. Full details can be seen in Figure A.2 at Appendix A. Still Thermal was the main source used, but the penetration of renewables is already remarkable also in this country.

The increasing penetration of RES in the energy portfolio has brought many particularities. First, due to their intrinsic characteristics, WP and PV units cannot be installed in every part of the grid, since they depend on the availability of the natural resource. Once installed, the conditions of the transmission system to supply far regions may not be helpful. The grid has been planned according to recurrent directions of power flows, from the traditional generating units installed to the main demanding centers. Once the generating units change, also changes direction of the power flows, as depicted in Figure 1.6. This may cause congestions (what may bring the necessity of curtailment) and voltage control issues.

Moreover, due to uncertainty, variability and unpredictability characteristics of most RES generation, a lot of flexibility is needed in the operation of a system that is traditionally not so flexible. As an example, WP and PV based units are non-dispatchable, what brings the risk of overgeneration in moments of minimum load or undergeneration in moments of high load. In conventional systems, flexibility is mainly provided by adjusting the output of generators to follow demand, which is very restrictive to

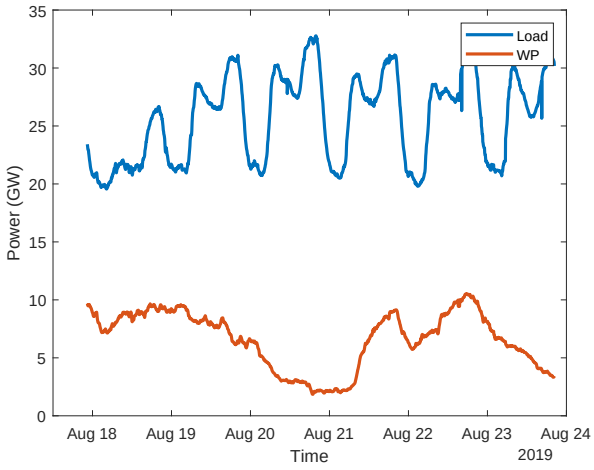

Figure 1.4: *Power generated in UK*

units that are able to provide that service. To improve the flexibility of the system, main solutions involve demand-side response, use of energy storage and retrofitting traditional units.

Another challenge of operating a modern power system that stands out is related to the stability of the system in high presence of RES. In this conditions, there is a change in local and interarea electromechanical modes, which may cause unexpected oscillations. In addition, the system may face higher frequency excursions then a conventional system, which requires new tuning of protection devices and defense plans, situation that may imply further catastrophic conditions if unforeseen.

1.1 Motivation of the work

The frequency behavior of the system during the transient period shortly after the occurrence of a power imbalance in the grid is governed by its equivalent inertia, which decreases when WP and PV units are connected to the grid. This is due to the fact that RES do not provide rotational inertia, once they are electrically decoupled from the grid by converters, such that the power output of these generators do not counteract frequency deviations of the grid. Systems with low inertia suffer from larger and faster frequency deviations from nominal values, which can lead to instability and loss of synchronism [10].

An illustrative example of the challenges of operating a system with high penetration of RES is the blackout that happened with the southern system of Australia, in 2016. Extreme weather conditions resulted in five electrical faults and the protection disconnected the southern part of the system from the main grid. However, a viable island operation could not be established because the frequency decayed very fast (with a rare of approximately 6Hz/s, double the level the load shedding counteract procedures could expect to operate in time to maintain the frequency of the isolated system). When the frequency reached 47 Hz, the remaining generators were tripped. The reason for this high Rate of Change of Frequency (RoCoF) was the low level of inertia which this part of the system was operating with, as it was identified and reported in [5].

Therefore, an arising stability requirement of modern power systems is to operate the system in a state that fulfills a minimum threshold level of inertia [11], [12]. A solution under study to guarantee that requirement and compensate low inertia levels is the so-called synthetic inertia [13]. This "virtual inertia"

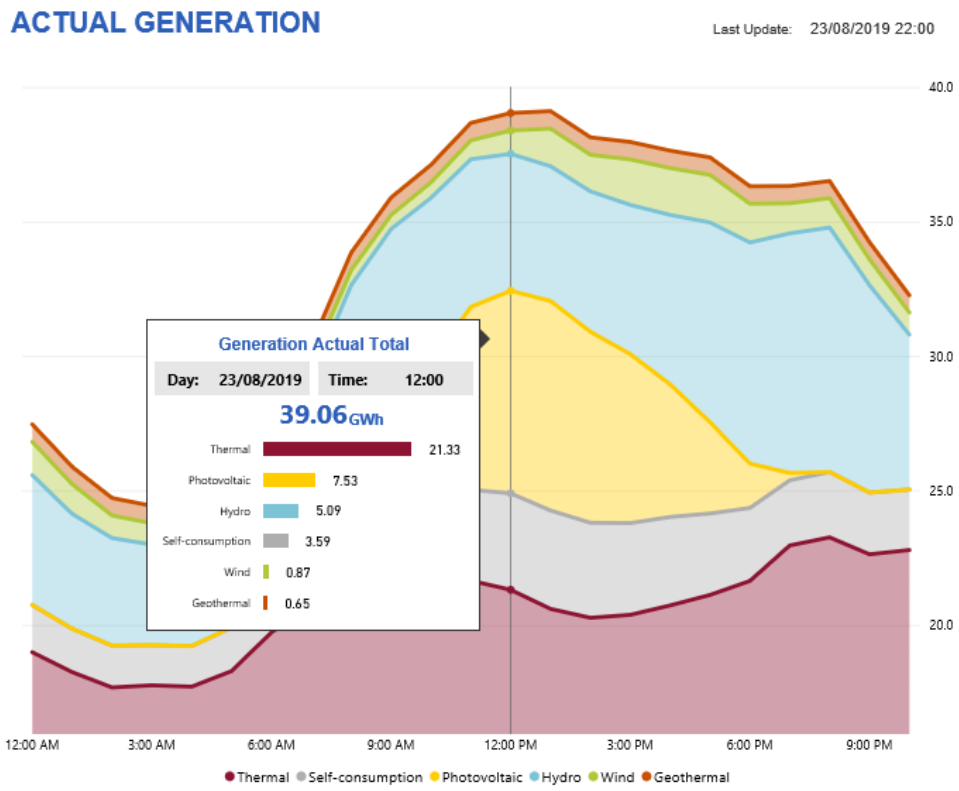

Figure 1.5: *Energy generated at midday, Italy, 23/08/2019, [9]*

consists in controlling power converters to mimic synchronous generators by delivering an active power response proportional to frequency variations. However, the question that arises is how a Transmission System Operator (TSO) or a Distribution System Operator (DSO) may know when the equivalent inertia of the system is low and needs compensation. Many traditional generators are not directly monitored, and moreover, most of the RES-based units are connected to medium and low voltage grids, leaving the TSO without the possibility of acquiring direct information in real-time about them. In these conditions, computing an equivalent inertia in real time is not an easy task, and the possibilities pass through methods for monitoring and estimation.

For what concerns grid monitoring, TSO worldwide traditionally adopted the Supervisory Control and Data Acquisition (SCADA) system to collect data from substations and to estimate states of interest in a power system. With the possibility of acquiring voltage magnitudes and power flows at the installed points with a resolution of one sample at every 2-4 seconds, the SCADA system has been widely used for steady-state analysis, such as supervising grid topology, active and reactive power control, load scheduling and historical data processing. Notwithstanding, due to the the limited resolution and to the fact that phase angles are not monitored, SCADA has not been often used for dynamic analysis.

As an alternative, the deployment of the Phasor Measurement Unit (PMU) has brought the possibility of acquiring measurements of current and voltage (magnitude and phase angles) in real-time in a precise and synchronized way with a resolution of 10-60 samples per second [14]. In other words, PMUs capture samples from measured waveforms and reconstruct phasors around the fundamental frequency of the waveform. Synchronizing all the measurements, the phasor concept can be extended from its static

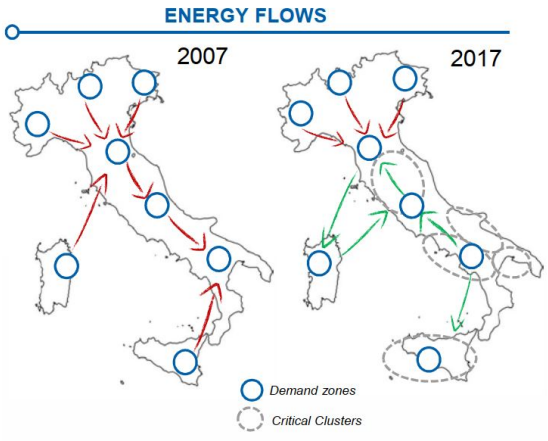

Figure 1.6: *The Italian case, [1]*

characteristics to dynamic characteristics, the so-called synchrophasors.

Due to the ease of working with phasors, and due to the high sampling rate, PMUs have been widely used for many applications [15], such as monitoring and detecting events, supervising relays and estimating parameters of interest. Likewise, many studies concerning on-line inertia estimation were developed in the past few years, normally divided in small-perturbation [16]–[18], large-perturbation [19]–[22] and steady-state [23], [24] approaches. Nonetheless, this field has still a lot of room for work, as [25] reports. The area has a lot of space for debate on modelling and analysis of low-inertia systems, which this work intends to contribute to.

1.2 Objectives of the work

The general aim of this work is to evaluate and develop methods for inertia estimation in real-time or near real-time, in practical conditions, based on synchrophasor measurements coming from PMUs installed on a transmission grid. The motivation comes from the necessity of TSOs to monitor equivalent inertia in real-time, for guaranteeing stability.

In the beginning of this work (2016), no method was identified as a definitive and general solution for online inertia estimation. Some of the methods require monitoring the terminals of each generating units [19], [22], some require monitoring coherent groups [16], some require monitoring the moving power [26]. At the moment of writing this thesis, the assumptions considered by the most recent studies are still the same [27]–[29].

However, commercial PMUs are still very expensive (reported as costing $40000 to $180000 in 2014, [30]), which limits its installation to strategic points on the grid defined following many different criteria other from just inertia estimation. In this context, how to make use of available spread PMUs to evaluate equivalent inertia is a topic not fully explored in the literature yet, with reported challenges and difficulties [31], but of high interest for TSOs worldwide. The topic involves many aspects: the determination of equivalent models; the effect of considering different measurement points, and how to relate them; the impact of loads on the estimations; the consideration of the location of the perturbation. Besides some of these aspects have individual solutions proposed in the literature, dealing with all of them with the purpose of estimating inertia is a field not yet explored.

Instead of focusing on developing and testing only one estimation method, applicable to a restricted set of cases, this work focuses on exploring the variety of practical situations and configurations that a transmission grid may present, and the possible mathematical models to approach it. As it explored many different solutions, no method was optimized to the definitive use. Consequently, the studies performed are limited to simulated data, under practical conditions though. Also, there were no specific studies on detecting and determining the time of a perturbation, neither bad data detection, as this has been explored in different works in the literature. This thesis contributes to the topic by proposing solutions to the cases other works did not explore directly.

Hence, the questions that arose and guided the specific objectives of this work were:

- Considering that PMUs are not necessarily installed at the terminals of every generator, is it still possible to gather any information regarding inertia?
- Is it possible to make use of PMUs spread on the grid to provide equivalent estimations of inertia in real-time?
- Is it possible to estimate an equivalent inertia based on a area delimited only by the measurement units available, regardless the behaviour of the rotating machines inside?
- What is the influence of loads on the estimations?
- What are the challenges and limitations of estimating equivalent inertia after a perturbation?
- Is it possible to monitor the inertia decrease following a substitution of synchronous generation by RES-based generation?
- Is it possible to monitor the inertia of the system under ambient conditions?

All of these questions were investigated having in mind to maintain the research practical and applicable with the conditions available nowadays, making reasonable assumptions with the amount of information a TSO should have.

1.3 Contributions of the work

This thesis approaches inertia estimation with Widea Area Monitoring Systems (WAMS) from two different perspectives: monitoring individually generating units considering PMUs installed at terminal buses or monitoring areas considering PMUs spread on the grid. Regarding the latter, this thesis presents innovative methods that are not based on delimiting the area following coherency criteria, as traditionally is done in the literature; in the proposed approach they are delimited by the assumption of PMUs installed at their boundaries. This practical assumption conduced to the development of different methods and strategies:

A novel Iterative-IME method was developed [32] to build dynamic equivalents and deal with perturbations, adapting the work proposed in [16] originally tailored to work with oscillations.

A strategy was developed to take advantage of spread PMUs in a system [33], defining a study area and using the measurements available to perform estimations of the dynamics of the Center of Inertia (COI) of the referred area. The technique makes use of Ward method to reduce the system and of the method proposed in [34] to build dynamic equivalents.

When dealing with an area that experiences an internal perturbation, the main challenge faced in this research was that the equivalent power of the referred area needs to be monitored or estimated. This condition increases drastically the requirements for practical use of the methods, such that a method to estimate the equivalent power was proposed. A paper on that topic is under submission.

Another contribution of this thesis is the study of inertia estimation in ambient conditions. The methods presented in [32] and [34] were tested with a strategy to estimate the equivalent moving power, with accurate results for generators individually monitored and with limited but practical results for area monitoring. Alternatively, considering generating buses monitored by PMUs, the method proposed in [35] was adapted in a novel approach for estimating inertia. A paper on that topic is under submission.

Figure 1.7 presents the summary of the above cited contributions.

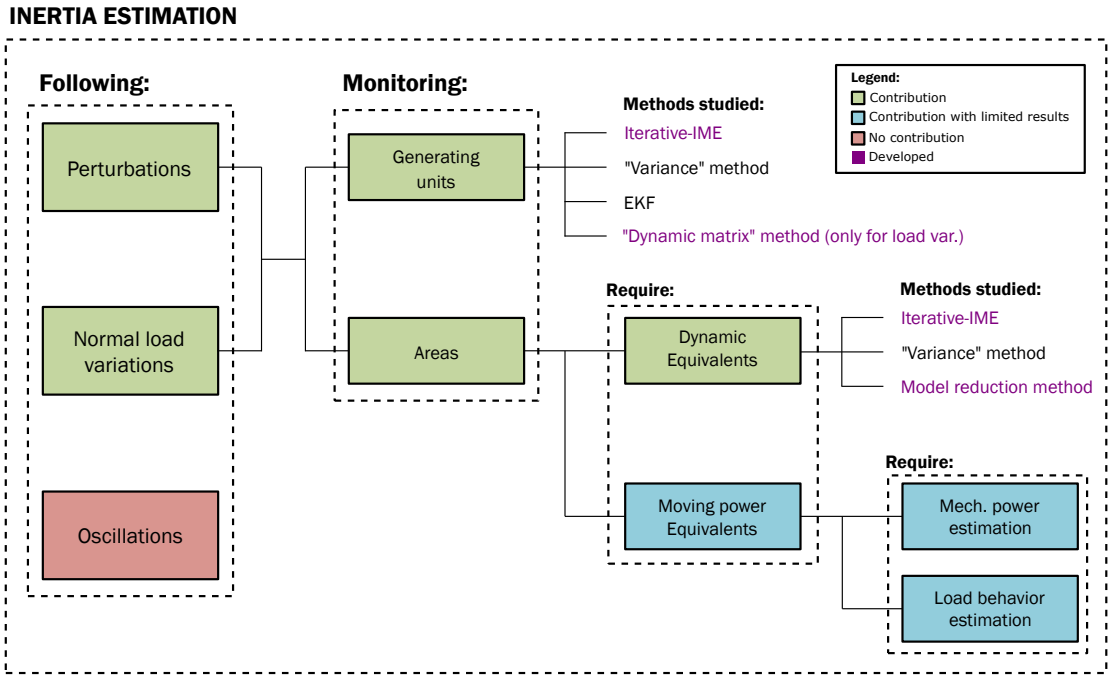

Figure 1.7: *Contributions of the thesis*

1.4 Structure of the Thesis

The remaining of the thesis is organized in the following way:

Chapter 2 brings a theoretical review on the power system's theory involved with the angle stability problem, constant of inertia and dynamic equivalents.

Chapter 3 presents the theory involving synchrophasor measurements and stability analysis.

Chapter 4 introduces the methods studied and proposed in this work, and a summary comparing the inputs, outputs, advantages and limitations of each one.

Chapter 5 presents the numerical results obtained.

Chapter 6 presents the final conclusions.

CHAPTER 2

Power system stability

The function of a power system is to supply electric energy to final customers, from generation through transmission and distribution. Moreover, the stable operation conditions must be provided, at minimum cost and minimum environmental impact, fulfilling standards of quality supply, such as constant frequency, constant voltage and reliable operation.

Due to the wide range of elements connected together to perform their function in the role of supplying electric energy, power systems are large and complex, such as the scheme of a generic power system depicted in Figure 2.1. As it can be seen, generating units are nowadays spread through different levels of transmission or distribution systems, operating at different voltage levels and supplying different types of customers. From the operating point of view, every aspect represented in Figure 2.1 has its influence and interest on this thesis.

A starting point regards the different types of generating units supplying the grid. The generation process consists in converting primary sources of energy (such as fossil, nuclear, water, wind and solar) to mechanical energy, later converted to electrical energy by the use of electrical generators.

Traditionally, the thermoelectric and the hydraulic processes are the most used. Figure 2.2 depicts a general scheme that represents the process of both thermoelectric, that uses steam (generated by a boiler heated by the combustion of fossil fuels or nuclear fission), and hydraulic, that uses water flow, to move the shafts of a turbine generating a mechanical torque (T_m) and a mechanical power (P_m). The mechanical power is converted to electrical power (P_e) through a synchronous generator. Basically, a synchronous generator requires the frequency of the stator (depending on the frequency of the grid) to be synchronized to the rotor mechanical speed to operate. Consequently, in a multi-machine system, the stator voltages and currents of all machines must have the same frequency also, such that a stable

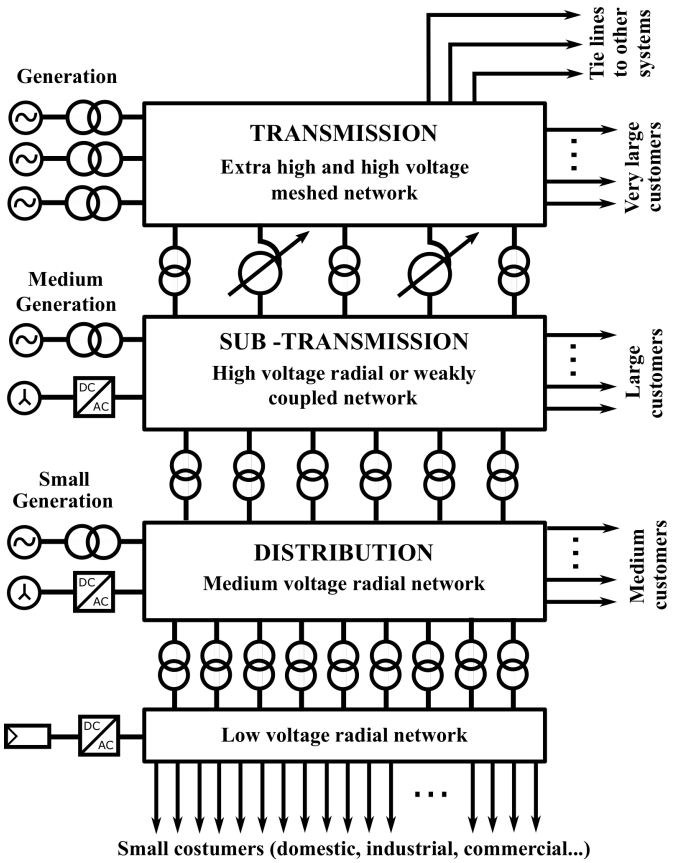

Figure 2.1: *Structure of a modern power system, adapted from [36]*

operation depends on that. Normally, these types of units are concentrated in specific points of the grid, with many generators able to provide energy to the part of the system through the transmission lines, as represented in Figure 2.1.

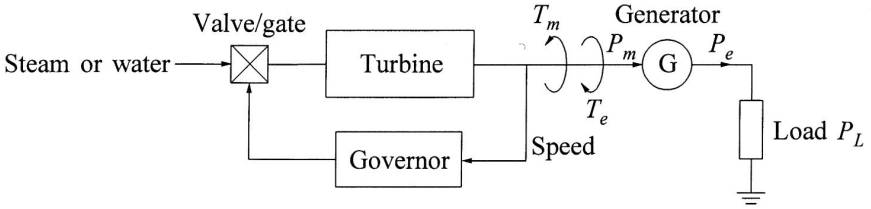

Figure 2.2: *Working principle of thermal and hydro generation, [37]*

Regarding the environmental impact of these traditional fonts, there are many issues. The process of combustion of fossil fuels is very pollutant, and the process based on nuclear fission has always the risk of contamination, that can be mitigated but not totally eliminated. The hydroelectric units do not exploit a resource that is in principle finite, since it exploits the power of moving water to generate electricity. However, the impact to the environment on the installation of hydroelectric units is a problem, and the places where they can be installed with limited impact are scarce. With the requirements of providing

solutions for energy generation that impacts less the environment, the search for RES brought WP and PV to highlight.

As an illustrative example, Figure 2.3 presents the working principle of wind-power generation. The mechanical power provided by the rotation of the shaft is converted either through an asynchronous generator, or through power electronic devices that decouple the generating process from the grid when delivering the electrical power. From the point of view of this thesis, the process used in PV units is similar to the process represented in Figure 2.3, because of the same decoupling provided by DC/AC converters. Normally, WP and PV can be installed in any part of the grid, but their use for distributed generation have been increasing recently, as represented in Figure 2.1 at medium and low voltage networks.

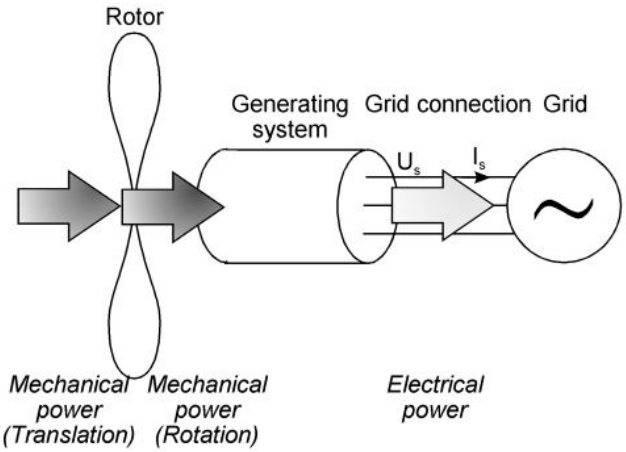

Figure 2.3: *Working principle of wind-power generation, [38]*

One of the main differences between synchronous generation and decoupled generation regards their inertial response to perturbations. In short, every rotating machine has a constant of inertia that "quantifies the kinetic energy of the rotor at synchronous speed in terms of the number of seconds it would take the generator to provide an equivalent amount of electrical energy when operating at a power output equal to its MVA rating" [36]. In other words, the dynamic effect of the perturbation on the units coupled to the grid (synchronous machines) is to release an amount of electrical energy that was previously stored in the form of kinetic energy in the shafts of these units. This amount of energy provided may mitigate the negative effect of the perturbation without affecting drastically the operating frequency of the system. However, decoupled units do not provide naturally a contribution to an inertial response, making the system weaker in terms of frequency changes. For that reason, control strategies are under development to provide the so-called synthetic inertia, an emulation of the synchronous inertial response making use of power electronic devices of decoupled generating units [39], [40].

This chapter aims at presenting the main concepts involving the operation of a multi-machine system with both synchronous and asynchronous/decoupled machines, such that one can understand the importance of inertia in modern power systems and the problems of stability under high penetration of RES-based generation. To delimit the field of study of this thesis, Section 2.1 presents the concepts involving Stability in Power Systems and defines the assumptions involved in these types of studies. After the field is delimited, Section 2.2 presents the general concepts and models of Synchronous generators

that will be adopted in this thesis. Section 2.3 describes the differences about types of generation based on machines decoupled from the frequency of the grid. Complementing, Section 2.4 discusses load modelling for stability studies and Section 2.5 presents a brief introduction to frequency control.

2.1 Stability in Power Systems

As previously presented, traditional power systems were based on operating the system at a synchronous speed, such that maintaining synchronism after a perturbation has always been one of the most challenging issues even before the increasing penetration of RES. In modern power systems, this type of problem is studied under the classification of large perturbation analysis, as represented in Figure 2.4.

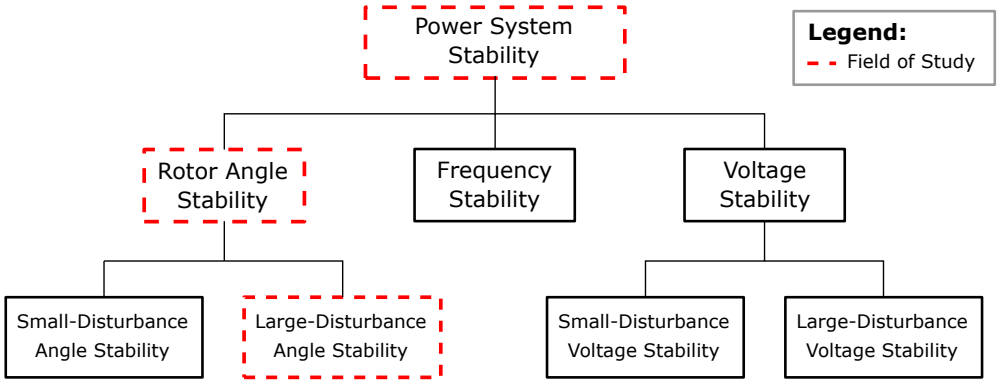

Figure 2.4: *Stability analysis classifications, [37]*

Formally, stability can be stated as *"the ability of an electric power system, for given initial operating condition, to regain a state of operating equilibrium after being subjected to a physical disturbance"* [37]. Hence, as a general concept, it can be extended to describe three different type of problems: rotor angle, voltage and frequency stability, differing mainly in the power system variable affected by the possible unstable behaviour. These classifications are important non only to define the field of study of this thesis, but also because it impacts on modelling assumptions of the studied methods.

The field of study of this work is rotor angle stability, traditionally divided in small perturbation angle stability (electromechanical oscillations) and large perturbation angle stability. Small-angle instability problems are normally related to insufficient damping. The large perturbation angle instability instead, is associated with the nonlinear power-angle relationship. The latter is normally a consequence of both the initial state and of the severity of the perturbation, and mainly occurs due to a lack of synchronizing torque [37]. According to the imbalance, the equilibrium between the mechanical and the electrical torques of a synchronous machine is affected, resulting in acceleration or deceleration of its rotor. Hence, according to the angle separation between the connected machines, the system may regain or lose synchronism. The time frame of interest in these type of studies range from the first seconds after the perturbation until 10-20s in very large systems.

To study rotor angle stability problems, a dynamic model of the grid is needed, either for simulation or analysis. Due to the complexity of real power systems, model simplification is not only acceptable but sometimes necessary, because of computational time and effort. The traditional approach consists in making simplifying assumptions according to the time constants of the phenomenon considered. Perturbations are usually classified in electromagnetic and electromechanical transients.

Much slower are the electromagnetic dynamics that take place in the machine windings following a disturbance, operation of the protection system or the interaction between the electrical machines and the network.

The fastest events are classified as electromagnetic transients, lasting mostly μs to ms [41]. This type of phenomena takes place in the machine windings, following disturbances, opening or closure of circuit breakers, specific actions of power electronic devices or equipment failures. Due to their fast rate of decay, electromagnetic transients deal with changes in voltages and currents, and they affect mostly transmission lines, transformers and protection devices. On the other hand, the inertia of the turbines, motors and generators are sufficient to prevent any significant change in the synchronous speed of the system [36].

Electromechanical transients, instead, last from ms to s. They are caused by mismatches between production and consumption following a disturbance, and their time scale is long enough to affect the rotor of the synchronous machines and some controls. Due to their faster behaviour, network voltages and currents (that change in the order of μs to ms) may be considered as passing from one steady state to another[42], which allows modelling their behaviour using algebraic equations, while the dynamic of synchronous machines are represented with differential equations.

2.2 Synchronous machine representation in stability studies

Synchronous machines consist basically of two elements: the field and the armature circuits. The field circuit (normally in the rotor) is excited with dc current, and driven by a prime mover, forms a rotating field that induces an emf in the armature winding (normally in the stator). The reaction of the induced currents in the stator is to produce a magnetic flux that rotates at the same speed as the rotor. The resulting flux regarding the excitation and the induced fluxes is stationary concerning the rotor motion, but rotates at synchronous speed in relation to the stator. In this way, the speed of the machine is proportional to the operating frequency of the network [36], [43]. Figure 2.5 depicts a three-phase machine with one pair of field poles, where ω_r is the rotor speed.

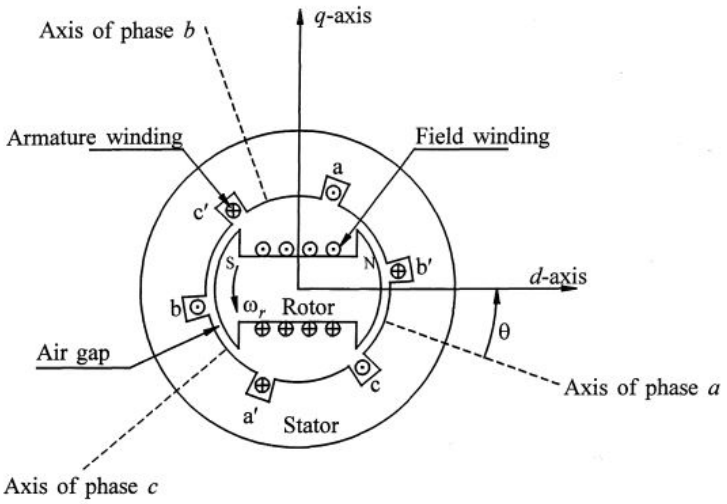

Figure 2.5: *Schematic diagram of a three-phase synchronous machine, [37]*

In developing a mathematical model for a synchronous machine, one need to write the differential equations that represent the magnetic and the electrical circuits. To do so, some assumptions are usually adopted: sinusoidal distribution of the stator windings along the air-gap (if the mutual effects with the rotor are considered), the rotor inductances don't vary significantly with the rotor position, magnetic hysteresis and saturation effects negligible. These assumptions are supported by field tests and measured performances.

From the mathematical models to represent synchronous machines available in the literature, the classical model, that consists in a voltage source behind a reactance, is the simplest and the easiest one to be used when explaining large perturbations in a multi-machine system. Moreover, it is the model that most benefit from phasor representation, relating to the intention of using data from PMUs, and a major trade-off (in this thesis) is whether a more detailed model is identifiable based on measurements and in practical conditions. The classical model is based on strong assumptions, but its use in stability studies is wide spread and recognized [42], [44], [45]. This section quickly reviews the main concepts related to it.

2.2.1 Classical model for synchronous machines

Considering the study of an isolated generator connected to an infinite power bus, the occurrence of a perturbation induces currents in the rotor circuits of the machine, that following the occurrence of the event, decay with different time constants. The parameters intrinsic to the machine that have a faster influence on the decay are the so called sub-transient parameters, the transient parameters are those related to slower decay, and the synchronous parameters are those related to sustained influence. The time constants corresponding to the rate of decay, together with the effective reactances seen from the terminals of the machine are related to the fundamental frequency of the transient, and are the main important quantities to define synchronous machines in transient analysis.

A particular figure of interest is the open-circuit transient time constant ($Td_0^{'}$). This constant is an operational parameter determined through an open-circuit test, and characterizes the time required for the transient alternating component of the open-circuit current to decay until 0.368 time its initial value. It is a characteristic of the construction of every machine, and it is a function of the inductances of the field and armature, with typical values reaching 10s for Hydro and Thermal units [42]. Typically, if the period of study is smaller than $Td_0^{'}$, the rotor flux linkages in the field of the machine can be considered constant. As a consequence, no differential equations are needed to represent the electrical characteristics of the machine.

Neglecting also the transient saliency of the rotors, the machine can be represented as a voltage source behind a transient reactance. Figure 2.6 shows the classical configuration for a generator, where $\mathbf{E}'$ and $\mathbf{E_T}$ are the transient internal voltage and terminal voltage, $\mathbf{I}$ is the current and x'_d is the transient reactance, respectively, and the use of bold letters denotes phasors quantities.

Using phasor notation, $\mathbf{E}' = E'\angle\delta$ can be calculated according to its pre-disturbance value

$$\mathbf{E}' = \mathbf{E}'_0 + jx_d\mathbf{I_0} \tag{2.1}$$

where the subscript 0 and x_d denote pre-disturbance quantities. The phasor notation is possible because only the fundamental frequency components of stator quantities are considered, once the phasors are defined in terms of d-q axis components of terminal voltages. The d-q axis are represented in Figure 2.5.

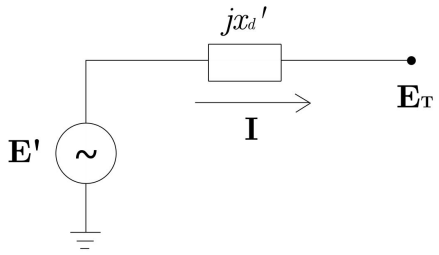

Figure 2.6: *Classical model of the generator*

As a consequence of the constant flux linkage hypothesis, the d-q components of the voltage $\mathbf{E}' = E_d + j * E_q$ can be considered constant throughout all the study period, and therefore $|\mathbf{E}'|$ can be considered constant. As the rotor speed changes, E' will have constant orientation in relation to its d-q components, as it can be seen in Figure 2.7. Hence, the phase angle δ can be used as an accurate approximation for the rotor angle of the synchronous machine in study. As δ varies, so does $\mathbf{I}$ and $\mathbf{E}_T$, according to Ohm's Law.

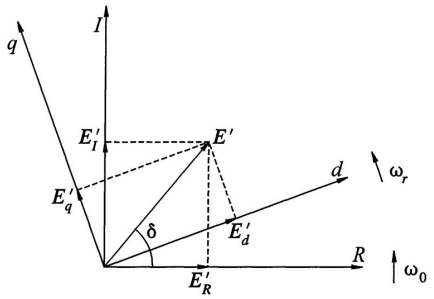

Figure 2.7: *The R-I and d-q coordinate systems, [42]*

2.2.2 The synchronous inertia

The expression that describes the motion of the rotor is the so called Swing Equation:

$$J\frac{d\omega_m(t)}{dt} = T_m(t) - T_e(t) \tag{2.2}$$

where J is the momentum of inertia, ω_m is the mechanical speed of the rotor in [mech. rad/s] in a fixed reference and T_m and T_e are the mechanical and electrical torque (in [Nm]), respectively [42].

The momentum of inertia, J, is a constant defined as

$$J \triangleq \int r^2 dm, \qquad kg.m^2 \tag{2.3}$$

where r is the distance to the pivot point and m is the mass of the body.

The mechanical speed of the rotor (ω_m) is given by the derivative of the rotor angular position ϑ_m,

expressed with reference to a fixed axis:

$$\omega_m(t) = \frac{d\vartheta_m(t)}{dt} \tag{2.4}$$

However, it is possible (and more convenient) to adopt a rotating reference at synchronous speed for ϑ_m, given by

$$\vartheta_m(t) = \omega_{0m}t + \delta_m(t) \tag{2.5}$$

where ω_{0m} is the mechanical synchronous speed and δ_m is the rotor angular position in the synchronously rotating frame, in [mech. rad].

Hence, Equation (2.2) may be rewritten substituting first Equation (2.4), and then Equation (2.5), giving:

$$J\frac{d^2\delta_m(t)}{dt^2} = T_m(t) - T_e(t) \tag{2.6}$$

Expressing (2.6) in terms of Power [W], there is

$$J\frac{d^2\delta_m(t)}{dt^2}\omega_m(t) = P_m(t) - P_e(t) \tag{2.7}$$

The momentum of inertia can be substituted by the so-called Inertia Constant (H), that is the ratio between the stored kinetic energy E_{SG} in [MWs] at synchronous speed and the machine rating power S_n in [MVA], given by

$$H' \triangleq \frac{E_{SG}}{S_n} \qquad [MWs/MVA] \tag{2.8}$$

The stored kinetic energy, in its turn, is given by

$$E_{SG} = \frac{J\omega_{0m}^2}{2} \tag{2.9}$$

As a representative example of Equation (2.8), if a Synchoronous Generator (SG) has $H' = 3s$, this means that the kinetic energy stored at the rotating parts of this machine can feed the rated load for 3s. Table 2.1 presents typical values.

Table 2.1: *Typical values of H', [42]*

Type	**H' [MWs/MVA]**
Thermal unit 2-pole 3600 r/min	2.5 to 6
Thermal unit 4-pole 1800 r/min	4 to 10
Hydraulic	2 to 4

Besides the unit of the defined constant H' is $[MWs/MVA]$, it is often used in the literature only [s], assuming the rated power of the generator is already taken into account. This will be the definition used in most of this thesis, represented by H.

It is also common in the literature to define other inertia constants in terms of H, [46], such as

$$M = \frac{2H}{\omega_0}, \qquad [s^2] \tag{2.10}$$

and

$$M' = 2H, \qquad [s] \tag{2.11}$$

Assuming $\omega_m(t) \approx \omega_{0m}$, Equation (2.7) becomes

$$\frac{2HS_n}{\omega_{0m}} \frac{d^2\delta_m(t)}{dt^2} = P_m(t) - P_e(t) \tag{2.12}$$

For power system studies, it is more useful to substitute the mechanical quantities δ_m and ω_m by their electrical correspondent, according to the number of the pole pairs (p) of the machine,

$$\delta = p\delta_m \tag{2.13}$$

$$\omega = p\omega_m \tag{2.14}$$

where δ is the rotor angular position (or simply rotor angle) in electrical [rad] and ω is the rotor speed in electrical $[rad/s]$.

Expressing (2.12) in terms of δ and ω, and dividing the right hand side of Eq. (2.12) by S_n, the Swing Equation can be written as

$$\frac{2H}{\omega_0} \frac{d^2\delta(t)}{dt^2} = P_m(t) - P_e(t), \qquad p.u. \tag{2.15}$$

Referring to Equation (2.15), when the per-unit mechanical power P_m provided by the generators no longer matches the per-unit electrical power P_e consumed by loads and losses, the per-unit angular speed of the generators (ω) increases or decreases, depending on the sign of the power mismatch. The imbalance ($P_m(t) - P_e(t)$) is also called accelerating power P_{acc}. As an illustrative example, Figure 2.8 presents the dynamic behaviour of a synchronous generator simulated using the classical model. After a load step (in $t = 5s$), the active power (P_e) produced increases to match the increase in the load, while the mechanical power (P_m) is kept constant (see Figure 2.8(a)). Consequently, the accelerating power right after the perturbation is negative, producing a decrease in the speed as it can be seen in Figure 2.8(b).

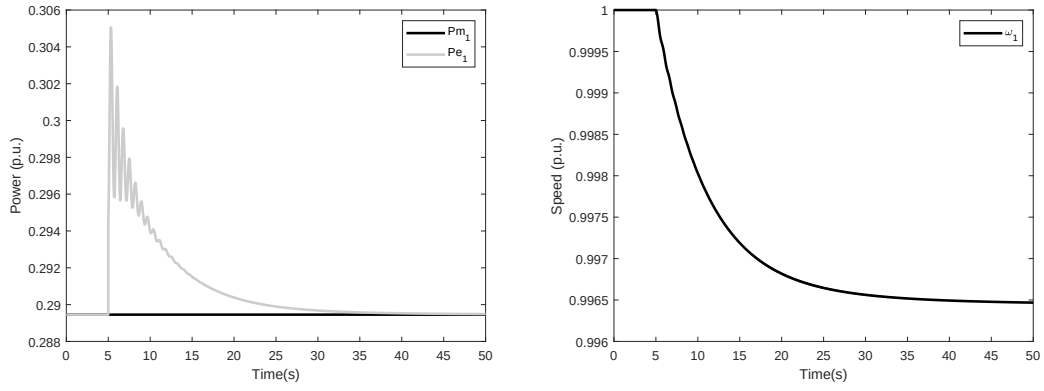

(a) Power behaviour

(b) Speed behaviour

Figure 2.8: *Dynamic response of a synchronous generator subject to a step increase on the load*

This variation could be limited by the damping torque (i.e., the product between the damping coefficient D and the difference between the current and rated per-unit angular speed of the generators ($\omega - \omega^0$), exerted by the damping windings of the generators and by the loads whose withdrawn power changes with the frequency. To consider the damping coefficient, Equation (2.15) can be rewritten as

$$\frac{2H}{\omega_0}\frac{d^2\delta(t)}{dt^2} + D\frac{d\delta(t)}{dt} = P_m(t) - P_e(t), \qquad p.u. \tag{2.16}$$

Or, alternatively,

$$\frac{2H}{\omega_0}\frac{d\omega(t)}{dt} + D\omega(t) = P_m(t) - P_e(t), \qquad p.u. \tag{2.17}$$

As it can be understood from Equations (2.15) and (2.16), the inertia constant H plays a very important role in the inertial response: considering a fixed amount of power imbalance, the higher the inertia, the lower the frequency variation right after a power disturbance.

2.2.3 Multi-machine systems

In a multi-machine system, where many generators and loads are interconnected by tie-lines, Equation (2.17) can be extended for everyone of the i machines connected [47]. Neglecting damping for the sake of simplicity, the general set of i equations is

$$\begin{cases} H_1\frac{d\omega_1(t)}{dt} &= (P_{m_1}(t) - P_{e_1}(t))\frac{\omega_0}{2} \\ H_2\frac{d\omega_2(t)}{dt} &= (P_{m_2}(t) - P_{e_2}(t))\frac{\omega_0}{2} \\ &\vdots \\ H_i\frac{d\omega_i(t)}{dt} &= (P_{m_i}(t) - P_{e_i}(t))\frac{\omega_0}{2} \end{cases}$$

An important concept to study the dynamics of a multi-machine system is the COI, a rotational analogy of the center of mass of an object. The dynamic behaviour of the synchronous machines tends to follow the speed associated to its COI [10], [13], [48], the so-called mean speed, determined by the following expression

$$\omega_{COI} \triangleq \frac{\sum_{j=1}^{i} S_{n_j} H_j \omega_j}{\sum_{j=1}^{i} S_{n_j} H_j} \tag{2.18}$$

Related to the COI, the equivalent inertia constant H_{COI} can be calculated with the following definition

$$H_{COI} \triangleq \frac{\sum_{j=1}^{i} S_{n_j} H_j}{\sum_{j=1}^{i} S_{n_j}} \tag{2.19}$$

In addition, the same concepts can be extended to define similarly an equivalent phase angle δ_{COI} and equivalent frequency f_{COI}:

$$\delta_{COI} \triangleq \frac{\sum_{j=1}^{i} S_{n_j} H_j \delta_j}{\sum_{j=1}^{i} S_{n_j} H_j} \tag{2.20}$$

$$f_{COI} \triangleq \frac{\sum_{j=1}^{i} S_{n_j} H_j f_j}{\sum_{j=1}^{i} S_{n_j} H_j} \tag{2.21}$$

The equivalent motion equation of the system with respect to its COI is given by

$$\frac{2}{\omega_0} \frac{\sum_{j=1}^{i} S_{n_j} H_j}{\sum_{j=1}^{i} S_{n_j}} \frac{d\frac{\sum_{j=1}^{i} S_{n_j} H_j \omega_j}{\sum_{j=1}^{i} S_{n_j}}}{dt} = (\sum_{j=1}^{i} P_{m_j}(t) - P_{e_j}(t)), \qquad p.u. \tag{2.22}$$

or alternatively

$$\frac{2}{\omega_0} H_{COI} \frac{d\omega_{COI}}{dt} = (P_{m_{Eq}}(t) - P_{e_{Eq}}(t)), \qquad p.u. \tag{2.23}$$

where $P_{m_{Eq}}(t) = \sum_{j=1}^{i} P_{m_j}(t)$ and $P_{e_{Eq}}(t) = \sum_{j=1}^{i} P_{e_j}(t)$.

To illustrate the behaviour of a multi-machine dynamics, a system consisting of three synchronous generators is taken as example. The behaviour of the COI of the system right after a load increase is represented in Figure 2.9, in comparison to the speed of the three machines of the system. It can be seen that the mean frequency gives the general trend of the decrease.

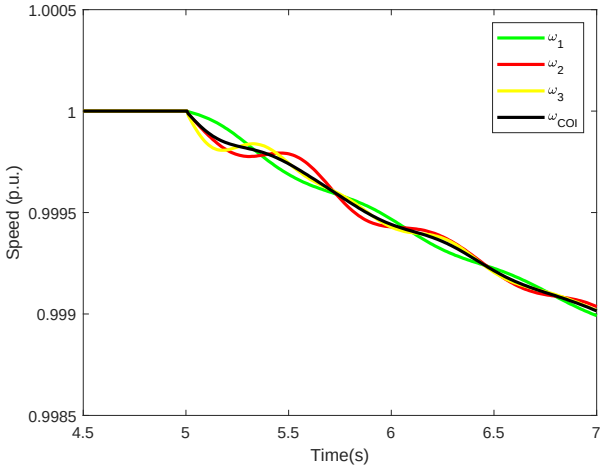

Figure 2.9: *Speed behaviour of the generators*

The effect of decreasing the inertia is represented in Figure 2.10 for the same perturbation, where ω_{COI_I} is the long term response of the same ω_{COI} presented in Figure 2.9, while $\omega_{COI_{II}}$ and $\omega_{COI_{III}}$ are the mean speed after the equivalent inertia of the system is reduced to half and to third, respectively.

Two other illustrative examples of multi-machine dynamics are represented in Figure 2.11. First, Figure 2.11(a) depicts the case when frequency controllers are included in the system, bringing the mean frequency back to 1 p.u. some seconds after the perturbation. In the legend, ω_{FC} denotes the case with frequency controllers, while ω_{W_FC} denotes the case without. At second, Figure 2.11(b) illustrates the case when the system is not able to handle the size of the perturbation applied, and the rotor angles increase indefinitely until the synchronism is lost. No frequency controllers are considered in this case.

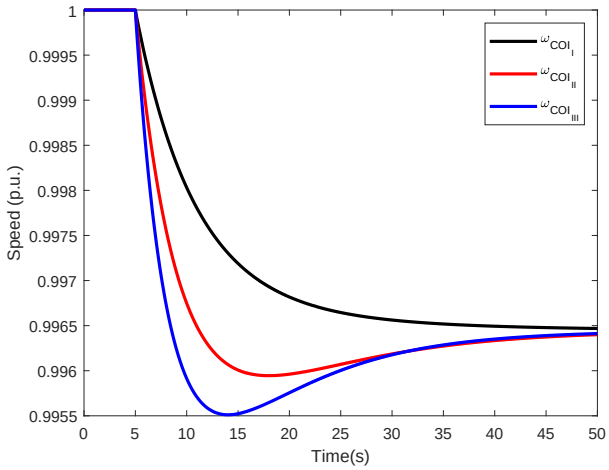

Figure 2.10: *COI behaviour with three different values of equivalent inertia*

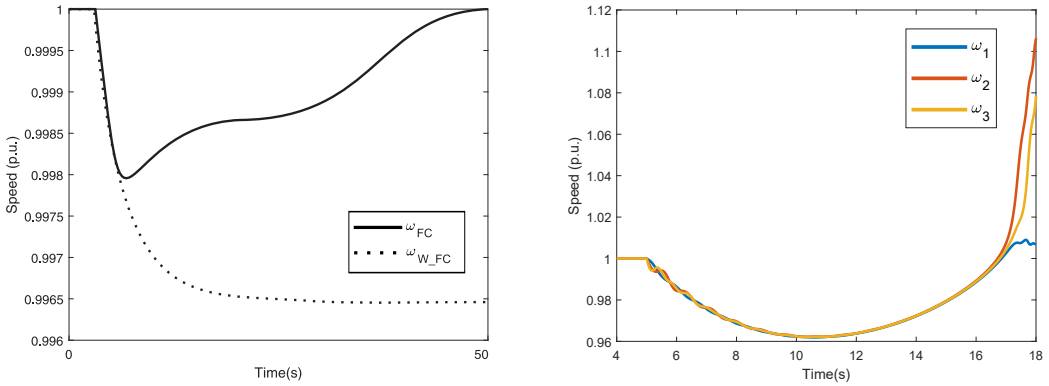

(a) Frequency control

(b) Loss of synchronism

Figure 2.11: *Speed behaviour - Illustrative cases*

2.3 Decoupled machine representation in stability studies

Specifically for stability studies, the most important variables regarding generating units connected to the system through power electronic devices are the outputs of the converter, since the other quantities are decoupled from the frequency of the grid. To reach this conclusion, this Section will give a brief explanation of the processes involved.

2.3.1 Wind power units

Wind Power generation units are composed basically by a wind turbine, a generator and a converter or transformer. Also, battery banks can be included to mitigate the intermittency of the source. The main topologies can be divided in:

- Fixed-speed topology:
  Speed set by the frequency of the grid, the gear and the generator characteristics, no matter the

wind speed. The mechanical power generated by the rotation of the turbine's blades is transformed into electrical power through the use of induction generators, the most common is the Squirrel Cage Induction Generator (SCIG). The generator is normally connected to the grid through transformers, capacitors banks and soft starters.

- Variable-speed topology:
  Designed to obtain maximum efficiency over a continuous range of wind speed, adapting the rotational speed of the rotor to the speed of the wind. The mechanical torque is approximately constant while the variations of wind are absorbed by the rotor speed of a synchronous or induction generator, that must be decoupled from the grid through power converters to allow this type of operation. The main used generators are the Doubly-Fed Induction Generator (DFIG) and the Direct Drive Synchronous Generator (DDSG).

Figure 2.12 depicts the most common schemes of connection of wind turbines to the grid. In the Figure, WRIG denotes Wound Rotor Induction Generator (a type of DFIG), PMSG denotes Permanent Magnet Synchronous Generator and WRSG denotes Wound Rotor Synchronous Generator.

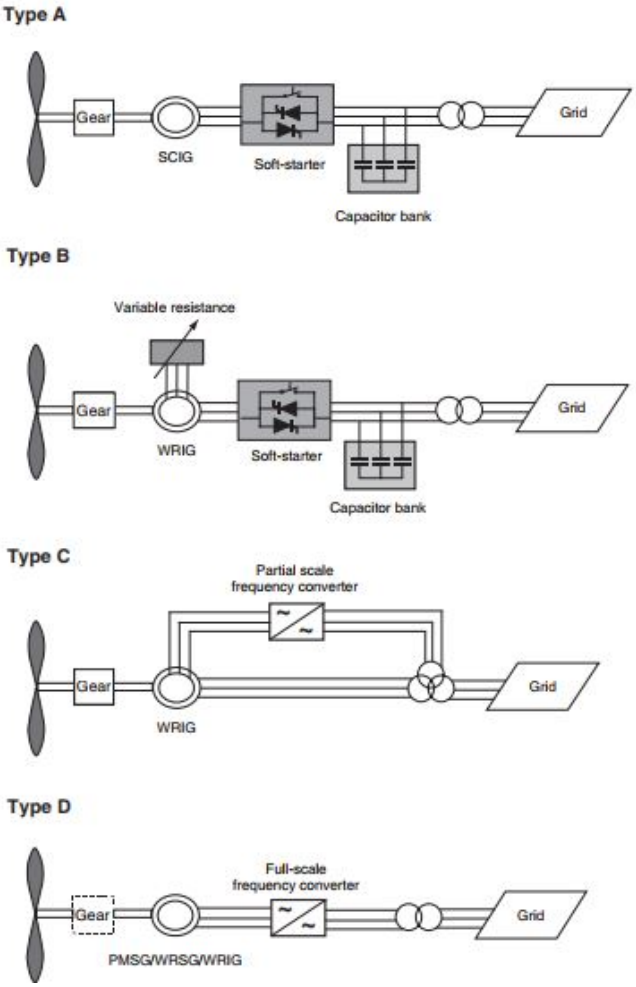

Figure 2.12: *Typical wind turbine configurations, [49]*

Regarding the wind turbines, the operation can be divided in four different zones, as depicted in Figure 2.13. In zones I and IV the turbine does not work, because the wind speed is less than the rated speed V_{in} or greater than the maximum speed V_{out}, respectively. In Zone II the turbine works with optimized efficiency, obtaining maximum conversion of the wind kinetic energy into electrical energy according to the generator used. In Zone III the power output remains constant no matter the wind speed, by controlling the blades of the turbine.

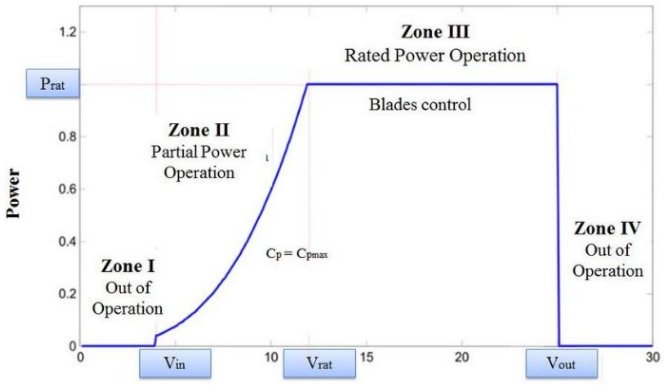

Figure 2.13: *Wind turbine operation zones, [50]*

According to the wind speed (v_W) and the operational zone, the mechanical power produced by a wind turbine is given by

$$P_W = \frac{1}{2} C_p \pi \rho r^2 v_W^3 \tag{2.24}$$

where $\rho r = 1.225 \frac{kg}{m^3}$ is the air density, r is the rotor radius and C_p is the efficiency coefficient of the wind turbine [49]. To transform the mechanical power into electrical, a generator is needed, either synchronous or asynchronous. Between the asynchronous generators, the induction machines are the most used.

While the principles of synchronous generators have already been presented, the principle of working of induction machines is based on applying an exciting Alternate Current (AC) to the stator, that creates a magnetic field rotating at the speed of the grid. If the rotor rotates with a speed different from the synchronous machine of the grid, a current is then induced in it's windings, which in turn creates a magnetic field that opposes the rotating field in the stator. The interaction between these two fields produces a mechanical torque in the rotor. The speed of the rotor, regarding induction generators, must be faster than the synchronous speed by a difference factor called slip (s_l):

$$s_l = \frac{\omega_s - \omega_r}{\omega_s} \tag{2.25}$$

where ω_s is the speed at the stator, therefore synchronous, and ω_r is the speed of the rotor. To generate power, induction generators vary their rotor speed and their slip, without acting on the frequency of the stator [43]. The variation of the slip in time is given by

$$\frac{ds_l}{dt} = \frac{1}{2H}[T_m - T_e] \tag{2.26}$$

where, similarly to synchronous machines, H is the constant of inertia, T_m and T_e are the mechanical and electrical torque, respectively.

Regarding the SCIG, the rotor speed variations may reach only 2% of its nominal speed. For this reason, they are often referred as constant speed machines, and consequently quantities depending on ω_r can also be considered constant. Normally these machines are designed with a suitable number of poles to provide two different power outputs (both a two different constant speed or slip values).

The equivalent circuit of a SCIG generator can be seen in Figure 2.14, in the d-q reference frame. The electric power output injected in the grid can be determined according to only stator quantities [49], as follows,

$$P_s = v_{ds} i_{ds} + v_{qs} i_{qs} \tag{2.27}$$

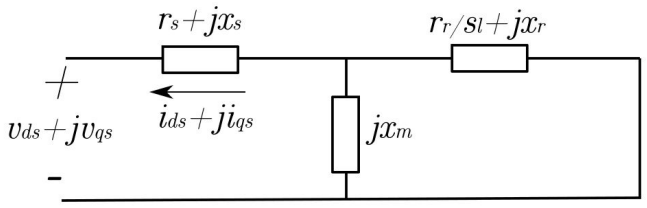

Figure 2.14: *Equivalent circuit of SCIG, [51]*

The other two machines, DFIG and DDSG, are instead variable speed systems, allowing a larger range of wind power to be explored. To allow the rotation of the rotor to vary without implications on the function of the machine, a power converter is needed to assure frequency decoupling. In the DFIG, the electrical frequency of the grid matches the electrical frequency of the rotor, that is therefore decoupled from the mechanical frequency of the rotor (rotation speed). In the DDSG, the decoupling between the grid and the generator is total, such that the generator side of the converter can be a voltage source or a diode rectifier to excite the field circuit of the machine [38].

Looking at the grid side, the electric power output of a converter can be expressed by

$$P_c = u_{dc} i_{dc} + u_{qc} i_{qc} \tag{2.28}$$

where, similar to Equation (2.27), the subscripts d and q denote direct and quadrature components of the voltage u and the current i at the grid side of the converter, denoted by c. The power P_c is consequently a function of the rotor power in terms of the efficiency of the converter, but is decoupled from the rotor speed dynamics.

2.3.2 Photovoltaic units

Photovoltaic units normally consist of one or more PV panels, a DC/AC inverter, a distribution panel or a transformer, and battery banks that can be used for benefit. Figure 2.15 presents some typical connection schemes.

In short, PV cells are crystalline-based featuring a p-n junction, whose positive and negative sides present a DC voltage, able to supply electricity. The material of the cell is able to absorb photons of light and release electrons, by the so-called photoelectric effect. The scheme of a PV cell is depicted in Figure 2.16.

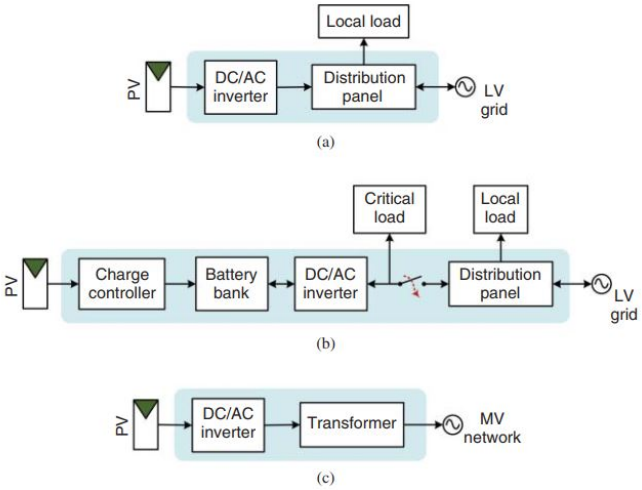

Figure 2.15: *Typical PV configurations, [52]*

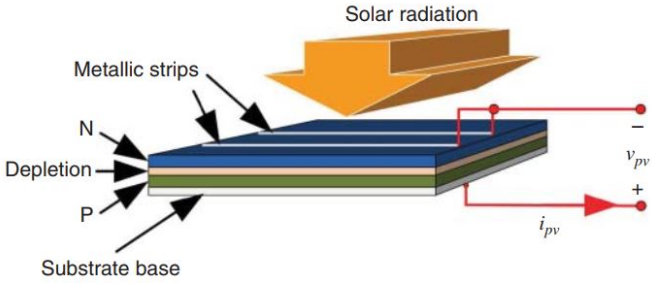

Figure 2.16: *Typical crystalline PV cell, [52]*

PV cells are direct current sources, such that the reverse flow of current should be prevented by the usage of blocking diodes. In addition, the full equivalent circuit of a PV cell includes a shunt resistor and a series resistor to model non-ideal factors [52]. Figure 2.17 depicts the equivalent circuit of a PV cell.

$$I_{PV} = I_{PH} - I_D - I_L = I_{PH} - I_0(exp(\frac{q(V + IR_s)}{AkT}) - 1) - \frac{V + IR_s}{R_L} \tag{2.29}$$

where I_{PH} is the PV photon current, I_D is the diode current and I_L is the inter-electronic leakage current. Also, I_0 is the diode reverse saturation current, q is the charge of the element, k is the Boltzmann constant, A is the diode constant and T is the temperature in the p-n junction. The characteristics of the expression of I_D are due to the Shockley theory for p-n junctions [52].

The output voltage V of a single cell is less than $1V$, such that these cells must be combined in series and parallel, forming bigger arrays. By using circuits theory, the equivalent DC output of the array can be determined. PV power plants are large-scale systems that include one or more PV arrays and multiple inverters to handle the connection with the grid, reaching the order of MW of power generation.

When using PV units for supplying power to AC grids, a DC/AC inverter is needed. The output of a typical inverter can be seen in Figure 2.18, here based on a frequency of 50Hz.

The output of the inverter is given by the dynamics of a DC Link for AC grid connections, that may

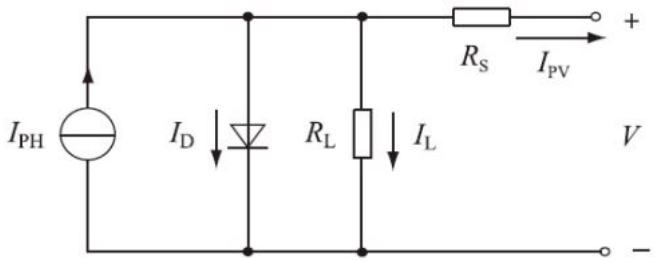

Figure 2.17: *Equivalent circuit of a PV cell, [53]*

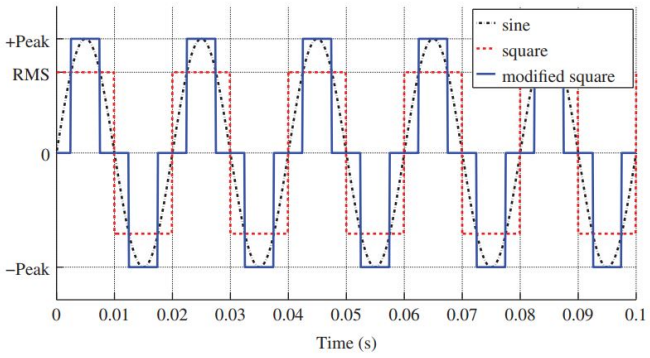

Figure 2.18: *Typical waveforms output of an inverter, [52]*

include a high capacitance to filter double-line frequency ripple if the connection is single phase.

The output current of the cell is given by

$$C_{dc}\frac{dV_{dc}}{dt} = \frac{P_{dc} - P_{grid}}{V_{dc}} \tag{2.30}$$

where C_{dc} is the filter capacitance, V_{dc} and P_{dc} are the voltage and power in the DC part, inputs for the inverter, and P_{grid} is the power at the side of the inverter, delivered to the grid. As it can be seen, the power output is a function of an operational capacitance and the efficiency of the device on the DC/AC conversion. When connected to medium voltage grids, transformers are normally required.

2.3.3 Multi-machine systems considering decoupled units

Figure 2.19 depicts a modern power system considering the presence of WP and PV generators.

In this illustrative example, the equivalent inertia of this system is given by the synchronous machines connected (Equation (2.9)), the only ones contributing to the mean frequency (the frequency at the COI, as defined in Equation (2.31)). For the moment, synthetic inertia is not considered.

$$f_{COI} \triangleq \frac{\sum_{j=1}^{i} S_{n_j} H_j f_j}{\sum_{j=1}^{i} S_{n_j} H_j} \tag{2.31}$$

However, the WP and PV are contributing in power generated to feed the loads. In this way, Equation (2.23) can be restated to include the decoupled machines,

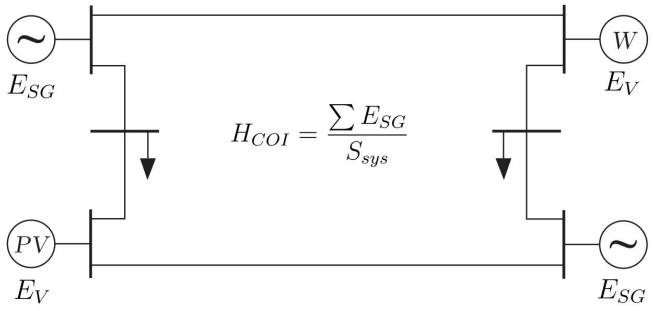

Figure 2.19: *Power system with RES units connected*

$$\frac{2}{f_0} H_{COI} \frac{df_{COI}}{dt} = P_s(t) + P_{dec}(t) - P_L(t) - P_j(t), \qquad p.u. \tag{2.32}$$

where P_s stands for the total power generated by synchronous machines, P_{dec} stands for the total power generated by decoupled machines, P_L is the total active power consumed by the loads and P_j is the total active power losses in the transmission lines, [25].

To illustrate the case, suppose a first situation with n synchronous generators with a total $H_{COI} = 12.5s$, at $f = 50\ Hz$, supply a total load of $10\ p.u.$, damping and losses neglected. If a step increase of $0.1\ p.u.$ occurs in the load, by Equation (2.23), the RoCoF is

$$\frac{df_{COI}}{dt} = \frac{(10 - 10.1) * 50}{2 * 12.5} = 0.2 \frac{Hz}{s}$$

Now suppose a second situation when 20% of the original load ($10\ p.u$) is supplied by an asynchronous generator, and the other 80% is supplied by synchronous generators totalizing $H_{COI} = 10s$. The inertia of the COI has decreased because, due to the connection of the decoupled generation, some synchronous generators were not needed anymore. In this conditions, and considering the same load step, Equation (2.32) gives

$$\frac{df_{COI}}{dt} = \frac{(8 + 2 - 10.1) * 50}{2 * 10} = 0.25 \frac{Hz}{s}$$

As it can be seen, the RoCoF increased form 0.2 Hz/s to 0.25 Hz/s. The drawbacks of higher RoCoF are very important. First, the RoCoF creates higher difference between rotor angles. The higher this difference, the lower the chances of the system to keep synchronism. At second, many protection devices are set to disconnect generation due to frequency thresholds, which may cause power imbalance and consequently blackouts.

The fact that the WP and PV units are not able to provide synchronous inertia to the grid is seen as a drawback by TSOs. However, it is possible to overcome this problem in some cases by controlling the power electronic devices used in the connection, and exploiting "hidden" energy stored in these units to provide the so-called synthetic (or virtual) inertia. Considering PV and WP units, the main sources of energy that can be exploited are the kinetic energy stored in the rotating masses of the blades of the wind turbine and the energy stored in batteries that might be connected to the power units [39], [54]. The synthetic inertia can be used in cases in which the equivalent inertia of the system is recognized as low, with the drawback of slowing down the turbine blades or decreasing the amount of energy stored in the

batteries.

To provide the synthetic inertia, the converters that decouple the generators from the grid can vary the energy exchange in terms of a measured frequency variation in the grid, as represented in the simplified scheme represented in Figure 2.20. In the scheme, the unit equipped provides a kinetic energy of $E_V = \frac{J_V \omega_e^2}{2}$, where J_V is the virtual moment of inertia of the unit. More complex and detailed schemes for virtual inertia provision are proposed in the literature. The interested reader may refer to [40].

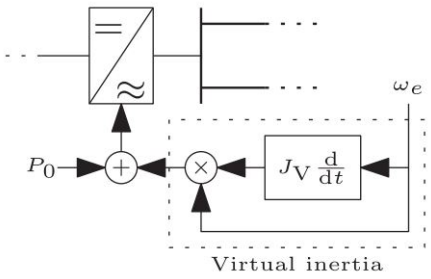

Figure 2.20: *Virtual inertia control, [13]*

Considering the synthetic inertia provision, the system depicted in Figure 2.19 is modified. In Figure 2.21, the units supplying this virtual kinetic energy are identified by E_V, now contributing to the equivalent inertia of the COI.

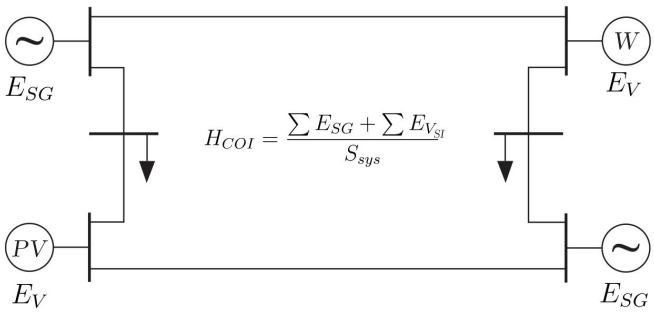

Figure 2.21: *Power system with synthetic inertia provision*

Figure 2.22 illustrates a comparison between the total amount of energy of a power system consisting only of traditional generators (system A), a power system where some of the traditional generators were substituted by decoupled generators that do not provide synthetic inertia (system B) and the same power system with synthetic inertia provision (system C). The horizontal side represent the amount of momentum of inertia of each system, while the vertical side represent the quantity $\frac{\omega_e^2}{2}$, that compose Equation (2.9). The area of each rectangle represents the total amount of stored kinetic energy, and the traced area represents the released kinetic energy after a perturbation, related to the decrease of $\omega_{e,0}$ to $\omega_{e,1}$.

The speed drop according to Equation (2.32) is smaller in the system that has more equivalent inertia. Consequently, referring to Figure 2.22, the system less affected is System A. However, the virtual inertia provided in System C brings an advantage in comparison to System C, as depicted in Figure 2.23.

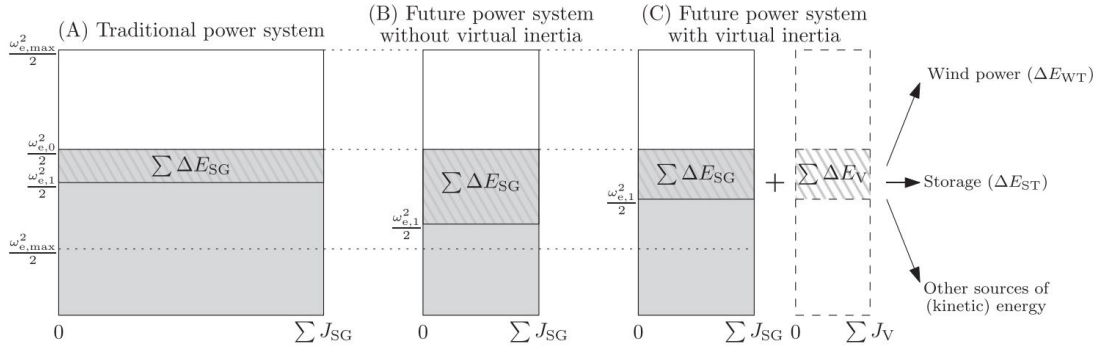

Figure 2.22: *Schematic representation of kinetic energy exchange, [13]*

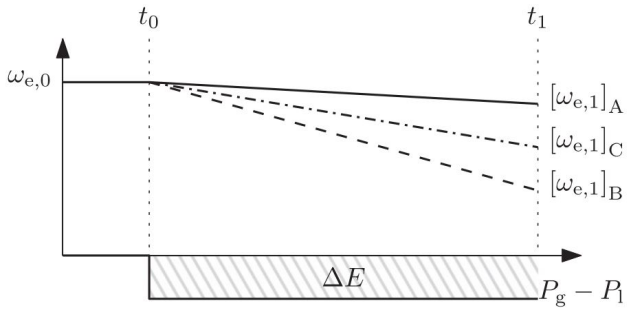

Figure 2.23: *Schematic representation of kinetic energy exchange, [13]*

2.4 Loads in stability studies

In power system stability studies, loads are modelled with a considerable degree of simplification. The amount of different types of loads connected to a single bus of a system is huge, such that their behavior is approximated by static or dynamic equivalent models. While static models express power at any instant of time as function of voltage and frequency at the load bus, the dynamic models consider variations in time through differential equations.

The dynamic model is used to represent rotating loads, through the swing equation. Mainly, dynamic loads are synchronous and induction machines, whose models were previously presented in this Chapter. When the load is connected directly to the system, it presents an inertial behaviour equal to synchronous inertia previously defined. To illustrate the inertial contribution of rotating loads in comparison to the contribution of the generators of a real system, Figure 2.24 presents some of the results of [55], obtained with a practical approach applied to the entire power system of Ireland and Northern Ireland. In the Figure, letters A to F denote the load inertia estimated considering the data recorded of 6 different outages, happening in different dates when the system had different levels of RES penetration and different levels of load connected. In the cases analyzed, the contribution of the inertial behaviour of the loads ranged from 2 to 15% of the total inertia of the system.

The static model, instead, is used for representing resistive and lighting load but also as an approximation of dynamic load components such as motor-driven loads [56]. In this model, the following algebraic equations represent the active (P_L) and reactive (Q_L) power components:

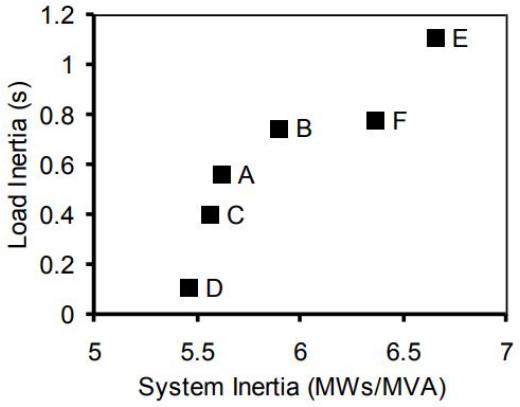

Figure 2.24: *Load inertia with respect to system inertia, [55]*

$$P_L = P_0(\frac{V}{V_0})^a \tag{2.33}$$

$$Q_L = Q_0(\frac{V}{V_0})^b \tag{2.34}$$

where the subscript 0 denotes the initial operating point, and the exponents a and b, equal to 0, 1 or 2 represent the characteristic of the load as constant power, constant current or constant impedance, respectively.

A composite load that comprises all the three characteristics can be represented by the so-called ZIP model, expressed by the following polynomial expressions

$$P_L = P_0[P_1(\frac{V}{V_0})^2 + P_2(\frac{V}{V_0}) + P_3] \tag{2.35}$$

$$Q_L = Q_0[Q_1(\frac{V}{V_0})^2 + Q_2(\frac{V}{V_0}) + Q_3] \tag{2.36}$$

where the subscripts 1, 2 and 3 identify the proportion of the load that presents constant impedance, constant current and constant power behaviours, respectively.

To represent frequency dependence, the ZIP model can be extended to

$$P_L = P_0[P_1(\frac{V}{V_0})^2 + P_2(\frac{V}{V_0}) + P_3](1 + K_{pf}\Delta f)) \tag{2.37}$$

$$Q_L = Q_0[Q_1(\frac{V}{V_0})^2 + Q_2(\frac{V}{V_0}) + Q_3](1 + K_{qf}\Delta f)) \tag{2.38}$$

where K_{pf} and K_{qf} are dependence factors, ranging from 0 to 3 in the case of K_{pf} and ranging from -2 to 2, in the case of K_{qf}, [57]. The quantity Δf is the variation of the frequency at the load bus.

2.5 Frequency control

Given the swing equation, the system faces a frequency variation whenever there is a power mismatch. In a multi-machine system operating at synchronous speed, the frequency response to the perturbation can be divided mainly in three phases, as depicted in Figure 2.25.

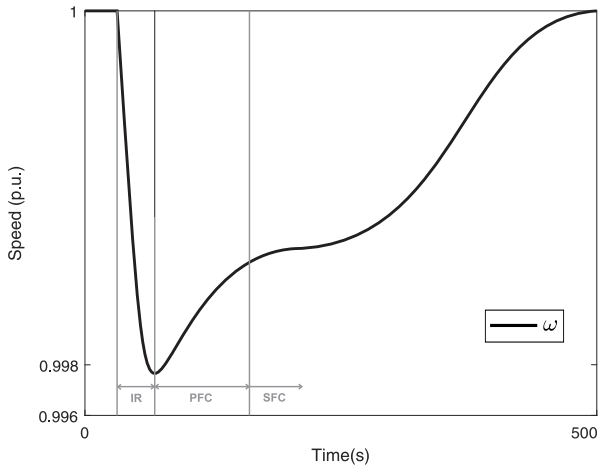

Figure 2.25: *Responses of a system with frequency control*

The first one is the inertial response (IR), as described in the previous Sections. Following the inertial response, the system may stabilize at a new speed or loose synchronism, as seen previously in Figures 2.11(a) and 2.11(b) respectively. Forcing the frequency of a machine back to the initial frequency of the system is done through the phases of Primary Frequency Control (PFC) and Secondary Frequency Control (SFC).

The main player in frequency control is the speed governor, that is part of the turbine system responsible for converting kinetic energy of the wind, water or thermal into mechanical energy, as represented in Figure 2.26.

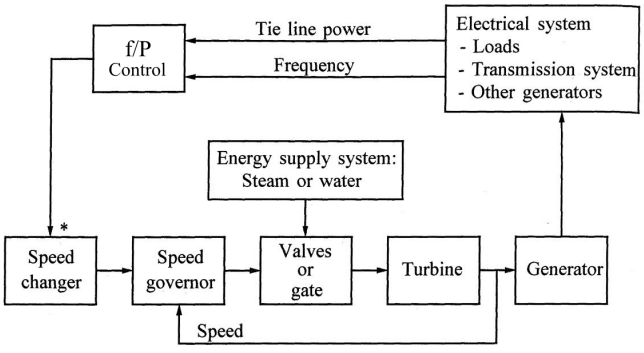

Figure 2.26: *Frequency control system, [42]*

Setting electronically a load reference for the turbine, according to a power-frequency characteristic, the governor is able to control the frequency of the generator. Figure 2.27 depicts the case, with two

different characteristic of a frequency-dependent load represented. First, the generator operating at a frequency f_1 supplies a load P_L^{old} at the operation point 1. After a load change, the system operates at point 2 (with frequency decrease). To force the machine back to $f1$, the system must operate at point 3, setting the power reference according to the x-axis.

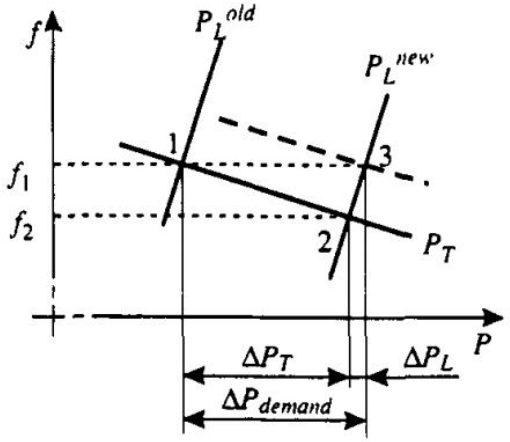

Figure 2.27: *Governor set-point example, [36]*

The equivalent block diagram of a steam turbine governing system, as an example, is represented in Figure 2.28, where R is the droop and T_G is the time constant of the governor. The PFC takes place after a delay of some seconds with reference to the perturbation, due to the time constants of the governors. The main objective is to contain the frequency decrease and to bring it back to stable acceptable values. The control of the setpoints is done exploring local measurements of frequency and power.

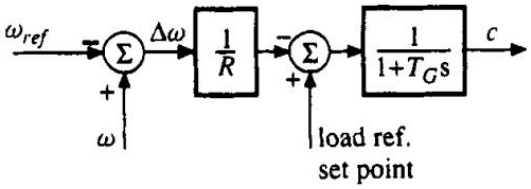

Figure 2.28: *Speed governor block diagram, [36]*

The SFC, instead, takes place after the PFC and aims at correcting set-points to compensate frequency errors that remained after the previous control phase, restoring the nominal frequency of the system. It explores measurements from SCADA and range from seconds to minutes. After SFC, a tertiary frequency control takes place for economic dispatch and generation rescheduling [36].

2.6 Conclusion of the chapter

This chapter presented the theoretical basis that involves the stability of a power system to large perturbations, considering synchronous and decoupled generators connected. Models of the machines were presented, together with descriptions on how they relate to the problems of interest.

CHAPTER 3

PMUs in Power Systems

The so-called Phasor Measurement Units (PMUs) are devices first invented in the 80s for computer based distance relaying, exploiting symmetrical component theory for power systems protection. The original project was motivated by the idea of developing a relay based on digital synchronized measurements able to compete with the analogical devices that were the market leaders in those days [15].

During the last years, PMUs showed advantages in many applications, not only in power system protection but also in monitoring, operation and control. The possibility of visualizing the grid behaviour through real-time measurements enabled communication, estimation and detection of parameters and events that are useful for backing up studies and decisions. With the deployment of PMUs on the grid, a real-time synchronized data acquisition system could be developed, under the name of WAMS.

This chapter aims at presenting the theoretical background involving the use of PMUs in power systems application, mainly focusing at making an introduction of the use of synchorphasors measurements for inertia estimation.

3.1 Phasors and Synchrophasors

The whole theory involved with PMUs is based on synchophasors, an extension of the concept of phasors.

A (static) phasor is a representation of a time invariant sinusoidal signal in terms of its magnitude

and phase angle. Consider the sinusoidal signal

$$\begin{cases} x(t) = Xcos(\theta(t)) \\ \theta(t) = \omega_s t + \phi \end{cases} \tag{3.1}$$

The phasor representation of (3.1) is

$$\mathbf{X} = \frac{X}{\sqrt{2}} e^{j\phi} = \frac{X}{\sqrt{2}} \angle \phi \tag{3.2}$$

and it is valid only for the single frequency ω_s component. Figure 3.1 depicts the signal and its phasor representation.

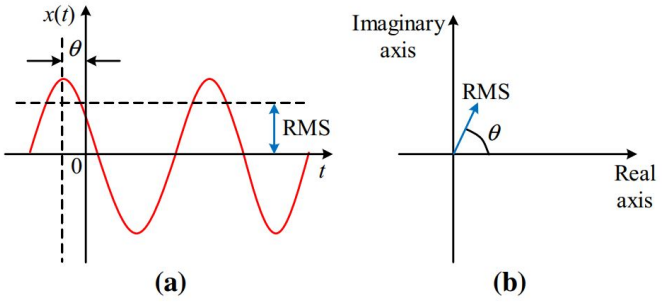

Figure 3.1: *A sinusoid and its representation as a phasor, [15]*

In electrical engineering, phasors are widely used for steady-state studies, since a common frequency allows linear combinations of the phasors involved, in the so-called phasor arithmetic. In RLC circuits, phasors also enable modelling the system with algebraic instead of differential equations, simplifying studies and calculations.

The concept can be extended to time-varying phasors, assuming that the signal under study is nearly sinusoidal and its amplitude and phase vary slowly over time. In power systems, the assumption is often valid as the system is stably operated around a nominal frequency of 50Hz or 60Hz.

Modelling the sinusoid as

$$\begin{cases} v(t) = V(t)cos(\omega_s t + \phi(t)) \end{cases} \tag{3.3}$$

where ω_s is the reference frequency and $\omega_s t$ is the reference phase, it is possible to represent it as the following phasor

$$\mathbf{X(t)} = \frac{X(t)}{\sqrt{2}} \angle \phi(t) \tag{3.4}$$

As an example, Figure 3.2 depicts the case where the signal is sinusoidal but nearly constant over a single 50Hz cycle. In fact, at t_1 and t_2, the signal present the same phase and the same magnitude, where (3.4) is a good representation for many applications. After t_2, sampling the signal at $T = \frac{2\pi}{\omega_s}$ (range of some ms), it is possible to evaluate a phasor representation at each time period.

In this way, as long as the signal does not suffer from a major change between each time interval, each phasor representation is a good approximation to the portion of the signal related. Due to this reason, it is possible to use dynamic phasors to study the system not only in steady state, but also under slow electromechanical transients (that last from ms to s, as seen in Section 2.1). This representation is

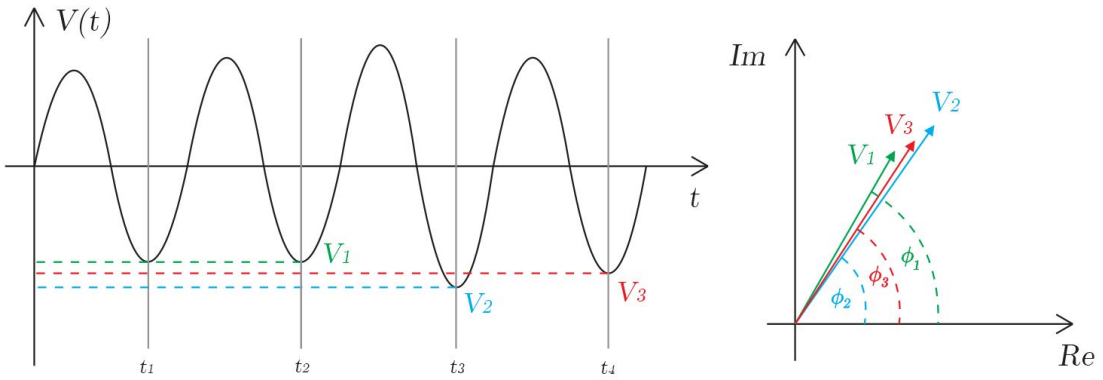

Figure 3.2: *Composing phasors*

not suitable for electromagnetic transients, as they last less than ms.

The most critical point in the use of time-varying phasor representation in power systems is the common frequency ω_s, as already said, but also a time reference for the measured phase angles is important. To evaluate the phase angle difference between the voltages at two buses in a phasor diagram, a reliable common reference is needed. The key contribution that PMUs brought is that they are able to address both points. First, PMUs are able to perform real-time phasor estimation, obtaining a fundamental frequency and a related phasor representation with high sampling rates. At second, they are able to synchronize each sampling process for different signals in different units through Global Positioning System (GPS) clocks, that provide a timing-reference stamp. With the stamp, every single phasor can be compared according to the same reference. The technology enabled to extend the concept of phasors to the concept of synchrophasors, with use in real-time applications [58].

3.2 Phasor Measurement Unit

A PMU is defined as a microprocessor based device that must be capable of providing synchrophasors, frequency and RoCoF estimations from voltage and current signals measured at 50Hz [59] typically at 48 samples per cycle (or 1 sample at every 0.4ms). Nowadays, modern units may reach up to 128 samples per cycle, i.e., 1 sample at every 0.16ms [60].

A general measurement scheme is depicted in Figure 3.3. First, current and voltage signals are measured from the phase conductor through Current and Voltage Transformers. Subsequently, the signals are processed through analog and digital filters and sampled, according to the Nyquist criterion. At the PMU, another processing step treats the input wave signal over a time window to track its fundamental frequency. After the fundamental frequency is tracked, the phasor calculation is performed (DFT or DFT-based techniques are the most common procedures adopted), and time-stamped at every 20ms (usually).

The fundamental frequency tracking is done through different ways, depending on the manufacturer, and respecting the standards defined in [59]. The most used techniques are the Complex Valued Least Squares (CLS), the Prony method, the Polynomial Fitting and the Phase-Locked Loop (PLL), [58]. This enables the detection of off-nominal frequency values over a range of ± 5 Hz, and in this case, a magnitude and angle correction is considered to account for the frequency deviation.

Once the fundamental frequency is determined, the PMU is able to provide the frequency measure-

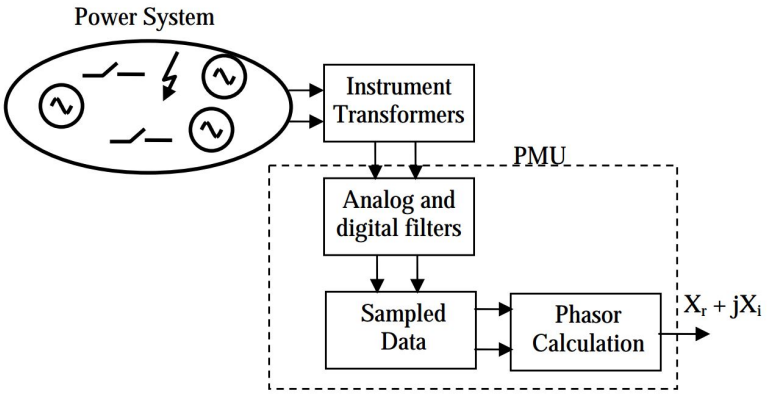

Figure 3.3: *PMU measurement chain, [60]*

ments, according to the following definition [59]. Considering the signal modelled in Equation (3.1), the frequency is defined as

$$f(t) = f_0 + \frac{1}{2\pi}\frac{d\theta(t)}{dt} = f_0 + \Delta f(t) \tag{3.5}$$

where $\Delta f(t)$ is the deviation of frequency from nominal.

The RoCoF is defined as

$$ROCOF(t) = \frac{d\Delta f(t)}{dt} \tag{3.6}$$

where all the quantities were previously defined. However, this definition may lead to noisy estimations. Better approaches are under development, and for the moment a polynomial fit is often suggested in literature [15].

The time-referencing for Synchrophasors is done exploiting the pulse-per-second emitted by GPS. The pulse is able to reach any receiver unit in Earth within $1\mu s$, with leap-second correction, to provide coordinated universal time, with reference to the Second-of-Century (SOC) counter.

A typical block diagram for a PMU representing the signal processing, the frequency tracking, the time stamping and the phasor estimation is depicted in Figure 3.4. At the end, output phasors, frequency and ROCOF measurements are sent to Data Concentrators through a modem.

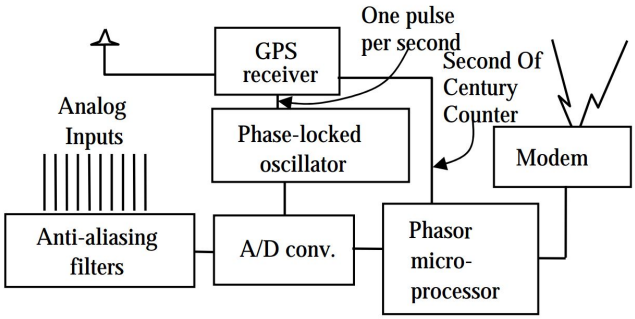

Figure 3.4: *PMU block diagram, [60]*

Regarding the types of transient phenomena described in Section 2.1, the response of a PMU depends

on the frequency components of the measured signal. The electromagnetic transients normally disappear within a short time, and the effect of high-frequency components (10^3 to 10^6 Hz) are strongly attenuated by the filters of the PMU. The exceptions are harmonics and some network resonances, with frequency components ranging less than 10^3 Hz [60]. Electromechanical transients are also slower than the 10^3 Hz and consequently fully observable. The signal seen at a busbar in a multi-machine system is then a superposition of the response of the many generators connected, with different frequency and magnitudes contributions. Besides of more complexity, the output signal can essentially be seen as an amplitude and phase modulation of the center frequency.

As long as the power system is operating close to nominal frequency (within ± 5 Hz range, [59]), the PMU will estimate the synchrophasors continuously at every new sample obtained. As long as the modulation frequencies are low, the estimated phasors will follow also the amplitude modulation. Regarding unbalanced inputs, a PMU is able to report positive sequence phasors under the same standards.

3.3 WAMS and SCADA

After the measurement acquisition and data processing, the PMUs, that are installed at power system substations, send the stamped data packages to Phasor Data Concentrator (PDC)s installed at remote locations following communication protocols defined in [61]. The main functions of the PDCs are gathering the packages, rejecting bad data, aligning the time-stamps and organize the temporary storage of the recorded data. On a wide system, a hierarchical structure of PDCs is used, constituting a WAMS able to monitor power system dynamics in real time and provide information to the system operators, for situational awareness, protection and control.

The PDCs are also able to communicate with the data centers of the so-called SCADA, an earlier monitoring system. The SCADA comprises common industrial instrumentations, sensors and measurement devices for data acquisition, that is transmitted through a communication system and processed by a dedicated unit. The SCADA have been used for monitoring general plants and equipments in different areas of applications, such as energy, oil, gas, etc [62]. Figure 3.5 depicts a general SCADA system.

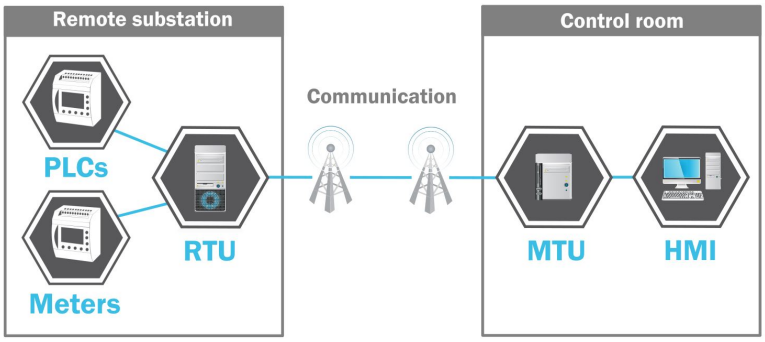

Figure 3.5: *SCADA general scheme*

Considering the application of SCADA in a Power System, first the data acquisition is performed by voltmeters, ammeters, power consumption meters and other analogical or digital sensors installed in the field to acquire data. At the substations, Programmable Logic Controllers (PLCs) that are able to perform logic functions to control switches, relays and timers, are also integrated. All theses devices

communicate with a Remote Terminal Unit (RTU), a microprocessor based unit in charge of collecting and transmitting data from the substation to the Master Terminal Unit (MTU), installed in a control room. The data is processed and then sent to the Human-Machine Interface (HMI), that provides data visualization of voltages, currents and power magnitudes, and also breaker switching status.

As the SCADA was a system developed to integrate the many measurement devices already in use, it has a limited resolution of data acquisition, of 1 sample every 2 to 4 seconds, which restricts its use for monitoring steady states only. Moreover, SCADA system is not able to do time stamping itself, which prevents phase angle acquisition, limiting the acquisitions to magnitude of the signals only. Figure 3.6 presents a comparison on voltage magnitudes acquired following a disturbance.

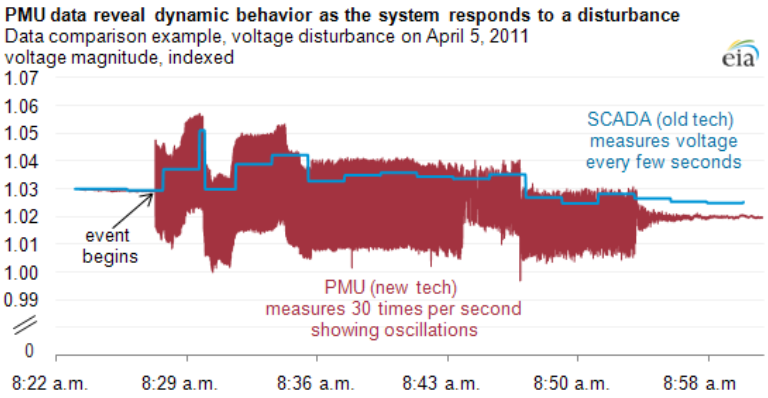

Figure 3.6: *Data comparison PMU vs SCADA, [63]*

However, besides the resolution and practical advantages of PMUs, the SCADA systems are a technology more spread, since it has been developed and deployed first. Consequently, data provided by SCADA systems are still useful to improve observability and monitoring in different applications, and one can make use of such data together with PMU data available. A general representation of a WAMS integrating both PMUs and SCADA is represented in Figure 3.7.

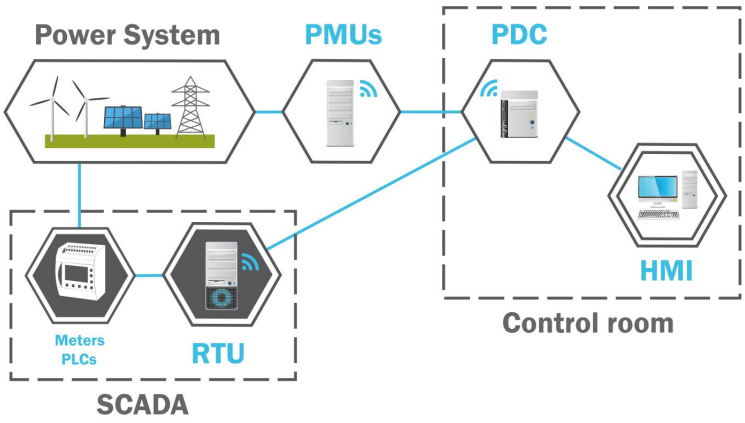

Figure 3.7: *PMU and SCADA integration*

A Summary of the differences between SCADA and PMU can be seen in Table 3.1, [60], [62].

Attribute	SCADA	PMU
Resolution	2-4 samples per cycle	Up to 128 samples per cycle
Measure	Voltage and power magnitudes	Voltage and current phasors, frequency and ROCOF

Table 3.1: *Comparisons between PMU and SCADA*

3.4 Applications of PMUs

Main applications of PMUs in power systems can be categorized as: system monitoring, state estimation, system protection and system control.

3.4.1 Monitoring

The advantage of providing voltage and current phasors, as well as frequency and ROCOF measurements in real-time enabled operators to monitor different aspects of the behaviour of the grid.

The phase angle and frequency monitoring in real time is an important tool for the operator to detect and study oscillations, perturbations, unbalance or stress indicators on the system, supporting counteracting decisions or investigating the reactions of automatic controls.

Some specific applications of monitoring are: phase angle difference assessment, detection and evaluation of disturbances and oscillations, voltage stability monitoring, thermal rating monitoring and islanding detection. As the topic of this thesis is related to rotor angle stability, the applications directly related to phase angles will be detailed below. The interested reader may refer to [60], [64] for the other ones.

3.4.1.1 Phase angle difference assessment

One application regarding direct phase angle monitoring is the assessment of the angle difference between voltages at different buses as an indicator of the stress of a system. Increasing voltage angle differences is a signal of increasing stress, as power flows are function of angle differences. As an example, Figure 3.8 presents the graphic interface of a software [65] indicating the stress between two voltage buses, indicated in red.

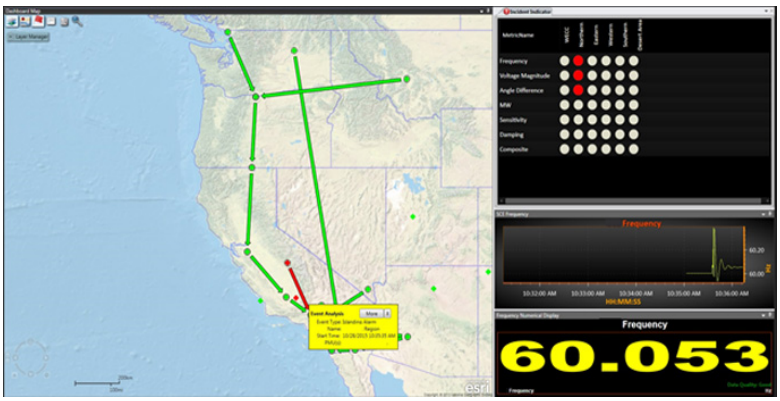

Figure 3.8: *RTDMS software - phase angle difference monitoring, [65]*

By monitoring phase angle differences, the operator may diagnose line, load or generation tripping, and counteracting actions including load shed, generation redispatch or provision of voltage support.

3.4.1.2 Detection and evaluation of oscillations

Another application, based on frequency monitoring, is the detection and evaluation of oscillations occurring with the interaction of the different machines connected to a power system. Processing the acquired data, it is possible to assess the modes of oscillation, classifying them according to their frequency range and according and evaluating the participation of each state variable. Figure 3.9 depicts the mode assessment of a measured signal.

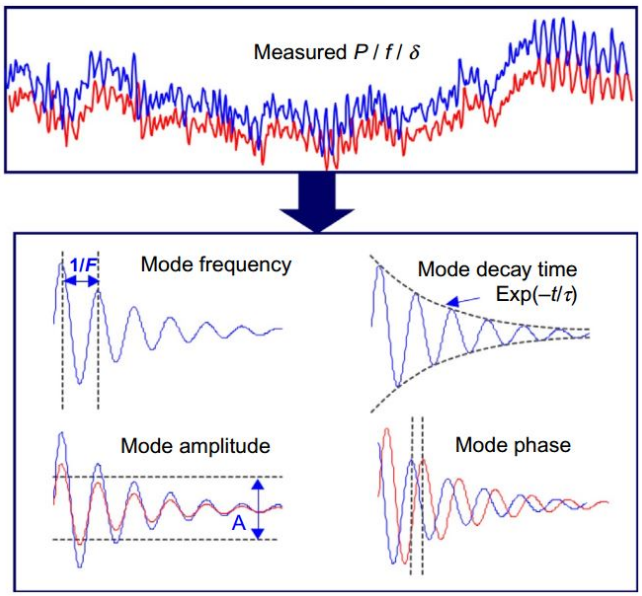

Figure 3.9: *Evaluation of oscillation modes, [64]*

With these types of diagnosis, the operator can extract stability parameters and tune controllers to damp the most critical modes. The consequences of oscillations range from stressing components, damaging plants, tripping protections, degrading power quality to even evolving to large frequency excursions, system separation and blackouts.

Traditionally, the type of oscillation mode that cause most concern are the electromechanical, ranging from 0.1 to 4 Hz, and normally affecting a wide area of the interconnected system. These modes can be further divided in local modes (1 to 4 Hz) and interarea (0.1 to 1 Hz). Here again, the decrease of inertia is also a reported problem [64], affecting the frequency characteristics and consequently the damping of these oscillation modes. Hence, the monitoring of oscillation modes in a system with high-penetration of RES shows its importance. Figure 3.10 presents an example of measured data presenting oscillations in a real grid.

3.4.1.3 Detection and evaluation of disturbances

Data recording enables post-event analysis disturbance detection, estimation of the time of disturbance, estimation of the magnitude of disturbance, dynamic modelling estimation and parameter calibration

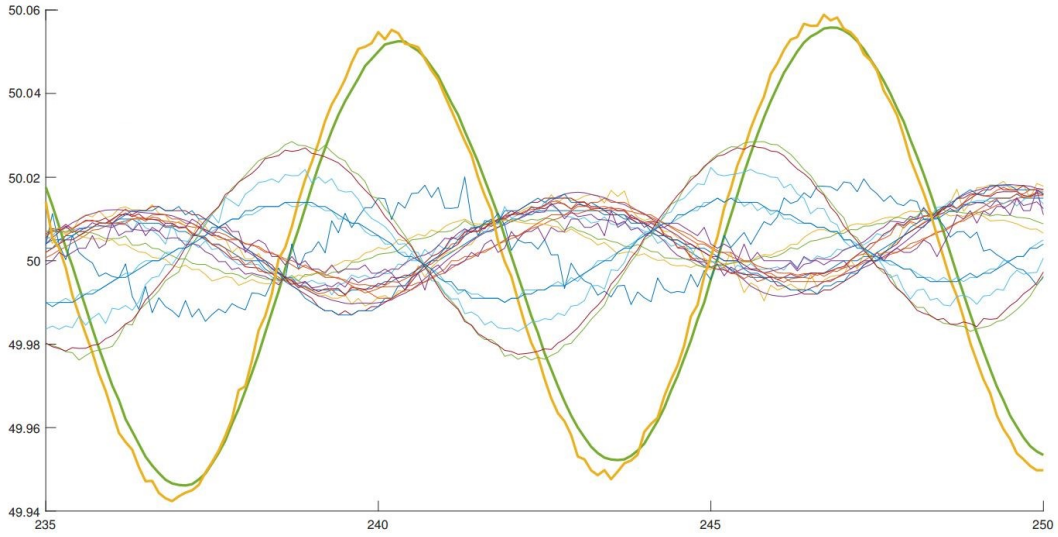

Figure 3.10: *Real oscillation event recorded, [66]*

(such as the inertia estimation, the topic of this thesis).

As an example, Figures 3.11 and 3.12 present power and frequency measured in a real event recorded in Italy in 2017 [67]. From Figure 3.11, it is easy to tell that a power generation loss has happened. Comparing with the recorded data at other points of the grid, it is possible also to identify the location where the disturbance happened, according to the impact seen in the measured quantities. This type of application is important to support system inspection, maintenance and repair.

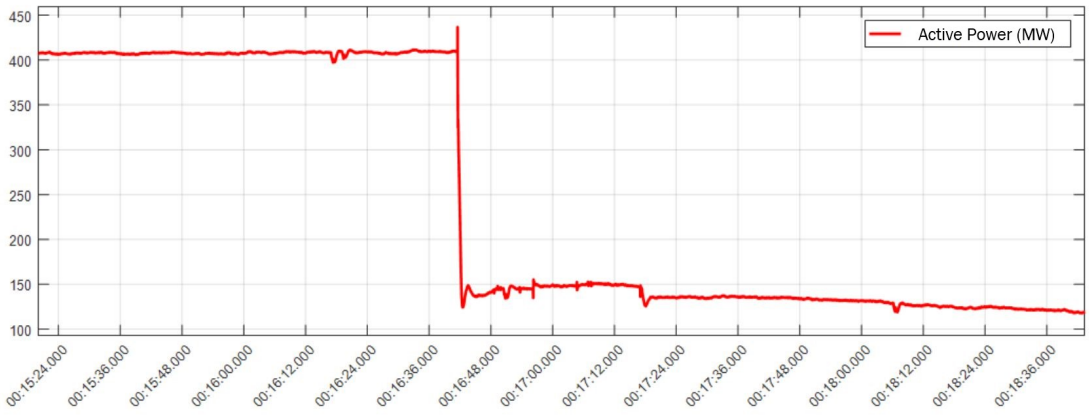

Figure 3.11: *Active power recorded, [67]*

From Figure 3.12 it is possible to study the RoCoF and to estimate equivalent inertias. Moreover, it is possible to evaluate the performance of the processes of frequency control and emergency control. Comparing frequency data acquired in many different points, it is possible also to identify coherent groups and study the dynamic behaviour of the system based on that model identification.

If a disturbance results in a system separation, each island formed will present a decoupled com-

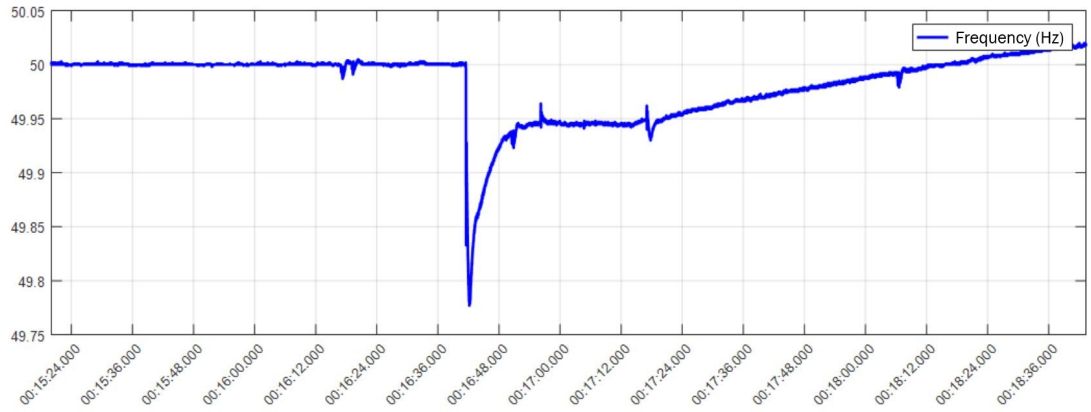

Figure 3.12: *Frequency recorded, [67]*

mon frequency, and voltage angles will rotate relative to other islands. These phenomena can be observed in PMUs interface. The application is not helpful only for detection but also for monitoring re-synchronization procedures. Before PMUs, islanding applications were based on topology (breaker status) estimation, without the possibility of observing out-of-step response of the generators.

3.4.2 State estimation

The process of state estimation consists in assigning a value to an unknown state variable based on redundant measurements obtained, treated according to a decided criteria. It has been widely used in power systems operation since its development to infer all the bus voltages (magnitudes and angles) and power injections of a system, from measurements obtained at specific points at the grid. Monitoring system states provides security assessment to system operators, bringing support to take possible security countermeasures or optimization decisions.

The first contribution that PMUs brought to state estimation regards higher accuracy and reliability on the measurements acquired. However, the contributions are much more than that. In state estimation, a first key point regards the observability of the system: a concept that defines how well the states of a system can be inferred from the measurements available. To improve observability, it is important to monitor as many states as possible, and PMUs brought the possibility of acquiring data of some state variables that were not directly measurable before (as voltage angles, for example). A second key point relies on the fact that increasing measurements redundancy allows to increase also the accuracy of the states estimated, since it enables the possibility of better detecting and processing bad data.

To illustrate, a conventional SCADA-based state estimation with bad-data processing is performed on a 30-bus test system [60], with results presented in Figure 3.13(a). Considering the integration of PMUs and SCADA, the results can be seen in Figure 3.13(b), with remarkable improvements.

Another major contribution is that before the deployment of PMUs, only static state estimation was possible. Due to the reasons described above, PMUs already contributed to that. But in addition, PMUs brought the possibility of not only monitoring voltages and currents over time during non-steady conditions, but also performing dynamic state estimation to track states such as rotor speeds and rotor angle positions. As already mentioned, PMUs enabled not only monitoring bus voltage and current angles, but also high sampling rates and precise time-synchronization, essential in dynamic state estimation.

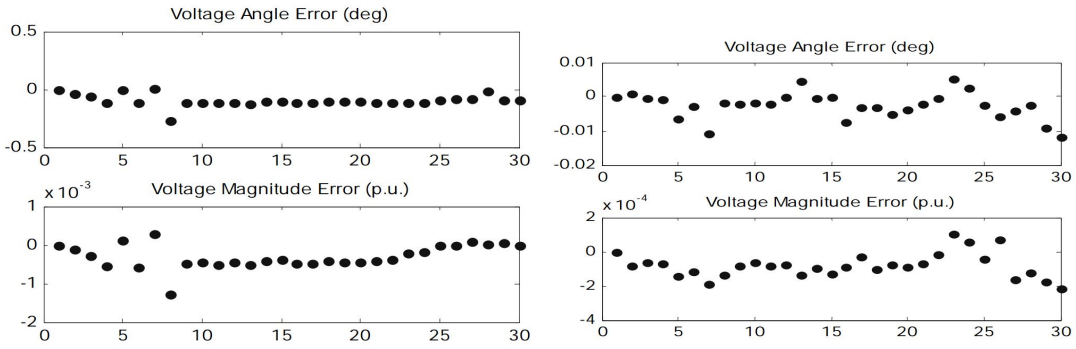

(a) SCADA-based SE

(b) PMU-based SE

Figure 3.13: *State Estimation (SE) - SCADA Vs. PMU, [60]*

3.4.3 System protection and control

PMUs have been developed for improving the performance of protection functions of slow time response, such as distance relays. However the impact in system protection is much wider, enabling the application of new functions based on phasors comparison, the coordination of protection devices trough communication of synchronized measurements and the development of adaptive schemes, where the devices involved react and adjust automatically to new conditions detected in the acquired data.

One example of new function enabled is the differential protection. In this type of application, voltages and current synchrophasors are used to evaluate the difference between the currents flowing in both ends of a monitored segment of transmission line, that can be used to detect the occurrence of faults. Another type of new function is the System Integrity Protection Scheme (SIPS), proposed in [15], [68]. The function is designed to detect and manage possible congestions in the monitored area, avoiding islanding and load shedding.

The adaptive protection schemes where developed as a solution to the cases where common protection schemes experienced in false trips and cascading events in conditions of normal operation, but with stressed system. Using real-time synchronized measurements, it is possible to relax some limits and conditions of detections in specific determined cases, adding an adaptive characteristic for the protection scheme. A first example is the adaptive out-of step protection, for detecting generators going out-of-step and interpret when the situation could evolve to instability, providing the corresponding countermeasure. Another example is the adaptive protection of transformers, used to adapt the protection according to off-nominal turn ratios in tap changes. Also important is the adaptive system restoration function, adapting the protection rules to back-up the re-energization of a blacked out system.

In control applications prior to the development of PMUs, the counteracting procedures were taken based on local measurements or by mathematical model of equivalent systems. The advent of PMUs made many control actions less model dependant, as many state variables are now observable remotely. Moreover, nonlinear optimal control became a feasible solution, since synchrophasor measurements can be used in comparison to the outputs of state models. Mainly, PMU-based control schemes are used for damping oscillations and assisting protection functions.

3.5 A focus on the research of PMUs

Through all the applications described in the previous section, PMUs have been extensively researched in academy since its invention. Figure 3.14 gives an idea on the crescent publication curve in IEEE journals about the topic, from 1983 to 2014.

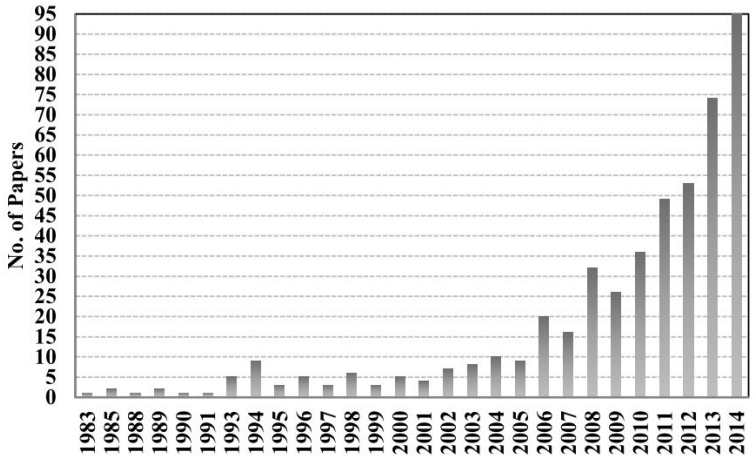

Figure 3.14: *Number of publications about PMUs in IEEE journals, [69]*

The first works approached software and hardware issues, addressing algorithms for tracking frequency and estimating phasors, [70]–[72], a topic that still receives contributions year by year [58], [73], [74]. With time, much attention has been devoted to defining standards, that evolved since 1994 [75] to 2011 [59], [61], the last published ones.

Through applications, grid monitoring and related aspects have been receiving wide attention. In [76], [77], the perspectives of grid monitoring with PMUs are discussed. Dividing in categories, many works have been published in event detection and location [19], [78]–[80], evaluation of oscillations [16], [81], [82], model validation and calibration [21], [22], [83], [84], and stability assessment [85]–[87].

At the same time, PMUs have been incorporated in State Estimation studies, as presented in Subsection 3.4.2. One type of studies involves the cooperation between PMUs and SCADA, [88]–[91]. Another type of studies concerns observability [92] and optimal placement of PMUs for state estimation, [93]–[95]. The optimal placement of PMUs for other type of applications has also been extensively addressed in the literature, [96]–[99].

In system protection applications, the original purpose for what PMUs have been developed, new special protection schemes have been developed, together with new algorithms, counteracting schemes and adaptive schemes, [100]–[104].

Regarding control applications, many approaches have been proposed to use PMU data for supporting preventive and corrective actions for guaranteeing stability [105]–[107]. Moreover, the field also has studies on designing control systems for improving the performance of operational devices, such as Power System Stabilizer (PSS), Automatic Voltage Regulators (AVR), High-Voltage DC (HVDC) transmission lines, etc [108]–[111].

Also a lot of effort is dedicated on developing low cost PMUs and open-source solutions of software and hardware [112]–[114], since commercial PMUs are still very expensive, reported as costing $40000

to $180000 in 2014, [30] and costing $15000 the device for distribution grids [115].

Besides conferences and journals, many theoretical and application books have been published totally dedicated [60], [64], [116], [117] or partially dedicated [17], [118], [119] to PMUs. Considering other types of media, two websites [120], [121] fully dedicated to PMUs are sustained to collect publications, softwares, disclose and organize related events. An educational simulator package for MATLAB-SIMULINK has been developed strictly for teaching about frequency measurement and phasor estimation [122].

3.6 PMUs around the world

Since the development of the technology, the increasing advantages of having PMUs installed on the grid spread their deployment all over the world.

USA, where the first prototype was developed, is still one of the countries most investing on PMUs. One of the catalysts that helped the technology to spread was ironically the blackout in the Northeast of the country, in 2003. Recorded data by existing PMUs at that time were useful to analyze the event and seemed promising to improve the reliability of the system operation for the future. Since that moment, more than 500 units have been installed in the grid until 2012, as depicted in Figure 3.15, and this number increased to more than 1500 in 2018, as reported in [15].

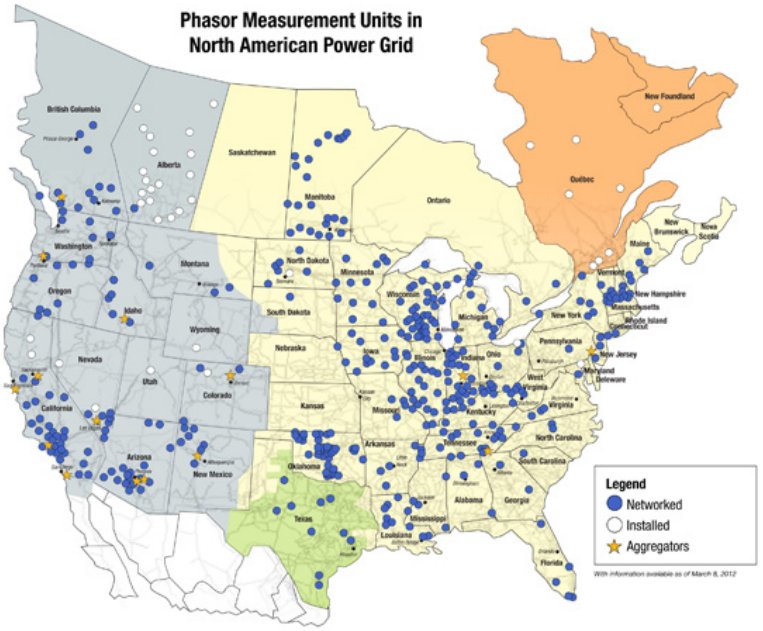

Figure 3.15: *PMUs in USA, [63]*

In Mexico the technology arrived right after its development in US. Nowadays 300 units installed in the country are reported, mostly used for oscillation analysis according to [15]. In 2005, WAMS supported the synchronization of four different electric systems to the Mexican grid, assisting the control.

In South America, the arrival of PMUs was done primarily through the MedFasee project, an initiative lead by the Federal University of Santa Catarina (UFSC), Brazil, in 2003 [123]. The project consisted in developing and installing PMUs in universities around the continent to monitor events in low voltage

grids, and soon expanded to more than 20 other participating universities in the country. As one of the outputs of the project, a real-time representation of the estimated phasors of the interconnected system can be visualized on [124]. Later on, the project was expanded to 12 other locations in Chile and Argentina [125], and recently to Portugal [126]. Figure 3.16 presents a screenshot of phasors captured at the Brazilian units that are part of the project. Recently, the Brazilian TSO made an agreement for the deployment of 45 PMUs in the transmission system, [127], with expected installation lasting until 2022.

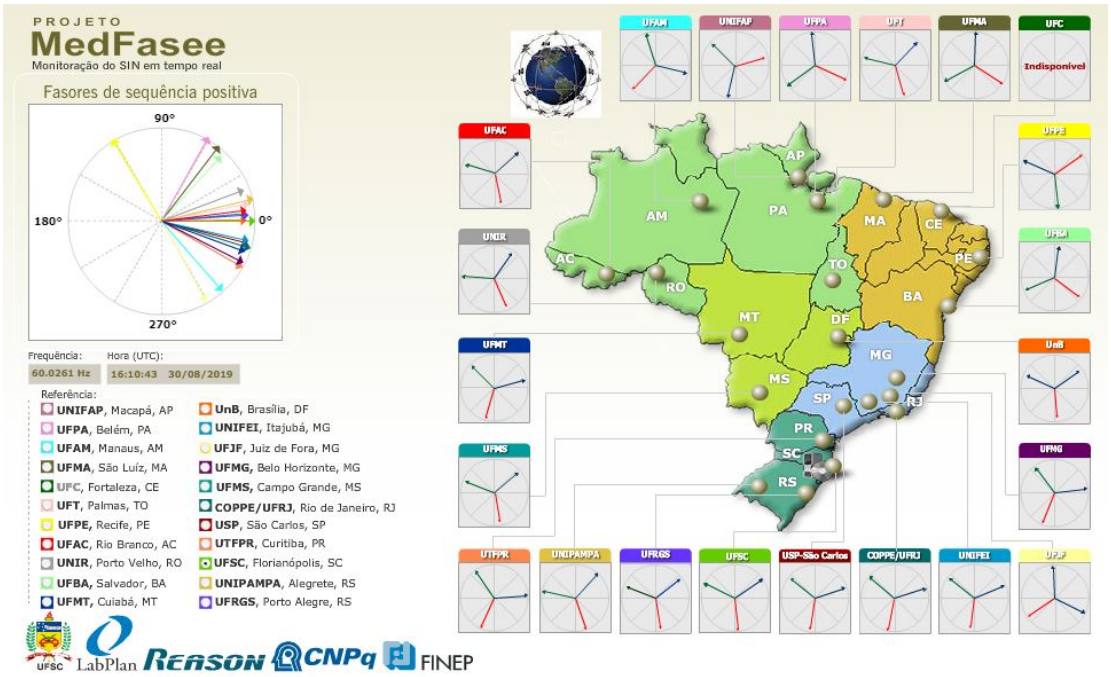

Figure 3.16: *MedFasee project, Brazil, [124]*

In Europe, PMUs are installed at universities as well, such as in Denmark and Sweden [15], and in England, where some of the works cited in this thesis were done [19], [80], [128]. Regarding transmission systems, many PMUs were installed in the continent, as depicted in Figure 3.17.

Specifically in Italy, the deployment started in 2004 and in 2015 the country reportedly counted with more than 60 units spread in the grid, with data exchange with three other countries, [130]. In 2019, the number of installed units have increased to more than 100.

In Asia, China, Japan and India are the highlights. China is probably the leading country in the world in numbers of PMUs installed, with more than 3000 units already commissioned. Reportedly all of their 500 kV and above substations, and the most important 220 kV substations are individually monitored, and so are all 100 MW and above power plants. In India, each region counts with an average between four and five units, and there are plans to install more than 4500 units in the upcoming years [15]. In Japan, a university-based project already installed 12 units around the country [131].

Regarding Oceania and Africa, not much information is accessible. Australia already has PMUs installed according to [132], but the number is unknown. Regarding New Zealand, 10 PMUs were installed during a local program in 2011, [133]. Kenya reportedly had 6 units installed in 2012 [134], while South Africa developed studies using 3 installed units in 2009, [135]. No further register was found.

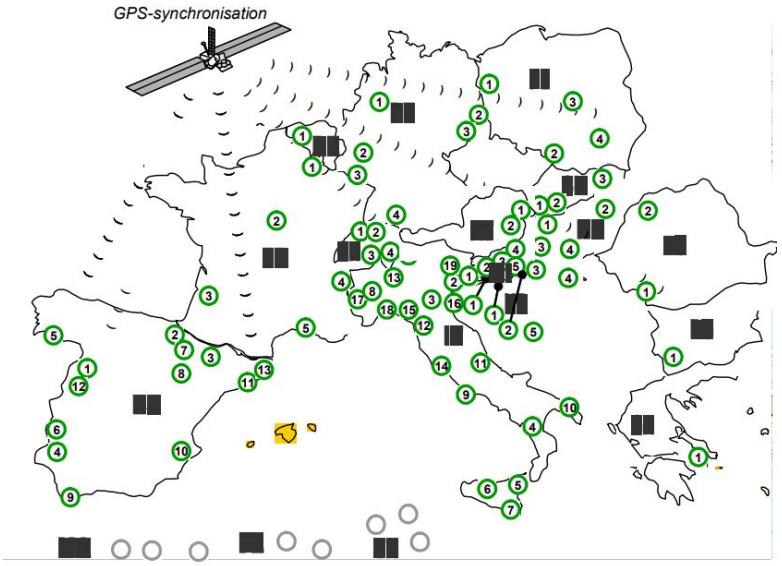

Figure 3.17: *PMUs in Europe, 2010, [129]*

3.7 Conclusion of the chapter

This Chapter presented an overview of the usage of PMUs in power systems. Also, a bibliographical review was presented to give an idea of the study of synchophasors in academy, and a panorama of the units installed worldwide was given.

CHAPTER 4

Determination of Power Systems Inertia

As seen in Chapter 2, the constant of inertia is related to rotating masses. Starting from the motion equations, one can describe the dynamic behavior of one or more machines, regarding power imbalances. The advent of the PMUs enabled monitoring of dynamic phasors in time, such that dynamic modelling and parameter estimation in real-time became possible and realistic.

This chapter presents the methodology adopted in this thesis to investigate the many possibilities of estimating inertia based on synchrophasor measurements. To approach the general and specific questions proposed in Section 1.2, the adopted methodology approached the problem in topics, as depicted in Figure 4.1. There, part of a grid is represented together with an illustrative example of the delimitation of each one of the topics approached.

Referring to Figure 4.1, the details of each topic are described below:

- Bibliographical review to identify the main methods for inertia estimation;
- Topic 1: Inertia estimation considering a PMU installed in the terminals of the generator:
  In this topic, different inertia estimation methods were proposed and tested with simulated data.
- Topic 2: Inertia estimation considering a PMU installed at the boundary of an area.
  Due to the complexity of this topic, it was divided into smaller subtopics to approach progressively all the aspects related to the elements that are inside the area monitored and that can interfere in the inertia estimations. The subtopics consist in estimating inertia considering:
  - 2.1: Area containing single generator, transformer and transmission lines; Perturbation outside;

  - 2.2: Area containing coherent and non-coherent generators, transformers and transmission lines; Perturbation outside;
  - 2.3: Area containing loads, coherent and non-coherent generators, transformers and transmission lines; Perturbation outside;
  - 2.4: Area containing loads, coherent and non-coherent generators, transformers and transmission lines; Perturbation inside;

- Topic 3: Inertia estimation considering spread PMUs:
  - 3.1: At the boundaries of an area (more than one boundary for each area);
  - 3.2: At the boundaries and inside the considered area;

- Topic 4: Inertia estimation following normal load variations in normal operating conditions. This topic involved two different approaches:
  - 4.1: Estimation using model estimation methods;
  - 4.2: Estimation using a state-space statistically-based identification method;

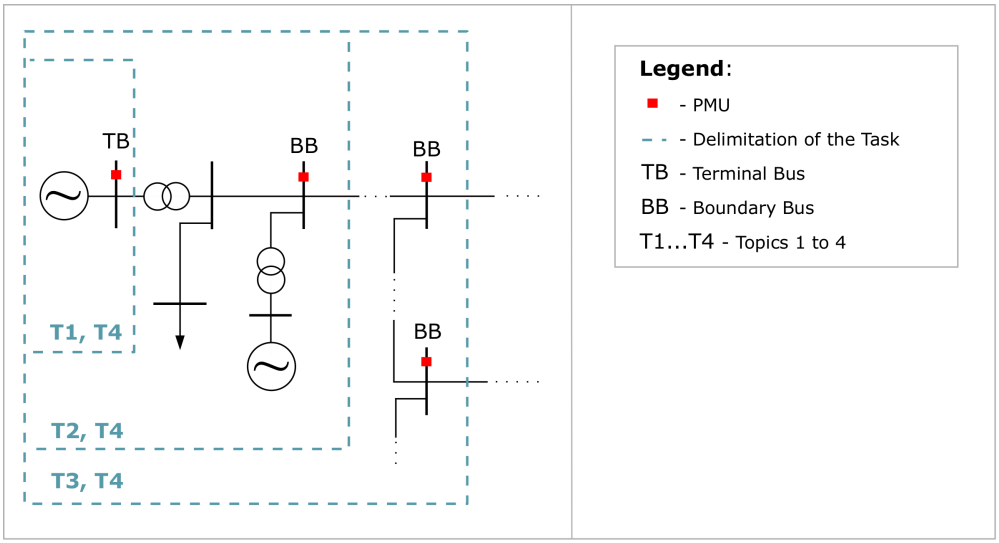

Figure 4.1: *Methodology infographic*

The organization of the remaining of this Chapter is divided according to the Topics list:

Section 4.1 presents a general bibliographical review, describing the state of the art of inertia estimation methods with PMUs.

Section 4.2 explain the estimation methods studied in this thesis, divided into:

- Subsection 4.2.1, presenting the Direct Least-Squares Method, used mainly in Topic 1;
- Subsection 4.2.2, presenting two Model Estimation Methods, with direct or auxiliary use in all Topics;
- Subsection 4.2.3, presenting the Extended Kalman Filter method, used in this thesis in Topics 1 and 2 for comparison;

- Subsection 4.2.4, presenting the auxiliary Ward Equivalent Method to perform inertia estimation with model reduction, useful in Topics 3 and 4;
- Subsection 4.2.5, presenting an auxiliary method to estimate the equivalent moving power of an area, useful mainly in Topics 2.4, 2.5, 3 and 4.1;
- Subsection 4.2.6, presenting an inertia estimation method for ambient conditions, used in Topic 4.2.

Section 4.3 brings a summary of the presented methods, comparing the requirements, assumptions, inputs and outputs.

Section 4.4 brings the final comments of the chapter.

4.1 General Bibliographical Review

As presented in Section 2.2.2, the inertia constant of a synchronous machine can be calculated from its definition, according to Equation (2.8). By knowing the geometry and the construction parameters, the constant of inertia of each machine is trivial. Then, if the TSO knew each synchronous unit connected to the grid, together with its manufacturer data, equivalent inertias could be calculated through (2.23), at least for generating machines. However, normally construction parameters are not known.

Since the unbundling of power systems, generation is open to competition of different companies. This makes it difficult for the TSO to have online information about every connected unit to the grid. Together with the inertia of rotating loads, they form a "hidden inertia" that TSO's cannot easily observe [31], [136]. Considering also the contribution of the upcoming synthetic inertia, the idea of estimating an equivalent inertia by the construction parameters of the connected synchronous units is an approximation that does not seem reasonable anymore. Hence, the necessity of finding other solutions arose, and with the advent of PMUs, the possibility of using synchrophasor measurements to estimate inertia in power systems looks promising.

Many studies regarding inertia estimation have been developed over the past few years. Roughly, they can be divided in large-perturbation, small-perturbation and ambient conditions approaches; besides, some of the techniques can be adapted to one or another purpose. On the field of large-perturbations, methods based on post-event analysis are proposed to estimate the inertia constant of one or more machines regarding the studied transient. Regarding the small-perturbations, normally inter-area oscillations are used for identifying the inertia of the contributing machines and of coherent areas. And under-ambient conditions, normal load variations are studied based on statistical and historical data to identify patterns and parameters.

A particular type of approach explored in the literature are the Kalman Filter (KF) based techniques. The KF is a prediction-correction type estimator that applies measurements observed to a model and simulates the response, calibrating the outputs over time. These methods have applications for parameter estimation considering perturbations or ambient conditions.

Large perturbation approaches

A method that proposes a selected window to analyze intervals of power and frequency measurements to estimate the inertia of a monitored generator is presented in [128]. The approach assumes small frequency deviations, neglecting the damping. In [19] the methodology is extended to detect and estimate

simultaneously the time of disturbance, which reduces false estimations of inertia. A similar approach is proposed in [20], exploring directly variations of power and frequency from measurements through the Swing Equation, neglecting damping and rotating loads.

In [27], a dynamic regressor extension and mixing procedure is proposed assuming monitored all the generators participating in primary frequency control. The perturbation considered are generator outages (large perturbation) and rescheduling events.

Reference [34] proposes a method to estimate an equivalent transient reactance of a generator, such that the rotor angle can be calculated and subsequently applied on the swing-equation, later solved through Least-Squares. Reference [84], instead, proposes a modified Least-Squares method for both parameter estimation and initial values of state variables, and compares the obtained results with other methods in the literature.

All the works cited present results on inertia estimation of single machines, not exploring equivalent areas. The method presented in [34], however, is suitable for area studies and is tested in this thesis for this purpose.

Small perturbation approaches

In [16], a method to estimate the inertia divided in three steps is proposed: first it performs a parameter estimation to obtain an equivalent transient reactance of a generator represented with the second-order model, then it carries out a modal decomposition and finally it identifies the inertia of the machine under study solving the Swing Equation. The approach is further explored in [17], [18], [137], [138]. In [139], the technique is expanded and applied for dynamic equivalencing to consider PMU installed at the boundary bus of an area that comprises coherent machines and transmission lines. For small-perturbation studies, these approaches are limited to coherent areas because they depend on modal decomposition, such that local oscillations between non-coherent units interferes on the method.

The paper [140] proposes a Least-Squares (LS)-based system identification method for a power subsystem. Equivalent machines can be obtained assuming coherency. In [141], a closed loop scheme is proposed to estimate inertia with the use of a probe. In [142], PMU measurements are used for modal decomposition, and a LS based approach that makes use of the Newton-Raphson method and the Modal Assurance Criterion is proposed for inertia estimation.

As one of the main focuses of this thesis is to consider spread PMUs installed following criteria that are not necessarily estimating inertia, coherency is a strong assumption to consider. When monitoring areas with non-coherent machines, the local oscillations make it difficult estimating inertia based on the modes of oscillation, such that this research direction was not followed in this thesis. However, some of the methods proposed that deal with oscillations can be adapted for other uses, such [16], that was adapted in this thesis for estimating inertia following large perturbations or normal load variations.

Normal load variation approaches

While the previous methods depend on the occurrence of a perturbation to work, few works in the literature approach normal load variations to estimate the inertia of the system through stochastic methods.

In [23], an algorithm is formulated as a Gaussian Mixture Model with temporal dependence encoded as Markov Chains, and the algorithm is trained with historical data of the system to be capable of identifying patterns and provide estimations following frequency measurements of PMUs. In [24], the grid is

represented with a full Differential Algebraic Equation system and the parameters are estimated through the solution of a Bayesian inverse problem, in a statistical inference procedure. The approach proposed is quite complex, and the author reported concerns regarding execution time for on-line applications. An autoregressive-moving-average (ARMAX) is used in [28] for polynomial modelling, expressing the relationship between inputs, outputs and noise. Inertia is estimated through system identification.

All the methods proposed require a large quantity of historical data and the knowledge of important parameters. Moreover, execution time is a major concern, since the techniques depend on data training, calibration and system identification.

Kalman Filter approaches

A KF is basically a method that proposes a predictor-corrector scheme to minimize the estimated error covariance between measurements and an assumed model for the system [143]. The approaches vary on how the model is stated, and which are the inputs and outputs. The minimum set of state variables are rotor angles and inertia, that are estimated according to assumed initial values during the evolution of the method.

In [21] and [22], an Extended Kalman Filter (EKF) is proposed, a version of the KF that approximates optimality of Bayes' rule through linearization. These approaches use the classic generator second-order set of equations as a predictive model for the system and use active and reactive power (that can be calculated in function of measured voltages and currents) as playback for the corrective part. In [83], instead, voltages and currents are proposed as playback equations, while active power is considered as an input. An Unscented Kalman Filter (UKF) is proposed in [144], that differs on how to deal with the approximations of Gaussian random variables in the core of the method, applying a Monte-Carlo simulation technique instead of the linearizations used in the EKF. Also, frequency control is considered in this paper in the prediction model.

Recently, new contributions have been added to the field of KF-based methods. In [26], a multi-area dynamic state estimation is proposed, solving an optimization problem with an EKF constraint. The areas are previously defined assuming coherency, and full observability is assumed. In [29], the EKF methodology is improved to gain robustness to errors and data loss, and results with ambient data are presented. Also, full observability is needed.

The main requirement of KF-based methods as seen in the literature is monitoring individually the units (or assuming full observability). Only in this condition it is possible to have a good initial estimate of the parameters to be calibrated, crucial for the accuracy of the method. Moreover, the convergence of the method depends on the difference between the model proposed and the system observed: this can be negligible when monitoring individual generators, but may be significantly different when dealing with areas with non-coherent units. Increasing the complexity of the models could improve the accuracy, but there is a limitation on the amount of variables that PMUs can directly observe. In other words, PMUs are able to monitor voltages, currents, powers and frequency. Other parameters such as transient reactances, constants of inertia, damping and parameters that model AVRs, PSSs and governors can only be observed and calibrated indirectly. Hence, increasing the complexity of the models without increasing the amount of information acquired from the measurement model may actually decrease the accuracy of the estimations, since the number of dependent variables to be estimated increases.

Summary of the review

Different methods and approaches have been proposed in the literature for estimating inertia.

Considering generators individually monitored, consistent methods have already been proposed. However, it was not possible to identify a definitive and general one, since the methods mostly depend on different requirements and assumptions. Hence, the field seems still open not only for comparison studies but also for proposing new methods and approaches.

Regarding area studies, few works could be found in the literature. All of them depend on full observability (which is similar to the assumption of monitoring individually the generating units) or depend on monitoring coherent groups. However, commercial PMUs are still very expensive and most of the Countries still do not count with a high number of units, as seen in Section 3.6. Hence, one may ask what type of information it is possible to achieve for the PMUs available on the system. In this condition, the study becomes challenging because the monitored area may contain generators that are not-coherent, loads and perturbations. These issues open many topics for studies.

4.2 Estimation methods

In this section, seven different methods are presented in the order they were needed in the research to approach the proposed topics. To clarify, some of the methods were already proposed in the literature and were tested in the context of this thesis, such as the 'Least-squares method', described in Subsection 4.2.1, the 'Variance method', described in Subsection 4.2.2.2 and the EKF, described in Subsection 4.2.3.

The novel methods, strategies and approaches are the 'Iterative-IME' method, presented in Subsection 4.2.2.1, the 'Inertia estimation with model reduction', presented in Subsection 4.2.4, the 'Equivalent moving power estimation method', presented in Subsection 4.2.5 and the 'Dynamic matrix method', presented in Subsection 4.2.6.

4.2.1 Inertia estimation through direct Least-squares method

Given the system presented in Figure 4.2, consider PMUs installed at bus 1 and 2 providing system frequency measurements, voltage ($V_i\angle\theta_i$) and current ($I_i\angle\alpha_i$) synchrophasors. Here, only one generator was assumed in each side of the radial path, but note that G_i can be an equivalent generator representing all the machines of that area.

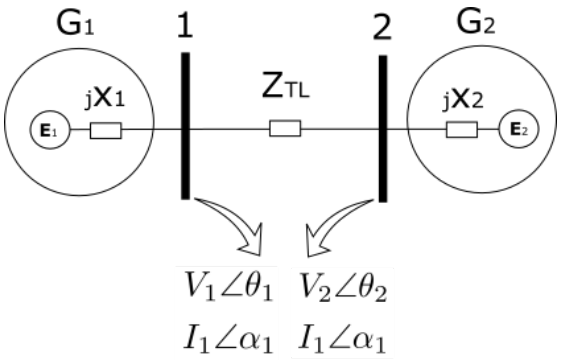

Figure 4.2: *Radial path*

Considering the second-order model for each synchronous machine, the swing equation for machine

i can be stated as:

$$\frac{H_i}{\pi f^0}\frac{d^2\delta_i(t)}{dt^2} + D_i\frac{d\delta_i(t)}{dt} = \Delta P_i(t), \qquad p.u. \qquad i = 1, 2 \tag{4.1}$$

where f^0 is the nominal frequency of the system [Hz], $\delta_i(t)$ is the angle [rad] of the internal voltage $\mathbf{E}_i$, H_i and D_i are the inertia [s] and the damping constant [p.u.], and ΔP_i is the power imbalance [p.u.] related to the machine i, respectively.

Some assumptions can be made to make Equation (4.1) dependent only on observed variables and on the unknown constants H_i and D_i:

- The active power exiting bus i through the interconnection line at time t can be calculated from the measured variables, i.e., voltages and currents (phasors). This variable will be represented by P_i;
- The moving power in comparison to the electromagnetic power generated by synchronous machines is assumed to have a slowly varying behavior, such that $\Delta P_i(t) \approx P_i^{st} - P_i(t)$, where P_i^{st} is the steady state value of P_i before the perturbation;
- The first and second derivatives of the rotor angle δ_i are calculated through finite differences method, again from PMU outputs;
- The difference between the angle of the internal voltage δ_i and the measured voltage angle θ_i is negligible (transient reactances considered negligible).

By doing so, the following overdetermined system can be stated:

$$\begin{bmatrix} \frac{d^2\delta_i(t_1)}{dt^2} & \frac{d\delta_i(t_1)}{dt} \\ \frac{d^2\delta_i(t_2)}{dt^2} & \frac{d\delta_i(t_2)}{dt} \\ \vdots & \vdots \\ \vdots & \vdots \\ \frac{d^2\delta_i(t_M)}{dt^2} & \frac{d\delta_i(t_M)}{dt} \end{bmatrix} \begin{bmatrix} \frac{H_i}{\pi f_0} & D_i \end{bmatrix}^T = \begin{bmatrix} \Delta P_i(t_1) \\ \Delta P_i(t_2) \\ \vdots \\ \vdots \\ \Delta P_i(t_M) \end{bmatrix} \tag{4.2}$$

Or, in matricial form:

$$A_i X_i = B_i \tag{4.3}$$

where:

$$A_i = \begin{bmatrix} \frac{d^2\delta_i(t)}{dt^2} & \frac{d\delta_i(t)}{dt} \end{bmatrix}, X_i = \begin{bmatrix} \frac{H_i}{\pi f_0} & D_i \end{bmatrix}^T, B_i = \begin{bmatrix} \Delta P_i(t) \end{bmatrix}$$

The system 4.3 can be solved through the Least-squares method,

$$\hat{X}_i = (A_i^T A_i)^{-1} A_i^T B_i \tag{4.4}$$

where $\hat{X}$ is the estimation of X that provides the optimum values of H_i and D_i, [34].

The solution of Equation (4.4) gives inertia and damping estimations related to the samples of power imbalance and ROCOF considered as input. If during the time window considered ΔP_i and $\frac{d^2\delta_i}{dt^2}$ do not

vary, it is not possible to estimate H_i. Hence, the method depends on selecting a proper time window for the post-event estimations.

For real time, a sliding time window can be adopted to provide continuous estimations of inertia, as depicted in Figure 4.3. In this graphic example, a time window of 300 samples (6s) was chosen to slide over the samples of power imbalance and ROCOF. Considering the data from t=15s to t=21s (TW1, represented in red), the inertia at t=21s is obtained. Sliding the window to consider the samples of ΔP and ROCOF between t=16s to t=22s (TM2, represented in green), the inertia at t=22s is obtained.

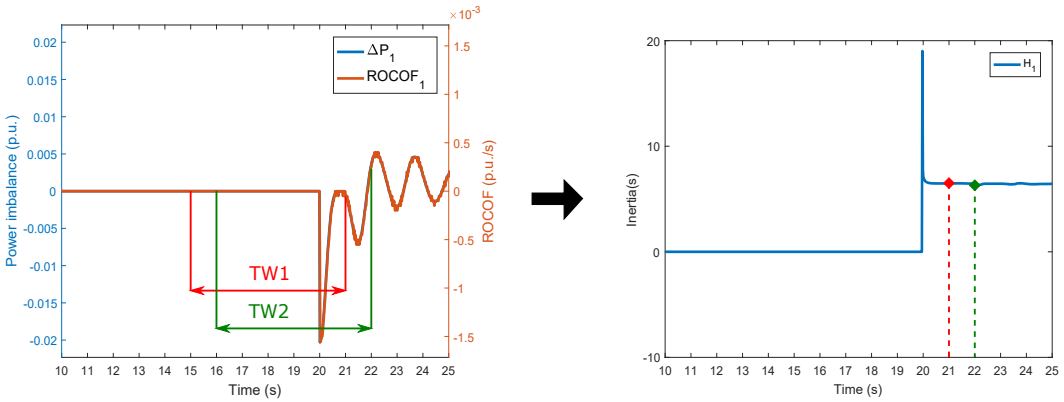

Figure 4.3: *Sliding time window scheme*

The advantage of the direct Least-Squares method is its practicality, and for that reason was the first one studied. The method was used to obtain the results presented in Section 5.1.1. The disadvantage is that the assumption of $\delta_i \approx \theta_i$ may lead to high errors on the estimations. In that case, methods to estimate the transient reactance are needed.

4.2.2 Model estimation methods

In cases where the difference between the angle of the internal voltage and the measured voltage angle (at a terminal bus or at a boundary bus) is not negligible ($\delta_i \neq \theta_i$, referring to Figure 4.2), an alternative approach is to represent the system as a dynamic equivalent and estimate properly the internal angle δ_i. For that purpose, two different methods were studied, each one with its properties. As in this thesis they are used with the same objective, i.e., building dynamic equivalents, they will be called here as Model Estimation Methods (MEM).

4.2.2.1 Iterative-IME Method

The Inter-Area Model Estimation (IME) method was first proposed in [17] for building dynamic equivalents of coherent areas and estimating inertia following oscillations. This method was adapted for the purposes of this thesis, to deal with perturbations and areas that are not necessarily coherent, and the work was published in [32].

Comparing [17] and [32], the first steps of the methods are the same, but some innovations were proposed in [32] for the following steps. First, a novel iterative approach was included to consider losses without the need of increasing the number of measurement points and without loosing accuracy. At second, the method aims at first estimating the transient reactance of the equivalent machine, then

calculates the internal voltage phasor and later estimates the equivalent inertia through LS method. This enables the use of the method following perturbations, and moreover, to study non coherent areas, as the modal decomposition step of the method proposed in [17] is not used. Due to the iterative strategy proposed here (and in [32]), this technique will be called as Iterative-IME method to differ from the method presented in [17].

Given the power system of Figure 4.2, where PMUs are monitoring the terminals of two generators, the goal is to estimate the transient reactances x_i and calculate the internal voltages $\mathbf{E}_i$ accordingly. Alternatively, if PMUs are instead monitoring the boundary of two different areas, the goal of this method is to find out the parameters of equivalent generators, as G_{A1} and G_{A2} in Figure 4.4. Each area is represented by a voltage source $\mathbf{E_1}$ and $\mathbf{E_2}$ behind its own equivalent reactance x_1 and x_2. The two areas are interconnected by an interconnection line with impedance $\mathbf{Z_{TL}}$. Measurements are assumed to be acquired at buses 1 and 2 by PMUs.

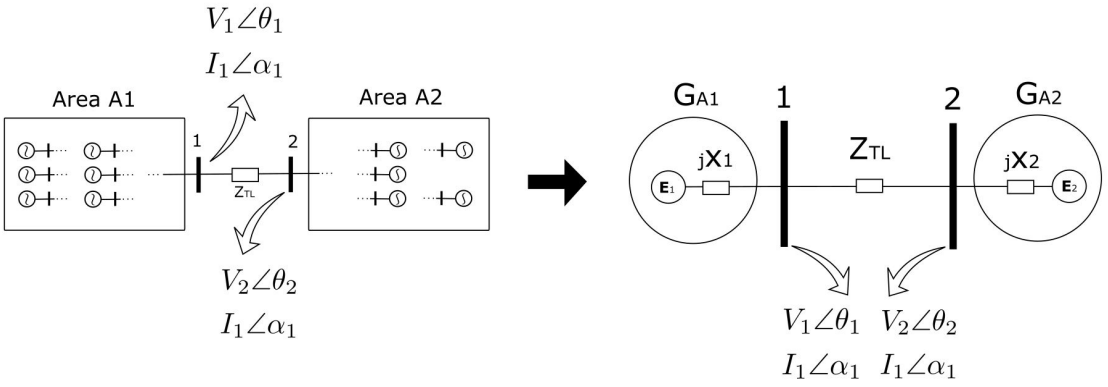

Figure 4.4: *Equivalent system*

The procedure to determine the equivalent parameters of each area requires the voltages and currents phasors in both ends of the radial path. With those phasors, it is possible to calculate the impedance Z_{TL}. Then, to estimate the transient reactances x_1 and x_2, and the internal voltages $\mathbf{E}_1$ and $\mathbf{E}_2$, the following steps are required:

Step 1: The voltage $\mathbf{V_i}$ of each measurement point *i*, can be expressed in terms of the electrical distance to the voltage sources $\mathbf{E_1}$ and $\mathbf{E_2}$:

$$\mathbf{V_i}(t) = \mathbf{Z_{i_{E2}}}\mathbf{E_1}(t) + \mathbf{Z_{i_{E1}}}\mathbf{E_2}(t) \tag{4.5}$$

where $\mathbf{Z_{i_{E2}}}$ is the electrical distance of point i to the voltage source $\mathbf{E_2}$ and $\mathbf{Z_{i_{E1}}}$ is the electrical distance of point i to the voltage source $\mathbf{E_1}$. Both $\mathbf{Z_{i_{E1}}}$ and $\mathbf{Z_{i_{E2}}}$ are functions of the unknowns X_1, X_2 and known Z_{LT}.

Step 2: Take the magnitude of $\mathbf{V_i}$.

$$V_i(t) = \sqrt{E_1(t)^2\Psi_{A_i}^2 + E_2(t)^2\Psi_{B_i}^2 + 2E_1(t)E_2(t)\Psi_{A_i}\Psi_{B_i}cos(\varpi_i(t))} \tag{4.6}$$

where E_1 and δ_1 are the magnitude and angle of the voltage $\mathbf{E_1}$, while E_2 and δ_2 are the magnitude and

angle of the voltage $\mathbf{E_2}$ and the other parameters are defined below.

$$\Psi_{A_i} = \frac{|\mathbf{Z_{i_{E2}}}|}{|\mathbf{Z_{Tot}}|} \tag{4.7}$$

$$\Psi_{B_i} = \frac{|\mathbf{Z_{i_{E1}}}|}{|\mathbf{Z_{Tot}}|} \tag{4.8}$$

$$\varpi_i(t) = \mu_{A_i} - \mu_{B_i} + \delta_1(t) - \delta_2(t) \tag{4.9}$$

$$\mu_{A_i} = \arctan \frac{imag(\mathbf{Z_{i_{E2}}})}{real(\mathbf{Z_{i_{E2}}})} - \arctan \frac{imag(\mathbf{Z_{Tot}})}{real(\mathbf{Z_{Tot}})} \tag{4.10}$$

$$\mu_{B_i} = \arctan \frac{imag(\mathbf{Z_{i_{E1}}})}{real(\mathbf{Z_{i_{E1}}})} - \arctan \frac{imag(\mathbf{Z_{Tot}})}{real(\mathbf{Z_{Tot}})} \tag{4.11}$$

$$\mathbf{Z_{Tot}} = jx_1 + jx_2 + \mathbf{Z_{TL}} \tag{4.12}$$

Step 3: Consider its variation ΔV_i with respect to a change in $\Delta\delta$ can be linearized about an equilibrium point 0

$$\Delta V_i = \frac{E_1(t)E_2(t)\Psi_{A_i}\Psi_{B_i}\sin\left(\varpi_i(t)\right)}{|V_{0i}|}\left[\Delta\delta_2 - \Delta\delta_1\right] \tag{4.13}$$

Step 4: Define the normalized voltage V_{ni} as

$$V_{ni}(t) \triangleq \Delta V_i(t) V_{0i} \tag{4.14}$$

where it is worth noticing that both $\Delta V_i(t)$ and $V_{ni}(t)$ are time dependent. As the PMUs will provide a number of samples within the considered time interval, the normalized voltages can be computed based on the PMU output. The approach for this step is different from the one proposed in [17], as it considers more than one point in the equations.

Step 5: Let us assume that three PMUs are installed at points 1, 2 and 3. Point 3 can be either a physical bus (where a real PMU is installed) or a virtual bus somewhere along the transmission line, where data can be computed based on the data coming from the PMUs installed at 1 and a 2 and known Z_{TL}.

Write the following expressions:

$$\frac{V_{n3}(t)}{V_{n1}(t)} = \frac{\Psi_{A_3}\Psi_{B_3}\sin\left(\varpi_3(t)\right)}{\Psi_{A_1}\Psi_{B_1}\sin\left(\varpi_1(t)\right)} \tag{4.15}$$

$$\frac{V_{n2}(t)}{V_{n1}(t)} = \frac{\Psi_{A_2}\Psi_{B_2}\sin\left(\varpi_2(t)\right)}{\Psi_{A_1}\Psi_{B_1}\sin\left(\varpi_1(t)\right)} \tag{4.16}$$

This expressions cannot be solved in this step because $\delta_1(t)$ and $\delta_2(t)$ (that appear inside the functions $\varpi_i(t)$) are not directly measured.

Step 6: Consider for the moment the resistance of the transmission line negligible (the relevant results are characterized by the subscript I): $R_{LT} = 0$.

Taking one of the generators as a reference (e.g. $\delta_1 = 0$), expressions 4.15 and 4.16 can be simplified to be dependent only on system parameters:

$$\frac{V_{n3_I}(t)}{V_{n1_I}(t)} = \frac{x_{3_{E2}}x_{3_{E1}}}{x_{1_{E2}}x_{1_{E1}}} \tag{4.17}$$

$$\frac{V_{n2_I}(t)}{V_{n1_I}(t)} = \frac{x_{2_{E2}} x_{2_{E1}}}{x_{1_{E2}} x_{1_{E1}}} \tag{4.18}$$

Call the right hand side of equations 4.17 and 4.18 as

$$\alpha_I = \frac{x_{3_{E2}} x_{3_{E1}}}{x_{1_{E2}} x_{1_{E1}}} \tag{4.19}$$

$$\beta_I = \frac{x_{3_{E2}} x_{3_{E1}}}{x_{1_{E2}} x_{1_{E1}}} \tag{4.20}$$

where the subscript I denotes the lossless case.

Rewrite expressions 4.17 and 4.18 as:

$$\underline{V_{n3_I}} = \alpha_I \underline{V_{n1_I}} \tag{4.21}$$

$$\underline{V_{n2_I}} = \beta_I \underline{V_{n1_I}} \tag{4.22}$$

where $\underline{V_{n1_I}}$, $\underline{V_{n2_I}}$ and $\underline{V_{n1_I}}$ are vectors consisting of a limited number of samples of the variables $V_{n1}(t)$,$V_{n2}(t)$ and $V_{n3}(t)$, respectively.

The over-determined systems (4.21) and (4.22) can be solved for α_I and β_I using the linear Least Squares method:

$$\hat{\alpha}_I = (\underline{V_{n1_I}}^T \underline{V_{n1_I}})^{-1} \underline{V_{n1_I}}^T \underline{V_{n3_I}} \tag{4.23}$$

$$\hat{\beta}_I = (\underline{V_{n1_I}}^T \underline{V_{n1_I}})^{-1} \underline{V_{n1_I}}^T \underline{V_{n2_I}} \tag{4.24}$$

With the solutions of (4.23) and (4.24), equations (4.19) and (4.20) can be solved for x_{1_I} and x_{2_I}, the internal reactances of the equivalent machines G_1 and G_2 for the lossless case.

Step 7: At this point, in order to take into account the resistive feature of the interconnection line, which is one of the contributions of the present method, the estimated x_{1_I} and x_{2_I} can be combined with the measurement coming from the PMUs to compute the estimate of internal voltages $\mathbf{E_{1_I}}(t) = E_{1_I}(t)\angle\delta_{1_I}(t)$ and $\mathbf{E_{2_I}}(t) = E_{2_I}(t)\angle\delta_{2_I}(t)$ through Ohm's law.

Step 8: The values of the internal voltages newly computed make it possible to come back to expressions (4.15) and (4.16). As $\delta_1(t)$ and $\delta_2(t)$ are not directly measured, the angles $\delta_{1_I}(t)$ and $\delta_{2_I}(t)$ obtained in Step 5 are used in this step as an approximation.

The values of the internal voltages newly computed make it possible to determine an improved linearization of voltage magnitudes at the installation point of PMUs and to provide updated expressions for the updated normalized voltages $\underline{V_{n1_{II}}}$, $\underline{V_{n2_{II}}}$ and $\underline{V_{n3_{II}}}$:

$$\frac{\underline{V_{n3_{II}}}}{\underline{V_{n1_{II}}}} = \frac{\Psi_{A_3}\Psi_{B_3}\sin(\mu_{A_3} - \mu_{B_3} - \underline{\delta_{1_I}} - \underline{\delta_{2_I}})}{\Psi_{A_1}\Psi_{B_1}\sin(\mu_{A_1} - \mu_{B_1} - \underline{\delta_{1_I}} - \underline{\delta_{2_I}})} \tag{4.25}$$

$$\frac{\underline{V_{n2_{II}}}}{\underline{V_{n1_{II}}}} = \frac{\Psi_{A_2}\Psi_{B_2}\sin(\mu_{A_2} - \mu_{B_2} - \underline{\delta_{1_I}} - \underline{\delta_{2_I}})}{\Psi_{A_1}\Psi_{B_1}\sin(\mu_{A_1} - \mu_{B_1} - \underline{\delta_{1_I}} - \underline{\delta_{2_I}})} \tag{4.26}$$

where the underline denotes vector and the subscript II denotes the present step, considering $R_{TL} \neq 0$.

Calling α_{II} the right hand side of equation (4.25), and β_{II} the right hand side of equation (4.26), both over-determined systems can be solved using least squares method to obtain updated $x_{1_{II}}$ and $x_{2_{II}}$, similar to what was done in Step 6.

At this point, again, the updated internal voltages $\mathbf{E_{i_{II}}}(t)$ can be computed by Ohm's law, using the

newly estimated $x_{1_{II}}$ and $x_{2_{II}}$.

Step 9: Test if $(x_{j_I} - x_{j_{II}})$ is lower than a tolerance (10^{-6} $p.u.$ used), where $j = 1, 2$ denotes the Area of the calculated equivalent reactance. If not, set $x_{j_I} = x_{j_{II}}$ and go back to Step 7. If yes, the iterative process of reactance estimation converged. Proceed to Step 10.

Step 10: In this step, the area equivalent inertia is estimated.

$$\frac{H_{A_j}}{\pi f^0}\frac{d^2\delta_i(t)}{dt^2} = \Delta P_{A_j}(t), \qquad p.u. \tag{4.27}$$

where H_{A_j} is the inertia constant and ΔP_{A_j} is the power imbalance of Area j $(j = 1, 2)$, f^0 is the nominal frequency of the system. Due to the slow behavior of the moving power in comparison to the electromagnetic power generated by synchronous machines, $\Delta P_j(t) \approx P^{st}_{int_j} - P_{int_j}(t)$, where P_{int_j} is the power exiting Area j through the interconnection line and $P^{st}_{int_j}$ is its value in steady state (before the perturbation). Equation (4.27) can be solved through Least Squares method for H_{A_j}. This step is another novel contribution in comparison to the method proposed in [16].

The method proposed here was used to obtain the results presented in Subsections 5.1.2, 5.1.3 and 5.2.1. The advantage of this method is the possibility of estimating both the inertia of an individually monitored generator and the inertia of an equivalent generator, representing an area composed by coherent or non-coherent machines. The disadvantage is the need of monitoring both ends of a radial interconnection path.

4.2.2.2 "Variance" Method

This method was proposed in [34] and studied in the context of this thesis for building dynamic equivalents, as an alternative to situations where the Iterative-IME method cannot be used (due to the requirement of radial paths).

To estimate the transient reactance of the equivalent machine, the method presented in [34] is based on the variance of the magnitude of the internal voltage, defined as a function of the variables of the grid. For the sake of simplicity, this method will be referred as the "Variance method" in this thesis.

Referring to Figure 4.4, this approach is based in stating equations to obtain x_1 and x_2 using Ohm's Law. The second order model for the equivalent machine G_{Ai} $(i = 1, 2)$ is assumed, with the magnitude of voltage $|\mathbf{E}_i|$ constant. Based on the expression of the variance of $|\mathbf{E}_i|$, the method is able estimate x_1 and x_2 without needing to know exactly $|\mathbf{E}_i|$. Later, the voltages $E_i\angle\delta_i$ are calculated based on the reactances estimated, and the inertia is estimated related to the behavior of the dynamic equivalents. The steps of the methodology can be summarized as follows:

Step 1: State the Ohm's Law for each equivalent area:

$$E_i(t)\angle\delta_i(t) = (jx_i)I_i(t)\angle\alpha_i(t) + V_i(t)\angle\theta_i(t) \tag{4.28}$$

Step 2: State the magnitude of $\mathbf{E_i}$. This procedure can be seen in Appendix B. The final expression is:

$$|\mathbf{E_i}| = \sqrt{x_i^2|\mathbf{I}_i|^2 + |\mathbf{V}_i|^2 + 2x_iQ_i} \tag{4.29}$$

such that

$$E_i^2 = x_i^2I_i^2 + V_i^2 + 2x_iQ_i \tag{4.30}$$

Step 3: Since the second order model for the synchronous machine is considered, i.e., representing the generator by a voltage source with constant magnitude (but with angular variation) behind a reactance, it can be stated that:

$$E_i \approx constant \rightarrow E_i^2 \approx constant \rightarrow Var(E_i^2) \approx 0 \rightarrow \overline{(E_i^2 - \overline{E_i^2})^2} \approx 0 \tag{4.31}$$

where Var denotes the Variance and $\bar{E} = mean(E)$.

Step 4: Fitting (4.30) into (4.31), write

$$\overline{(E_i^2 - \overline{E_i^2})^2} \approx 0 \rightarrow (x_i^2 I_i^2 + V_i^2 + 2x_i Q_i) - (x_i^2 \overline{I_i^2} + \overline{V_i^2} + 2x_i \overline{Q_i}) \approx 0 \tag{4.32}$$

Step 5: Rearranging, state the following equation for every time step t,

$$x_i^2(\overline{I_{i_t}^2} - I_{i_t}^2) + x_i(2(\overline{Q_{i_t}} - Q_{i_t})) \approx (V_{i_t}^2 - \overline{V_{i_t}^2}) \tag{4.33}$$

Expression (4.33) can be solved for x_i using nonlinear least squares techniques. In the present work, a Matlab function (*lsqnonlin* function) is used in its default configuration.

This method was directly used to produce the results presented in Subsections 5.1.3, 5.2.1, 5.3.1 to 5.3.3, and partially used to produce the results presented in Sections 5.2.3, 5.4.2 and 5.5.1. The advantage of this method is the requirement of only one measurement point to estimate the inertia of a generator individually monitored or to estimate the inertia of an area monitored at its boundary bus. Due to this advantage, this method was used in combination with the Ward equivalent method in the methodology proposed in Subsection 4.2.4.

4.2.3 Extended Kalman Filter

The EKF was studied in the context of this thesis for comparison with the MEM on inertia estimation of single machines or equivalent machines. The EKF is a method for parameter calibration, updating the initial estimations of the parameters of interest according to measurements acquired at the system.

Traditionally, angle stability analysis has been seen as a direct mathematical problem. The classical second order generator model is used to represent the dynamic behavior of a synchronous machine following a perturbation, and by feeding the model with the internal parameters of the machine one can predict the post-fault rotor swings, key point to assess stability. Figure 4.5 depicts this problem.

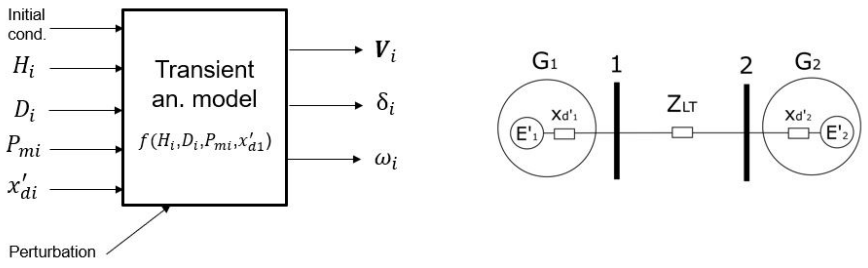

Figure 4.5: *Rotor swings direct problem*

The transient analysis model reported in Figure 4.5 refers to the application of the second order model

of the generator, described in Equation (4.34).

$$\begin{cases} \dot{\delta}(t) = \omega(t) \\ \dot{\omega}(t) = \left[P_m - \frac{E(t)V(t)\sin(\delta(t)-\theta(t))}{x'_d} - D\omega(t)\right]\frac{\omega_0}{2H} \qquad p.u. \end{cases} \tag{4.34}$$

where all the variables were previously defined.

The parameter estimation problem is depicted in Figure 4.6, and could be faced as an inverse problem of the one represented in Figure 4.5. The idea is to make use of measurements of voltage ($\mathbf{V}_i$) and current ($\mathbf{I}_i$) coming from PMUs to determine the internal parameters of the machine under study, using a Kalman Filter as an observer of the dynamic process. The other inputs required in the method will be discussed later in this subsection.

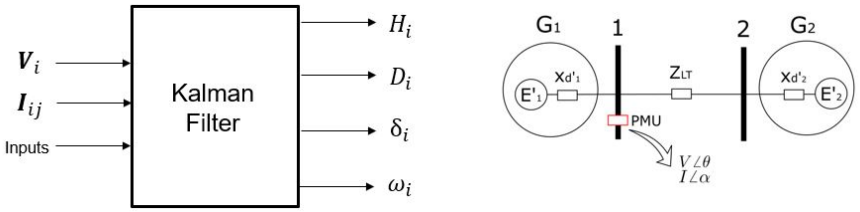

Figure 4.6: *Parameter estimation inverse problem*

The Kalman Filter (KF) is a prediction-correction method based on modelling a dynamic process in state-space equations and comparing their predictions with observations over time. In statistical terms, it minimizes the estimated error covariance when some determined conditions are met. The Extended Kalman Filter (EKF), which will be described in this Section, is a version of the KF where a linearization about the current mean and covariance is proposed to deal with nonlinear processes, [143].

Consider that the dynamic process is governed by

$$x_k = f(x_{k-1}, u_k, w_{k-1}) \tag{4.35}$$

where x_k is the state variable x at the discrete time instant k, f is a nonlinear function of the previous state of x, represented by x_{k-1}, the input u_k and the process noise w_{k-1}.

The measurement model is governed by

$$z_k = g(x_k, v_k) \tag{4.36}$$

where z_k is the observation variable, g is the nonlinear algebraic function that relates z_k to x_k and v_k, that is the measurement noise.

Providing the initial estimates for the 'a priori' state variable $\bar{x}_0^A$ and for the 'a priori' estimate error covariance matrix P_0^A, the prediction-correction scheme depicted in Figure 4.7 is executed for every time step k. In the figure, the subscript 'A' denotes the variables 'a priori' and the subscript 'F' denotes the variables 'a posteriori'. Also, $F_k = \frac{df}{dx}$, $W_k = \frac{df}{dw}$, $G_k = \frac{dg}{dx}$, $V_k = \frac{dg}{dv}$, Q_k is the process noise covariance matrix, R_k is the measurement noise covariance matrix and I is identity.

The matrix Q_k enables the method to consider a gap between the process model and the measurement

acquired. In practical terms, this brings robustness to the method to consider a model with a certain degree of simplification in respect to the real process. Similarly, the matrix R_k brings robustness against small measurement errors. Both Q_k and R_k must be known or tuned according to the system under study. One may refer to [143] for further details on the EKF theory.

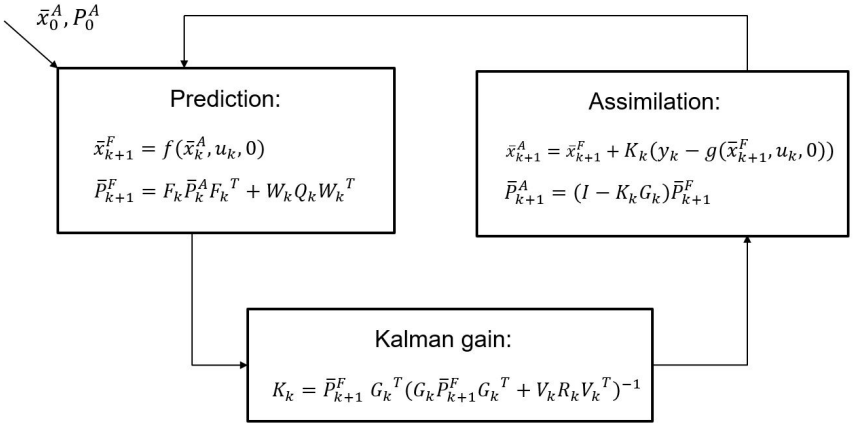

Figure 4.7: *EKF scheme*

Following the approach proposed in [22], the EKF is suggested as an observer of a dynamic model of a synchronous generator, calibrating inertia and damping parameters through the comparison between the state variable predictions and corrections based on the measurements from the machine's terminals.

The dynamic process is represented by

$$\begin{cases} \dot{\delta}(t) = \omega(t) + w_1 \\ \dot{\omega}(t) = \left[P_m - \frac{E(t)V(t)\sin(\delta(t)-\theta(t))}{x'_d} - D\omega(t)\right] \frac{\omega_b}{2H} + w_2 \end{cases} \tag{4.37}$$

where $w_j,\ j = 1, 2$ are variables that represent the noise of the selected process model.

The measurement model is

$$\begin{cases} P_e(t) = \frac{E(t)V(t)\sin(\delta(t)-\theta(t))}{x'_d} + v_1 \\ Q_e(t) = -(\frac{V(t)^2 - E(t)V(t)\cos(\delta(t)-\theta(t))}{x'_d}) + v_2 \end{cases} \tag{4.38}$$

where v_1 and v_2 are the noise variables related to the measurement model and P_e and Q_e are the active and reactive power injected in the grid at the connection point. Apart the fact the active and reactive power are not directly measured by PMUs, they can be calculated from the voltages and current injections measured. Many PMU manufacturers provide the results of these calculations together with their degree of accuracy.

Discretizing the systems (4.37) and selecting as state variables δ_k, ω_k, $N_k = \frac{\omega_b}{2H_k}$ and D_k, we have

$$\begin{cases} \delta_{k+1} = \omega_s t_s + \delta_k + w_{1_k} \\ \omega_{k+1} = \left[P_m - \frac{E_k V_k \sin(\delta_k - \theta_k)}{x'_d} - D_k \omega_k\right] N_k t_s + \omega_k + w_{2_k} \\ N_{k+1} = N_k + w_{3_k} \\ D_{k+1} = D_k + w_{4_k} \end{cases} \tag{4.39}$$

where E_k, V_k, θ_k, x'_d and P_m are inputs. Regarding x'_d, some approaches like [18] propose to estimate it together with the other internal parameters of the machine. However, it reports a decrease in accuracy on the results obtained, that is natural due to the amount of parameters to be estimated based on only two variables measured. In this research, specific methods to estimate x'_d were proposed, such that x'_d is considered known for the application of the studied EKF.

Discretizing (4.38), we have

$$\begin{cases} P_{e_k} = \frac{E_k V_k \sin(\delta_k - \theta_k)}{x'_d} + v_1 \\ Q_{e_k} = -(\frac{V_k^2 - E_k V_k \cos(\delta_k - \theta_k)}{x'_d}) + v_2 \end{cases} \tag{4.40}$$

The discrete models are then applied to the scheme presented in Figure 4.7.

Results of the presented method can be found in Subsection 5.2.2. The advantage of this method is to deal with noise in a prediction-correction way. However, the measurement model is able to provide direct feedback only for a restricted number of variables (i.e., rotor angle and speed), and the other variables (such as H and D) need to be calibrated indirectly. This makes the method strongly dependent on the initial guess of H and D, and on the tuning of the matrix Q.

4.2.4 Inertia estimation with model reduction

4.2.4.1 Contextualization

The previous methods were first proposed and tailored to work using measurements acquired at a terminal bus or a boundary bus, in the case of an equivalent area well defined and connected by a single interconnection. However, PMU placement depends on the multiple functions these devices need to carry out. One may ask if it is possible to have a dynamic equivalent of the system seen from spread PMUs available on the grid. In the literature, this topic is not approached in this way. Most of the methods previously discussed assume full observability of the system to consider they have measurements at the terminals of every generator or at least at the boundary of coherent areas. However, the question is whether these pre-defined divisions are still the best configuration to provide insights about the inertia distribution of a system when intermittent RES units are connected, and moreover, if they are reasonable from the economic point of view.

The idea here is to propose a method that allows one to take advantage of the available PMUs to have a fingerprint of the inertia distribution of the system, regardless coherency. In this sense, the areas or subareas under study may be defined according to the measurements available. Moreover, once generators are not approached in their terminal buses, an equivalent that also takes into account the inertial

behaviour of loads can be built. To do so, it is necessary to reduce the system around the measurement points available.

System reduction methods were first developed in the literature for speeding up calculations and simulators [36]. Consequently, some of the criteria to reduce the system may not be reasonable to assume for practical purposes, as they were tailored for model simulation, but some techniques may be adopted. The Ward Equivalent method is a generalization of the Thévenin equivalent, widely used with phasorial representation in steady-state studies, that can be extended to represent part of grid in quasi-static conditions. Here, the idea is to retain the buses where PMUs are available, eliminating the others. The dynamic of hidden generators will be represented together in the dynamic equivalent obtained with the addition of the "Variance method".

The Ward Equivalent Method requires the knowledge of the topology of the system. This topic has been widely discussed in the literature, in techniques that involve the combination of measurements coming from SCADA and/or PMUs to monitor circuit breakers status, [89], [91], [145]. Once the admittance matrix of the system is obtained, the Ward Equivalent decomposes it in different sub-matrices according to the buses to be excluded and retained.

4.2.4.2 Method

Consider a generic power system with PMUs installed in N buses among the total N_t buses of a system, as depicted in Figure 4.8(a). By means of system reduction, the aim is to obtain the equivalent represented in Figure 4.8(b).

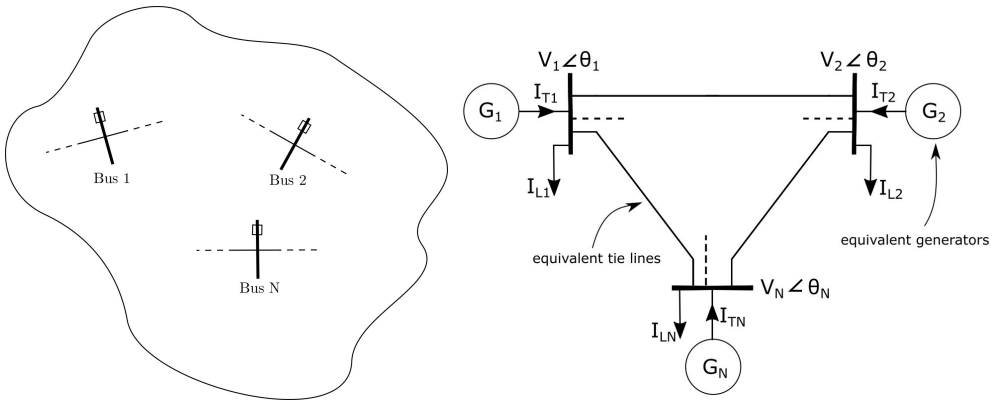

(a) PMUs installed in N buses (b) Equivalent system

Figure 4.8: *Ward Equivalent Method, [67]*

The construction of this equivalent starts from the full algebraic equations, which is valid for each time step $i = 1, \ldots, M$ when considering the transient evolving under quasi-static conditions and small frequency variations. By Ohm's law,

$$\mathbf{Y}_{BUS}\mathbf{V}_{Bi} = \mathbf{I}_{Bi} \tag{4.41}$$

where $\mathbf{Y}_{BUS}$ is the admittance matrix of the system (without including generator and load admittances), with dimensions $N_T \times N_T$. The vectors $\mathbf{V}_{Bi}$ and $\mathbf{I}_{Bi}$ are respectively the bus voltages and current injections vectors at time step i, with dimensions $N_T \times 1$.

Regarding a generic bus j, the current injection $\mathbf{I}_{Bi}^{(j)}$ can be written as:

$$\mathbf{I}_{Bi}^{(j)} = \mathbf{I}_{Gi}^{(j)} - \mathbf{I}_{Li}^{(j)} \tag{4.42}$$

where $\mathbf{I}_{Gi}^{(j)}$ is the generator current of bus j, $\mathbf{I}_{Li}^{(j)}$ is the load current and $\mathbf{I}_{Bi}^{(j)}$ is the injected current in the grid.

Defining the buses where PMUs are installed as the set of buses to be retained ($R = \{1, 2, \ldots, N\}$), the $N_T - N$ remaining buses compose the set to be eliminated ($E = j \notin R$). Using the subscripts R and E to denote retained and eliminated, respectively, Equation (4.41) can be reorganized as:

$$\begin{bmatrix} Y_{RR} & Y_{RE} \\ Y_{ER} & Y_{EE} \end{bmatrix} \begin{bmatrix} V_R \\ V_E \end{bmatrix} = \begin{bmatrix} I_R \\ I_E \end{bmatrix} \tag{4.43}$$

Since all the quantities involved are complex numbers, for the sake of simplicity, they are not represented in bold anymore. Also, the subscript i is neglected here.

From Equation (4.43),

$$Y_{ER}V_R + Y_{EE}V_E = I_E \;\Rightarrow\; V_E = Y_{EE}^{-1}I_E - Y_{EE}^{-1}Y_{ER}V_R \tag{4.44}$$

Now substituting V_E in the upper line of Equation (4.43), it is possible to obtain

$$(Y_{RR} - Y_{RE}Y_{EE}^{-1}Y_{ER})V_R = I_R - Y_{RE}Y_{EE}^{-1}I_E \tag{4.45}$$

Where quantities of interest are defined as

$$Y_{EQ} = Y_{RR} - Y_{RE}Y_{EE}^{-1}Y_{ER} \tag{4.46}$$

and

$$I_{EQ} = I_R - Y_{RE}Y_{EE}^{-1}I_E \tag{4.47}$$

In Equation (4.47), the vector $I_W = Y_{RE}Y_{EE}^{-1}I_E$ takes into account the generators and loads current injections at eliminated buses, and reduces to the retained buses the global power behaviour of the system. Alternatively,

$$I_{EQ} = Y_{EQ}V_R \tag{4.48}$$

It is important to observe that I_{EQ} can be calculated through Equation (4.48) considering the voltage phasors at the retained buses and the reduced admittance matrix Y_{EQ}, therefore practical conditions.

However, in systems where all the generators are individually monitored, the total current injection I_{EQ} can be expressed as

$$I_{EQ} = I_T - I_L \tag{4.49}$$

where I_T is the total current injected by the generators and I_L is the total load currents. This Equation is not required in the method for the practical estimation of inertia, but brings additional information that will be exploited later in this thesis to provide insights on the impact of the loads in the inertia estimation. It‘s important to point out that Equation 4.49 denotes the equivalent injections after the application of

the Ward reduction, differing from the generic bus injections expressed in Equation 4.42 before the application of the method.

Therefore, given the N-PMU measurements and the admittance matrix Y_{BUS}, one can derive the equivalent matrix Y_{EQ} and calculate the equivalent current injections with Equation(4.48), obtaining the equivalent system depicted in Figure 4.8(b).

After the equivalent system is obtained, with the measured V_R and the calculated I_{EQ}, the "Variance method" presented in Subsection 4.2.2.2 can be applied to obtain the equivalent inertias of each machine.

The procedure can be summarized in the following steps:

Step 1: Build the admittance matrix Y_{BUS} of the system. Topology must be known or estimated.

Step 2: Obtain the equivalent matrix Y_{EQ} through Equation (4.46) defining the retained and eliminated buses.

Step 3: Calculate I_{EQ} through Equation (4.48) according to the measurements of V_R in time.

Step 4: With I_{EQ} and V_R, apply the "Variance method" to estimate the transient reactances of each equivalent machine.

Step 5: Solve the swing equations of the equivalent generators through LS method to estimate the equivalent inertias. These generators are an equivalent built in terms of the PMU measurements available at the retained buses. This step is equivalent to the step of the MEM to estimate the inertia for equivalent machines.

This method was directly used to produce the results presented in Subsections 5.2.3 and partially used to produce the results seen in Subsections 5.3.3 to 5.5.1. The advantage is to enable the use of more measurements available in one area to build the dynamic equivalents, instead of considering only one measurement point when the MEM are applied alone. Consequently, with additional information, the method is able to provide a more accurate picture of the dynamics of the COI of the area.

4.2.5 Equivalent moving power estimation method (auxiliary)

4.2.5.1 Contextualization

The methods presented in Subsections 4.2.1 and 4.2.2, based on solving the swing equation through LS, rely on a strong assumption: the consideration that the mechanical power of a machine changes slowly in comparison to the electrical power generated by the machine. This assumption is reasonable and often used in the literature for single machines, [41], [42]. However, when dealing with equivalent machines that represent an entire area, this assumption becomes unreasonable in the case of an internal loss of generation or in the case which the the perturbation is a change on the mechanical power of one of the machines.

The aggregated swing equation (2.23) (defined in Subsection 2.2.3) considers $P_{m_{Eq}}(t) = \sum_{j=1}^{i} P_{m_j}(t)$, and is valid when all the generators are connected to the same bus or when all the power generated is known. However, one may want to monitor an area installing a PMU at the boundary bus of an area and exploit the Model Estimation Methods (MEM) presented previously, as depicted in Figure 4.9.

In this case, the equivalent equation of motion of the COI of Area A becomes:

$$H_{COI_A}\frac{df_{COI_A}}{dt} = (P_{mov_A}(t) - P_{e_A}(t))\frac{\omega_0}{2}, \qquad p.u. \tag{4.50}$$

where the subscript A denotes Areas A, P_{mov_A} is the equivalent moving power and P_{e_A} is the active power exiting the area.

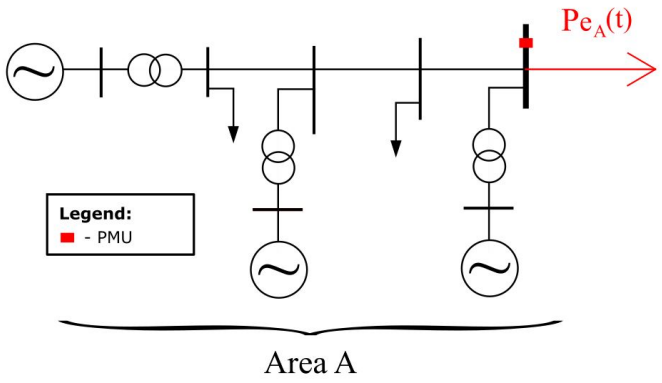

Figure 4.9: *Area monitored by a PMU*

The equivalent moving power (P_{mov_A}) can be calculated as

$$P_{mov_A}(t) = \sum_{n=1}^{n_g} P_m - \sum_{n=1}^{n_l} P_L - \sum_{n=1}^{n_{tl}} P_{losses} \tag{4.51}$$

where $\sum P_m$ denotes the sum of the mechanical powers of each of the n_g generators, $\sum P_L$ denotes the active power consumed by the n_l loads and $\sum P_{losses}$ are the losses in the n_{tl} transmission lines in the area.

Figure 4.10 depicts the area monitored by the PMU and its correspondent equivalent.

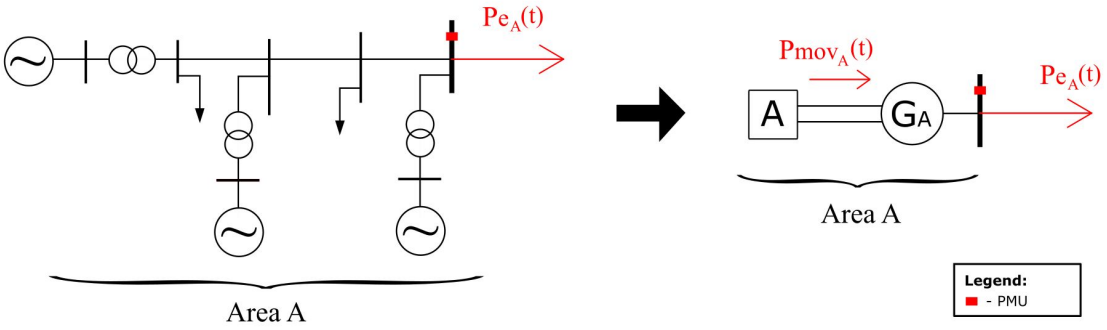

Figure 4.10: *Dynamic equivalent of the monitored area*

In these conditions, the equivalent moving power $P_{mov_A}(t)$ may not move slower in comparison to P_{e_A}, due to perturbations inside the area or due to the voltage and frequency dependance of loads, that make the variation of power consumed to vary fast and intense, [146]. When using the MEM directly with dynamic equivalents making the assumption of slow moving power, consequently, this inconsistence with the model may cause negative estimations for the inertia [147]. Knowing the load behavior and estimating the moving power of an area therefore improves the assumption of slow moving power variation to a more realistic approach. The objective of this section is to evaluate the possibility of performing these estimations in a practical way starting from PMU measurements.

4.2.5.2 Specific bibliography review

Many different papers discuss the use of PMUs for monitoring, studying or estimating load behavior using PMUs. In [148], the voltage dependance of the loads is identified as the main contributor to load changes, neglecting frequency dependance. In [149] the use of a PMU to monitor and estimate the behavior of induction motors is addressed, detailing practical limitations. The works [150] and [151] propose different approaches for dynamic load modelling in distribution grids.

In [152], a practical approach based on modelling the load as constant current is presented. The methodology assumes the total load pre-disturbance is known, and by weighting voltage measurements at different buses is able to estimate an equivalent load behavior of an area. The works [153] and [154], instead, are model-identification based. They make use of optimization for estimating the parameters of the ZIP model [154] or exponential voltage/frequency dependance model [153].

4.2.5.3 Methodology

As the idea here is to estimate an equivalent moving power as an auxiliary method to the estimation of inertia, the approach [152] was chosen to address load estimation, as it seemed the most practical and flexible. The method was adapted to the assumptions considered in this thesis, and combined with a strategy for estimating the equivalent mechanical power of the area and compose the equivalent moving power.

The load model proposed in [152] is the constant current, expressed by

$$P_L(t) = \sum_{i=1}^{l} P_{L0_i} \frac{V_{L_i}(t)}{V_{L_i}(0)} \tag{4.52}$$

where $P_L(t)$ is the total load demand at time t, P_{L0_i} and $V_{L_i}(0)$ are the initial values of load demand and voltage at bus i respectively, $V_{L_i(t)}$ is the voltage at time t and l is the number of connected loads.

However, these quantities are not always known or directly monitored. Based on 4.52, the total load demand at time t can be approximated in a more practical way by

$$P_L(t) = P_{prod} V_{set}(t) \tag{4.53}$$

where P_{prod} is the total load reference, that can be approximated by the average value of the total load in the time window studied. The variable $V_{set}(t)$ is a weighted sum of the voltage measurements at selected buses.

In [152], loads are represented using the constant current and the selected set considers the terminal buses of the generators, as

$$V_{set}(t) = \frac{1}{n} \sum_{i=1}^{n} \frac{V_{G_i}(t)}{V_{G_i}(0)} \tag{4.54}$$

where n is the number of generators and the subscript G stands for the terminal buses of the generators.

Regarding the load representation, if the case is to use the constant impedance model instead of the constant current, Equation (4.53) may be adapted to

$$V_{set}(t) = \frac{1}{n} \sum_{i=1}^{n} \frac{V_{G_i}^2(t)}{V_{G_i}^2(0)} \tag{4.55}$$

Deciding for a specific model or for a composite model depends on the historical load characteristics of the area under study. If the load parameters in the ZIP model (Equation (2.35)) are known or previously estimated, Equation (4.53) can be adapted to consider a composite model.

Equations (4.54) and (4.55) are defined as functions of V_{G_i}, following the approach proposed in [152]. However, this implies in the requirement of monitoring the terminal buses of the generators. In that conditions, the inertia of each machine could be estimated individually and the COI could be evaluated without the need of estimating the equivalent moving power of the area. Moreover, as it is shown in the chapter of results (Subsection 5.4.2), considering the terminal buses of generators is not the best choice to compose V_{set} and estimate $P_L(t)$. For the tested cases, considering measurements obtained with PMUs at load or transfer buses brought more accuracy to the estimations. Hence, monitoring the terminals of the generators is not a requirement of this method, and Equation (4.55) can be modified to Equation (4.56).

$$V_{set}(t) = \frac{1}{n}\sum_{i=1}^{ns}\frac{V_{Bus_i}^2(t)}{V_{Bus_i}^2(0)} \tag{4.56}$$

where V_{Bus_i} denotes the magnitude of voltages at the ns buses present in the selected set, to be defined according to the PMUs available.

To estimate an equivalent mechanical power behaviour, the quasi-steady state conditions both before and after the perturbation may be exploited. In steady state, it is possible to write

$$P_{e_A}^{st} = P_{mov_A}^{st} \tag{4.57}$$

where the superscript st denotes the steady-state.

As P_L was already estimated with Equation 4.53 and P_{e_A} is measured (as assumed in Figure 4.10), only P_m and P_{losses} are left to be estimated in Equation (4.51). Here, P_m and P_{losses} will be estimated together, such that for the sake of simplicity the variable

$$P_{ML} = \sum_{n=1}^{n_g} P_m - \sum_{n=1}^{n_{tl}} P_{losses} \tag{4.58}$$

is defined.

Hence, substituting Equations (4.57) and (4.58) in Equation 4.51,

$$P_{e_A}(t) = P_{ML} - \sum_{n=1}^{n_l} P_L \tag{4.59}$$

Defining $st1$ the steady state before the perturbation and $st2$ the steady-state after the perturbation, it is possible to rewrite Equation (4.59) in the following forms

$$P_{ML_A}^{st1} = P_{e_A}^{st1} + \sum_{n=1}^{n_l} P_L^{st1} \tag{4.60}$$

$$P_{ML_A}^{st2} = P_{e_A}^{st2} + \sum_{n=1}^{n_l} P_L^{st2} \tag{4.61}$$

such that the quantities $P_{ML_A}^{st1}$ and $P_{ML_A}^{st2}$ can be calculated in terms of the measured $P_{e_A}^{st1}$ and $P_{e_A}^{st2}$, and

the estimated $\sum_{n=1}^{n_l} P_L^{st1}$ and $\sum_{n=1}^{n_l} P_L^{st2}$.

The behaviour of P_{ML_A} during the time window between the points $P_{ML_A}^{st1}$ and $P_{ML_A}^{st2}$ can be estimated according to the droop characteristics of the area. Assuming a slow response of $\sum P_m(t)$ in relation to $P_{e_A}(t)$ (note that is not the same of assuming a slow response of $P_{mov_A}(t)$), it is possible to project a linear behaviour between the two steady-states and obtain $P_{ML_A}(t)$. This can be done in two different ways.

The first approach assumes that the major change in the equivalent mechanical power ($\sum_{n=1}^{n_g} P_m(t)$) happens only in the few seconds following the perturbation, which can be observed in $P_{e_A}(t)$. Therefore, measuring the time constant t_i of the major variation of $P_{e_A}(t)$ enables to project $P_{ML_A}(t)$ according to the illustrative Figure 4.11.

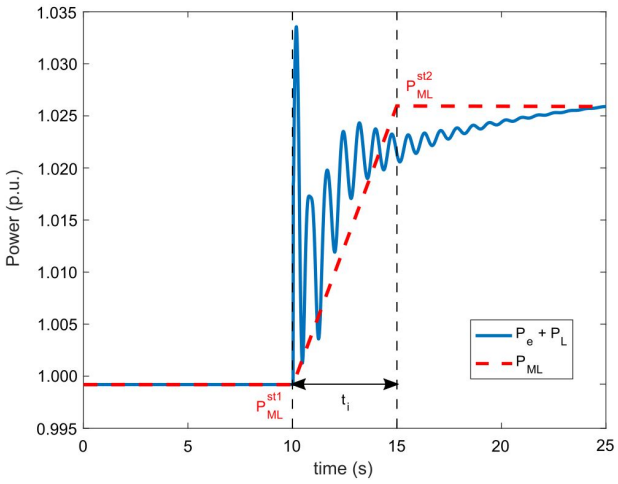

Figure 4.11: *Projected* $P_{ML}(t)$

The disadvantage of this first approach is that it needs visual inspection or defining a criteria for determining the time constant t_i.

A second possible way to obtain $P_{ML_A}(t)$ is related to the droop of the machines present in the area of study. The droop can be defined as a percentage of speed regulation, i.e., it determines the percentage of frequency variation according to a percentage of mechanical power variation, according to Figure 4.12.

The expression that models the droop (R) is

$$R = \frac{\Delta f}{\Delta P_m} \tag{4.62}$$

where Δf and ΔP_m are the frequency and the mechanical power variation of the unit under study. Assuming a value for R, and knowing Δf, it is possible to estimate ΔP_m in Equation (4.62). Typical values of R usually range from 2% to 10%.

In the present case, measuring Δf with PMUs and assuming typical values for R, it is possible to obtain ΔP_{ML_A}. Starting from Equation (4.62),

$$R_A = \frac{\Delta f_A}{\Delta P_{ML_A}} \rightarrow R_A = \frac{f_A(t) - f_A^{st1}}{P_{ML_A}(t) - P_{ML_A}^{st1}} \tag{4.63}$$

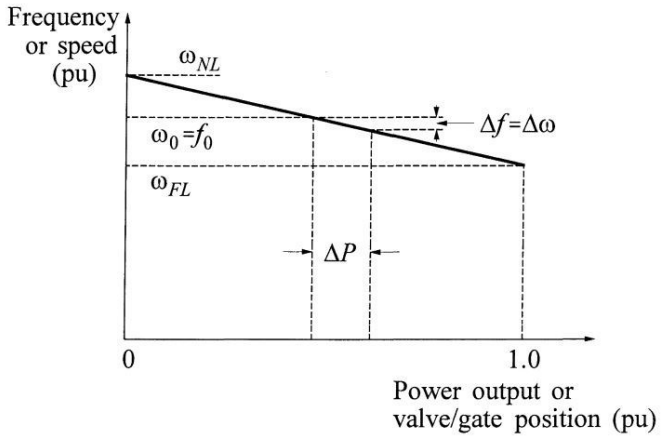

Figure 4.12: *Ideal steady-state characteristics of a governor with speed droop, [42]*

it is possible to rewrite as

$$P_{ML_A}(t) = \frac{RP_{ML_A}^{st1} + f_A(t) - f_A^{st1}}{R} \tag{4.64}$$

The disadvantage of this second approach is that it requires the knowledge of typical values of R for the studied area. At second, losses are considered when $P_{ML_A}^{st1}$ was defined, but are neglected during the procedure to determine $P_{ML_A}(t)$ defined in Equation (4.64). Hence, they need to be taken into account considering an additional percentage of the total $P_{ML_A}(t)$ or otherwise $P_{ML_A}(t)$ may be underestimated.

This method can be used as an auxiliary method to the inertia estimation methods proposed previously in Section 4.2. The results obtained are presented in Section 5.4.2.

4.2.6 Dynamic matrix method

4.2.6.1 Contextualization

This approach is based on the method presented in [35], [155], that combines model/topoology knowledge with PMU measurements in ambient conditions for parameter estimation. In [155], the covariance matrices related to voltage and currents measured are used to provide information on the proximity to instability. The work was adapted in [35], where inertia and damping constants are assumed as known to identify the dynamic state Jacobian matrix, useful for applications like identification of topology change.

Here, the idea is to adapt the method for the aim of this thesis: estimate inertia from PMU measurements under normal load variations. In that case, a perturbation is not needed to identify inertia, but the method is able to monitor the inertia in normal conditions. For this estimation to be practical, three main items are required:

- The topology (admittance matrix) of the grid;
- An estimation of a reference load (or mean load);
- The dynamic equivalent seen from each measurement point, i. e., the transient reactances and the previous inertia estimations for each equivalent generator. This parameters can be obtained with one of the MEM presented in Section 4.2.2.

With the requirements fulfilled, it is possible to estimate the inertia continuously following normal load variations. If, due to a perturbation, the parameters of the area or the unit represented by the dynamic equivalent changes, the MEM needs to be executed again.

4.2.6.2 Methodology

The method is modelled in terms of the internal nodes of each generator. To do so, the admittance matrix of the system needs to be modified to include loads and transient reactances in a first moment, and then is reduced around the internal nodes. This procedure is shown in Appendix C.

The motion equation of the $i-th$ synchronous generator presented in (2.15) can be expressed as a second-order system of equations,

$$\begin{cases} \dot{\delta}_i & = \omega_i \quad p.u \\ M_i\dot{\omega}_i & = P_{m_i} - P_{e_i} - D_i\omega_i \quad p.u. \end{cases} \tag{4.65}$$

where the subscript i denotes each of the n generators of the system, $M_i = \frac{2H_i}{\omega_0}$ and the other variables were previously defined in Section 2.2. The electrical power P_{e_i} here is obtained with

$$P_{e_i} = \sum_{j=1}^{n}[E_iE_j(G_{ij}\cos(\delta_i - \delta_j) + B_{ij}sin(\delta_i - \delta_j))] \quad p.u. \tag{4.66}$$

where E and δ are the magnitude and phase angle of the internal voltage of each machine, and G_{ij} and B_{ij} are the conductance and susceptance terms of the reduced admittance matrix that connects each of the machines.

The System (4.65) is represented considering an infinite bus as a static reference for angle and speed of the generators. The same equations can be represented in the COI frame, assuming the angle of the COI as a rotating reference for the generators [156]. This procedure is shown in Appendix C. This model has been traditionally used for direct stability determination, among other models, because it deals with path-dependent terms in a easier way [46].

The COI angle and the COI frequency were already defined in Section 2.2.3. Here, they are repeated for convenience, but expressed in terms of M (instead of H) and considering that all the generators have the same nominal power (for simplicity of the following deductions). Hence,

$$\delta_{COI} \triangleq \frac{\sum_{i=1}^{n} S_{n_i}M_i\delta_i}{\sum_{i=1}^{i} S_{n_i}M_i} \quad rad \tag{4.67}$$

$$\omega_{COI} \triangleq \frac{\sum_{i=1}^{n} S_{n_i}M_i\omega_i}{\sum_{i=1}^{i} S_{n_i}M_i} \quad rad/s \tag{4.68}$$

All the rotor angles and speed of the system can be expressed by $\tilde{\delta}_i = \delta_i - \delta_{COI}$ and $\tilde{\omega}_i = \omega_i - \omega_{COI}$.

The system of equations becomes

$$\begin{cases} \dot{\tilde{\delta}}_i & = \tilde{\omega}_i \quad p.u \\ M_i\dot{\tilde{\omega}}_i & = P_{m_i} - P_{e_i} - D_i\tilde{\omega}_i - \frac{M_i}{M_T}P_{COI} \quad p.u. \end{cases} \tag{4.69}$$

where $M_T = \sum_i^n M_i$ is the sum of all inertias and the term P_{COI} can be defined as

$$P_{COI} = \sum_{i=1}^{n} [P_{m_i} - P_{e_i}] \quad p.u. \tag{4.70}$$

and represents the power imbalance at the COI, a function of all n generators.

The motion of the n^{th} generator can be determined as a function of the others through Equations (4.67) and (4.68), as presented in Appendix C. The final expressions are:

$$\tilde{\delta}_n = -\frac{\sum_{k=1}^{n-1} M_k \tilde{\delta}_k}{M_n} \quad rad \tag{4.71}$$

$$\tilde{\omega}_n = -\frac{\sum_{k=1}^{n-1} M_k \tilde{\omega}_k}{M_n} \quad rad/s \tag{4.72}$$

Expressions (4.71) and (4.72) can be substituted in the System (4.69) to reduce the order of the system, that becomes

$$\begin{cases} \dot{\tilde{\delta}}_k & = \tilde{\omega}_k \quad p.u. \\ M_k \dot{\tilde{\omega}}_k & = P_{m_k} - P_{e_k} - D_k \tilde{\omega}_k - \frac{M_k}{M_T} P_{COI} \quad p.u. \end{cases} \tag{4.73}$$

where $k = 1...n-1$ is the new index. Note that P_{e_k} is a function of $\tilde{\delta}_n$, and consequently P_{COI} is also. Hence, when calculating P_{e_k}, the variable $\tilde{\delta}_n$ must be substituted by Equation (4.71).

Considering the constant impedance model for loads, and assuming a Gaussian variation around a base case loading, the load variation can be represented in the diagonal elements of the reduced admittance matrix

$$Y_{ii}^{new} = Y_{ii}(1 + \sigma_i \xi_i) \angle \phi_{ii} \quad p.u. \tag{4.74}$$

where σ_i is the standard deviation of load variation and ξ_i is a independent standard Gaussian variable, that comes from the representation of the stochastic variation as a Wiener Process [35], [157]. As it can be seen, the variation affects only the magnitude of $Y(i,i)$, while the phase angle remains unchanged.

Applying Equation (4.74) in (4.66), the power consumed by the load connect to the node i due to the load variation is

$$P_{e_i} = E_i^2 G_{ii} \sigma_i \xi_i \quad p.u. \tag{4.75}$$

an expression that does not depend on the variables at the other buses. Hence, it is possible to include the effect of (4.75) separately in the system (4.73) without the need of modifying the expression of P_{e_k}, that accounts the power consumed by the base loads. This makes the following mathematical deductions easier.

Considering Equation (4.75) into system (4.73), the model becomes

$$\begin{cases} \dot{\tilde{\delta}}_k & = \tilde{\omega}_k \\ M_k \dot{\tilde{\omega}}_k & = P_{m_k} - P_{e_k} - D_k \tilde{\omega}_k - E_k^2 G_{kk} \sigma_k \xi_k - \frac{M_k}{M_T} P_{COI} + - \frac{M_k}{M_T} P_{L_{COI}} \end{cases} \tag{4.76}$$

where $P_{L_{COI}} = \sum_i^n E_i^2 G_{ii} \sigma_i \xi_i$, and all the other variables has been previously defined.

The system (4.76) can be linearized around a stable steady state point and represented as

$$\begin{bmatrix} \tilde{\boldsymbol{\delta}} \\ \tilde{\boldsymbol{\omega}} \end{bmatrix} = \begin{bmatrix} \mathbf{0} & \mathbf{I} \\ \mathbf{J} & \mathbf{K} \end{bmatrix} \begin{bmatrix} \tilde{\boldsymbol{\delta}} \\ \tilde{\boldsymbol{\omega}} \end{bmatrix} + \begin{bmatrix} 0 \\ -\mathbf{M}^{-1}\mathbf{E}^2\mathbf{G}\boldsymbol{\Sigma} \end{bmatrix} \boldsymbol{\xi} \tag{4.77}$$

where $\tilde{\boldsymbol{\delta}} = [\tilde{\delta}_1, ..., \tilde{\delta}_{n-1}]^T$, $\tilde{\boldsymbol{\omega}} = [\tilde{\omega}_1, ..., \tilde{\omega}_{n-1}]^T$, $\mathbf{M} = diag([M_1, ..., M_{n-1}])$, $\mathbf{E} = diag([E_1, ..., E_{n-1}])$, $\mathbf{G} = diag([G_{11}, ..., G_{(n-1,n-1)}])$, $\boldsymbol{\Sigma} = diag([\sigma_1, ..., \sigma_{n-1}])$, and $\boldsymbol{\xi} = [\xi_1, ...\xi_{n-1}]^T$.

The matrices $\mathbf{0}$ and $\mathbf{I}$ are $(n-1) \times (n-1)$ null and identity matrices, respectively.

The matrix $\mathbf{J}$ can be obtained by

$$\mathbf{J} = -\mathbf{M}^{-1}(\frac{\partial \mathbf{P_e}}{\partial \tilde{\boldsymbol{\delta}}})_{COI} \tag{4.78}$$

where

$$(\frac{\partial \mathbf{P_e}}{\partial \tilde{\boldsymbol{\delta}}})_{COI} = (\frac{\partial \mathbf{P_e}}{\partial \tilde{\boldsymbol{\delta}}} + \mathbf{M}\frac{1}{M_T}\frac{\partial P_{COI}}{\partial \tilde{\boldsymbol{\delta}}}) \tag{4.79}$$

and the derivatives $\frac{\partial \mathbf{P_e}}{\partial \tilde{\boldsymbol{\delta}}}$ and $\frac{\partial P_{COI}}{\partial \tilde{\boldsymbol{\delta}}}$ can be found in Appendix C.

The matrix $\mathbf{K}$ can be obtained by

$$\mathbf{K} = diag([-\frac{D_1}{M_1}, ..., -\frac{D_{n-1}}{M_{n-1}}]) \tag{4.80}$$

Coming back to System (4.77), the same equations can be represented in a standard simplified form as

$$\dot{\mathbf{x}} = \mathbf{A}\mathbf{x} + \mathbf{B}\boldsymbol{\xi} \tag{4.81}$$

where $\mathbf{x} = [\boldsymbol{\delta}, \boldsymbol{\omega}]^T$, $\mathbf{A} = \left[\begin{smallmatrix} 0 & I \\ J & K \end{smallmatrix}\right]$ and $\mathbf{B} = [0, -\mathbf{M}^{-1}\mathbf{E}^2\mathbf{G}\boldsymbol{\Sigma}]^T$.

If the system is stable, an important property can be exploited, based on the stationary covariance matrix $\mathbf{C_{xx}} = \left[\begin{smallmatrix} \mathbf{C}_{\tilde{\delta}\tilde{\delta}} & \mathbf{C}_{\tilde{\delta}\tilde{\omega}} \\ \mathbf{C}_{\tilde{\omega}\tilde{\delta}} & \mathbf{C}_{\tilde{\omega}\tilde{\omega}} \end{smallmatrix}\right]$. This matrix is normally unknown in practice, but approximations can be obtained as it will be discussed later in this section. As the method here described is proposed to identify inertia following small load variations under normal operation, stability can be assumed, such that in that conditions the matrix $\mathbf{C_{xx}}$ satisfies the so-called Lyapunov Equation [158],

$$\mathbf{A}\mathbf{C_{xx}} + \mathbf{C_{xx}}\mathbf{A}^T = -\mathbf{B}\mathbf{B}^T \tag{4.82}$$

Combining equations (4.77) and (4.82),

$$\begin{bmatrix} \mathbf{0} & \mathbf{I} \\ \mathbf{J} & \mathbf{K} \end{bmatrix} \begin{bmatrix} \mathbf{C}_{\tilde{\delta}\tilde{\delta}} & \mathbf{C}_{\tilde{\delta}\tilde{\omega}} \\ \mathbf{C}_{\tilde{\omega}\tilde{\delta}} & \mathbf{C}_{\tilde{\omega}\tilde{\omega}} \end{bmatrix} + \begin{bmatrix} \mathbf{C}_{\tilde{\delta}\tilde{\delta}} & \mathbf{C}_{\tilde{\delta}\tilde{\omega}} \\ \mathbf{C}_{\tilde{\omega}\tilde{\delta}} & \mathbf{C}_{\tilde{\omega}\tilde{\omega}} \end{bmatrix} \begin{bmatrix} \mathbf{0} & \mathbf{J}^T \\ \mathbf{I} & \mathbf{K}^T \end{bmatrix} + \begin{bmatrix} \mathbf{0} \\ -\mathbf{M}^{-1}\mathbf{E}^2\mathbf{G}\boldsymbol{\Sigma} \end{bmatrix} \begin{bmatrix} \mathbf{0} & -\mathbf{M}^{-1}\mathbf{E}^2\mathbf{G}\boldsymbol{\Sigma} \end{bmatrix} = 0 \tag{4.83}$$

From Equation (4.83), its possible to write:

$$\mathbf{C}_{\tilde{\delta}\tilde{\omega}} + \mathbf{C}\tilde{\omega}\tilde{\delta} = \mathbf{0} \tag{4.84}$$

$$\mathbf{J}\mathbf{C}_{\tilde{\delta}\tilde{\delta}} + \mathbf{K}\mathbf{C}_{\tilde{\omega}\tilde{\delta}} + \mathbf{C}_{\tilde{\omega}\tilde{\omega}} = \mathbf{0} \tag{4.85}$$

$$\mathbf{J}\mathbf{C}_{\tilde{\delta}\tilde{\omega}} + \mathbf{K}\mathbf{C}_{\tilde{\omega}\tilde{\omega}} + \mathbf{C}_{\tilde{\omega}\tilde{\delta}}\mathbf{J}^T + \mathbf{C}_{\tilde{\omega}\tilde{\omega}}\mathbf{K}^T + \mathbf{\Psi} = 0 \tag{4.86}$$

where $\mathbf{\Psi} = [-\mathbf{M}^{-1}\mathbf{E}^2\mathbf{G}\mathbf{\Sigma}][-\mathbf{M}^{-1}\mathbf{E}^2\mathbf{G}\mathbf{\Sigma}]^T$.

The term $\mathbf{K}\mathbf{C}_{\tilde{\omega}tilde\delta}$ in Equation (4.85) is typically negligible. This assumption was made in [35] and verified in the tests with the method. Hence, substituting Equation (4.78) in Equation (4.85) and neglecting $\mathbf{K}\mathbf{C}_{\tilde{\omega}\tilde{\delta}}$ [35], it's possible to obtain

$$\mathbf{M} = (\frac{\partial \mathbf{P_e}}{\partial \tilde{\boldsymbol{\delta}}})_{COI}\mathbf{C}_{\tilde{\delta}\tilde{\delta}}\mathbf{C}_{\tilde{\omega}\tilde{\omega}}^{-1} \quad [s^2] \tag{4.87}$$

The matrix $(\frac{\partial \mathbf{P_e}}{\partial \tilde{\boldsymbol{\delta}}})_{COI}$ can be obtained from the Equations described in the Appendix C, as function of the known topology and outputs of a previous execution of a MEM.

The covariance matrix $C_{\tilde{\delta}\tilde{\delta}}$ can be obtained from

$$C_{\tilde{\delta}\tilde{\delta}} = \begin{bmatrix} C_{\tilde{\delta}_1\tilde{\delta}_1} & C_{\tilde{\delta}_1\tilde{\delta}_1} & \cdots & C_{\tilde{\delta}_1\tilde{\delta}_n} \\ C_{\tilde{\delta}_2\tilde{\delta}_1} & C_{\tilde{\delta}_2\tilde{\delta}_2} & \cdots & C_{\tilde{\delta}_2\tilde{\delta}_n} \\ \vdots & \vdots & \ddots & \vdots \\ C_{\tilde{\delta}_{n-1}\tilde{\delta}_1} & C_{\tilde{\delta}_{n-1}\tilde{\delta}_2} & \cdots & C_{\tilde{\delta}_{n-1}\tilde{\delta}_{n-1}} \end{bmatrix} \tag{4.88}$$

The matrix $C_{\tilde{\omega}\tilde{\omega}}$ can be defined in a similar way.

The individual terms of (4.88) can be obtained from

$$C_{\tilde{\delta}_i\tilde{\delta}_j} = E[(\tilde{\delta}_i - \mu_i)(\tilde{\delta}_j - \mu_j)] \tag{4.89}$$

where μ_i is the mean of $\tilde{\delta}_i$.

For the practical proposed application, it is unfeasible to use Equation (4.89) because of limited data. Hence, an approximation must be done considering the window of data available. In this conditions, the sample covariance matrices $\mathbf{Q}_{\tilde{\delta}\tilde{\delta}}$ and $\mathbf{Q}_{\tilde{\omega}\tilde{\omega}}$ can be calculated by

$$\mathbf{Q}_{\tilde{\delta}_k\tilde{\delta}_j} = \frac{1}{N-1}\sum_{r=1}^{N}(\tilde{\delta}_{rk} - \overline{\tilde{\delta}_k})(\tilde{\delta}_{rj} - \overline{\tilde{\delta}_j}) \tag{4.90}$$

$$\mathbf{Q}_{\tilde{\omega}_k\tilde{\omega}_j} = \frac{1}{N-1}\sum_{r=1}^{N}(\tilde{\omega}_{rk} - \overline{\tilde{\omega}_k})(\tilde{\omega}_{rj} - \overline{\tilde{\omega}_j}) \tag{4.91}$$

where the overline denotes the sample mean of the referred quantity and N is the number of samples.

Hence, $\mathbf{M}$ can be estimated from Equation (4.87) in relation to the sample interval selected to calculate $\mathbf{Q}_{xx}$, for generators $k = 1...n-1$. The constant $\mathbf{M}$ can be estimated in time considering a sliding window of selected samples.

The constant M of the $n-th$ generator can be calculated in terms of the M constants of the $n-1$ generators previously calculated and the samples of $\tilde{\boldsymbol{\delta}}$, solving Equation (4.71) through Least-Squares, as follows:

$$M_n = (\tilde{\delta}_{n_r}^T\tilde{\delta}_{n_r})^{-1}\tilde{\delta}_{n_r}^T(-\sum_{k=1}^{n-1}M_k\tilde{\delta}_{k_r}) \quad [s^2] \tag{4.92}$$

where $r = 1...N$ and N is the number of samples considered.

This method was used to produce part of the results presented in Section 5.5.2. The advantage is the possibility of identifying inertia under normal load variations without the necessity of estimating the load behaviour. The disadvantage is the high number of requirements.

4.3 Summary of the methods

This subsection present a summary of all the methods presented, enumerating the general assumptions taken, the main requirements in terms of variables and measurement points, and the procedure necessary to estimate the inertia in each method. Advantages and disadvantages are presented in Section 5 of numerical results, together with specific assumptions taken in each test.

General assumptions:

- The active and reactive power exiting bus i through the interconnection line on time t can be calculated from the measured variables $\mathbf{V}_i(t)$ and $\mathbf{I}_i(t)$.
- The moving power in comparison to the electromagnetic power generated by synchronous machines has a slow behavior, such that $\Delta P_i(t) \approx P_i^{st} - P_i(t)$, where P_i^{st} is the steady state value of the active power P_i before the perturbation. An alternative is to use the auxiliary method presented in Subsection 4.2.5.

Specific characteristics of the Least Squares Method for inertia estimation:

- Further assumptions:

  - The difference between the angle of the internal voltage and the measured voltage angle is negligible $(\delta_i(t) \approx \theta_i(t))$.

- Requirements to estimate H_i:

  - One measurement point, at the terminal of each synchronous machine;

  - $V_i\angle\theta_i$, $I_i\angle\alpha_i$;

- Procedure:

  - Solve directly the Swing Equation filled with the measured data through Least Squares method.

Specific characteristics of the Iterative-IME method:

- Assumptions:

  - The variation $\Delta V_i(t)$ of the measured voltage $V_i(t)$ with respect to a change in $\Delta\delta$ can be linearized about an equilibrium point 0;

  - The measurement points are in the same radial path;

- Requirements to estimate H_i:

  - Two measurement points in a radial path;

  - $V_i\angle\theta_i$,$I_i\angle\alpha_i$ with $i = 1, 2$;

- Procedure:

  - Obtain the internal parameters of the equivalent machine i, i.e., the transient reactance and the internal voltage angle to build a dynamic equivalent;

  - Estimate the inertia solving the swing equation related to the equivalent machine through the Least Squares method.

Specific characteristics of the "Variance" method:

- Assumptions:

  - The expressions are stated fitting $E \approx constant$ and $Var(E^2) \approx 0$.

- Requirements to estimate H_i:

  - One measurement point;

  - $V_i \angle \theta_i$, $I_i \angle \alpha_i$;

- Procedure:

  - Obtain the internal parameters of the equivalent machine i, i.e., the transient reactance and the internal voltage angle to build a dynamic equivalent;

  - Estimate the inertia solving the swing equation related to the equivalent machine through the Least Squares method.

Specific characteristics of EKF method:

- Assumptions:

  - The dynamic of the studied system can be represented by the classical second-order differential equations for synchronous machines;

- Requirements to estimate H_i:

  - One measurement point, at the terminal of the synchronous machine;

  - P_i, Q_i;

- Procedure:

  - Prediction-Correction method that compares estimations produced with a chosen process model and measurements acquired from the grid.

Specific characteristics of the inertia estimation with system reduction method:

- Assumptions:

  - The static elements (lines and transformers) of the reduced portion of the grid are considered in steady state during the period of analysis;

- Requirements to estimate H_i:

  - Knowledge of the network topology (Y matrix);

  - Two or more measurement points*;

  - $V_i\angle\theta_i$, $I_i\angle\alpha_i$;

- Procedure:

  - Reduce the system around the measurement points using the Ward equivalent method;

  - Obtain the internal parameters of the equivalent machine i through the "Variance" method;

  - Estimate the inertia solving the swing equation related to the equivalent machine through the Least Squares method.

*Obs.: Depending on the boundaries of the area to be represented. If there is only one boundary bus, only one measurement point is necessary to estimate the equivalent inertia of this area, due to the use of the "Variance method", whose related assumptions and requirements are still valid. However, the proposed method for system reduction is useful to study areas with more than one boundaries and or areas with PMUs inside, from which additional information can be achieved to improve the inertia estimations.

Specific characteristics of the dynamic matrix method:

- Assumptions:

  - The system is stable and under normal load variations;

  - The system can be linearized around an equilibrium point and represented as with the state-space model.

- Requirements to estimate H_i:

  - Knowledge of the network topology;

  - An estimation of a reference load (or mean load);

  - The outputs of a previously performed MEM, i.e., the transient reactance and the previous inertia estimated for the equivalent generator.

  - One measurement point;

  - $V_i\angle\theta_i$, $I_i\angle\alpha_i$;

- Procedure:

  - Reduce the system around the measurement points using the Ward equivalent method;

  - Obtain the internal parameters of the equivalent machine i through the "Variance" method;

  - Calculate the Jacobian of the system, including the previous load reference point and the inertia previously estimated;

  - Calculate the covariance matrices of the estimated rotor angle and speed;

  - Estimate the inertia through Equation (4.87).

4.4 Conclusion of the Chapter

In this chapter the possibilities of estimating inertia in power systems using synchrophasor measurements were discussed. A literature review was presented, divided in the main types of approaches found. The methodology proposed in this thesis was explained, together with the methods studied and proposed.

CHAPTER 5

Numerical results

This Chapter presents the numerical results obtained with the application of the methods proposed in Chapter 4. The Chapter is divided in different sections, each one containing a different study conduced according to the guiding specific objectives enumerated in Section 1.2 and the Topics defined in Chapter 4, here recalled in a short summary:

- Topic 1: Inertia estimation considering a PMU installed in the terminals of the generator;
- Topic 2: Inertia estimation considering a PMU installed at the boundary of an area;
- Topic 3: Inertia estimation considering spread PMUs;
- Topic 4: Inertia estimation following normal load variations in normal operating conditions.

To investigate the Topics, every study was performed according to the following procedure:

1. Simulate the response of the test system according to a perturbation or normal load variations;
2. Assume the presence of PMUs installed in specific points of the grid, according to the study;
3. Save the simulated data related to the PMUs considered;
4. Process the data and apply the methods described in Chapter 4;
5. Analyze the results.

The organization of this chapter is as follows:

In Section 5.1, preliminary studies are presented evaluating base cases for identifying the main challenges on inertia estimation. Topic 1 is investigated, with the aim of estimating inertia considering PMUs installed at terminal buses of generators.

In Section 5.2, the idea was to estimate inertia considering PMUs installed at boundary buses of a portion of the grid, the purpose of Topics 2 and 3. In addition, the section also brings further observations regarding Topic 1 too.

In Section 5.3, results are presented considering the integration of RES-based generation. Inertia estimation was performed from the point of view of Topics 1 to 3.

In Section 5.4, complementary studies are presented. In the first study of this section, a probe is considered to generate a measurable signal to estimate inertia. In the second, the moving power estimation method proposed in Section 4.2.5.3 is tested.

In Section 5.5, normal load variations are studied, as proposed in Topic 4. Two different approaches are considered and comparisons are carried.

The Section 5.6 presents the final conclusions of the Chapter, summarizing the results obtained and making comparisons between the methods.

5.1 Preliminary studies

The aim of Topic 1 is to evaluate inertia of a generator considering a PMU installed at its terminals, and for this purpose the methods presented in Sections 4.2.1 and 4.2.2 were tested with simulated data in these preliminary studies.

In Subsection 5.1.1, Study 1 presents the application of the direct Least-Squares method for estimating the inertia of a radial system. In Subsection 5.1.2, Study 2 propose the IME method to improve the accuracy of the results obtained in Study 1. In Subsection 5.1.3, Study 3 presents a comparison between the MEM studied, evaluated with two different perturbations.

5.1.1 Study 1 - Least-squares direct method

This subsection introduces the first study approaching Topic 1. The Least-Squares direct method, presented in Section 4.2.1, is tested for estimating inertia of a generator from measurements acquired by PMUs installed at its terminals.

For this study, a simulation was performed in Matlab, with the following details:

- Test-system used: Test-system A presented in Section D.1, chosen due to its simplicity.
- Simulation software: Euler numerical integration method as proposed in [41], implemented in Matlab.
- Perturbation simulated: disconnection of Generator 1 at t=0s and reconnection at t=0.2s;
- Model used for the synch. machines: Second order model (as presented in Subsection 2.2.1);
- Machine parameters: according to Table 5.1;
- Model of the loads: constant impedance;
- Losses: neglected;

- The sampling time used is 10ms. The total simulation lasts 10s.

The values of inertia (H), damping (D) and transient reactance (x'_d) for both generators used in the simulations can be seen in Table 5.1. The values are merely theoretical and do not reproduce real cases.

Table 5.1: *Study 1 - Machine parameters*

	H[s]	**D**	$\mathbf{x_i[p.u.]}$
$\mathbf{G_1}$	30	10	0.054
$\mathbf{G_2}$	300	50	0.054

During the simulations, the following variables coming from the generators were recorded: internal voltage phasors ($E_i\angle\delta_i$), generated power (P_i) and mechanical power (P_{m_i}) where $i = 1, 2$. These variables are not measurable by PMUs, but here they were recorded for testing the preliminary tests with the studied method. From the interconnection line, assuming PMUs installed at buses 1 and 2, the voltage phasors ($V_1\angle\theta_1$ and $V_2\angle\theta_2$) at the buses and the power flows (P_{12} and P_{21}) were recorded. Figure 5.1 depicts the recorded variables.

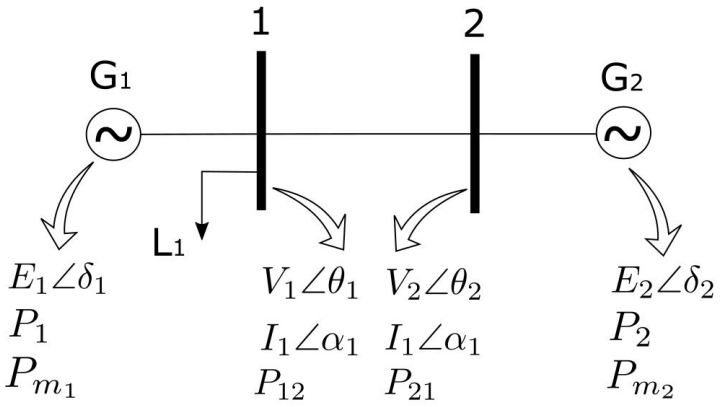

Figure 5.1: *Study 1 - Simulated system and recorded variables*

The results of the simulation are presented in Figure 5.2. As it can be seen in Figure 5.2(a), the speed ω_1 increases after G1 is disconnected, while ω_2 decreases. When G1 is reconnected to the grid, at t=0.2 s, the situation changes and ω_1 rapidly decreases, meanwhile ω_2 rapidly increases. This happens because G2 act as a generator to feed the load while G1 was disconnected. When G1 is reconnected, G2 starts to perform as a motor to counteract the power generated by an accelerated G1, until they reach a steady-state and only G1 feeds the load (that is installed at bus 1).

5.1.1.1 Results of Study 1

A first test was performed applying the Least-Squares method described in Subsection 4.2.1 with the data coming from the generators, i.e., applying δ_i, P_i and P_{m_i} directly in Equation (4.1). This test is identified as "Study 1 - Test 1". In this conditions, H_i and D_i were estimated with less than 1% of error, which validates the method in the situation considered. However, this test does not take into consideration practical conditions, as rotor angles δ are not directly measurable by PMUs.

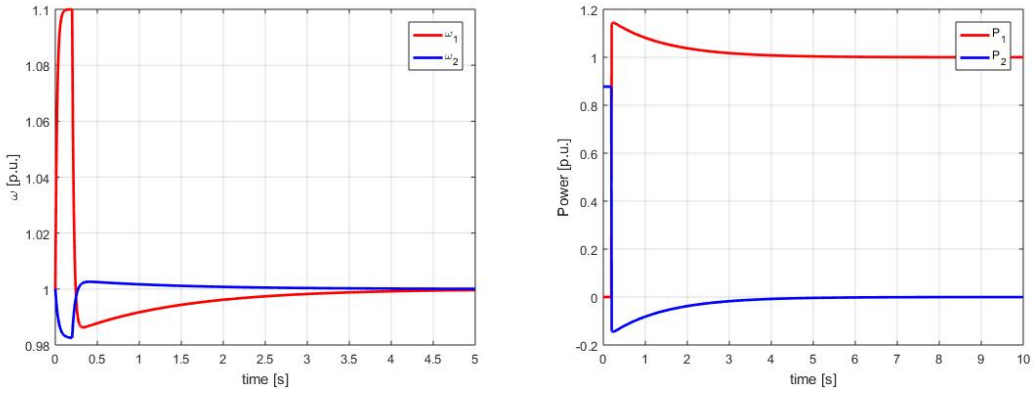

(a) Speed behaviour

(b) Power generated

Figure 5.2: *Study 1 - Simulations*

In a second test, still non-practical, the recorded data of the power flow from bus 1 to bus 2 were considered as the generated power of Generator 1 ($P_1 \approx P_{12}$), and the same was considered in the reverse direction $P_2 \approx P_{21}$. The rotor angles δ_i were used to complete the set of required data to apply the method. In these conditions, the results presented in Table 5.2 were estimated. This test is identified as "Study 1 - Test 2".

Table 5.2: *Study 1 - Test 2*

	Simulated		**Estimated**	
	H [s]	**D**	**H [s]**	**D**
$\mathbf{G_1}$	30	10	11.9438	3.0883
$\mathbf{G_2}$	300	50	300.0000	50.0000

It can be seen that the estimations for Generator 1 are not accurate. In comparison to the Test 1, it is noticeable that the load interfered. The assumption $P_1 = P_{12}$ didn't consider the presence of the load at bus 1, such that it doesn't reflect the true generated power by the studied machine. Meanwhile, the estimations for Generator 2 presented an error of less then 1%.

To follow the direction of a practical approach, a third test is performed taking out one the non-practical assumption of monitoring rotor angles. Hence, the phase angles of the terminal voltages at buses 1 and 2 (θ_1 and θ_2) were used as an approximated measure of the internal voltage angles (δ_1 and δ_2) in the (4.1). The assumption of $P_i = P_{ij}$ is still kept for this test. The results are presented in Table 5.3, and this test is identified as "Study 1 - Test 3".

Table 5.3: *Study 1 - Test 3*

	Simulated		**Estimated**	
	H [s]	**D**	**H [s]**	**D**
$\mathbf{G_1}$	30	10	-3.5620	-0.0198
$\mathbf{G_1}$	300	50	9.6978	0.0460

As it can be seen, the results are very far from the true values. Regarding Generator 1, the assumptions lead to negative estimations. Comparing to Generator 2, the only difference between the assumptions about the topology of both sides is the presence of the load at bus 1. The voltage dependence of the load affects the assumption $P_1(t) = P_{12}(t)$ leading to different signal in relation to the change in $\theta_i(t)$; this implies negative estimations for inertia and damping. This issue is further explored in Studies 4, 6 and 11, in Subsections 5.2.1, 5.2.3 and 5.4.2, respectively.

Regarding Generator 2, the approximation $\delta_1 \approx \theta_1$ also led to high errors. Hence, the assumption that the difference between the angle of the internal voltage and the angle of the measured voltage at the terminal bus is negligible (stated in Section 4.2.1) does not hold. The difference between δ_i and θ_i comes from the fact that the transient reactance of each machine is not taken into account, and it is clearly interfering in the results, showing the need of estimating it.

5.1.1.2 Conclusions of Study 1

This section presented preliminary tests where the Least Squares method was applied to solve the swing equation to estimate inertia and damping of synchronous machines.

The method was only accurate when data from the rotor angle or internal voltage angle were used. When data coming from the terminal buses were used, the method failed to estimate the constants of interest with acceptable accuracy.

The main reason identified was the approximation that considered the difference between rotor angles and the phase angles at terminal buses as negligible, which does not hold, due to the effect of transient reactances. Hence, it was identified the necessity of studying methods to build dynamic equivalents, mainly estimating the transient reactance of the studied generator. Moreover, the voltage dependence of the load was also identified as an issue. The following studies approach these problems.

5.1.2 Study 2 - IME method

This subsection presents a second study involved with Topic 1, approaching one of the issues identified in the previous section. For this study, the Test-system B presented in Subsection D.2 is used. The system is similar to Test-system A, with the difference that the load at bus 1 was excluded and now a generator feeds a motor. These modifications were done to approach the issue identified in Study 1 regarding the negligence of the effect of the transient reactances, without the interference of the load behaviour as seen in the same study. The impact of the load, instead, is further investigated in Studies 4, 6 and 11, in Subsections 5.2.1, 5.2.3 and 5.4.2, respectively.

The details of the simulations for this study are:

- Test-system used: Test-system B presented in Section D.2.
- Simulation software: Euler numerical integration method as proposed in [41], implemented in Matlab.
- Perturbation simulated: disconnection of Generator 1 at t=0s and reconnection at t=0.2s;
- Model used for the synch. machines: Second order model with damping (as presented in Subsection 2.2.1);
- Machine parameters: according to the case;

- Model of the load: dynamic (motor);
- Losses: neglected;
- Sampling time: 10ms. The total simulation last 10s.

Two different tests were simulated. The first one, identified as "Study 2 - Test 1", considered the parameters presented in Table 5.1, as in Study 1. A second test ("Study 2 - Test 2") considered the parameters presented in Table 5.4, a variation produced to test the IME method.

Table 5.4: *Study 2 - Test 2 - Machine parameters*

	H[s]	**D**	$\mathbf{x_i[p.u.]}$
$\mathbf{G_1}$	50	20	0.07
$\mathbf{G_2}$	500	60	0.07

The dynamic response of the synchronous machines can be seen in Figure 5.3.

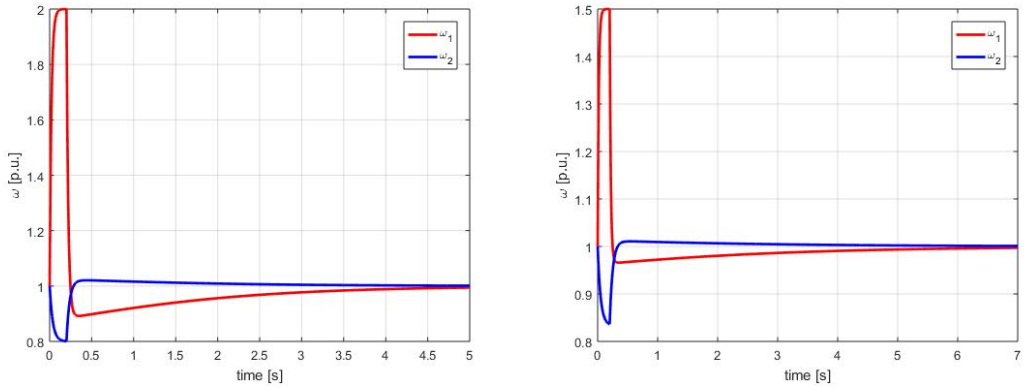

(a) Test 1 (b) Test 2

Figure 5.3: *Study 2 - Simulations*

5.1.2.1 Results of Study 2

Only variables at the terminal buses were considered as measured, giving a practical characteristic for the present study. According to Figure 5.1, the variables recorded were: $V_1\angle\theta_1$, $V_2\angle\theta_2$, $I_{12}\angle\alpha_{12}$.

The method presented on Subsection 4.2.2.1 was tested skipping the steps 8 and 9 of the algorithm, as the system is lossless. Due to this reason, this method is identified as "IME" in this Study, leaving the "Iterative" prefix term.

The results are presented in Table 5.5.

It can be seen that the results are very accurate for both cases. The Least Squares method, used in the Step 10 of the algorithm, proves to be accurate when applied to the swing equation supplied with the data of the internal voltage angles calculated with the IME-iterative method proposed.

Different tests were performed varying the values of the parameters presented in Table 5.1 and also the number of samples considered. The maximum error obtained was of $e = 5.83\%$ for the estimation of the transient reactances and less than 2% for both inertia and damping.

Table 5.5: *Study 2 - Results*

Test 1						
	Simulated			**Estimated**		
	H[s]	**D**	**x**	**H[s]**	**D**	**x**
G_1	30	10	0.054	30.0023	10.0005	0.0539
G_2	300	50	0.054	299.9772	50.0036	0.0539
Test 2						
	Simulated			**Estimated**		
	H[s]	**D**	**x**	**H[s]**	**D**	**x**
G_1	50	20	0.07	49.9541	19.9770	0.0699
G_2	500	60	0.07	497.8747	59.7885	0.0701

5.1.2.2 Conclusions of Study 2

The IME method proposed by [17] for oscillations was adapted and applied to estimate the inertia following perturbations. Data coming from the terminal buses were considered and applied to estimate the internal parameters of the synchronous machines in study, and the method produced accurate results in terms of transient reactance, inertia and damping estimated. The method solves the limitation of the methodology applied in Study 1, where the application of the Least Squares method on the swing equation fed with data from terminal buses did not produce good results.

5.1.3 Study 3 - Model Estimation Methods

In this subsection, the Iterative-IME and the "Variance" method are tested and compared considering different data simulated.

5.1.3.1 Study 3 - Test 1

In this first test, simulations are performed with Test-System B in the same conditions of Study 5.1.2, but now losses are considered in the transmission line. Summarizing:

- Test-system used: Test-system B presented in Section D.2, chosen due to its simplicity.
- Simulation software: Euler numerical integration method as proposed in [41], implemented in Matlab.
- Perturbation simulated: disconnection of Generator 1 at t=0s and reconnection at t=0.2s;
- Model used for the synch. machines: Second order model (as presented in Subsection 2.2.1);
- Machine parameters: according to Table 5.6.
- Model of the load: dynamic (motor);
- Losses: considered. The relation $\frac{X}{R}$ depended on the test;
- Sampling time: 10ms. The total simulation last 10s.

Table 5.6: *Study 3 - Test 1 - Machine parameters*

	H[s]	D	$\mathbf{x_i[p.u.]}$
$\mathbf{G_1}$	50	20	0.054
$\mathbf{G_2}$	500	60	0.054

The simulations are performed considering different $\frac{X}{R}$ relations for the transmission line. Only variables at the terminal buses were considered as measured, remaking the practical conditions of Study 2. The inclusion of a resistance in the transmission line didn't produce a big impact on the dynamic response of the machines involved; this is why no Figures presenting the responses are depicted for this case. However, the impedance of the radial path interferes on the transient reactance estimation and consequently on the inertia estimation of the machines, justifying this study.

The acquired data is used to produce a dynamic equivalent of each generator, according to Figure 5.4. To build each equivalent, the first step is to estimate the transient reactances x_1 and x_2. Then, the internal voltages can be calculated accordingly and the inertia can be estimated through the solution of the swing equation.

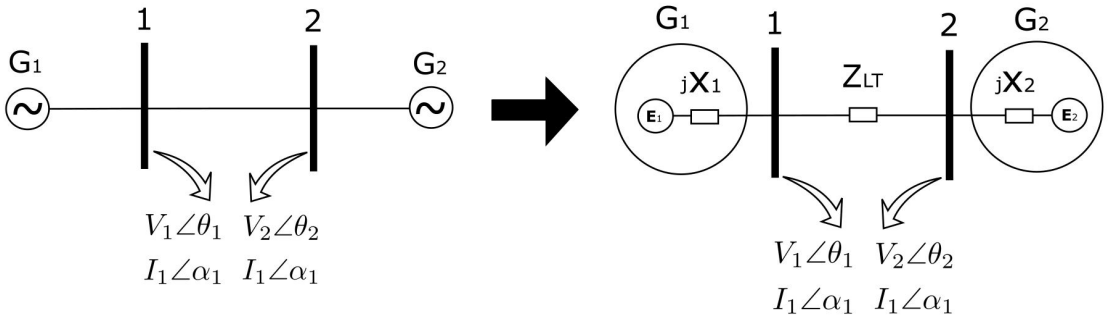

Figure 5.4: *Study 3 - Test 1 - Dynamic equivalents*

To evaluate the effect of the considered impedance on the estimations, three methods were tested: the IME method without the iterative loop, as used in Study 2, the Iterative-IME method as presented in Section 4.2.2.1, with tolerance of 10^{-6}, and the "Variance" method, as presented in Section 4.2.2.2. Results obtained with two different $\frac{X}{R}$ relations are presented in Table 5.7.

Table 5.7: *Study 3 - Test 1 - Transient reactances*

	Simulated		IME		It.-IME		"Variance method"	
	$\mathbf{x_1}$	$\mathbf{x_2}$	$\mathbf{x_1}$	$\mathbf{x_2}$	$\mathbf{x_1}$	$\mathbf{x_2}$	$\mathbf{x_1}$	$\mathbf{x_2}$
$\frac{\mathbf{X}}{\mathbf{R}} = \mathbf{5}$	0.054	0.054	0.0512	0.0518	0.0520	0.0529	0.054	0.054
$\frac{\mathbf{X}}{\mathbf{R}} = \mathbf{10}$	0.054	0.054	0.0507	0.0506	0.0518	0.0528	0.054	0.054

It can be seen in Table 5.7 that the Iterative loop brought improvements to the estimation of x_i in comparison to the simple IME method, specially when the the relation $\frac{\mathbf{X}}{\mathbf{R}}$ is higher. However, for the evaluated tests, the "Variance" method was the one that performed better.

Taking the case in which $\frac{X}{R} = 10$, the estimations of inertia and damping can be seen in Table 5.8, where the errors obtained in the estimation of x_i were reflected also in the estimation of H_i and D_i.

Table 5.8: *Study 3 - Test 1 - Inertia and damping ($\frac{X}{R} = 10$)*

	Simulated		**IME**		**It.-IME**		**"Variance method"**	
	$\mathbf{G_1}$	$\mathbf{G_2}$	$\mathbf{G_1}$	$\mathbf{G_2}$	$\mathbf{G_1}$	$\mathbf{G_2}$	$\mathbf{G_1}$	$\mathbf{G_2}$
$H(s)$	50	500	51.4423	493.5332	50.0447	499.8092	50.0000	500.0000
D	20	60	20.2365	62.2773	20.0026	60.0034	20.0000	60.0000

5.1.3.2 Study 3 - Test 2

For this test, a different type of perturbation is simulated in Test-System B: G2, acting as a motor, is set to consume 10% more power in t=0.2s. A governor and an AVR are implemented for Generator 1, according to [42].

- Test-system used: Test-system B presented in Subsection D.1, chosen due to its simplicity.
- Simulation method: Euler numerical integration method as proposed in [41], implemented in Matlab.
- Perturbation simulated: step increase of 10% in the mechanical power of G2 at t=0.2s;
- Model used for the synch. machines: Second order model (as presented in Subsection 2.2.1);
- Model of the loads: dynamic (G2 acts a motor).
- Losses considered with $\frac{X}{R} = 10$.
- The sampling time used is 10ms. The total simulation last 25s.
- According to Table 5.6.

The dynamic behaviour of G1 and G2 are presented in Figure 5.5 and 5.6. In Figure 5.5, the mechanical power (P_{m_i}) and the power generated (P_i) of G1 and G2 are presented. It can be seen that P_{m_1} follows the step imposed in P_{m_2} thanks to the action of the governor. In Figure 5.6, the speed of the machines are presented.

With the Iterative-IME method, the transient reactances estimated were $x_1 = x_2 = 0.0558$, while with the "Variance" method $x_1 = x_2 = 0.054$. Table 5.9 present the inertia and damping estimated. It can be seen that the Iterative-IME performed better for Generator 1 then Generator 2 in this case. However, once again, the "Variance" method performed better.

5.1.3.3 Conclusions of study 3

This section expanded Study 2 to consider losses on the transmission lines and also to include tests with another type of perturbation. The Iterative-IME method presented in Subsection 4.2.2.1 and the "Variance method" presented in Subsection 4.2.2.2 were tested, with accurate results, with the "Variance method" in advantage in the cases evaluated in this study. The differences between the methods are further investigated in Subsection 5.2.1, where results obtained with a more complex test-system are analyzed.

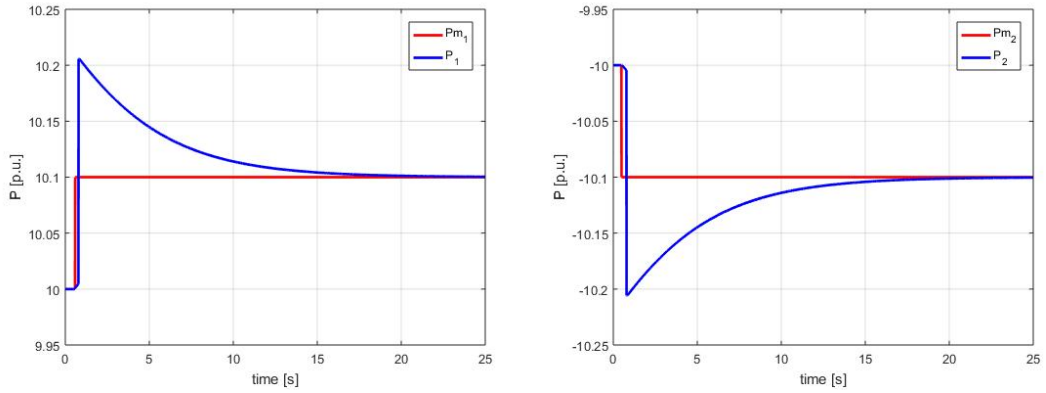

(a) Powers of G1 (b) Powers of G2

Figure 5.5: *Study 3 - Test 2 - powers simulated*

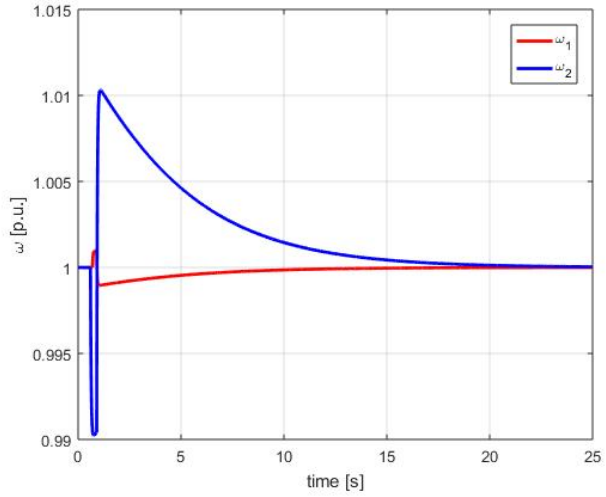

Figure 5.6: *Study 3 - Test 2 - speeds simulated*

Table 5.9: *Study 3 - Test 2 - Inertia and damping estimated*

	Simulated		**It.-IME**		**"Variance method"**	
	$\mathbf{G_1}$	$\mathbf{G_2}$	$\mathbf{G_1}$	$\mathbf{G_2}$	$\mathbf{G_1}$	$\mathbf{G_2}$
$H(s)$	50	500	49.8183	493.4876	50.1355	501.0247
D	20	60	19.8974	51.2776	19.9354	59.3604

5.2 Area equivalent studies

In this section, more complex test-systems are used to evaluate dynamic equivalents and inertia estimation from terminal buses, boundary buses and spread units installed on the grid.

Subsection 5.2.1 presents Study 4, presenting area studies considering non-coherent generators and debating the effect of loads and perturbation inside the area of study.

Subsection 5.2.2 presents Study 5, an evaluation of the EKF method in comparison to the MEM. Besides most of the results present in this subsection are related to single machines, the discussion of the results is pertinent to area studies.

Subsection 5.2.3 presents Study 6, where the results obtained with the method described in Section 4.2.4 are shown.

5.2.1 Study 4 - MEM

In this subsection, the Iterative-IME and the "Variance" method are evaluated for building dynamic equivalents and estimating inertia of an area, approaching the proposed Topic 2.

With the aim of studying the applicability of the methods with more complex systems, simulations were performed in PowerFactory2018 with the original test-system from [42], widely used in academy. The details of this test-system is presented in Section D.3, but the diagram is reproduced here for convenience.

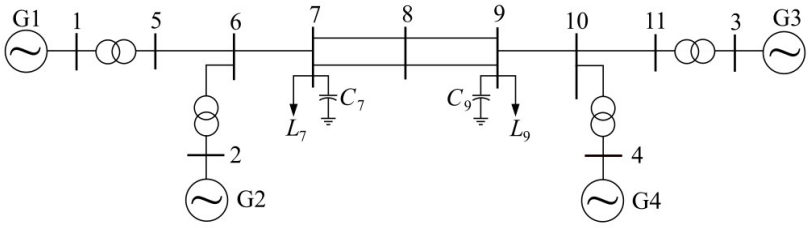

Figure 5.7: *Study 4 - Test-system C*

With this test-system it is possible to test the MEM considering a higher-order model for the synchronous machines in the simulation in relation to the second order model used to build the dynamic equivalents, and evaluate the possible limitations of this representation. Moreover, Governor, PSS and AVRs were modelled and considered in the simulations, what may also interfere in the performance of the studied methods.

- Test-system used: Test-system C, presented in Section D.3;
- Simulation software: PowerFactory2018;
- Perturbations simulated: load steps;
- Model used for the synch. machines: two-axis IEEE standard detailed Model 2.2 [45];
- Machine parameters: according to Table D.2.
- Model of the loads: constant impedance;
- Losses: considered;
- Controllers: Governor, PSS and AVRs modelled using standards models and parameters available in PowerFactory2018;
- Sampling time: 20ms.

For the purpose of this study, the chosen test-system is divided in two areas. Traditionally, areas are divided in power system studies according to coherent group of machines, such that their dynamic behaviour can be studied altogether. However, in this study the areas are divided accordingly to the assumed presence of a PMU at boundary buses. This choice is motivated by the fact that PMUs are installed in the grid according to many factors [94], [97], [98], such as observability, or other applications, as protection. Consequently, available PMUs may monitor groups of generators that are not necessarily coherent, and this study aims at investigating the implications of that.

The study considers PMUs installed at the boundary buses 5 and 6, such that Area 1 is defined by the boundary bus 5, and contain only one generating machine (G_1), and Area 2 is defined by the boundary bus 6, composed by three non-coherent generating units (G_2, G_3, G_4). The data acquired from the simulator are highlighted in Figure 5.8, that is a snipping of Figure 5.7. The voltage at bus 5 is represented as $V_5\angle\theta_5$ and the current injection exiting Area 1 is $I_{56}\angle\phi_{56}$. Similar for the other area, $V_6\angle\theta_6$ is the voltage at bus 6 and and $I_{65}\angle\phi_{65}$ is the current injection exiting Area 2. The Iterative-IME method and the "Variance method" were then applied to estimate the parameters of the equivalent system depicted in Figure 5.9 in two different cases considering a perturbation in each one of the areas.

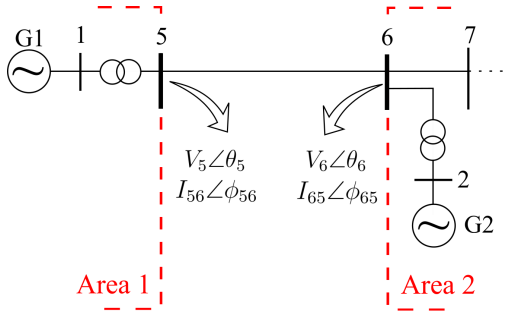

Figure 5.8: *Study 4 - Snipping of Test-system C*

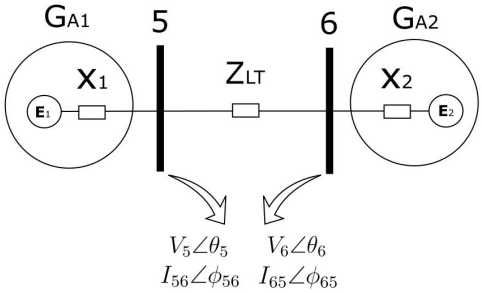

Figure 5.9: *Study 4 - Dynamic equivalent*

5.2.1.1 Test 1 - Perturbation inside Area 2

Test 1 is based on a simulated step increase of 20% in the load of bus 9 (see Figure 5.7). In this case, G1 and G2 oscillates against G3 and G4. However, considering bus 6 as the boundary of Area 2, the dynamic behaviour of this area is dominated by G3 and G4. Figure 5.10 shows the frequency behavior of the COI of Area 1 (composed only by G1) and the behaviour of Area 2 (Composed by G2, G3 and G4). The area division allows the MEM to be tested for estimating the parameters of a single machine (in case of Area 1) and estimating the parameters of an equivalent of non-coherent machines (Area 2).

The Iterative-IME method was tested with a selected time window of 2s around the moment the perturbation occurred, considering 0.5s before and 1.5s after. The process converged in 8 iterations. The internal reactances estimated were $x_1 = 0.034$p.u. and $x_2 = 0.185$p.u. The "Variance method" produced $x_1 = 0.0272$p.u. and $x_2 = 0.0692$p.u. It is important to observe that, since the model used during the simulations for synchronous machines is of a higher-order, the transient reactances estimated by both methods are an equivalent of the static internal parameters of each area, and each method depend on different assumptions to obtain them. In this way, it is not possible to compare directly these partial results.

With x_1 and x_2, the internal voltages $E_1(t)\angle\delta_1(t)$ and $E_2(t)\angle\delta_2(t)$ are calculated. The electrical

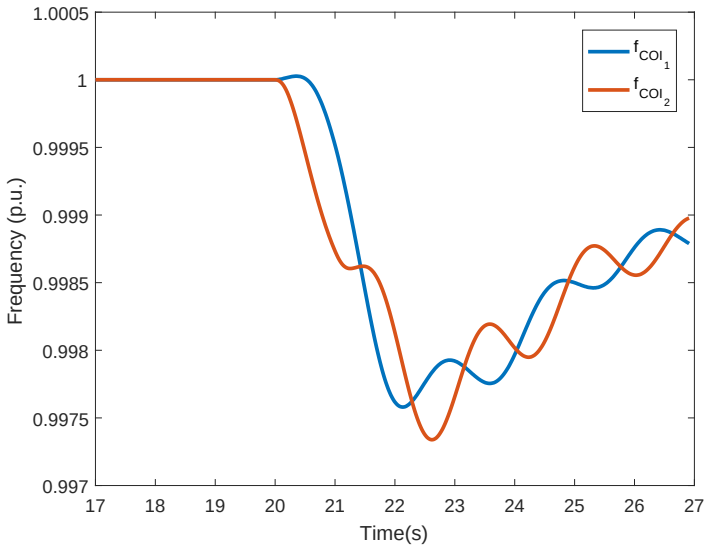

Figure 5.10: *Study 4 - Test 1 - Frequencies*

frequencies related to each equivalent generator are calculated according to Equation (3.5), making use of the obtained $\delta_i(t)$. After calculating the frequency, a median filter is applied to reduce the peaks caused by the application of the finite difference method to calculate the derivative in Equation (3.5).

To evaluate the dynamic equivalents obtained, the calculated electrical frequency of each equivalent machine (denoted by f_{calc_i}) is compared with the mean frequency (f_{COI}) of each area (defined in Section 2.2.3) obtained from the simulation. The results obtained with the Iterative-IME method are presented in Figures 5.11(a) and 5.11(b). Despite of the difference between the Iterative-IME and the "Variance method", the results obtained for the frequency were pretty similar in the scale studied. For this reason, only the results obtained with the Iterative-IME method are presented here.

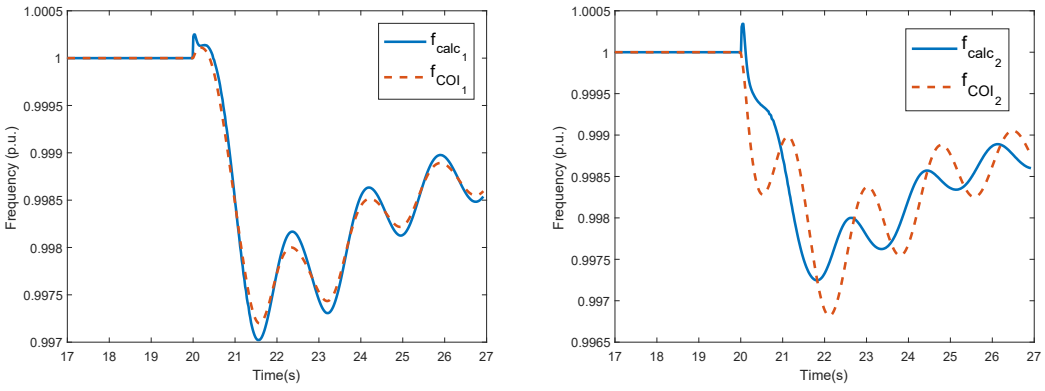

(a) Frequency - Area 1

(b) Frequency - Area 2

Figure 5.11: *Study 4 - Test 1 - Frequencies estimated*

It can be seen that the estimated frequency of area 1 is very close to the mean frequency of that area, which is expected since this area has only one generator. The differences are due to numerical

inaccuracies of the methods used. About area 2, instead, the behavior of f_{calc_2} is slightly different from f_{COI_2}. This happens because the measurement point is electrically closer to the Generator 2 than to the hypothetical COI of the system, such that the influence of the frequency of the generator 2 (f_{G2}) brings the estimated f_{calc_2} closer to its behavior. This can be seen in Figure 5.12, where f_{G2}, f_{G3} and f_{G4} are the actual frequencies of each generator of area 2 following the diagram of the test system (Figure 4.4).

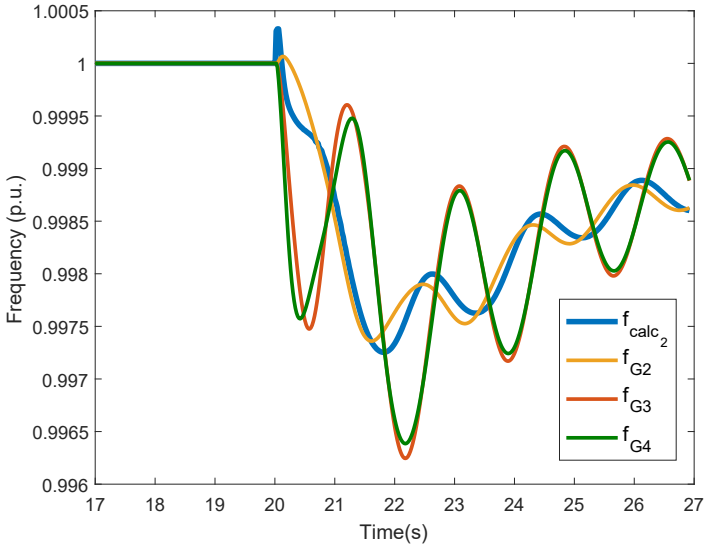

Figure 5.12: *Study 4 - Test 1 - Frequencies of Area 2*

However, it is worth observing in Figure 5.12 that the influence of f_{G3} and f_{G4} is also present in f_{calc_2}. Between $t = 20s$ and $t = 21s$ it can be seen that f_{calc_2} presents a peak, following the behavior of f_{G2}, but right after it decreases like f_{G3} and f_{G4} instead, such that the equivalent inertia related to f_2 takes into account the contribution of all the machines of area 2.

The estimated inertia results for Test 1 obtained with the same time window used to estimate the transient reactances (2s around the perturbation occurence) can be seen in Table 5.10, where "COI" denotes the simulated inertia at the COI (here presented as reference for comparisons), "It.-IME" denotes the inertia estimated with the Iterative-IME method and "Var. method" denotes the inertia estimated with the "Variance method".

Table 5.10: *Study 4 - Test 1 - Inertia estimations*

	COI (sim.)	**It.-IME**	**Var. method**
Area 1	6.5	6.2504	6.0760
Area 2	18.85	-0.7719	-0.1531

It can be seen that the inertia estimated for Area 1 is very close to the inertia of the COI of this area (that is equal to the inertia of G1). In this test, the Iterative-IME produced better results than the "Variance method". However, both methods failed to estimate the inertia for Area 2. This happens because the assumption for the mechanical power assumed in Step 8 of the method doesn't hold for this area, due to the fact that the perturbation is located inside Area 2. The perturbation alters the moving

power such that it oscillates together with the loads of the area, as shown in Figure 5.13, plotted with data coming from the simulation. The legend Pe_{A2} stands for the active power exiting Area 2 and Pm_{A2} represents the moving power related to the area computed according to the formula

$$Pm_{A2} = \sum_{i=2}^{4} Pm_{Gi} - \sum P_{loads} - \sum P_{losses} \tag{5.1}$$

where Pm_{Gi} stands for the mechanical power of the generators $i = 2, 3, 4$ of the area, and P_{loads} and P_{losses} are the sum of the active power consumed by the loads and the active power losses in the area, respectively. In this part of the study, simulated data was used in this approach, to provide insights on the results obtained in Table 5.10.

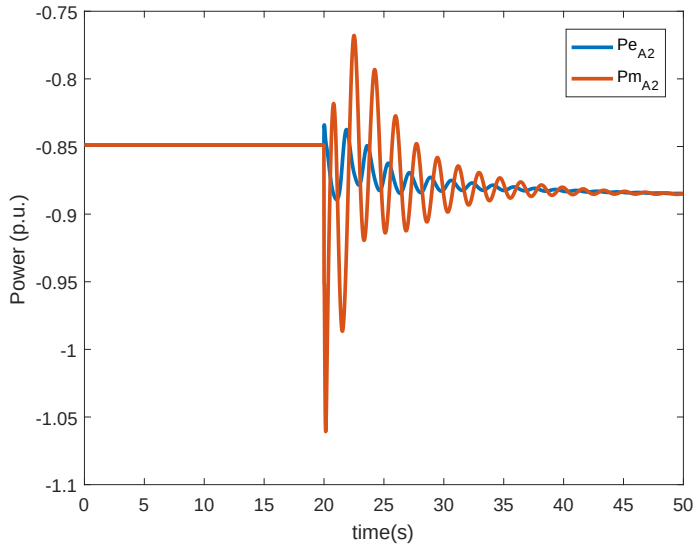

Figure 5.13: *Study 4 - Test 1 - Moving power and active power of Area 2*

Considering the moving power as known, the method is tested again and the estimations obtained for Area 2 are $H_{It-IME} = 19.03s$ and $H_{Var} = 18.5510s$, less than 1% different from the H_{COI}. Hence, to estimate properly the inertia of an equivalent area containing a perturbation and/or loads with high voltage dependence, a complementary method to estimate the equivalent moving power is needed. This motivated the method proposed in Section 4.2.5.3, tested for this purpose in Study 11 (Subsection 5.4.2).

5.2.1.2 Test 2 - Perturbation inside Area 1

A second experiment (named Test 2) is performed including a new load of 150MW and 50Mvar in Area 1, and a step increase of 20% in the active power consumption is simulated in this area.

For this case, the reactances estimated with the Iterative-IME method were $x_1 = 223.0201$ p.u. and $x_2 = 0.1249$ p.u, considering a time window of 2s around the moment the perturbation occurred. The increase of load in Area 1 was reflected direclty on the estimated x_1, much higher than in Case 1, while the estimations of x_2 were not so different. This happens because the presence of three generating units in Area 2 partially compensates the perturbation locally, such that the load increase has not a big impact

seen from the equivalent point of view. In Area 1, instead, the impact of a local load increase is much bigger because the area is limited to only one generating unit.

Regarding the inertia constants estimated with the obtained equivalent reactances, Table 5.11 present the results for the named Test 2.

Table 5.11: *Study 4 - Test 2 - Inertia estimations*

	COI (sim.)	It.-IME	Var. method
Area 1	6.5	-22.2999	-34.7167
Area 2	18.85	18.7216	14.7812

Results in Table 5.11 show that the method was accurate to estimate the equivalent inertia of Area 2, but struggled again when trying to estimate the inertia of the area that contains the perturbation (for the same reasons presented in Case 1). When the moving power of Area 1 is considered as known, the estimations obtained with the Iterative-IME method improved to $H_{est} = 7.179s$ for Area 1, while the "Variance method" obtained $H_1 = 6.5030s$. Despite the "Variance method" produced results more accurate for Area 1, regarding Area 2 the Iterative-IME performed better. In general, it can be said the methods are equivalent in terms of performance for estimating inertia.

Considering a sliding time window of 100 samples (2s), as defined in Section 4.2.1, the results presented in Figure 5.14 were obtained. In this case, the moving power of Area 1 was considered as known. In the legend, H_1 and H_2 refer to the estimated inertia of the equivalent machines of area 1 and 2, respectively. The black dashed lines represent the true value of the inertia of each area.

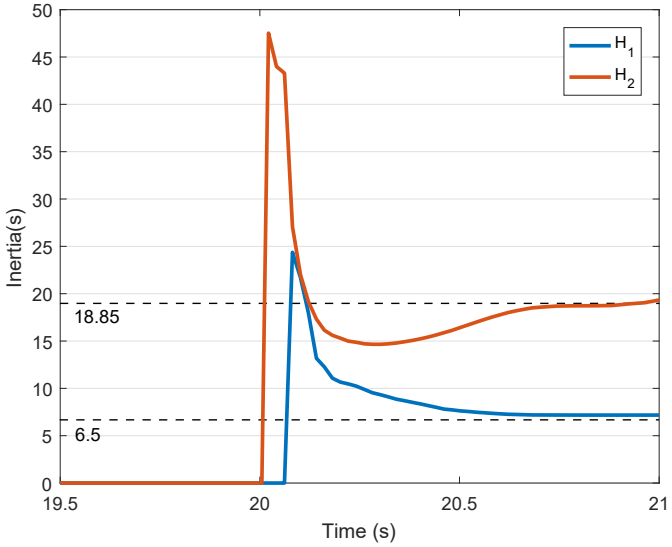

Figure 5.14: *Study 4 - Test 2 - Inertias estimated*

The method did not present high sensitivity for the size of the time window, such that the results were similar to every length tested (1.5s to 5s). It can be seen that the inertias estimated for both areas presented a peak in the first milliseconds after the perturbation, and later presented a nearly constant behavior. The peaks are due to the use of finite difference method to calculate the first and second

derivative of the equivalent rotor angle. The use of filtering reduced those peaks, but they can still be observed in both resulting signals.

5.2.1.3 Conclusions of Study 4

To compare the two methods studied in this Subsection, new tests were proposed, varying the type and the location of the perturbation. Some of the perturbations considered were load step, load ramp, loss of generation and short circuits. To summarize, results were accurate and practical when estimating the inertia of the areas that does not include a perturbation. For the area that contains a perturbation, the methods work but require the knowledge of the equivalent moving power of the area in time, which is addressed later on in this thesis in Study 11 (Subsection 5.4.2), using the method presented in Section 4.2.5. Otherwise, the result will be negative inertia.

In terms of accuracy on the estimations of the equivalent inertias in comparison to the COI, no method presented a definitive superior performance. For this reason, no method was discarded. It is important to point out that the reactances estimated with both methods are not directly comparable in the cases studied, as they depend on different assumptions and represent different equivalent circuits obtained with data simulated using a higher-order model.

5.2.2 Study 5 - Extended Kalman Filter

Two tests were performed in this study to evaluate the method proposed in Section 4.2.3 similarly to how the other methods were evaluated.

5.2.2.1 Test 1

First the EKF was fed with data provided by simulations with the Test-system B presented in Subsection D.2, with the following conditions:

- Test-system used: Test-system B presented in Section D.2.
- Simulation software: Euler numerical integration method as proposed in [41], implemented in Matlab.
- Perturbation simulated: disconnection of Generator 1 at t=0s and reconnection at t=0.2s;
- Model used for the synch. machines: Second order model (as presented in Subsection 2.2.1);
- Machine parameters: according to Table 5.12;
- Model of the load: dynamic (motor);
- Sampling time: 10ms. The total simulation last 10s.

According to the diagram presented in Figure D.2, the following variables were considered measured: $V_1\angle\theta_1$, $V_2\angle\theta_2$, $I_{12}\angle\alpha_{12}$.

Regarding the inputs of the method proposed in Section 4.2.3, the active and reactive power were calculated as function of the measured voltages and currents. The transient reactance was considered as known, as methods to calculate it have already been presented in this thesis and could possibly be used. The mechanical power P_m was also considered known and equal to P_e^{st}.

Table 5.12: *Study 5 - Test 1 - machine parameters*

	H[s]	**D**	$\mathbf{x'_d[p.u.]}$
$\mathbf{G_1}$	5	2	0.054
$\mathbf{G_2}$	50	20	0.054

Considering as initial estimates $H_1^0 = 7$ and $D_1^0 = 1$ for machine 1, the results presented in Figure 5.15 were obtained.

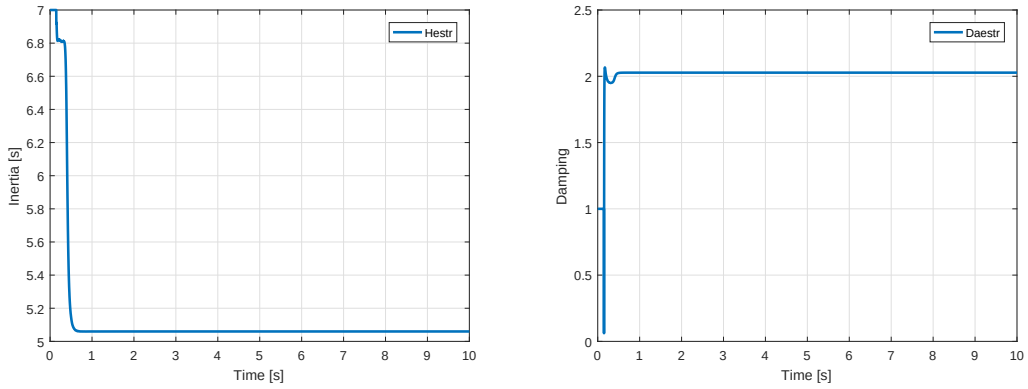

(a) Inertia estimation

(b) Damping estimation

Figure 5.15: *Study 5 - Test 1 - Estimation results*

It can be seen that the estimations obtained converge to values close to the expected (presented in Table 5.12). Variating the initial estimates, the results were similar. For an initial estimate 100% greater than the correct parameters, however, the process diverged, showing a dependence on the initial estimates. The estimations regarding Generator 2 followed the same behaviour, and did not bring any interesting information to add to the discussion of this subsection.

An important observation, however, is that the process noise covariance matrix (Q_k, in Figure 4.7) was considered null in this test. This parameter allows the method to consider modelling errors between the assumed model and the true one, such that in practical applications Q_k should be non-null. However, in this test the process model adopted is exactly the same model used in the simulations, so considering Q_k non null would only bring inaccuracy to the method.

5.2.2.2 Test 2

The simulations to provide the data were carried out in the same conditions of Study 4, i.e., with the Test-system C. Summarizing:

- Test-system used: Test-system C, presented in Section D.3;
- Simulation software: PowerFactory2018;
- Perturbations simulated: load step in L9;
- Model used for the synch. machines: two-axis IEEE standard detailed Model 2.2 [45];

- Machine parameters: according to Table D.2.
- Model of the loads: constant impedance;
- Losses: considered;
- Controllers: Governor, PSS and AVRs modelled using standards models and parameters available in PowerFactory2018;
- Sampling time: 20ms.

Here, the process noise covariance matrix (Q_k) was considered non-null, as in the EKF the process was modelled with the second order model for synchronous machines and in the simulations the machines were modelled according to the two-axis IEEE 2.2 standard model defined in [159]. As Q_k is the matrix that allows the EKF to process the difference in the models, it has to be well tuned. Different tests were made choosing a relaxation of 1 to 20% to rotor speeds and rotor angles, 1 to 50% to inertia and damping calibration, according to the order of the units of each variable.

The results obtained for speed and rotor angle for Area 1 can be seen in Figure 5.16, where blue represents the simulated response and red represents the estimated one.

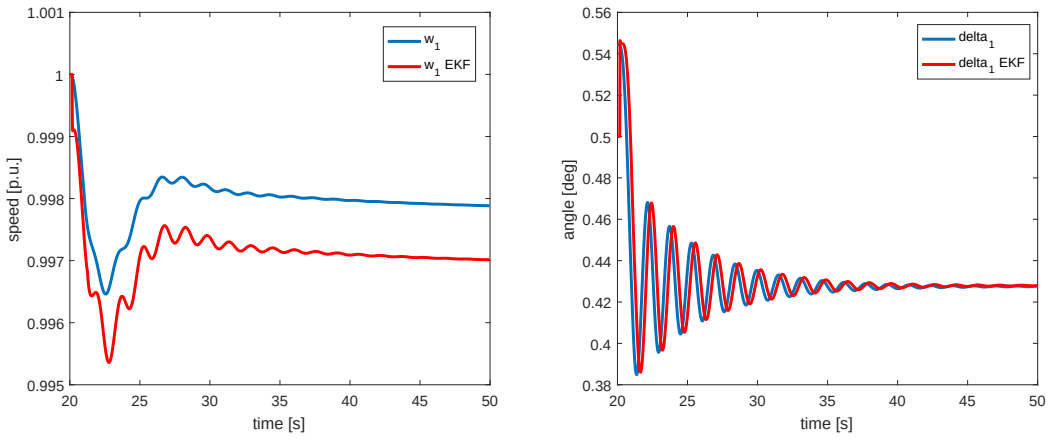

(a) Speed estimation

(b) Rotor angle estimation

Figure 5.16: *Study 5 - Test 2 - Estimation results*

It can be seen that the method estimated the rotor angle with acceptable error, but the speed was estimated with higher errors. These results were very dependant on Q_k. As this matrix allows the algorithm to consider the difference between the process model and the model used in simulations, it had to be tuned to produce accurate results. However, in any case it was not possible to obtain accurate values for the inertia of the equivalent machine of Area 1. Figure 5.17 presents the result obtained.

As it can be seen, the method was not able to converge to the correct result. The value of the inertia estimated increased with time, no matter the initial value used in the algorithm. Also the sampling rate was changed looking for better results, but it did not have an important impact. Regarding Area 2, not even the frequency estimated was close to the mean frequency of that area. For this reason, the results of Area 2 were suppressed. Other tests were performed considering different perturbations, with similar results. The work [160] suggests reducing the sampling time (through interpolation) to improve accuracy

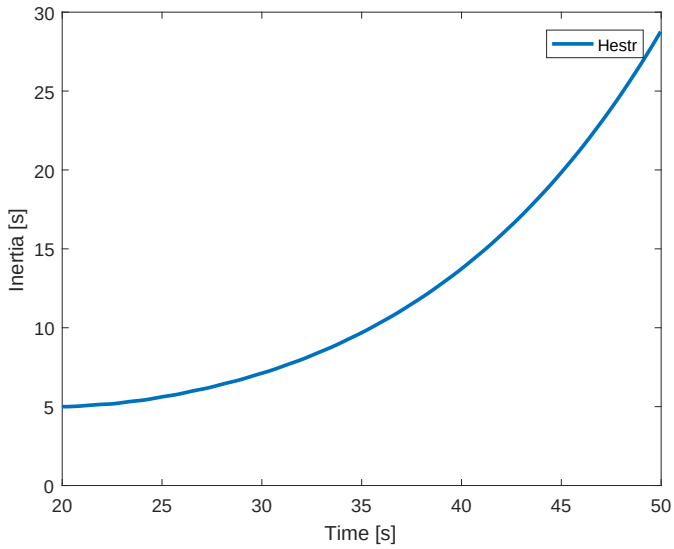

Figure 5.17: *Study 5 - Test 2 - Inertia estimated*

and obtain convergence. However, [160] also reports strong difficulties of the method when dealing with differences between the model simulated and model adopted in the EKF method.

5.2.2.3 Conclusions of Study 5

The method, in the way it was modelled in this thesis, showed to be limited for the interest of this research. Using the classical model for generators as the process model of the EKF worked when the data used was provided by simulations using the same models for the machines. When the method was tested with simulations that consider a higher-order model for the generators, which is a more realistic approach, the results were inaccurate in terms of inertia constant estimated. In this case, not only the model of the generator was different, but also the presence of frequency control was taken into account in the simulations.

In the literature, other works already provided some advance in this field. In [83], a different set of algebraic equations is proposed as the measurement model of the EKF, and the results seemed to show more robustness to handle differences in the process model. Also, the work [144] proposed the process model considering speed control, what could probably improve the results in the conditions of this study. Both works, however, are based on measurement models that only provide feedback information of the rotor angle in the EKF prediction-correction loop. Explaining, the variables that can be measured by PMUs can only be represented by algebraic equations that are functions of rotor angles, and not function of inertia or damping. Hence, the only direct feedback that can be provided by the measurement model is related to rotor angles, such that the other variables must be calibrated on a dependent indirect way.

This modelling issue bring concerns on the application of KF-based methods to wider applications. When adopting higher order models, or extending the model to consider frequency control, the number of parameters to be estimated are increased without increasing the number of variables that the measurement model may provide direct feedback on. In other words, the complexity of the model increases without increasing the amount of information acquired from the measurements available, what seems limiting.

Moreover, it was observed a strong dependence of the EKF on the tuning of the initial estimates and on the tuning of the process noise covariance matrix. These issues may be overcome when only one synchronous machine is evaluated, but may be a bigger problem to more complex studies, such as the proposed idea of evaluating dynamic equivalents based on measurements obtained on the boundaries of an area.

On a literature research, all the KF-based works found depend on individual monitoring of each generating unit. Only the work [29] proposes the use of an EKF for evaluating the properties of the COI, but it depends on full observability, what in practice is the same as monitoring each generating unit. As debated in Section 3.6, the deployment of PMUs is still preliminary on many countries, such that assuming observability of all the machines connected seem an assumption limited to very specific locations or part of the grids.

As one of the goals of this project is to study the inertia estimation based on few available measurement points on the grid, regardless their position on the terminals of the generators, the Iterative-IME and Variance method together with the Least Squares method showed more promising results for this purpose. Moreover, recently the work [84] showed a study with Least Squares methods outperforming KF methods. For these reasons, it was decided to focus on the LS based methods and discontinue the studies on KF-methods in the following.

5.2.3 Study 6 - Inertia estimation with system reduction

In this Study, the method proposed in Section 4.2.4 is used to evaluate test cases with more than one PMUs installed at each area, according to Topic 3.

A benchmark test-system proposed in [161] with 66 buses was used, due to its bigger size in comparison to the previous test systems.

The details of the simulations are:

- Test-system used: Test-system D, presented in Section D.4;
- Simulation software: PowerFactory2018;
- Perturbations simulated: disconnection of generators;
- Model used for the synch. machines: two-axis IEEE standard detailed Model 2.2 [45];
- Machine parameters: according to Table 5.13.
- Model of the loads: constant impedance;
- Losses: considered;
- Controllers: Governor, PSS and AVRs modelled using standards models and parameters available in PowerFactory2018;
- Sampling time: 20ms.

The equivalent inertias for each area of the system are given in Table 5.13, with reference to [161].

A simplified representation of the test-system is represented in Figure 5.18(a). Assuming PMUs installed at the boundary buses (A1, A2, B1, B2, C1 and C2), measuring voltages and currents, and considering the topology as known, the network is then reduced around those buses using the Ward

Table 5.13: *Study 6 - Equivalent Inertias of the Test-system*

	Num. of Generators	H_{COI} [s]
Area A	6	36.85
Area B	5	69.46
Area C	5	43.22

equivalent method. Note that any bus with a PMU can be considered a boundary bus to delimit an area with the Ward equivalent method. Here, the boundary buses were selected according to area previously delimited in [161]. The equivalent circuit to be determined can be seen in Figure 5.18(b), and each of the equivalent machines obtained will be identified by the name of the bus where it is connected (i.e., A1, A2, B1, B2, C1 and C2).

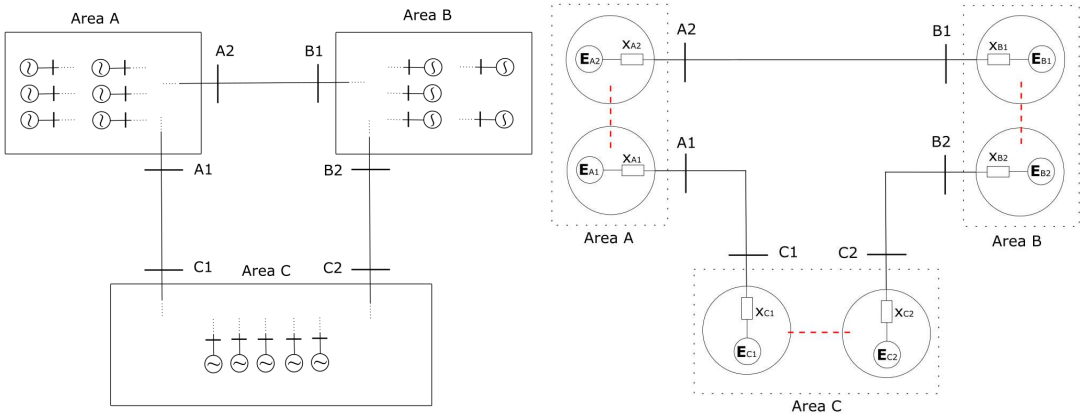

(a) Interarea connections (b) Dynamic equivalent

Figure 5.18: *Study 6 - Test-system and dynamic equivalent*

5.2.3.1 Test 1 - Perturbation inside Area B

The parameters of the equivalent generators are then estimated according to the occurrence of a perturbation in the simulations. Case 1 considers the disconnection of generator B2bG, of 1295MVA nominal power, connected at bus B2b (check D.4) inside Area B. Referring to Figure 5.18(b), the reactances estimated were respectively $x_{A1} = 0.2150$, $x_{A2} = 0.3949$, $x_{B1} = 0.3504$, $x_{B2} = 0.0585$, $x_{C1} = 0.1499$, $x_{C2} = 0.0602$ p.u.

The electrical frequencies $f_j(t)$ related to each equivalent generator are calculated according to Equation (3.5), where the subscript j refers to each of the equivalent machines $A1, A2, B1, B2, C1, C2$. After calculating $f_j(t)$, a median filter is applied to reduce the peaks caused by the finite difference method.

To be compared with the results of the simulation, the dynamic behavior of the COI of the equivalent machines in Figure 5.18(b) is evaluated. Equation (2.21) is applied for Area A, considering the equivalent machines $j = A1, A2$, obtaining $fcalc_{COI_A}$. The same is done for Area B, considering the machines $j = B1, B2$, and for Area C, considering the machines $j = C1, C2$, and obtaining respectively $fcalc_{COI_B}$ and $fcalc_{COI_C}$. The frequency behavior of each Area can be seen in Figure 5.19, in

comparison to the true mean frequency of each area recorded from the simulations and identified in the legend as f_{COI_A}, f_{COI_B} and f_{COI_C}.

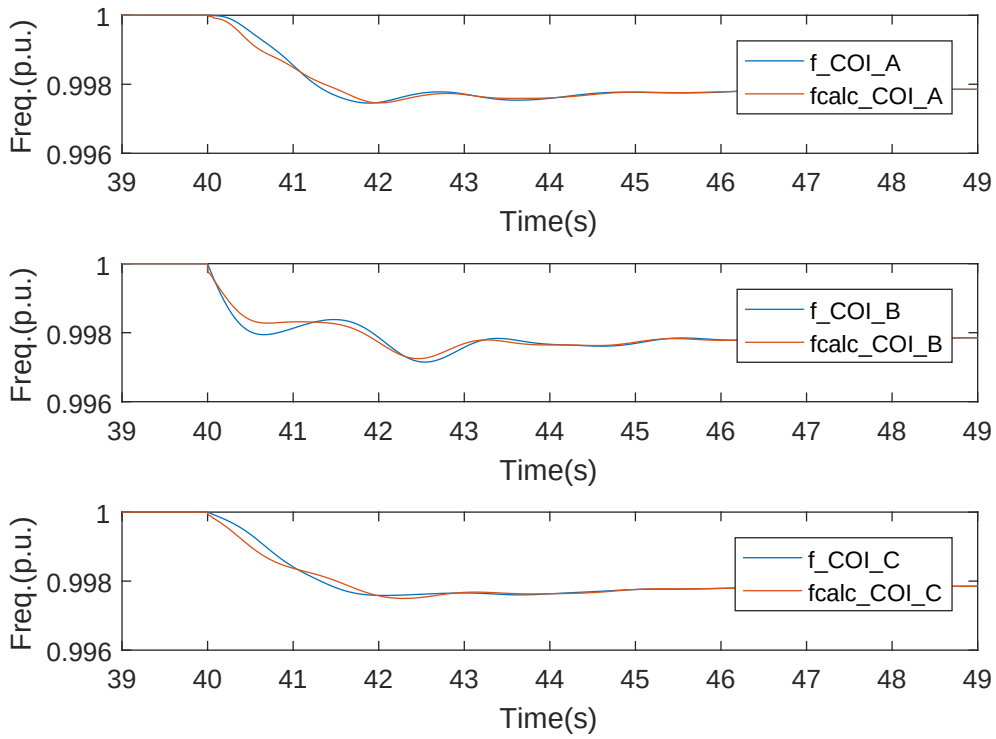

Figure 5.19: *Study 6 - Test 1 - Mean Frequency of each Area*

It can be seen that the differences are in the order of 10^{-4}, while the frequency decrease due to the perturbation is in the order of 10^{-3}, such that the estimations can be considered as good representations of the dynamic behavior of these areas.

Coming to the estimation of single inertias, additional insight can be gained on the phenomena considered. Using a time window of 5s around the time instant of the perturbation occurrence, the inertia constants can be estimated solving the Swing Equation. Table 5.14 presents the results obtained for each one of the six equivalent machines, and for the respective equivalent COI of each area.

Table 5.14: *Study 6 - Test 1 - Equivalent inertia estimated [s]*

Area A		**Area B**		**Area C**	
H_{A1}	45.38	H_{B1}	-63.99	H_{C1}	91.35
H_{A2}	29.31	H_{B2}	-127.39	H_{C2}	307.47
H_{COI}	74.70	H_{COI}	-191.38	H_{COI}	398.82

Comparing the estimated inertia at the COI with the simulated values seen in Table 5.13, it can be seen that the estimation of H_{COI_A} and H_{COI_C} were far from the expected, and the estimation of H_{COI_B} was negative. This does not prevent the frequency overall dynamic behaviour to be accurate:

all H estimates, both positive and negative, if used together, provide correctly the overall frequency response.

Negative H estimates of Area B result because the perturbation is located inside this area. In this situation, the assumption of slow behavior of the moving power in comparison to the generated power is violated. This can be seen in Figure 5.20 with results obtained from the simulation of the complete system, where P_{int_j} is the power exiting Area j and P_{mov_j} is the equivalent moving power of Area j, according to Equation (4.51).

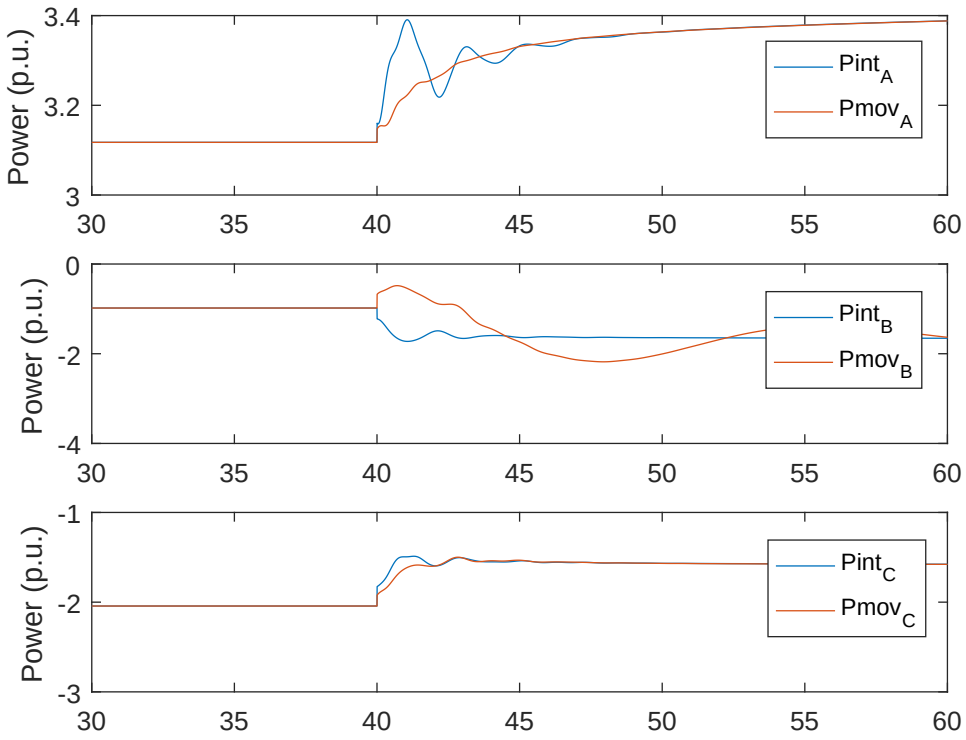

Figure 5.20: *Study 6 - Test 1 - Moving and generated powers*

A second issue is related to the load model. In the considered case, loads are assumed as voltage-dependent and therefore they are changing in time, as it can be seen in Figure 5.21 for Area A. This still affects Equation (4.51) and the estimations of inertia of Table 5.14, which are actually significantly different from those in Table 5.13. Due to this reason, the equivalent inertias estimated represent not only the inertias of the synchronous machines, but also the inertial behavior of the change in the load. This can be seen in Equation (4.49), considering that the calculated I_{EQ} with the Ward equivalent is made by both the equivalent generator current injection and the load current. This inertial response will be called *overall inertia* (H_{ov}), to differ from the equivalent inertia of the synchronous machines, that will be represented for now on in this study as H_{syn} (instead of only H).

Considering all machines of Area A monitored, is possible to calculate the current injection I_T of (4.49) and distinguish the inertial response of the synchronous machines from the overall inertia for theoretical investigations. Using a sliding time window of 5s, Figure 5.22 represents the synchronous inertia estimated for Area A in this conditions, using the proposed methodology. The dashed line represents the

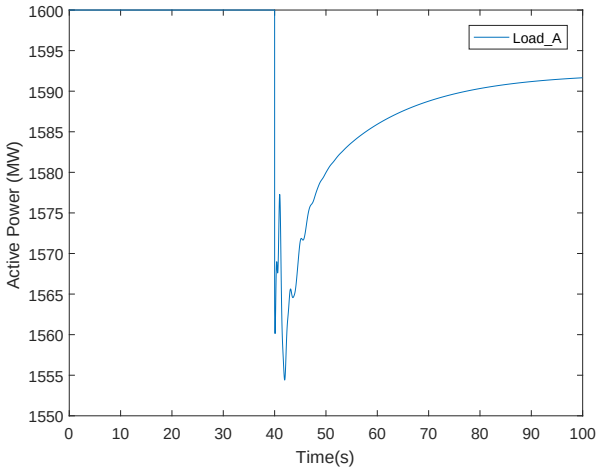

Figure 5.21: *Study 6 - Test 1 - Total load of Area A*

true value.

It can be seen that between 42s and and 44s, the synchronous inertia estimated was very close to the equivalent inertia of $H_{syn_A} = 36.85s$ shown in Table 5.13. After $t = 45s$, the frequency control takes part and the inertia estimation is affected, not representing anymore the equivalent inertia of the generators of Area A.

An alternative to monitoring all generators is to use the method proposed in Section 4.2.5.3 to estimate the equivalent moving power of this area. The studies with the referred method are presented in Section 5.4.2.

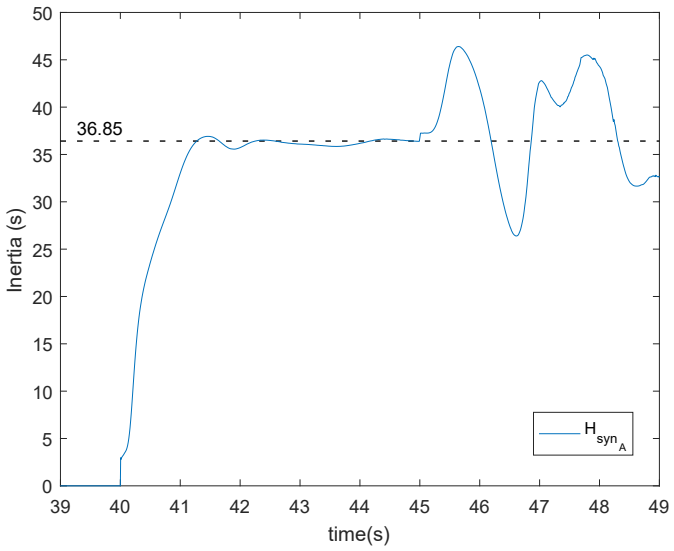

Figure 5.22: *Study 6 - Test 1 - Inertia estimated of Area A*

5.2.3.2 Test 2 - Perturbation inside Area A

Test 2 considered the loss of the Generator A6G (494MVA) inside Area A. The equivalent inertias can be seen in Table 5.15, where H_{OV} stands for the Overall inertia estimated and H_{SYN} stands for the equivalent inertia estimated related to the synchronous machines, disregarding the behavior of the load inside the Areas of study.

Table 5.15: *Study 6 - Test 2 - Equivalent inertias estimated [s]*

	Area B	**Area C**
H_{OV}	200.55	69.14
H_{SYN}	67.39	44.03

As it can be seen, the estimated H_{SYN} were very close to the values in Table 5.13. In addition, it can be concluded that the fault simulated has caused a higher impact in Area B than in Area C, due to the load variation associated to voltage dependence. This can be seen by the difference between H_{OV} and H_{SYN} of each area.

5.2.3.3 Conclusions of Study 6

This study presented estimated equivalent inertias based on measurements provided by PMUs spread in the system. The methodology assumes the topology as known, and uses the Ward equivalent method to reduce the system around the measurement points. Dynamic equivalents are built to represent the dynamic behavior of the areas connected to the boundary buses, and the inertia of each equivalent machine is estimated.

Considering measurements provided by PMUs installed in boundary buses, the proposed methodology is able to estimate the overall inertia of an area in practical conditions. The advantages of considering internal measurement points are discussed properly in the studies 9 to 12, presented in Subsections 5.3.3 to 5.5.1.

Considering the specific case when all the synchronous machines of an area are monitored, the study presents insights on the influence of the inertial response of the loads in the overall inertia. The possibilities of estimating the equivalent load behaviour is discussed in Study 11 (Subsection 5.4.2).

5.3 RES integration studies

In this Section, the dynamics of the grid are studied in the presence of RES, connected to the grid through converters.

First, the "Variance method" is used to check the possibility of estimating equivalent inertias considering as perturbation the connection of a wind power generator to a grid with only traditional synchronous machines.

At second, the disconnection of a synchronous generator with the same power capacity of the connected RES-unit is evaluated, in such a way that the power imbalance at the moment of the intervention is approximately null. This practical situation is evaluated to see if the dynamics involved are enough to produce variations detectable by the inertia estimation methods.

5.3.1 Study 7 - Connection of a RES-based generator

For this study, the simulation performed had the following characteristics:

- Test-system used: Based on Test-system C, presented in Section D.3;
- Simulation software: PowerFactory2018;
- Perturbations simulated: Load step at t=10s. Connection of a wind-power generator at t=70s;
- Model used for the synch. machines: two-axis IEEE standard detailed Model 2.2 [45];
- Machine parameters: according to Table D.2.
- Model of the loads: constant impedance;
- Losses: considered;
- Controllers: Governor, PSS and AVRs modelled using standards models and parameters available in PowerFactory2018;
- Sampling time: 20ms.

The test-system was modified to include a Wind power generator connected to bus 8, according to Figure 5.23. All the other parameters of the grid are kept as original. The areas are defined around the same boundary buses as Study 4. To recall the most important parameters, the inertias of G1, G2, G3 a G4 are $H_1 = H_2 = 6.5s$ and $H_3 = H_4 = 6.175s$, respectively, such that the equivalent inertia at the COI of Area 1 is $H_{A1} = 6.5$ and the equivalent inertia at the COI of Area 2 is $H_{A2} = H_2 + H_3 + H_4 = 18.85s$.

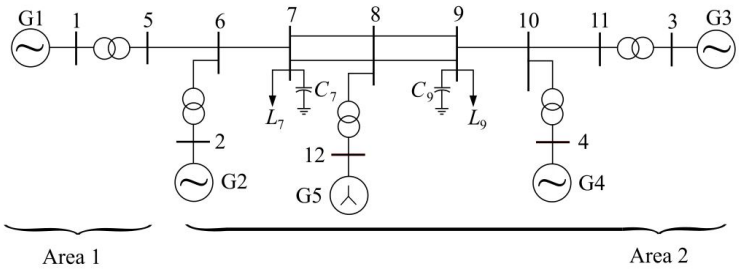

Figure 5.23: *Study 7 - Test-system*

The Wind power generator (identified in Figure 5.23 as G5) is set to generate constant 20MW and 6.6Mvar when integrated to the grid, which is much smaller than the generators already connected (that generate around 700MW each in the base case solution). The simulation lasts 100s, sampled at t=0.02s, and two different events are inserted: at t=10s there is a load increase of 5% in the active and reactive power of Load 7 (that was originally $S = 967MW + i100Mvar$), and at t=70s the Wind Power generator is connected. The first event is inserted just to serve as base of comparison with the second event in terms of magnitude of variations of frequency and power. The speed of the generators can be seen in Figure 5.24.

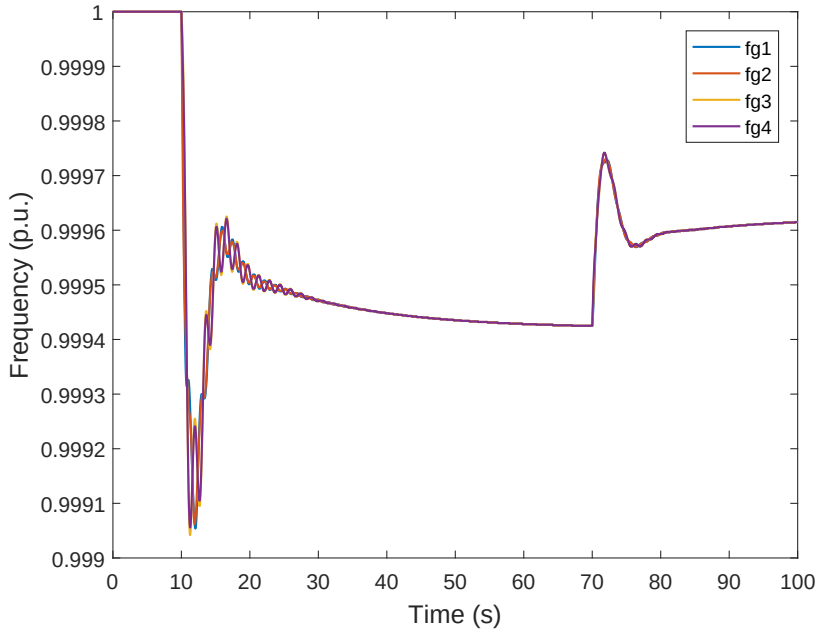

Figure 5.24: *Study 7 - Frequencies of the generators*

5.3.1.1 Results of Study 7

Considering PMUs installed at bus 5 and 6, the "Variance method" is applied to build the dynamic equivalents of each area and then estimate the equivalent inertias. Figure 5.25 presents the frequencies calculated as an output of the method (identified by f_{calc}) in comparison to the true frequency of the COI of each area obtained from the simulations.

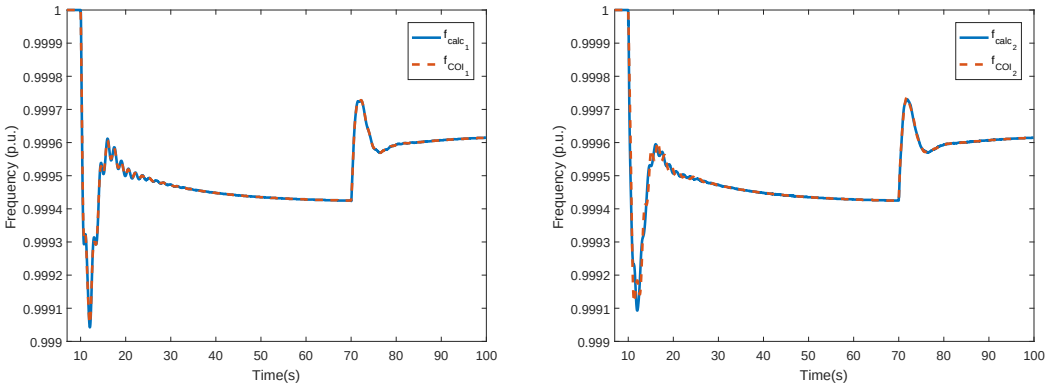

(a) Area 1 (b) Area 2

Figure 5.25: *Study 7 - Frequencies of the equivalent machines*

Resembling the results of Study 4, the frequency estimated to Area 1 follows the frequency of the COI of this Area perfectly, since this area is composed only by one generator. For Area 2, instead, the frequency estimated is highly influenced by the electrical distance between boundary bus 6 (where the

measurements are acquired) and Generator 2, such that naturally the influence of the frequency of G2 in the estimated frequency of the area is higher than the others. To observe better these phenomena, Figure 5.26 presents a zoom on the dynamic behaviour during the first perturbation.

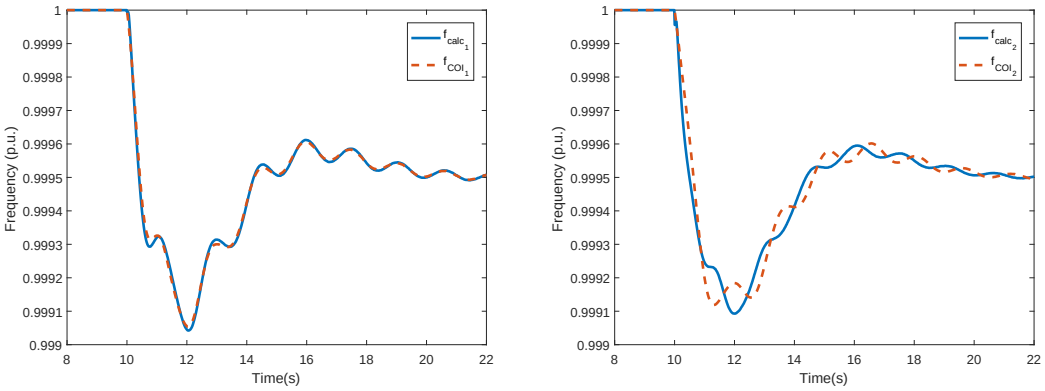

(a) Area 1 (b) Area 2

Figure 5.26: *Study 7 - Frequencies of the equivalent machines - Zoom*

To estimate the inertia of both areas, the following procedure is adopted: As Area 1 doesn't contain loads neither the perturbation, the practical approach of considering the mechanical power as constant in the seconds following the perturbation is used. For Area 2, instead, this assumption doesn't hold and may result in negative inertias estimated, due to the behaviour of the moving power, as seen in the previous sections of this thesis.

In the presence of a RES unit, the moving power of Area 2 can be expressed by

$$P_{mov_{A2}}(t) = \sum P_m(t) + \sum P_{dec}(t) - \sum P_L - \sum P_{losses} \tag{5.2}$$

where $P_m(t)$ stands for the total mechanical by synchronous machines and $P_{dec}(t)$ for the RES unit, that in this study is considered constant. The other quantities were previously defined in Equation (4.51). In this study, the moving power is considered as known.

Considering a sliding window of 300 samples (6s), the inertia of both areas was continuously estimated in time and presented in Figure 5.27, where the dashed horizontal line represents the true values of the COI. As it can be seen in Figure 5.27(a), the inertia estimated for Area 1 was very close to the expected value for more than 5s after the occurrence of both perturbations. Later on, the estimation degrades due to two reasons: first, the assumption of constant mechanical power does not hold for long, as it slowly increases to match the new load demand. At second, the inertial response ends and the dynamic of Area 1 is governed mostly by its controllers. In the case considered, the time constant of the controllers is around 4s. Considering the sliding window of 6s used, the response of the controllers start to appear in the inertia estimated approximately 10s after the occurrence of the perturbation.

Regarding Area 2, Figure 5.27(b) shows also accurate estimations with respect to the expected equivalent inertia of the COI. It is important to observe that this result was obtained assuming the moving power as known, which is a strong assumption. Here, the assumption is made to demonstrate that the connection of a wind power generator to the grid is an observable event that enables the methods studied to estimate the equivalent inertia of the related area accordingly. To be fully practical, i.e., obtain the

estimation of inertia based only on the measurements of the grid without assuming any other quantity as known, it is necessary to estimate the moving power. A method to estimate it was presented in Section 4.2.5.3, with results presented in Section 5.4.2.

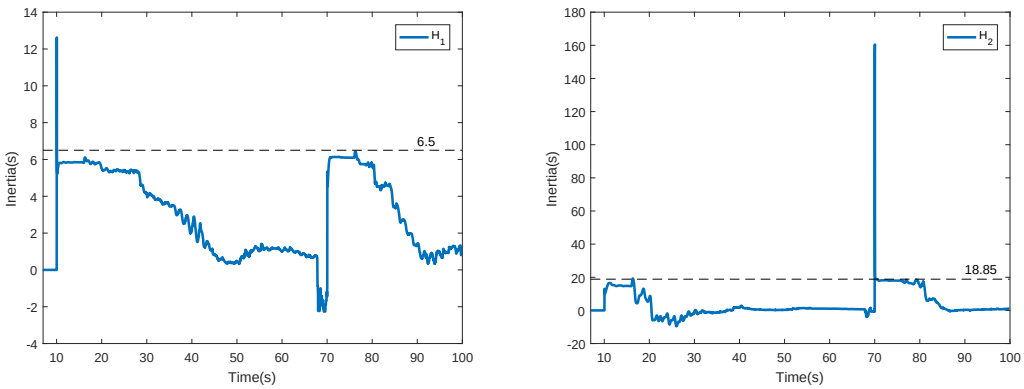

(a) Area 1 (b) Area 2

Figure 5.27: *Study 7 - Equivalent inertias*

To have an idea on the power and frequency variations following the event, Figure 5.28 depicts the results regarding Area 2. As it can be seen, the impact of the connection of the wind power unit was similar to the load step previously applied, both in terms of frequency and power. Hence, both events produced imbalances with a magnitude high enough for the methods to make use of the data and estimate inertia.

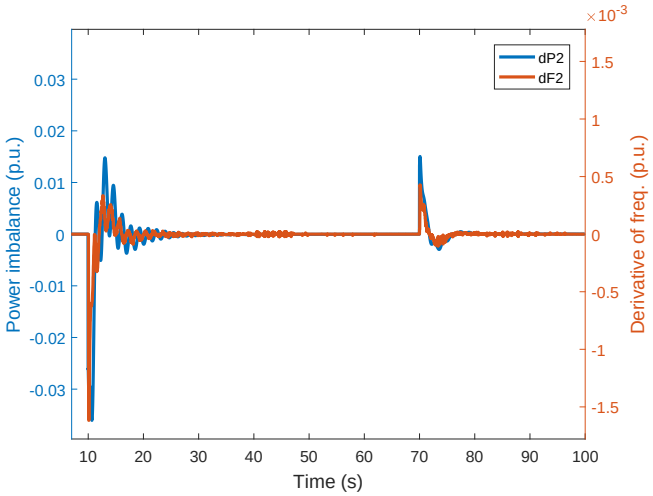

Figure 5.28: *Study 7 - Frequency and Power variations at Area 2*

5.3.1.2 Conclusions of Study 7

In this study, the connection of a wind power generation was evaluated as an event and measurements from the grid were used to estimate the equivalent inertias in the transient period. The estimations

were performed considering the delimitation of two areas. Regarding the area where the generator was connected inside, the moving power was assumed as known and imported from the simulator. Regarding the other area, instead, practical approaches were used. The inertias were accurately estimated in the conditions considered.

5.3.2 Study 8 - Substitution of a small synchronous generator by a RES-based generator

For this study, the Test-system C is modified according to Figure 5.29. A synchronous machine (identified as G6) is connected to bus 8 in the base case and the new power flow solution is obtained. The new unit generates 20MW and 6.6Mvar, and has a nominal power of 100MVA with H=5s of inertia constant (H=0.55s, scaled to the nominal power of G1,...,G4). Different simulations were performed, varying the outputs of the RES unit connected.

The characteristics of the simulations are as follows:

- Test-system used: Based on Test-system C, presented in Section D.3;
- Simulation software: PowerFactory2018;
- Perturbations simulated: Load step at t=10s. Connection of a wind-power generator and simultaneous disconnection of synchronous generation at t=70s;
- Model used for the synch. machines: two-axis IEEE standard detailed Model 2.2 [45];
- Machine parameters: according to Table D.2.
- Model of the loads: constant impedance;
- Losses: considered;
- Controllers: Governor, PSS and AVRs modelled using standards models and parameters available in PowerFactory2018;
- Sampling time: 20ms.

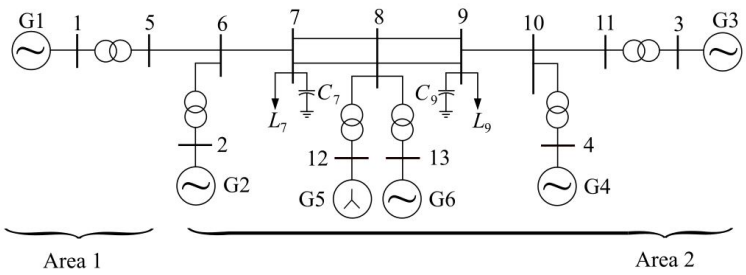

Figure 5.29: *Study 8 - Test-system*

5.3.2.1 Test 1

In this test, three events were considered in the same simulation. First, the same load step of Study 7 is applied at t=10s. At t=70s, G6 is disconnected while G5 is connected generating exactly the same amounts of active and reactive power that G6 was generating at that moment.

The variance method is applied, and the calculated frequencies of Area 1 and 2 can be seen in Figure 5.30, identified by f_{calc} and compared with the true frequency of the COI of each area (identified by f_{coi}), obtained from the simulations. As it can be observed, the frequencies were well estimated. However, it is not possible to observe significant variations following the event at t=70s. The same can be said about the ROCOF an the power imbalance related to each area, as depicted in Figure 5.31.

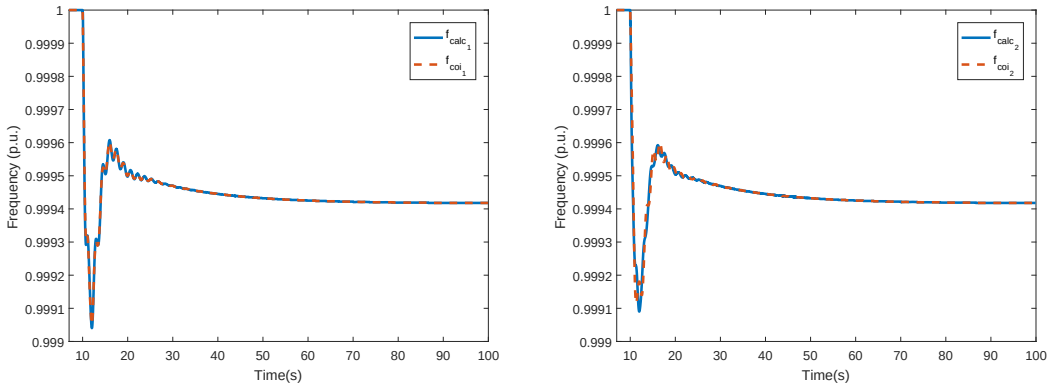

(a) Area 1 (b) Area 2

Figure 5.30: *Study 8 - Test 1 - Frequencies of the equivalent machines*

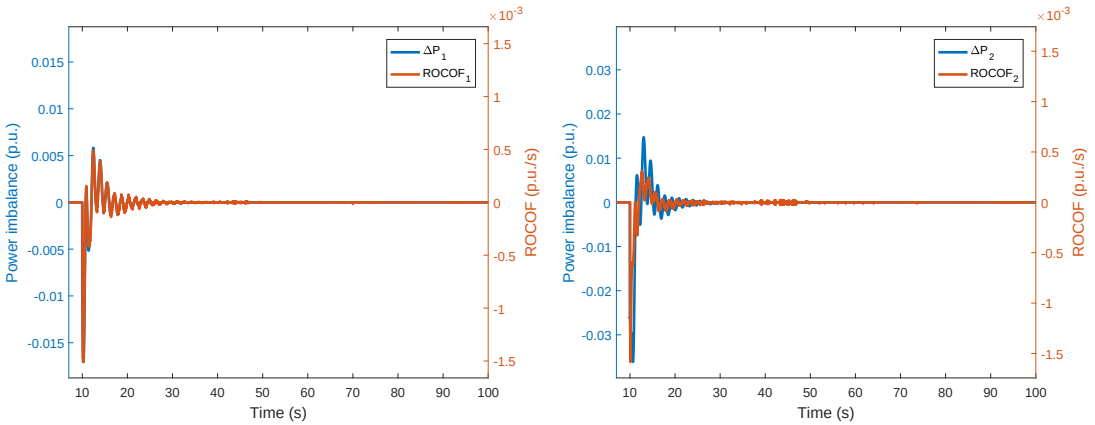

(a) Area 1 (b) Area 2

Figure 5.31: *Study 8 - Test 1 - ROCOF and power imbalances*

Consequently, the methods failed to estimate the inertia following the events happening at t=70s. The resulting inertias can be seen in figure 5.32(a). The negative inertias obtained after t=70s for Area 2 is due to a very small frequency variation, close to the limits of the integration method used in PowerFactory, as it can be seen in Figure 5.32(b).

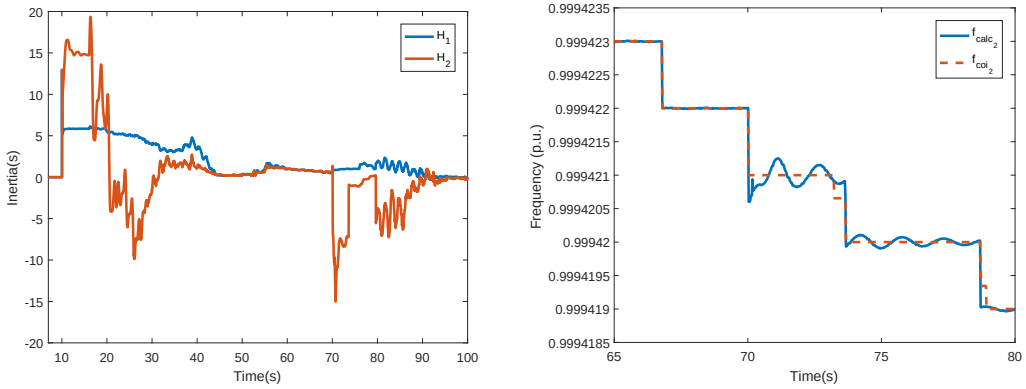

(a) Equivalent inertias estimated

(b) Zoom - Frequency of Area 2

Figure 5.32: *Study 8 - Test 1 - Results of Area 2*

However, it is important to point out that this case is quite extreme. The wind power unit G5 is connected generating the same amount of reactive power of G6, which is not expected in real life, as the RES-based machines work differently than the traditional ones in terms of generating reactive power. Hence, at least a reactive power imbalance should be seen, which may lead to further active power flows and active power imbalances. To test this hypothesis and to provide a test case more realistic, Test 2 was carried out, modifying the injected reactive power of the wind power unit.

5.3.2.2 Test 2

In this test, the test-system is re-simulated with G5 generating Q=2Mvar when connected. This detail forced the reactive power to be rebalanced, implying variations in the power flows and also variations in the frequencies around the system. As it can be seen in Figure 5.33, now the event at t=70s is noticeable, besides the variations are much smaller than the load increase applied at t=10s.

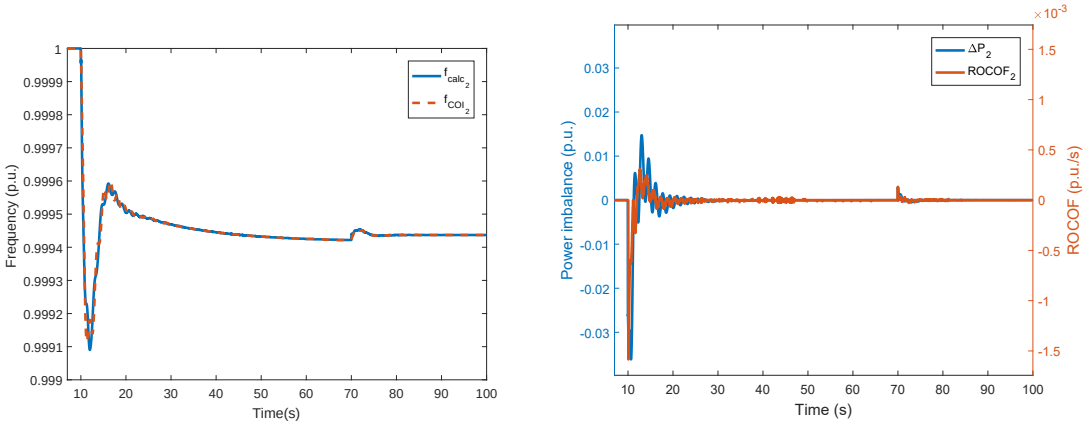

(a) Frequency

(b) Frequency and power variations

Figure 5.33: *Study 8 - Test 2 - Variations at Area 2*

Figure 5.34 depicts the estimated inertias for both Areas, with a sliding window of 6s. The black

dashed horizontal lines represent the true inertia of each COI. In Figure 5.34(b), the green horizontal lines depicts a representative value for the estimated inertias. The following criteria was used: if the inertia estimated varied less than 5% during 25 samples (0.5s), it is considered constant and the average value of the inertia estimates is taken as representative.

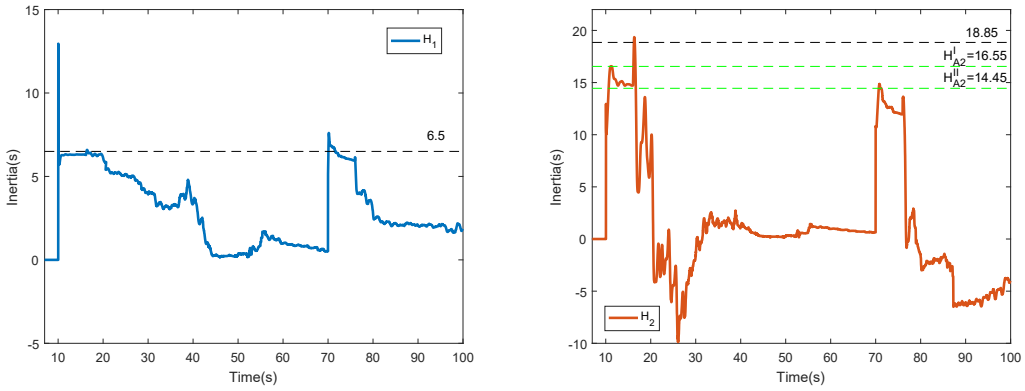

(a) Area 1 (b) Area 2

Figure 5.34: *Study 8 - Test 2 - Equivalent inertias estimated*

Using the criteria defined for estimating a representative value of inertia, after the first event the estimation obtained was $H^I_{A2} = 16.55s$, while after the second $H^{II}_{A2} = 14.45s$. As it can be seen, the results show a decrease in the inertia estimated for Area 2, meaning that the estimation method was able to detect the event and estimate the inertia of the area. However, the generator G6 is very small in terms of nominal power and inertia in comparison to the other synchronous machines connected. Due to this reason, the contribution of this generator to the equivalent inertia of Area 2 is very small and within the deviation that the inertia estimations are presenting until now. Hence, it is possible to observe an inertia decrease, but it is not possible to affirm yet that the decrease is due to the contribution of the generator disconnected or due to inaccuracy of the method, since the frequencies and power imbalances registered were much smaller than the ones registered following the first event. To investigate the inertia decrease quantitatively, another study was performed considering bigger generating units, and is presented in the next section.

5.3.2.3 Conclusions of Study 8

In this study, the connection of a wind power generator was performed at the same time as a synchronous generator was taken out of service. In the specific case when both generators are small and the wind power generator is connected supplying exactly the same active and reactive power that traditional unit was providing in the instant before the connection, it was not possible to observe frequency and power variations and hence to estimate equivalent inertias. However, simulating a scenario where the wind power generator is connected supplying a slightly different reactive power was already enough to provide frequency and power variations that applied to the methods leaded to reasonably acceptable monitoring of inertia variation. This seems to be a more realistic case, once the wind power and the synchronous generators differ on the way they produce or consume reactive power.

5.3.3 Study 9 - Substitution of a big synchronous generator by a RES-based generator

For this study, Test-system C is again taken as base. At t=5s the load step is applied at step increase of 5% at load 7. At t=20s, G4 is disconnected and a wind power generator (identified as G5) of the same size of G4 (900MW nominal power) is connected to bus 10, as depicted in Figure 5.35. The expected equivalent inertias at the COI of area 2 are $H^{I}_{COI_{A2}} = 18.85$ while G1...G4 are connected and and $H^{II}_{COI_{A2}} = 12.675$ after the disconnection of G4.

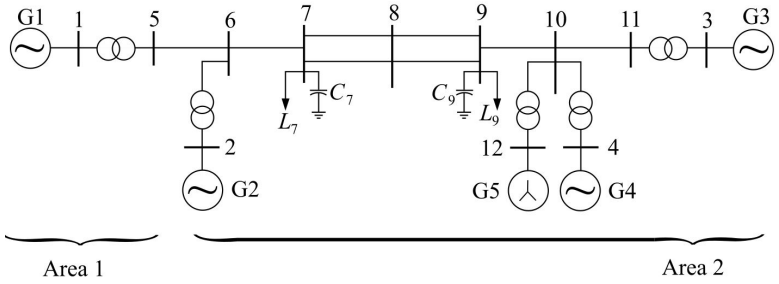

Figure 5.35: *Study 9 - Test-system*

The characteristics of the simulations are as follows:

- Test-system used: Based on Test-system C, presented in Section D.3;
- Simulation software: PowerFactory2018;
- Perturbations simulated: Load step at t=5s. Connection of a wind-power generator and simultaneous disconnection of synchronous generation at t=20s;
- Model used for the synch. machines: two-axis IEEE standard detailed Model 2.2 [45];
- Machine parameters: according to Table D.2.
- Model of the loads: constant impedance;
- Losses: considered;
- Controllers: Governor, PSS and AVRs modelled using standards models and parameters available in PowerFactory2018;
- Sampling time: 20ms.

In the present, case G5 is set to generate 711.4MW and 192.9Mvar, exactly the power supplied by G4 one instant before its disconnection, resembling the previous study. However, it was not possible to impose exactly the same quantities. Due to particularities of the scenario, the simulator connected the wind power unit generating 719MW and 195Mvar instead of the imposed values. These is due to how the software refers the quantities. The input is referred to a nominal voltage, which is not the current operating point in the moment of the imposed event. As this was a study imposing quite extreme conditions, as seen in the previous subsection, it was decided that investigating this software issue to

perform a perfect simulation in terms of power connection and disconnection was not worth, and it was decided to continue the study with the data provided by the simulation as it was described.

As it can be seen in Figure 5.36 that the magnitude of the variations of frequency and power related to Area 2 were significant.

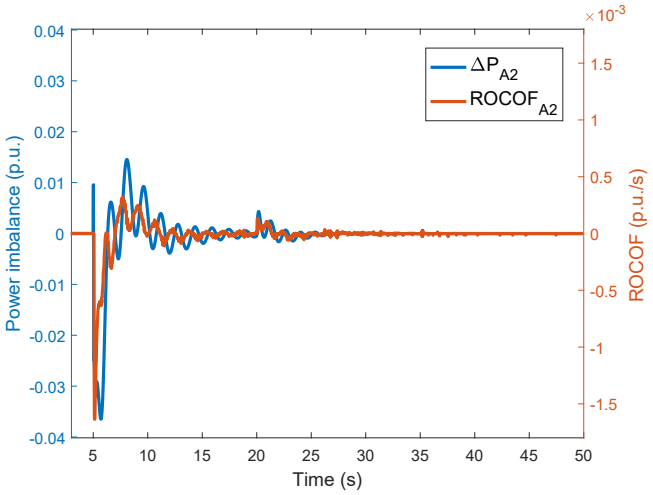

Figure 5.36: *Study 9 - Simulation results*

5.3.3.1 Results of Study 9

Considering the moving power of the area as monitored, the equivalent inertia of Area 2 was estimated with a time window of 6s. Results can be seen in Figure 5.37, where the black dashed lines are the actual values of inertia before (H=18.85) and after (H=12.675) the disconnection of G4. The green lines are the representative estimations chosen considering the same criteria adopted in the previous section, i.e., if the inertia estimated varied less than 5% during 25 samples (0.5s), it is considered constant and the average value of the inertia estimate is taken as representative.

The first comment that can be made is that clearly the estimated equivalent inertia after the second event decreased in comparison to the first. For a quantitative comparison, after the first event the representative inertia estimated was $H^I_{A2} = 14.74s$, while after the second event, the representative inertia estimated was $H^{II}_{A2} = 8.84s$. The difference is $H^I_{A2} - H^{II}_{A2} = 5.9s$, which is very close to the inertia of the disconnected generator ($H_{G4} = 6.175s$).

A second observation regards the negative inertia estimated between 15s and 20s. This is due to the action of the controllers present in the grid, which the methods are not able to take into consideration. Hence, these estimations are misleading. To differentiate these estimations from the true estimations of inertia following the perturbation, the criteria for defining a representative estimation can be used. Following the first seconds after the perturbation, the inertia estimations are constant for more than 0.5s and the representative estimation $H^I_{A2} = 14.74s$ was obtained. This is valid until t=10s, when the inertia starts to variate and does not become constant until the other perturbation happens. Considering the period between t=10s and t=20s, it can be said that the estimations obtained in this time window are not representative. Three different causes can be enumerated: whether the inertia of the area is varying substantially every second (which is not common, since it would need connections/disconnections of

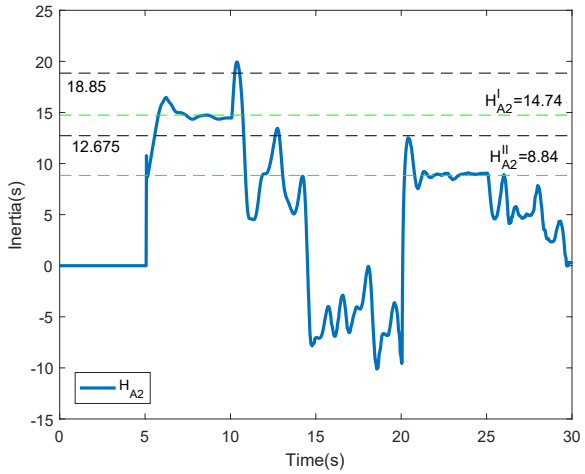

Figure 5.37: *Study 9 - Equivalent inertia of A2*

generators), whether many different perturbations are happening one after the other, with high impact, whether the frequency is oscillating due to the controllers. The latter is the most common one.

An additional comment that can be made is that both H^I_{A2} and H^{II}_{A2} were much smaller than the true inertia of the COI of Area 2 ($H^I_{COI_{A2}} = 18.85$ and $H^{II}_{COI_{A2}} = 12.675$). This happens because bus 6 (the boundary bus of Area 2, where the PMU is considered to be installed) is electrically closer to G2 than to the other generators, such that the estimated frequency of Area 2 (f_{calc_2}) is much closer to the frequency of G2 (f_{G2}) than to the frequency of the COI of Area 2 (f_{COI}), as it can be seen in Figure 5.38(a). However, it can be seen in Figure 5.38(b) that right after t=20s, f_{calc_2} follows a concave curve influenced by the dynamics of G3 and G4, and similar to the curve that f_{COI} presents. After t=20.5s, f_{calc_2} follows the convex trend of f_{G2}. This explains the first peak right after t=20s and the following decrease after 20.5s.

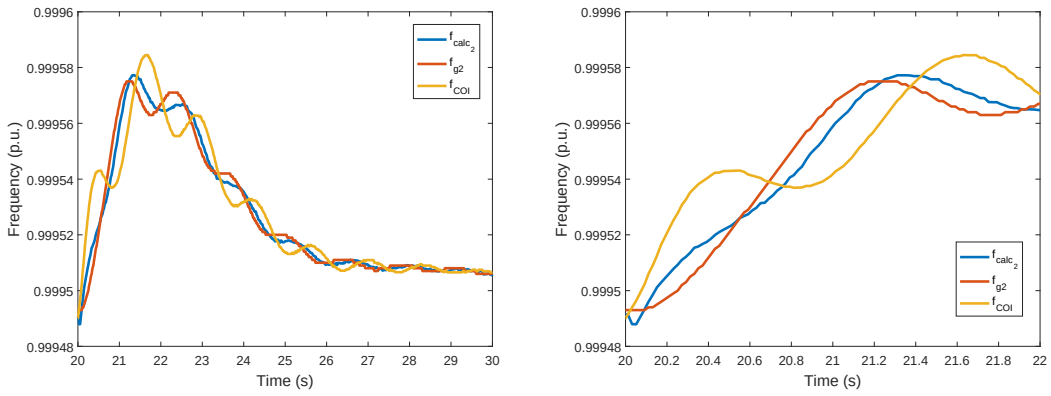

(a) Frequencies

(b) Frequencies - Zoom

Figure 5.38: *Study 9 - Results of Area 2*

Despite of that, one may be interested on having a more accurate information of the dynamic behaviour of the COI of the studied Area, not a information biased by the electrical distance of the mea-

surement point to the closest and to the other generator. For that, advantages can be taken if data coming from more measurement points are available.

Considering a PMU installed at bus 3, and applying the Ward equivalent method presented in Section 4.2.4, the results of Figure 5.39 are obtained. It can be seen in Figure 5.39(a) that now the frequency estimated follows much closer the trend of the COI frequency of the referred area. Moreover, it can be seen in Figure 5.39(b) that the equivalent inertia estimated matches the values of $H_{COI_{A2}}$ following the first event, and was close to the expected value after the second event. Although the oscillations are not ended up when the second event takes place, the correct values of the moving power of Area 2 provide enough information for the method to estimate correctly the inertia in most of the time window evaluated.

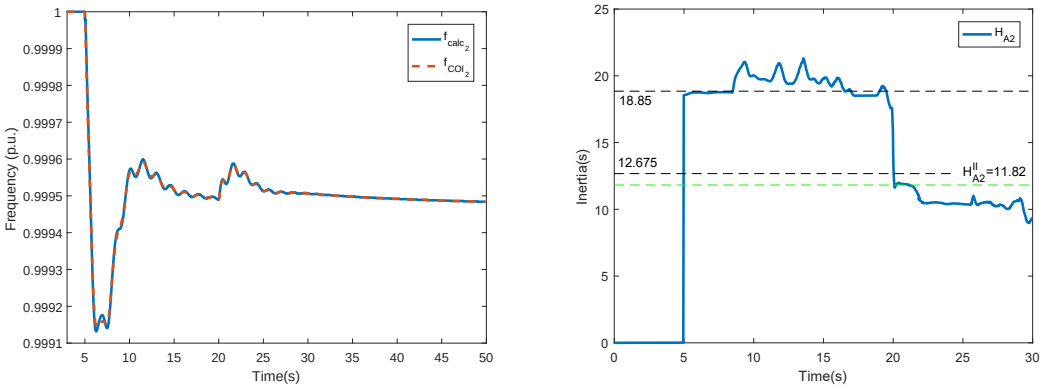

(a) Frequency

(b) Inertia estimated

Figure 5.39: *Study 9 - Results of Area 2 considering more PMUs*

5.3.3.2 Conclusions of Study 9

In this study it was possible to see that the substitution of synchronous generation by a decoupled generation generates a dynamic response of the grid that can be monitored by PMUs and used to estimate equivalent inertias from the points of measurements. Moreover, the decrease in inertia according to the disconnected synchronous machine is observable quantitatively in a sliding window approach. This study also showed the advantage of making use of more measurement points spread on the grid, which may provide a better picture of the COI of an area, while using only data acquired on the boundary bus gives estimations biased by the electrical distance of the generators involved.

5.4 Additional studies

In this section, two different studies are presented, in complement to the previous ones.

In study 10, a probed output signal that can be treated as a perturbation to estimate the inertia of the area is proposed, in complement to the previous studies that considered the occurrence of non-controlled events.

In Study 11, the method proposed in Section 4.2.5.3 to estimate the equivalent moving power of an area is tested with two different types of perturbation, and is further used to estimate the equivalent inertia of an area in a practical approach, in complement to the previous sections where the equivalent moving power was considered as known.

5.4.1 Study 10 - Tests considering a Probe

All the previous studies presented depended on observing a perturbation on the grid to estimate inertia. The load steps are common events, but still non controlled by the TSO, such that the power imbalance over a time window may be too small to be observed by the inertia estimation methods studied. This topic is approached in Section 5.5. In the present study, the idea is to evaluate the use of a probe to generate a controlled power imbalance to estimate inertia.

Here, Test-system C was used as base and modified according to the needs of the study. A Probe was connected in the intermediate bus 8, as depicted in Figure 5.40. It was simulated in PowerFactory by a constant PQ load varying its magnitude according to an input square wave. It is important to observe that the whole system counts with approximately 3250 MW of installed capacity, from which Area 2, where the probe is installed, counts with approximately 2500 MW.

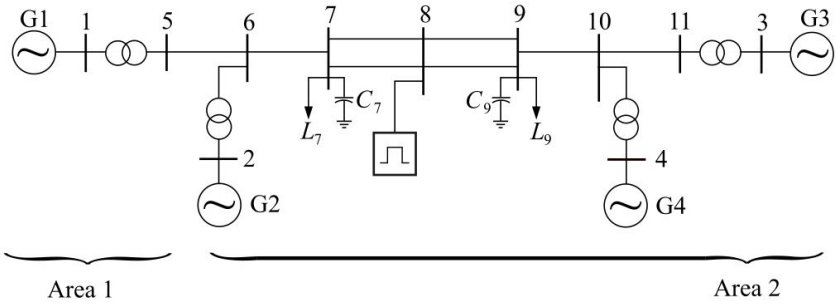

Figure 5.40: *Study 10: Test-system*

The characteristics of the simulations are:

- Test-system used: Based on Test-system C, presented in Section D.3;
- Simulation software: PowerFactory2018;
- Perturbations simulated: Probe (controlled square wave);
- Model used for the synch. machines: two-axis IEEE standard detailed Model 2.2 [45];
- Machine parameters: according to Table D.2.
- Model of the loads: constant impedance;
- Losses: considered;
- Controllers: Governor, PSS and AVRs modelled using standards models and parameters available in PowerFactory2018;
- Sampling time: 20ms.

5.4.1.1 Test 1 - 20MW peak-to-peak

In this study, the profile imposed to the probe was 20MW peak-to-peak, with a period of 10s as depicted in Figure 5.41.

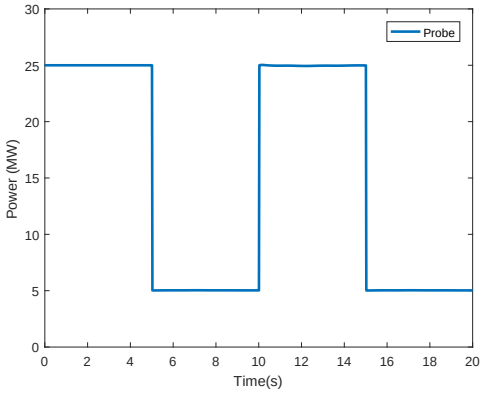

Figure 5.41: *Study 10 - Test 1 - Probe*

Considering 20s of simulation, the "Variance method" was applied to build the dynamic equivalents of each area considering PMUs installed at the boundary buses 5 and 6, and in the "internal" bus 10. The frequencies estimated can be seen in Figure 5.42.

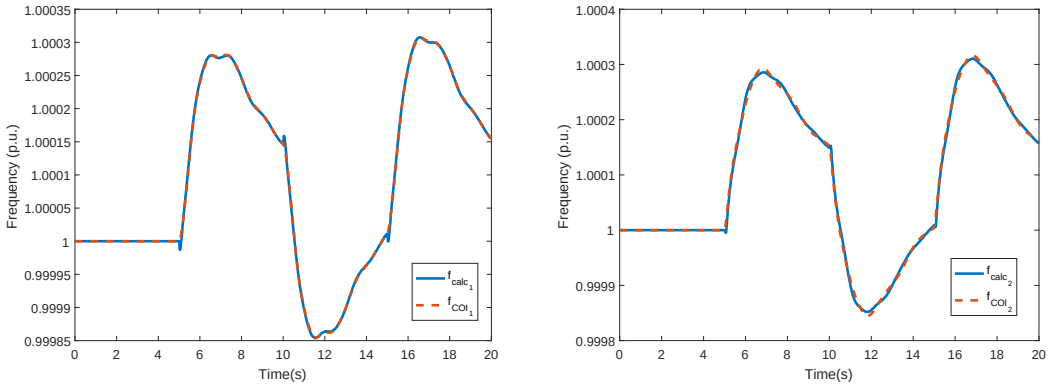

(a) Area 1 (b) Area 2

Figure 5.42: *Study 10 - Test 1 - Frequencies*

Once again, the assumption of slow moving power was adopted for Area 1 while for Area 2 the probe and the loads were considered as monitored. Both the inertias were well estimated, as it can be seen in Figure 5.43, considering a sliding time window of 5s.

For the tested 20MW peak-to-peak probe, the maximum frequency variation observed was 0.46mHz peak-to-peak.

5.4.1.2 Test 2 - Perturbation size vs accuracy of the method

In this study, the probe profile imposed was reduced in terms of peak-to-peak power consumed, to observe the accuracy of the Least-squares method for estimating the inertia vs the size of the probe. In this test, none of the MEM were used. Instead, the outputs of the simulation in terms of COI frequencies and power imbalances were considered, because here the idea is to evaluate the minimum power imbalance

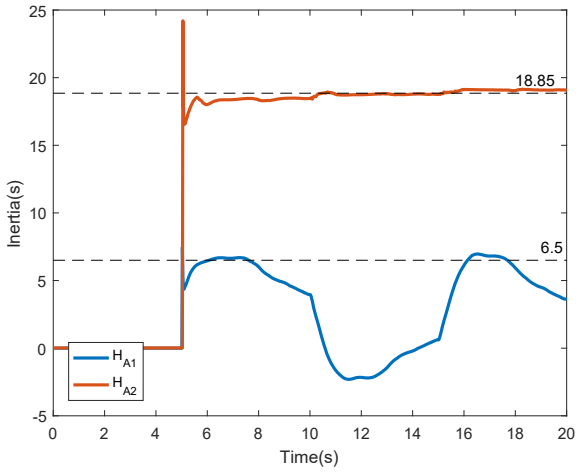

Figure 5.43: *Study 10 - Test 1 - Inertias estimated*

that can still provide accurate estimations of inertia in terms of an approach based on solving the swing equation through least squares, regardless the MEM used.

To investigate the proposed question, different simulations were performed. First, a probe of 10 MW peak-to-peak was used. Results can be seen in Figure 5.44, obtained with a sliding time window of 5s. The peak-to-peak variation of frequency observed was 0.225mHz, and the inertia estimated was close to the expected values, as it can be seen in Figure 5.44(b).

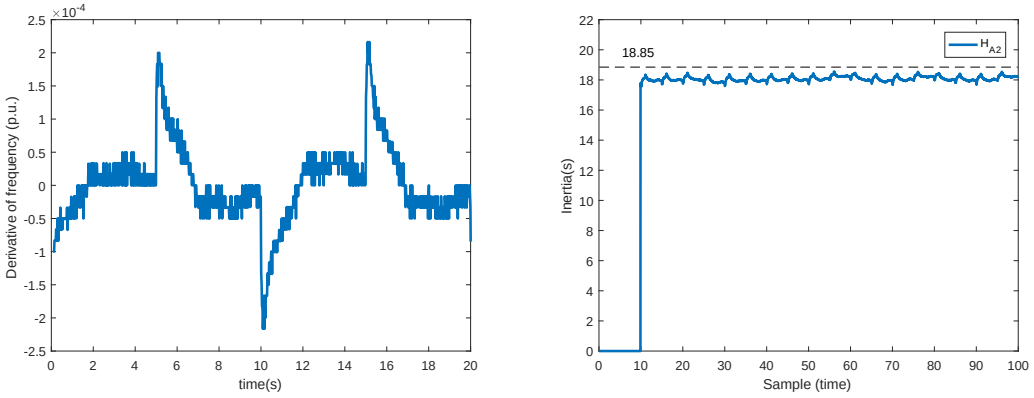

(a) Derivative of frequency - Area 2

(b) Inertia estimated - Area 2

Figure 5.44: *Study 10 - Test 2 - Probe of 10MW peak-to-peak*

Later, the peak-to-peak power input of the probe was reduced until it started to influence on the results. The length of the sliding window was kept the same for every test (5s). The estimations were still accurate until a probe of 5MW was used, with a related frequency variation around 0.1 mHz peak-to-peak. Below 5 MW, the inertia estimation degraded as it can be seen in Figure 5.45(b) for a probe of 4 MW. This is due to the degree of accuracy of the integration method used in PowerFactory2018, such that the finite difference operation involved in frequency and ROCOF calculations were affected. The peak-to-peak recorded frequency variation was 0.0901 mHz.

This behaviour is aggravated in the simulation considering the probe of 2 MW. Comparing the derivative of frequency between the probe of 2 MW (Figure 5.46(a)) and the probe of 10 MW (Figure 5.44(a)), the difference in accuracy is visible.

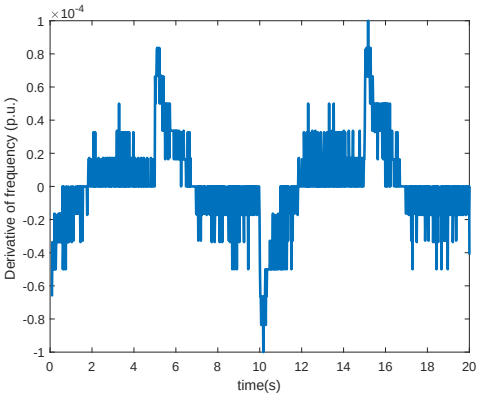

(a) Derivative of frequency - Area 2

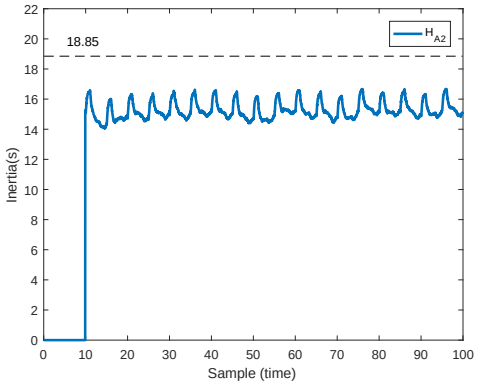

(b) Inertia estimated - Area 2

Figure 5.45: *Study 10 - Test 2 - Probe of 4MW peak-to-peak*

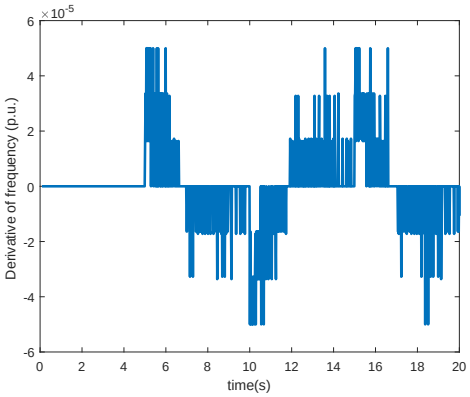

(a) Derivative of frequency - Area 2

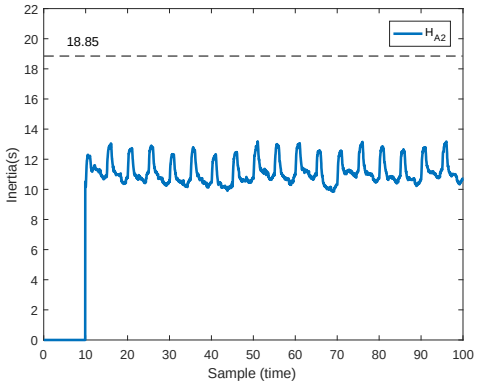

(b) Inertia estimated - Area 2

Figure 5.46: *Study 10 - Test 2 - Probe of 2MW peak-to-peak*

A summary of the results can be seen in Figure 5.47, where the error obtained in the inertia estimations is plotted against the size of the probe. It was necessary a probe of at least 5 MW peak-to-peak to obtain estimations with error smaller than 10%. In this case, the minimum frequency variation necessary was 0.1mHz, and the probe was tested in an Area of 2500MW power capacity. The study didn't consider noise on measurements, and the limit was established according to the numerical limitations of the integration method used.

Considering real cases, the limitation is the relation between the magnitude of variations of frequency in comparison to the measurement noise. If the magnitude of the noise is known, and also the typical constant of inertia the area where the probe should be installed, the minimum size of the probe can be determined according to the swing equation. Considering this test an example, for an area of 18s of inertia and 2500MW installed, the minimum peak-to-peak frequency variation needed was 0.1mHz to

estimate inertia with an error of less than 10%, obtained with a probe of 5 MW peak-to-peak.

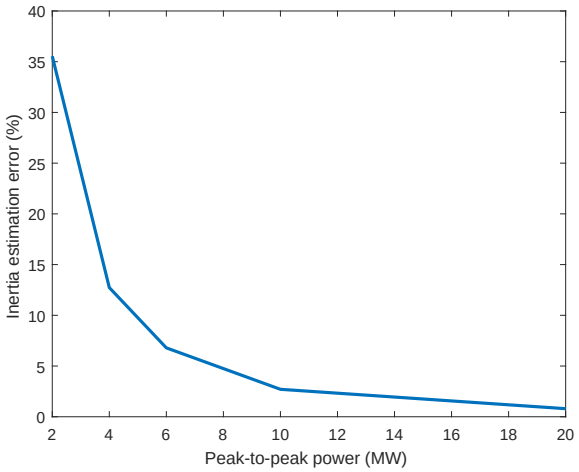

Figure 5.47: *Study 10 - Accuracy of the tests*

5.4.1.3 Conclusions of Study 10

This section presented simulations and results considering a Probe as a font of power imbalance to estimate the equivalent inertias of the system. In the first test, with a Probe of 20MW peak-to-peak, inertia could be well estimated in the conditions considered.

In the second test, the accuracy of the Least-Squares method was evaluated vs the size of the perturbation. The inertia estimation degraded when a probe of less than 5MW peak-to-peak was used in the test-system studied (in an area of 2500 MW installed capacity). This happened due to numerical limitations of the integration method used in the simulations. In real cases, the limitations of estimating inertia using a probe would depend on how small are the variations of frequency due to the power imbalance imposed by the probe in comparison to the noise on the measurement obtained.

5.4.2 Study 11 - Inertia estimation considering moving power estimation

As seen in the previous studies, the assumption of a slow moving power was the cause of many estimation errors when dealing with an equivalent area containing a perturbation and/or voltage dependent loads. In those cases, assuming the generators or otherwise the loads as monitored allowed therefore accurate estimations of the equivalent inertia at the COI of an Area. However, it is a strong requirement for real power systems.

An alternative is to estimate the equivalent moving power through the method presented in Section 4.2.5. In this study, simulations were performed using Test-system C, and considered two different types of perturbation. The main details of the simulations are as follows:

- Test-system used: Test-system C, presented in Section D.3;
- Simulation software: PowerFactory2018;
- Perturbations simulated: depending on the test;

- Model used for the synch. machines: two-axis IEEE standard detailed Model 2.2 [45];
- Machine parameters: according to Table D.2.
- Model of the loads: constant impedance;
- Losses: considered;
- Controllers: Governor, PSS and AVRs modelled using standards models and parameters available in PowerFactory2018;
- Sampling time: 20ms.

5.4.2.1 Test 1 - Load behaviour estimation

In this first test, the perturbation considered was a three-phase solid short-circuit. Case 1 considers a short-circuit at bus 5 and Case 2 considers a short-circuit at bus 11. All the perturbations were assumed at t=20s and the simulations lasted 50s. The short-circuits considered in each case were cleared after 0.5s.

During the simulation, the voltages at all the buses are recorded. Applying Equation (4.56), the voltage profiles presented in Figure 5.48 were obtained with different set of buses. Following the legend of the Figure, V_{Ls} refers to the set of load buses (i.e. bus 7 and bus 9), V_{Gs} refers to the set of generation buses of Area 2 (bus 2,3,4) and V_B refers to the boundary bus of Area 2 (bus 6). These comparisons were made because [152] suggests to use the voltages at generation buses to estimate the load behaviour, if load buses are not directly monitored (as showed in Equation (4.55)). However, as it can be seen in both cases, the voltage profile of the boundary bus (V_B) was closer than V_{Gs} to the set of load buses (V_{Ls}).

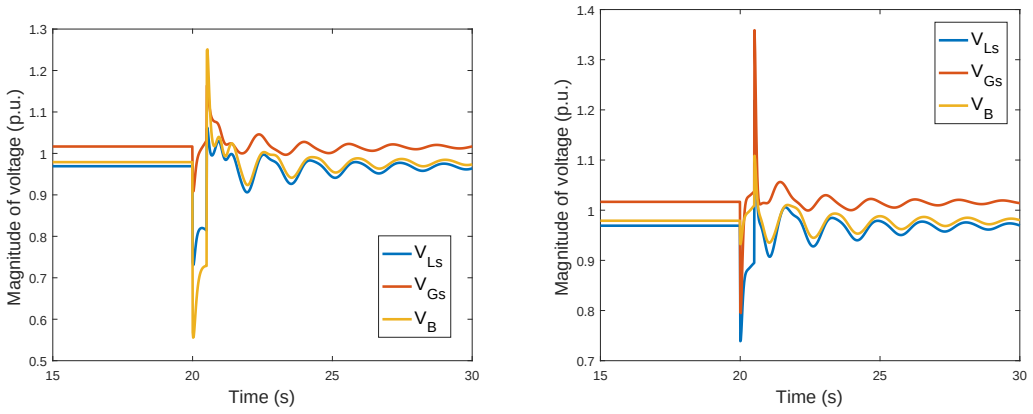

(a) Case 1 - SC at bus 5

(b) Case 2 - SC at bus 11

Figure 5.48: *Study 11 - Test 1 - Voltage magnitudes*

Moreover, it is possible to obtain a voltage profile closer to V_{Ls} if the voltage of more buses within the area is monitored by a suitable number of PMUs. The best case would be obviously monitoring directly the load buses. So, disregarding this possibility, the second best solution obtained applying Equation (4.56) was obtained monitoring the boundary bus 6 and the transfer buses 8 and 10, what will be referred here as $Set1$. Whenever the voltage at the generation buses were considered, the behaviour

of the equivalent voltage deviated from V_{Ls}. Figure 5.49 presents V_{Set1}, the voltage profile of the loads (V_{Ls}) and the voltage at the boundary bus (V_B). As it can be seen, V_{Set1} presents a closer behavior to V_{Ls} than V_B, showing the advantage of having more measurement points for this finality.

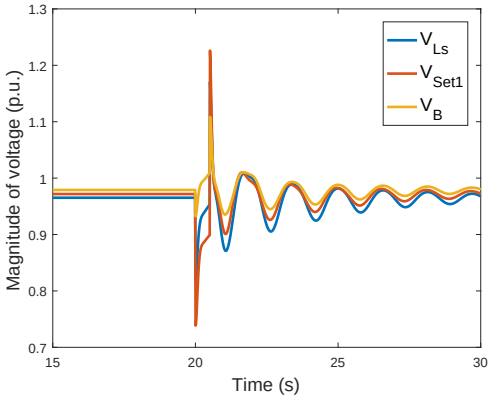

Figure 5.49: *Study 11 - Test 1 - Case 2 - Voltage profiles*

Applying (4.53) to $Set1$, the results presented in Figure 5.50 were obtained. Following the legends, P_{loads} is the true power consumed by the loads recorded during the simulation, while $P_{l_{est}}$ represents the estimated power. As it can be seen, the use of it was possible to estimate the load behaviour with errors smaller than 10% without monitoring directly the load buses. The use of the estimated load power for inertia estimation is approached in the next test.

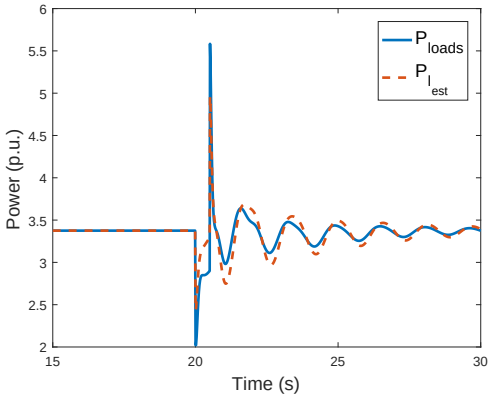

Figure 5.50: *Study 11 - Test 1 - Case 2 - Load behavior*

5.4.2.2 Test 2 - Moving power estimation

In this second test, a step in Load 7 is applied at t=20s. The voltage profiles can be seen in Figure 5.51 where all the legends respect the same quantities defined in the previous test.

The behaviour of the equivalent load of Area 2 is estimated using Equations (4.53) and (4.56). Here, the total load after the disturbance is considered as the reference P_{prod} in Equation (4.53). The results obtained using $Set1$ are presented in Figure 5.52, where P_{loads} is the true behaviour of the loads (acquired

from the simulator) and $P_{l_{est}}$ is the estimated one. As it can be seen also in this test, $Set1$ produced acceptable results, showing that monitoring the voltage at all load buses is not necessarily mandatory. Therefore, PMUs are considered available at bus 6 and at buses 8 and 10 ($Set1$) for the remaining of this test, and the estimated power behaviour P_L related to this set is used for means of inertia estimation.

Stating the expression of the equivalent the moving power of Area 2,

$$P_{mov_{A2}}(t) = \sum_{i=2}^{5} P_{m_{Gi}}(t) - \sum P_L(t) - \sum P_{losses}(t)$$

the remaining term $P_{ML} \triangleq \sum_{i=2}^{5} Pm_{Gi} - \sum P_{losses}$ still needs to be estimated.

Using the method proposed in Section 4.2.5.3 with an assumed droop of 5%, the result can be seen in Figure 5.53, where $P_{ML_{sim}}$ denotes the reference output of the simulator and $P_{ML_{Est}}$ denotes the signal obtained with the proposed approach.

Considering the estimated P_{ML} and P_{Loads}, finally the moving power (P_{mov}) of Area 2 can be obtained. The result can be seen in Figure 5.54 identified as $P_{mov_{est}}$ and compared with output of the simulator identified as $P_{mov_{sim}}$. As it can be seen, the results obtained were accurate during more than 10s after the perturbation. The later mismatches are due to the frequency control, that resulted in differences between the projected P_{ML} and the real one, as seen in Figure 5.53.

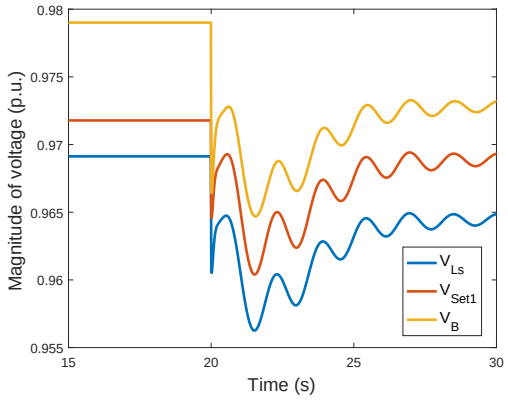

Figure 5.51: *Study 11 - Test 2 - Voltage profiles*

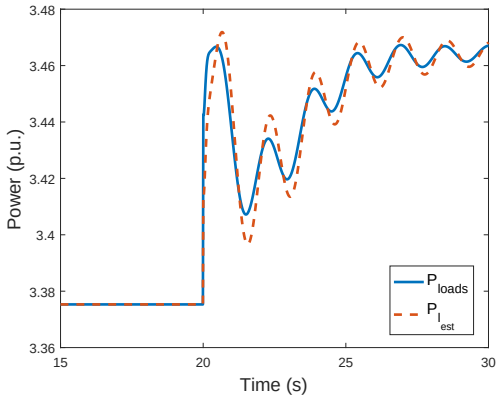

Figure 5.52: *Study 11 - Test 2 - Load behaviour*

With the obtained moving power of Area 2, it is possible to use one of the inertia estimation methods and obtain the equivalent inertia of Area 2. As in this study PMUs were considered available at buses 6, 8 and 10 (the defined $Set1$), the data coming from these units were used to build a dynamic equivalent that presents a dynamic behaviour that represents better the behaviour of the COI. If instead only the data of bus 6 was used, the dynamic equivalent obtained would be biased by the proximity of this bus and Generator 2, as seen in Study 9 (Subsection 5.3.3).

Hence, the system reduction method (Section 4.2.4) was applied and the estimated inertia at the COI of Area 2 can be seen in Figure 5.55, obtained with a sliding window of 6s. Following the legend, H_{A2_I} refers to the use of the old assumption of slow behaviour of the moving power, here presented for comparison, and $H_{A2_{II}}$ refers to the inertia obtained using $P_{mov_{est}}$ presented in Figure 5.54. The black dashed line, referred as $H_{COI_{A2}}$ depicts the true value of the inertia at the COI of Area 2. The green dashed line (H_{A2_r}) refers to the representative value estimated for $H_{A2_{II}}$ obtained using the following

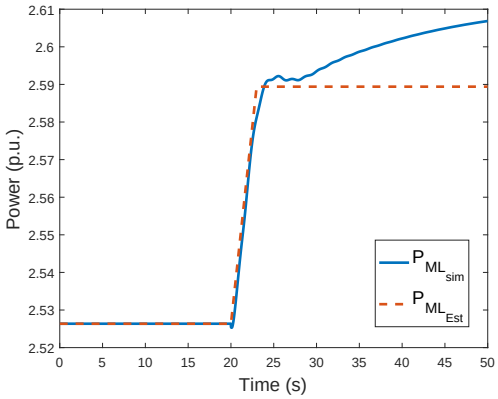

Figure 5.53: *Study 11 - Test 2 - P_{ML} of Area 2*

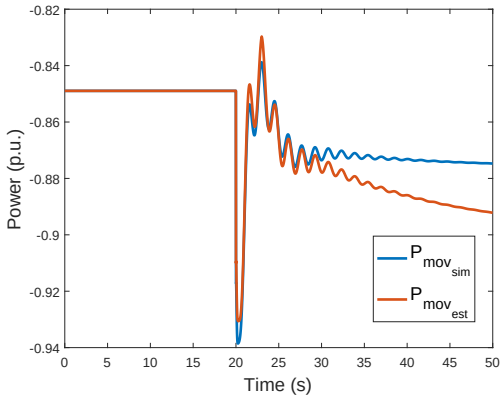

Figure 5.54: *Study 11 - Test 2 - P_{Mov} of Area 2*

criteria: if the inertia estimated varied less than 5% during 25 samples (0.5s), it is considered constant and the average value of the inertia estimates is taken as representative.

As it can be observed in Figure 5.55, the proposed method to estimate the equivalent moving power enabled estimating positive values for the inertia of the area containing the perturbation, and therefore solves this issue. The errors obtained in comparison to the true inertia at the COI were smaller than 10%. This result shows that it is possible to estimate the equivalent inertia of an area in a full practical way based on PMU measurements.

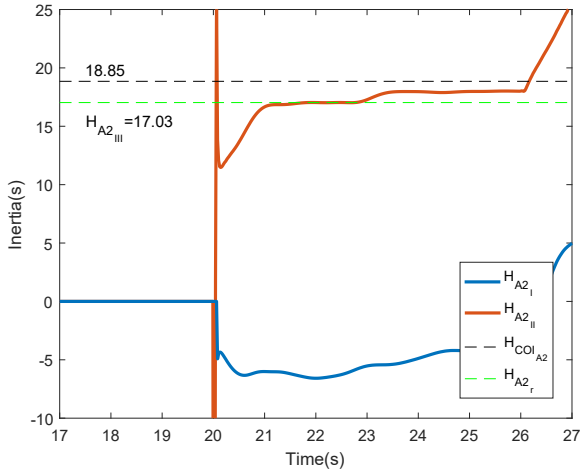

Figure 5.55: *Study 11 - Test 2 - Inertia estimations*

5.4.2.3 Conclusions of Study 11

In this study, the estimation of the equivalent moving power of an area was approached. The study was divided in three main steps: estimating the load behavior, estimating the moving power and estimating the inertia.

A method to estimate the equivalent behaviour of loads was tested, assuming the knowledge of an average estimation of the total power consumed by loads of the area in steady-state. For the simulations

performed, the method succeeded in estimating the equivalent load behavior of an area that contained two different loads. Two different types of perturbations were tested: short-circuits and load steps.

It is important to point out that the estimations were performed considering the constant impedance model for the load both in the simulations and in the method. So far in this thesis, which motivated the study of a method to estimate the load behaviour was the voltage dependence of the loads. As reported in [148], the frequency dependence has lower impact in inertia estimation studies. Hence, the constant impedance model was adopted in detriment of the ZIP or a frequency dependent ZIP model. For applications with real data, the approach [154] can be considered for identifying the proportions of the ZIP model in this case, adapting the method presented in Section 4.2.5.3 according to Equation (2.37).

The moving power of the studied area was composed by the estimated equivalent load behaviour and an estimation of the mechanical power and losses together. The obtained moving power was accurate with the outputs of the simulator for the fist 10s after the perturbation. Finally, the inertia of the studied area was estimated using the moving power obtained, with errors smaller than 10%.

The section also showed the advantages of using data from spread PMUs available in the area. For the point of view of the equivalent load behaviour, the use of a set of measurements obtained at transfer buses enabled to increase the accuracy of the estimations in comparison to only measuring at the boundary bus. To recall, Study 9 (Subsection 5.3.3) had already shown that the use of data coming from spread PMUs inside the area of study enables to build a dynamic equivalent that represents better the behaviour of the COI of the referred area. Hence, both steps of estimating the equivalent inertia of an area have benefits when more PMUs are available.

5.5 Normal load variation studies

In this section, two different studies are presented. The first one approaches the use of the MEMs to estimate inertia after normal load variations. The second one approaches the dynamic matrix method presented in Section 4.2.6.

5.5.1 Study 12 - MEM with moving power estimation method

This study tests the "Variance" method (Subsection 4.2.2.2) together with the moving power estimation method (Section 4.2.5.3) to evaluate inertia estimation following normal load variations. In the previous sections, these methods were already used to estimate the inertia of an equivalent area after the occurrence of a load step, with accurate results. Here, in this study, the idea is to test how the methods perform with normal load variations (i.e., very small changes at every second), instead of just one large load step. For the following studies, PMUs were considered installed at bus 5, 6, 8 and 10, as depicted in Figure 5.56.

- Test-system used: Test-system C, presented in Section D.3;
- Simulation software: PowerFactory2018;
- Perturbations simulated: normal load variation;
- Model used for the synch. machines: two-axis IEEE standard detailed Model 2.2 [45];
- Machine parameters: according to Table D.2.

- Model of the loads: constant impedance;
- Losses: considered;
- Controllers: Governor, PSS and AVRs modelled using standards models and parameters available in PowerFactory2018;
- Sampling time: 20ms.

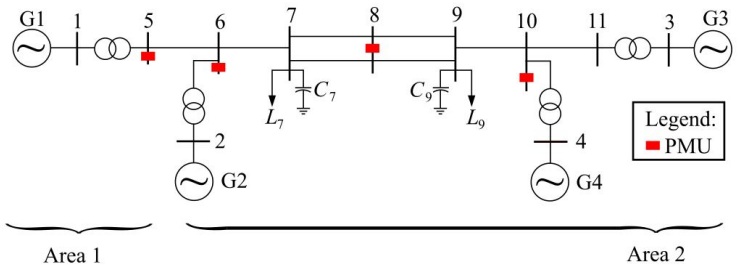

Figure 5.56: *Study 12 - Considered PMUs*

To simulate "normal load variations", an input profile was applied to the load connected to bus 7. The profile consisted in five sequential load steps applied at every second from t=20s to t=25s, varying from increase and decrease of magnitudes up to 10% of the nominal values of the active and reactive power of the load ($S = 967MW + i100MVAr$). The profile can be seen in Figure 5.57.

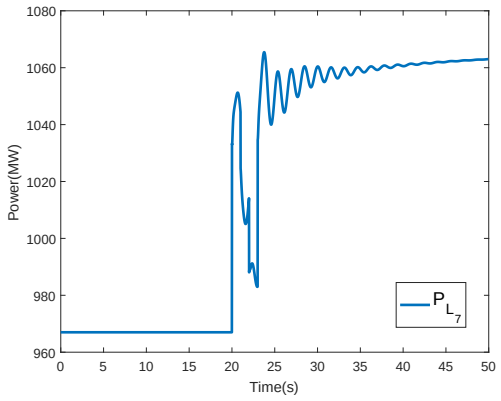

Figure 5.57: *Study 12 - Load profile imposed*

Regarding the dynamic equivalents, the transient reactances of Area 1 and Area 2 were estimated using a time window of 5s from 18.5s to 23.5s. As this load profile is expected to represent normal load variations, it is expected that the transient reactances estimated are good equivalents for the whole period of variations, and then kept constant from this time on. In this study, the limit of a normal load variation considered was 10%, as it was simulated. If, instead, a higher load step was applied, it could be studied alone as a single perturbation, as in the previous sections, with a transient reactance estimated exclusively for that event.

After the transient reactances are calculated, the internal voltages of each equivalent machine can be calculated. Using Equation (3.5), it is possible to calculate the frequencies of each area. Figure 5.58 presents the frequencies of the equivalent machines obtained (f_{calc_j} in the legend), against the frequencies of the COI of each area (f_{COI_j} where $j = A1, A2$ represents the area). The frequency obtained for Area 1 is based only on the measurement of bus 5, while the frequency of Area 2 is obtained taking advantage of the measurements at bus 6,8 and 10. As seen before in this thesis, the use of measurements coming from buses inside the considered Area 2 enables a more accurate estimation of the COI frequency, which is easier to interpret in comparison to the frequency estimated only using the measurements at bus 6.

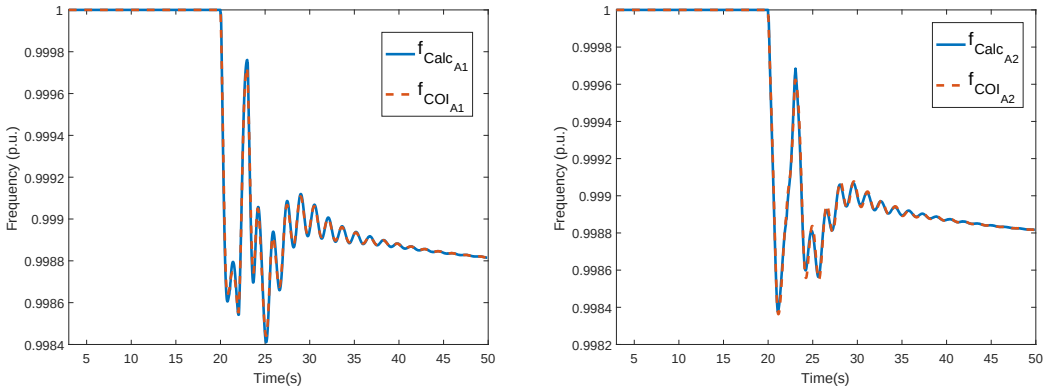

(a) Area 1 (b) Area 2

Figure 5.58: *Study 12 - Frequencies estimated*

Here, resembling Study 11, the total load after the analyzed interval is considered as the reference P_{prod} in Equation (4.53). Results are presented in Figure 5.59, where P_{loads} refers to the output signal of the simulator and $P_{l_{est}}$ refers to the estimated quantity. This approach is identified as Approach I.

As it can be seen in Figure 5.59, the estimations can be considered satisfactory for most of the time window analyzed. Only between t=22s and t=23s the estimated load did not follow accurately the trend of the original loads. This happens because, when considering the total load after the analyzed interval as the reference value P_{prod}, the method "understands" that there was a total load increase from t=20s to t=25s. However, between t=22s and t=23s what happens is a momentary decrease, which is not properly "seen" by the method. If instead P_{prod} is updated continuously, the accuracy of the load power estimations increases. Considering P_{prod} updated at every 2s, the results can be seen in Figure 5.60, identified as Approach II. However, this demands a knowledge of a total load power at time intervals smaller than the time window analyzed, which is not always practical.

With the same approach used in Subsection 5.4.2 to estimate together the trend of the equivalent mechanical power and the losses, the equivalent moving power of Area 2 was composed, with results presented in Figure 5.61. Referring to the legend, $P_{mov_{sim}}$ is the output signal of the simulator and $P_{mov_{est}}$ refers is estimated quantity.

Figure 5.62 presents the estimated inertia of both areas 1 and 2, obtained with a sliding time window of 5s. Starting from Area 1, as it can be seen the inertia was accurately estimated in comparison to the expected value ($H_1 = 6.5s$). It can be concluded that the load variations imposed in Area 2 produced variations of power and frequency high enough for the methods studied to perform as expected. Hence,

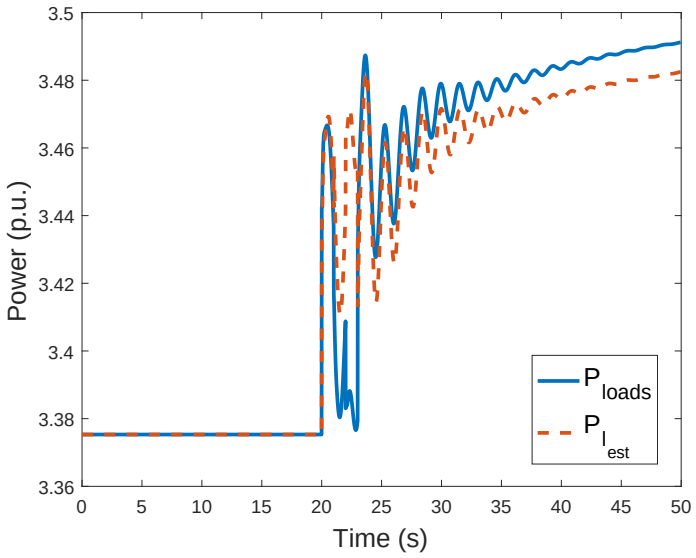

Figure 5.59: *Study 12 - Approach I - Load estimation*

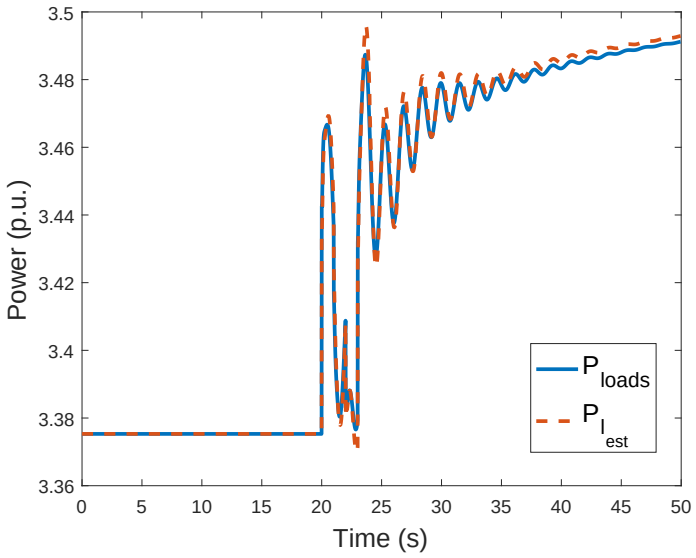

Figure 5.60: *Study 12 - Approach II - Load estimation*

it can be said that the MEM are able to estimate inertia following normal load variations when generators are individually monitored.

Regarding the estimation of the inertia of Area 2, it can be seen in Figure 5.62(a) that the estimation using Approach I was quite close to the expected values (estimated $H_{A2_r} = 16.38$) from t=20s to approximately t=23s. Later, the accuracy decreased following the mismatches on the estimated moving power presented in Figure 5.61(a). After t=25s, there are no load variations and the inertia estimated is influenced by the controllers of the grid. With Approach II, the reference inertia estimated $H_{A2_r} = 16.43$ did not deviate from the result obtained with Approach I, but the difference is after t=23s. The continuous

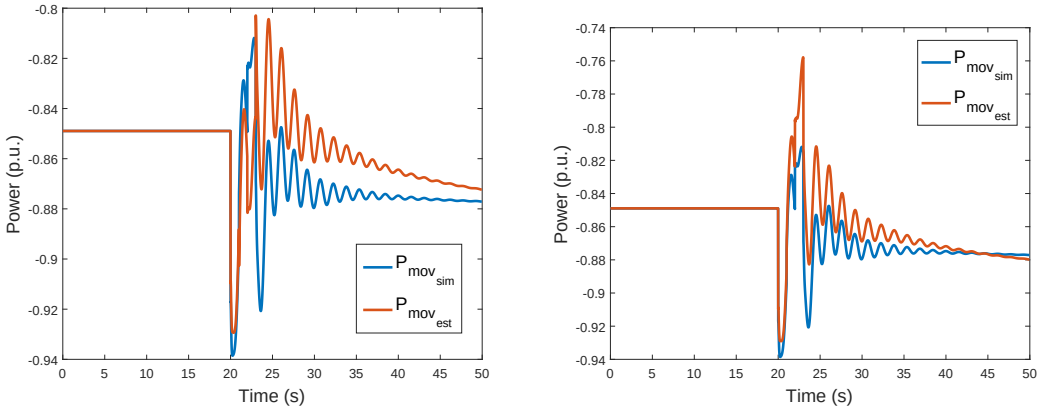

(a) Approach I (b) Approach II

Figure 5.61: *Study 12 - Moving powers estimated of Area 2*

update of P_{prod} improved the estimations for the remaining time interval analyzed.

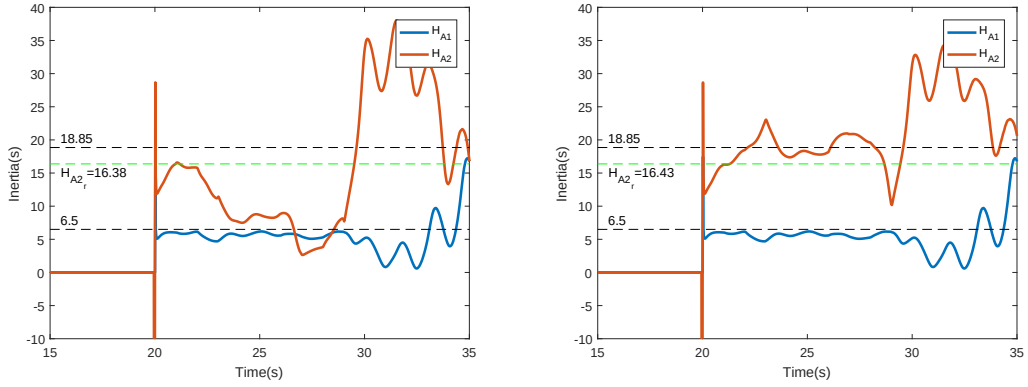

(a) Approach I (b) Approach II

Figure 5.62: *Study 12 - Inertias estimated*

Therefore, the conclusion that can be made for the use of the MEM for estimating the equivalent inertia of an area following normal load variations inside the area is that the method works, but is strongly dependent on monitoring or estimating the equivalent moving power. By monitoring the equivalent moving power, it can be understood by whether monitoring the loads whether the generators (what falls in the case of Area 1, which works well without further limiations). By estimating the equivalent moving power, the accuracy of the method is dependent on how often there is information about the total load of the area. This is a strong requirement when monitoring an area nowadays, where this information may be dependent on SCADA in most systems. Therefore, the topic has room for further studies on load behaviour estimation methods that could relax this requirement and make the proposed method more practical.

5.5.1.1 Conclusions of Study 12

In this study, the MEM were tested together with the moving power estimation method presented in Section 4.2.5.3 for estimating inertia following normal load variations. The MEM performed well, as it could be seen for the individually monitored generator of Area 1, such that it is possible to state that the methods studied work also in ambient conditions.

However, when dealing with equivalent areas with loads inside, the method strongly depends on the moving power estimation, which may decrease the accuracy of the estimations. Analyzing a time window of 5s with loads varying at every second, two approaches were considered. A first approach considered the knowledge of the total load of the area after the time window is concluded, which is a practical assumption. This approach produces acceptable estimations of inertia in the first seconds of the analyzed time window, degrading after it. A second approach considered the knowledge of the total load at every 2.5s, which improved the estimations. The conclusion is that, to estimate the inertia of the area containing the loads, not necessarily the loads must be individually monitored, but the accuracy of the estimations are dependant on how often there is knowledge of a total load of the area.

5.5.2 Study 13 - Dynamic matrix method

In this study, the method proposed in Section 4.2.6 is evaluated. To provide the data, the Test-system E is simulated in Matlab. The multi-machine system is represented with the second-order model in the COI frame, as proposed in [35], [162].

- Test-system used: Test-system E, presented in Section D.5;
- Simulation software: Euler numerical integration method as proposed in [41], implemented in Matlab;
- Perturbations simulated: normal load variation;
- Model used for the synch. machines: second-order model referred to the COI frame, according to Equation (4.76);
- Machine parameters: according to the test;
- Model of the loads: constant impedance;
- Losses: considered;
- Controllers: not implemented;
- Sampling time: 20ms.

To apply the method, the admittance matrix of the system is required, as well as voltage and currents at the terminals of each generator. Moreover, the outputs of a MEM are needed, i.e., rotor angles, frequencies, transient reactances and a previous estimation of inertia. As seen in the previous sections, the MEM performed well in every condition tested when the terminals of the generators were monitored. Consequently, this Study will not contemplate again the performance of the MEMs. Instead, these quantities will be assumed as known and the outputs of the simulator will be directly used, such that the dynamic matrix method proposed in Section 4.2.6 can be evaluated individually.

5.5.2.1 Test 1

For this test, the machine parameters presented in Table D.5 were simulated. In the simulation performed, all the three loads varied randomly every 0.02s, with constant power factor and a standard deviation $\sigma = 0.1$ around the base load. Figure 5.63 presents the load variations simulated, according to Equation (4.75). The outputs of the simulation can be seen in Figure 5.64, where rotor angle and speeds are presented in the COI frame.

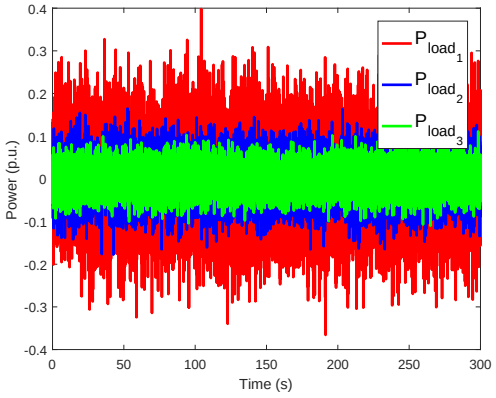

Figure 5.63: *Study 13 - Test 1 - Load behaviour simulated*

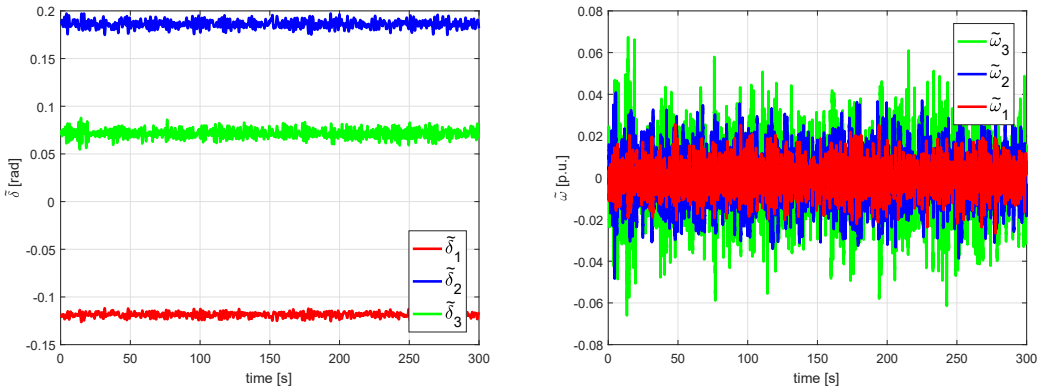

(a) Angles (b) Speeds

Figure 5.64: *Study 13 - Test 1 - Simulations*

The inertia is estimated through Equation (4.87), here repeated for convenience:

$$\mathbf{M} = (\frac{\partial \mathbf{P_e}}{\partial \tilde{\boldsymbol{\delta}}})_{COI} \mathbf{C}_{\delta\delta} \mathbf{C}_{\omega\omega}^{-1} \quad [s^2]$$

If there is no load variation, the term $(\frac{\partial \mathbf{P_e}}{\partial \tilde{\boldsymbol{\delta}}})_{COI}$ is constant and can be calculated through Equations (C.20) to (C.23) as presented in Appendix C. As in this study normal load variations are considered, $(\frac{\partial \mathbf{P_e}}{\partial \tilde{\boldsymbol{\delta}}})_{COI}$ varies around its base state, with no large excursions, since stable ambient conditions are assumed. In the calculations, the previously estimated transient reactances and initial estimates of M_i

are needed. For this simulation,

$$(\frac{\partial \mathbf{P_e}}{\partial \tilde{\boldsymbol{\delta}}})_{COI} = \begin{bmatrix} 8.063 & 1.236 \\ 2.815 & 5.084 \end{bmatrix}$$

Using a sliding time window of 200 samples (4s), the sample-weighted covariance matrices $\mathbf{Q}_{\delta_k \delta_j}$ and $\mathbf{Q}_{\omega_k \omega_j}$ can be calculated for the referred samples of rotor angles and rotor speeds. Hence, $\mathbf{M}$ is calculated in function of the constant $(\frac{\partial \mathbf{P_e}}{\partial \tilde{\boldsymbol{\delta}}})_{COI}$ and the window-based matrices $\mathbf{Q}_{\delta_k \delta_j}$ and $\mathbf{Q}_{\omega_k \omega_j}$. The results for M_1 and M_2 can be seen in Figure 5.65, where the dashed red line represent the expected value.

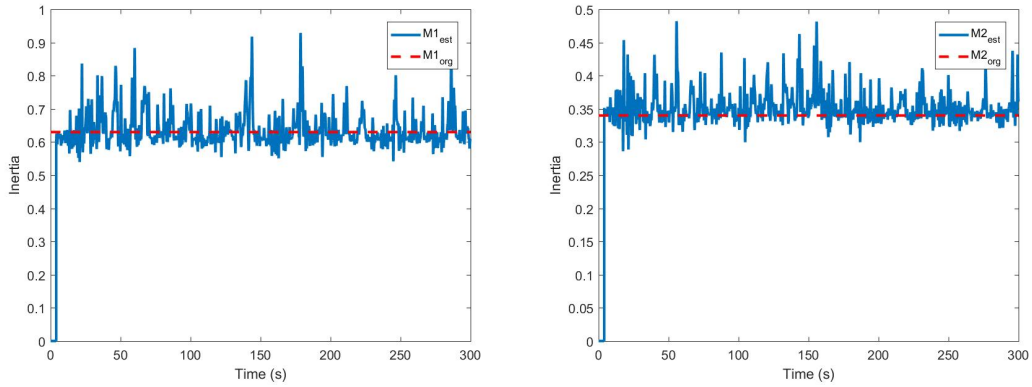

(a) Angles (b) Speeds

Figure 5.65: *Study 13 - Test 1 - Estimated M_1 and M_2*

M_3 cannot be directly calculated from Equation (4.87) because the $n-th$ generator is not represented in the model adopted when the COI reference frame is used, as seen in Section 4.2.6. Hence, it is estimated through Least-squares according to Equation (4.92), using the previous obtained M_1 and M_2. Results can be seen in Figure 5.66.

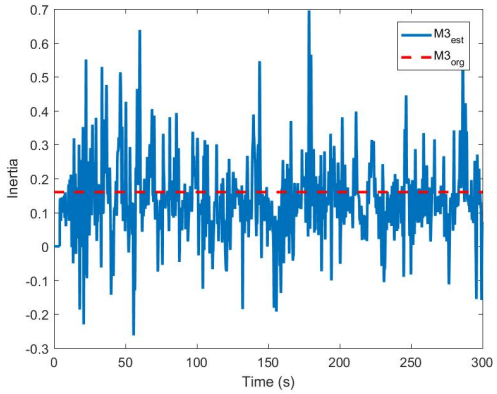

Figure 5.66: *Study 13 - Test 1 - Estimated M_3*

As it can be seen in Figure 5.65, at every sample the estimation changed, but the average is very close

to the expected value highlighted in red. Regarding M_3, the estimations varied with a higher standard deviation, since M_3 is calculated indirectly from the previously estimated M_1 and M_2. But even with a higher standard deviation, the average of the estimations is close to the expected constant of inertia also for Generator 3, as it can be seen in Figure 5.66.

The simulation is performed again five times, with the same standard deviation and sampling time for the load variation. The results can be seen in Table 5.16, where the columns "Sim 1" to "Sim 5" denote everyone of the five simulations performed, and $\overline{M_i}$ denote the mean average of the estimated values of the inertia of machine i.

Table 5.16: *Study 13 - Test 1 - Results*

	Exact	**Sim 1**	**Sim 2**	**Sim 3**	**Sim 4**	**Sim 5**
$\overline{M_1}$	0.63	0.6601	0.6549	0.6524	0.6435	0.6242
$\overline{M_2}$	0.34	0.3565	0.3560	0.3472	0.3446	0.3542
$\overline{M_3}$	0.16	0.1668	0.1596	0.1784	0.1705	0.1135

As it can be seen, $\overline{M_1}$ and $\overline{M_2}$ were accurately estimated according to the expected values in all the simulations performed. The highest errors (in terms of the mean value) obtained are around 5% for both generators. For Generator 3, however, the error is around 10% in the first four simulations, but reached almost 30% in Simulation 5, since it is influenced by the propagated errors of $M_1(t)$ and $M_2(t)$. These estimations of $M_3(t)$ may be improved by the usage of weighted LS method, taken into consideration the mean errors of $M_1(t)$ and $M_2(t)$.

5.5.2.2 Test 2

Further tests were performed changing the period of the load variations and changing the standard deviation.

First the standard deviation was changed to 0.05, instead of 0.1 used in Test 1. The period of variation of the loads was kept as 0.02s. The results can be seen in Table 5.17, identified by Test 2 - Case 1. Results were similar to those obtained in Test 1 for $\overline{M_1}$ and $\overline{M_2}$. For $\overline{M_3}$ the accuracy decreased in some of the simulations.

At second, the standard deviation was kept as original ($\sigma = 0.1$) while the period of variation of the load was changed. The simulations were performed considering a load change at every 0.1s, while data was recorded at 0.02s. Results can be seen in Table 5.18, identified by Case 2. As it can be seen, all the results did not deviate much from the results obtained in Test 1 (Table 5.16). The worst estimation of $\overline{M_3}$ in Test 2 - Case 2 presented an error around 26%.

The period of load variation is increased once again, to 1s, and results are presented in Table 5.19, identified as Case 3. As it can be seen, the accuracy degraded, ranging 100% of error. This happens because the slow variation of the loads in comparison to the sampling rate of data acquisition interferes in the calculations of the sample-weighted covariance matrices. Once the data is acquired faster, the load does not vary for consecutive samples until it jumps abruptly. Hence, the covariance between two samples may be very different, according to the samples considered, affecting the calculation of the final entrances of the sampled matrices. Consequently, it can be said that the method fails to estimate inertia following loads variations that are slow in comparison to the sampling data acquired.

Table 5.17: *Study 13 - Test 2 - Case 1*

	Exact	**Sim 1**	**Sim 2**	**Sim 3**	**Sim 4**	**Sim 5**
$\overline{M_1}$	0.63	0.6294	0.6296	0.6349	0.6535	0.6646
$\overline{M_2}$	0.34	0.3645	0.3724	0.3622	0.3510	0.3487
$\overline{M_3}$	0.16	0.0954	0.0752	0.1104	0.1702	0.1948

Table 5.18: *Study 13 - Test 2 - Case 2*

	Exact	**Sim 1**	**Sim 2**	**Sim 3**	**Sim 4**	**Sim 5**
$\overline{M_1}$	0.63	0.6845	0.6689	0.6765	0.6868	0.6736
$\overline{M_2}$	0.34	0.3665	0.3653	0.3721	0.3598	0.3598
$\overline{M_3}$	0.16	0.1817	0.1588	0.1538	0.2023	0.1804

Table 5.19: *Study 13 - Test 2 - Case 3*

	Exact	**Sim 1**	**Sim 2**	**Sim 3**	**Sim 4**	**Sim 5**
$\overline{M_1}$	0.63	1.1148	1.1356	1.2551	1.2430	1.2089
$\overline{M_2}$	0.34	0.5773	0.6041	0.5630	0.6548	0.6649
$\overline{M_3}$	0.16	0.3531	0.3178	0.6101	0.3529	0.2746

5.5.2.3 Test 3

In this test, different constant of inertia were used in the simulations. The idea was to evaluate the method with more cases, and also investigate the influence on the choice of the n-th generator which inertia will be estimated depending on the others. Results are presented in Tables 5.20 to 5.22.

Regarding the estimations of $\overline{M_1}$ and $\overline{M_2}$, the method performed similarly in every case, with maximum errors around 10%. Regarding $\overline{M_3}$, the worst estimations were obtained in Case 2, where G_3 played a bigger role in the inertia of the COI in comparison to the other two generators in the other cases analyzed. Hence, it is possible to say that the smaller the inertia of G_3 in comparison to the other two, the smaller the errors in the estimations of M_3. So, when applying the method, selecting the smaller generator as the $n-th$ unit in the modelling is the best option.

Table 5.20: *Study 13 - Test 3 - Case 1*

	Exact	**Sim 1**	**Sim 2**	**Sim 3**	**Sim 4**	**Sim 5**
$\overline{M_1}$	1.26	1.3829	1.4245	1.1148	1.3804	1.3513
$\overline{M_2}$	0.68	0.7348	0.7817	0.5773	0.7527	0.7338
$\overline{M_3}$	0.32	0.3811	0.3282	0.1922	0.3310	0.3304

Table 5.21: *Study 13 - Test 3 - Case 2*

	Exact	**Sim 1**	**Sim 2**	**Sim 3**	**Sim 4**	**Sim 5**
$\overline{M_1}$	0.90	1.0300	1.0058	1.0701	0.9728	0.9914
$\overline{M_2}$	0.50	0.4899	0.4622	0.4716	0.5122	0.5160
$\overline{M_3}$	0.65	0.9947	1.0207	0.1503	0.7890	0.8227

Table 5.22: *Study 13 - Test 3 - Case 3*

	Exact	**Sim 1**	**Sim 2**	**Sim 3**	**Sim 4**	**Sim 5**
$\overline{M_1}$	0.50	0.5384	0.5638	0.5500	0.5198	0.5531
$\overline{M_2}$	0.50	0.5124	0.5024	0.4717	0.4900	0.5411
$\overline{M_3}$	0.50	0.6805	0.9013	0.9767	0.6842	0.6186

5.5.2.4 Conclusions of Study 13

In this study, the Test-System E was simulated considering normal load variations, and the method presented in Section 4.2.6 was applied for estimating the inertia of the generators involved. The method requires the knowledge of the topology, the monitoring of the generators and the outputs of a previously performed MEM (transient reactances and an initial inertia estimation).

Recalling the procedure, due to modelling characteristics, the method estimates directly the inertia of all generators but one. The estimation of the last generator is done indirectly, as a function of the estimated inertia of the others. The accuracy of the estimations were evaluated in terms of the mean value, such that the method performed well in every direct estimation. Regarding the indirect estimation, the results depended much on the case tested. The best results were obtained when this selected generator had a smaller role in comparison to the others in terms of inertia. A possible way to improve these estimations is to assign weights to the inputs of the Least-Squares method, according to the magnitude of the errors observed in the direct estimations.

5.6 Conclusion of the chapter

This chapter presented all the studies performed considering the methodologies proposed and Topics defined in Chapter 4.

Section 5.1 presented preliminary results on the application of the direct LS method, showing its limitations, and the MEMs, as solution. The Iterative-IME and the "Variance" methods were compared considering the simple Test-sytems A and B. The perturbation considered was a generator disconnection, and loads were represented in the constant impedance model and in the dynamic model (synchronous generator), depending on the study. Considering PMUs installed at the terminal buses of generators, the MEMs succeeded in estimating inertia in the cases tested.

Section 5.2 presented studies on inertia estimation considering area equivalents. The studies were performed considering PMUs installed at the boundary buses of an area, and the equivalent inertia of the area was evaluated in terms of the measurements available. The studies considered the presence of the perturbation and the presence of loads inside the area, showing the limitations and the difficulties of this type of study. It was observed that, when there is a perturbation and/or voltage-dependent loads

inside the area, the equivalent moving power of the area must be estimated or monitored (i.e., monitoring individually loads or generators). Otherwise, the inertia estimated may be negative due to the violation of the assumption of slow equivalent moving power in comparison to the active power generated. The section also presented the results of the innovative methodology proposed in Section 4.2.4, that enables the evaluation of equivalent inertia of an area in terms of more than one PMUs installed at the boundary and at the internal of the studied area.

Section 5.3 presented studies considering the presence of RES. The connection of a wind-power unit was considered as an event that can be evaluated and used to estimate the equivalent inertia of the system. The simultaneous connection of a wind-power unit and disconnection of a synchronous unit was also evaluated, with accurate results obtained. The section also analyzed, using a time window, the further decrease in inertia due to the events considered. Therefore, it can be concluded that the proposed methods are able to estimate inertia following the connection and disconnection of synchronous or decoupled generators, and moreover are able to observe the change of inertia in time.

Section 5.4 presented two additional studies. First, the possibility of generating a controlled power output signal to estimate the inertia was analyzed. Considering a Probe modelled as PQ constant load, the studies showed that not only it is possible to estimate the inertia using the MEM studied, but it is possible to have an idea of dimensioning the probe, evaluating the limits of accuracy of the methodology. At second, the section brought studies using the proposed "Moving power estimation method" (proposed in Section 4.2.5.3). The method is complementary to the MEM because it enables area studies with perturbations and loads inside, without the requirement of full observability. The simulations were performed considering two different types of perturbation: short-circuits and load steps. The results were obtained considering the constant impedance model for loads, since this model is voltage dependent and this dependence was reportedly considered as the most contributor to load changes. The studies can be extended to consider different models for loads, if the load parameters are known or previously estimated.

Section 5.5 presented the results of two different studies considering inertia estimation under normal load variations on the grid. The first study was performed considering the direct application of the MEM to estimate the inertia. For the generator directly monitored, the method performed well. For equivalent inertia estimation seen from a boundary bus, the method depends on the load behaviour estimation, that, for continuous estimation of normal load variation, is dependent on how often there is information about the total load of the area. The second study was performed with the "dynamic matrix method" presented in Section 4.2.6. This method is complementary to the MEMs, since it needs their outputs from a previous performed application. The performance of the method was evaluated in terms of the mean average of the estimations obtained, with direct estimations with less than 10% of error. The indirect estimation of the inertia of the $n-th$ generator, however, presents higher errors due to its dependence on the previously performed direct estimations.

Connecting all the studies performed, some general observations can be made. To estimate the equivalent inertia of an area containing a perturbation and/or voltage dependent loads, one of the following options is needed: whether monitoring the generators independently, whether monitoring the equivalent moving power of the area, whether estimating the moving power of the area. Estimating the moving power of the area depends on how much information the TSO has on the loads of the area under study, such as an estimation of the total load of the area and the load characteristics. The inertia of the COI of an area may be estimated from the terminal buses of all generators, but also from a boundary bus with a

PMU installed. Regarding the latter, the estimation improves if more PMUs are available inside the area.

To summarize, the chapter presented many different studies, considering perturbations such as generator disconnections, connection of RES units, short-circuits and load steps. The simulations were performed considering different representations for the loads, using the dynamic model, the constant impedance model and the constant PQ model, depending on the study. The studies presented the results of the methodologies proposed and brought innovative insights on inertia estimation in areas defined by PMUs available.

CHAPTER 6

Conclusions

This thesis focused on estimating inertia using WAMS. Recently, the equivalent inertia of modern power systems have been degrading with the increasing penetration of RES, such that assessing this parameter in real-time is a necessity for TSOs. At present, no method for inertia estimation has arose as definitive. This Chapter presents and discusses conclusions about the methods and cases studied, highlighting the results obtained, the challenges identified and the needs for future studies.

6.1 General conclusions

This section presents the conclusions of this thesis divided in three different subsections.

First, Subsection 6.1.1 presents the conclusions regarding inertia estimation if generating units are monitored individually. The application of the methods, the requirements and the results obtained are commented both for inertia estimation following perturbations and following normal load variations.

At second, Subsection 6.1.2 debates the results obtained considering PMUs spread in the system, not necessarily at generator terminals, monitoring areas from their boundaries and from buses inside. This type of approach is new for the literature, where normally all the generating units are assumed as monitored or at least the monitored area is assumed as coherent.

At last, the contributions of the studies with a probe and considering the connection of RES-based generation are discussed in Subsection 6.1.3.

The studies were performed with different test-systems, ranging from 2 to 66 buses. Different models for the synchronous machines were used, and also primary frequency control was considered, depending on the study. Loads were represented with constant PQ, constant Impedance and dynamic model

(synchronous motor), also depending on the study. Different types of events were considered, such as load steps, normal load variations, short-circuits, connection and disconnection of generator, etc. Also, the possibility of using a testing probe was evaluated, and studies considering the presence of RES were performed.

6.1.1 Considering generating units monitored individually

Considering this purpose, five different methods were studied to estimate inertia.

First, the Direct Least-Squares method was evaluated and the results obtained showed significant limitations. The method requires the assumption of negligible difference between rotor angles and phase angles measured by PMUs at terminal buses, which does not hold in most cases, as the transient reactance is usually not negligible.

As an alternative, Model Estimation Methods (MEMs) were studied to overcome the limitations of the previous method. The acronym MEMs was created due to the common objective of both the Iterative Inter-area Model Estimation method (Iterative-IME) and the "Variance method": estimating the transient reactance and building a second-order dynamic equivalent for the studied machine. With this aim, the Iterative-IME method was developed adapting the work [16] (originally for oscillations) for the use with perturbations in a novel iterative strategy, one of the contributions of this thesis. The method is able to consider losses in the interconnected paths evaluated without increasing the number of PMUs required. Accurate results were obtained in the cases tested, and the method showed to be useful for monitoring the system considering perturbations and also normal load variations. The method showed robustness to deal with complex test-systems, where both higher order models to represent synchronous machines were adopted and primary frequency control was considered. The main limitation of the method is the need of monitoring at least two points in a radial path.

The "Variance method" proposed in [34] was the second MEM studied, as an alternative to the Iterative-IME method. The advantage of this method is the necessity of monitoring only one point. Both MEM performed similarly in the cases tested. However, as both methods depend on different assumptions to work, the results varied according to the case studied in terms of which method performed better. In some cases the Iterative-IME outperformed the "Variance method", in some cases it happened the opposite, such it was not possible to define the best of them.

The fourth method studied was the Extended Kalman Filter (EKF), a prediction-correction method that is based on assuming a model to represent a system, and calibrate it with the feedback provided by measured variables in time. The model proposed in [22] was tested in this thesis under the same conditions of the MEM. In the studies performed, the EKF did not performed well. It showed a strong limitation to deal with more complex test-systems, when a higher order model was assumed for the synchronous machines in comparison to the model adopted in the EKF. This flaw has already been overcome in the literature by further approaches that model the problem differently and showed more robustness. However, the different forms of modelling the problem are always limited in the amount of information that the measurement units can provide. The variables and parameters to be estimated by the method are more than the measurement model can provide direct feedback on, such that their estimation depend on indirect updating. Moreover, it was observed a strong dependence of the EKF on the tuning of the initial estimates and on the tuning of the process noise covariance matrix. These issues may not be a problem when synchronous machines are individually monitored, but may become a significant limitation to apply the method for area studies.

The fifth method, referred in this thesis as "Dynamic matrix method", is proposed specifically for estimating inertia under normal load variations. By stating the dynamic matrix and the Lyapunov equations of a stable equivalent system, it is possible to relate measured quantities and estimate parameters. The methodology is based on [155] and [35], dealing with different applications. In this thesis, it was adapted for inertia estimation in a novel approach. The requirements are the knowledge of the topology of the system, a general characterization of the loads, and the parameters of the dynamic equivalents of the generating units, which can be obtained by MEM. The method is able to estimate the inertia continuously in the presence of normal load variations, without the necessity of monitoring directly the loads nor estimating their dynamic behaviour.

To conclude, if the TSO is able to monitor individually each generating unit of its interest, then the methods studied in this thesis seem to address most of the situations without any identified limitation, considering perturbations, normal load variations (as showed in this thesis) or oscillations, as showed in [17].

6.1.2 Considering PMUs monitoring an area

Monitoring every generating bus of the grid is quite a strong assumption. As described in Section 3.6, the deployment of PMUs is still in starting condition in many countries. For this reason, the possibility of estimating equivalent inertias seen from spread PMUs installed on the grid was evaluated. At the moment, this may be the only possibility to evaluate inertia of isolated or poorly monitored regions. This subsection summarizes the conclusions of the studies performed on this topic.

The preliminary studies on this topic started with the assumption of monitoring two areas interconnected by a radial path, with PMUs installed at their boundary buses. For this purpose, the MEM were used to estimate the dynamic equivalent of each area, that consists on estimating the equivalent of the transient reactance and the equivalent of the internal voltage in time. Subsequently, the method states the swing equation with the equivalent generators and estimate the equivalent inertias through Least-Squares (LS) method. In this step, it was assumed that the equivalent moving power of the studied area has a slow behaviour in relation to the generated power.

The first issue that comes with monitoring an area with non coherent units by a single boundary bus regards estimations biased by the electrical distance between the PMU and the generators. The generator that is located closer to the PMU influences the equivalent frequency obtained and consequently influences the estimation of the inertia. Hence, the frequency and inertia obtained do not represent accurately the dynamics of the COI of the area. In this case, one may make use of the data coming from additional PMUs possibly installed in the considered area to acquire a better picture of the COI once the measurement points are spread enough among the non-coherent groups of generators. To build the complete equivalent, considering the equivalent interconnection lines between the measurement points, a system reduction method was studied.

To reduce the system around the measurement points, the Ward equivalent method was adopted. With this method, it is possible to evaluate an area with more than one interconnections to other areas, monitored by its boundaries, and/or by measurement points inside the area. The method consists in calculating equivalent interconnections and equivalent current injections between the buses selected. From that point on, the "Variance method" is applied to calculate each of the dynamic equivalents seen from the retained buses. Later, the equivalents of one area can be associated together in terms of their COI, giving a picture of the equivalent dynamics of the whole area.

However, the main issues that come with area equivalents regard the study of an area that contains a perturbation inside and/or loads with high voltage-dependence. In this case, the assumption of slow moving power used to solve the swing equation in practical conditions does not hold, and the inertia estimated may result negative. To overcome this problem in this thesis, a method for estimating the equivalent moving power of an area was proposed. The method is based on dividing this task in two: estimating the equivalent load behaviour first, and then estimating the equivalent mechanical power of the connected units together with the losses in the system.

The equivalent load behaviour is estimated assuming a load model to represent it. In this thesis, the constant impedance model was selected because it is the one with higher voltage dependence, the characteristic that was most affecting the inertia estimation of the area. However, it is possible to consider a composite model if the TSO knows properly the historical characteristics of the load in the area of study, or by estimating it using methods available in the literature such as [153], [154]. Once the load behaviour is estimated, the remaining part of the equivalent moving power can be estimated based on steady-state values of the generated power and typical values of the droop of the area. The method was tested for a load step and produced satisfactory results. For monitoring normal load variations, however, the method needs to be updated from time to time with the information of the total load of the area. The accuracy depends on how often this information is available.

To summarize, performing area studies with PMUs require to monitor the boundaries of the area, because the power generated is a needed input for the methods studied. If the monitored area neither include a perturbation nor high voltage-dependent loads, then the MEMs perform well without additional difficulties. However, if it includes one of these two elements, further additional requirements are needed. The dynamic behaviour of the loads and the perturbation influences on the moving power of the area, that cannot be assumed slow in comparison to the generated power. Hence, it is required to either monitor individually the generators, monitor the loads, filter out the load behaviour or estimate the equivalent moving power. The latter is an attempt of mitigating the requirements to monitor the inertia of an area in the most practical conditions. However, the problems of estimating the moving power are basically two: it also has its own required inputs, and it conditions the accuracy of the inertia estimations to the accuracy of the equivalent moving power estimations.

Therefore, the minimum set of PMUs to estimate the inertia of an area in general (without making assumptions) should include units at the boundaries to monitor the power generated, one or more PMUs close to the COI of the area to enable accurate estimations of the mean frequency, and one or more PMUs installed at load or transfer buses to estimate the load behaviour.

6.1.3 Application studies

The studied methods were tested with two different applications. The first one considered the presence of RES-based generation in the system. The second application was resumed in testing the possibilities of estimating inertia using a controlled probe.

Regarding the studies with RES, the connection of a wind-power generator was considered as an event that impacts the system such that its dynamic response can be used to estimate the inertia of the rest of the system. The methods proposed performed well in most of the cases tested, and moreover it was possible to observe the inertia decrease due to the disconnection of a synchronous generator following the connection of the wind-power generator. The only case when the methods were not able to estimate inertia was the case when the connected wind-power unit was connected generating exactly the

same active and reactive power of the synchronous unit disconnected. In this case, no power imbalance was produced and no possibility to observe a frequency change. However, this is quite extreme and unrealistic, because wind-power generators generate and consume reactive power differently then synchronous machines. Even a small imbalance in the reactive power generated was already enough to force the connected machines to react and consequently produce also a small active power imbalance, that could be observed and used to estimate the inertia of the system.

The studies with the probe were performed modelling it as a constant PQ load. As in the previous studies, the MEM performed well to estimate equivalent inertia. For the test-system used, the experiment was taken to the limit of accuracy of the simulation software, giving an idea on how to size a probe for practical use. In this case, the minimum magnitude of the power produced by the probe should be at least 10 times over the magnitude of the error of the PMU monitoring the area.

6.2 Future studies

This thesis presents some methods to estimate power system inertia according to some conditions and assumptions. However, the work highlighted some research topics worth to be further investigated.

The first topic approaches operational aspects of the application of the methods with real data. Further studies are needed to investigate different levels and types of measurement errors, presence of outliers and missing data. Some of the techniques that may bring advantages are filtering, re-sampling and interpolation. When dealing with perturbations, filtering could be investigated to eliminate the impact of load variations in the power imbalance of the area, such that estimating the equivalent load behaviour would not be necessary.

Considering the MEM, defining specific criteria to set the sliding window lengths and selecting the representative estimations of the estimate transient reactance may improve the accuracy of the dynamic equivalents and consequently the accuracy of the equivalent inertias estimated. Methods that detect the presence and estimate the exact time of occurrence of a perturbation seem also useful to improve the accuracy, besides the MEM can also work without this feature. When using the equivalent moving power method to deal with normal load variations, methods and criteria to determine the time interval of analysis and update the inputs are indispensable for practical applications.

A second topic is to improve specifically some of the models and methodologies. Further studies on modelling and estimating load behaviour may bring benefits for estimating the equivalent moving power, in terms of increasing accuracy and reducing requirements. Regarding the "dynamic matrix method", there is room for improvement on the way the method estimates the inertia of the $n-th$ generator, as in this thesis it is done indirectly depending on the inertia estimations of the other generators. Furthermore, another interesting study with this method would be evaluating its performance for estimating inertia considering equivalent areas instead of monitoring individually the generators. Also, the method have strong requirements, and further studies to mitigate them may be interesting to make it more practical. The same can be said about the requirements of the moving power estimation method, that can have benefit also from a whole study on load characterization and load behaviour estimation from boundary buses.

Another topic for future investigations is estimating equivalent inertia in a system capable of providing synthetic inertia. A possible study includes modelling these units and evaluating the proposed methods for estimating inertia in that situation.

Appendices

APPENDIX A

Power and energy generated in Europe

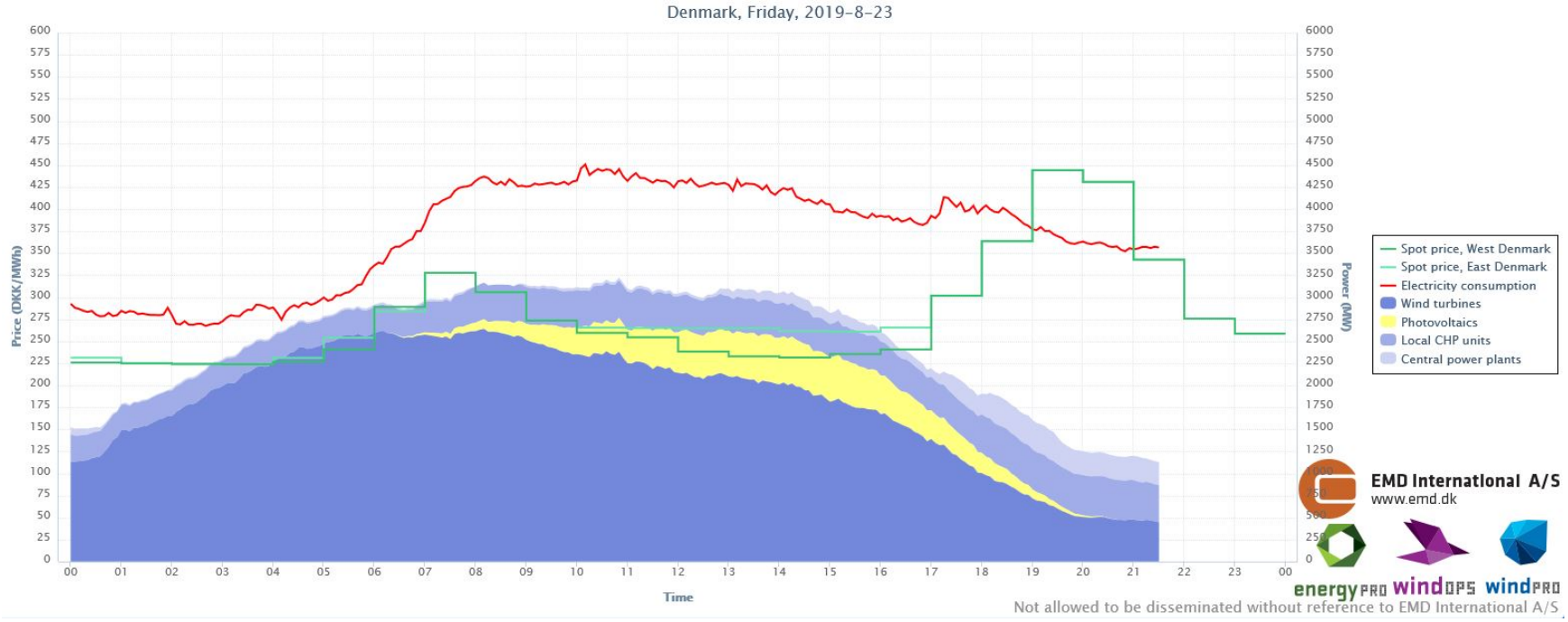

Figure A.1: *Power generated, Denmark, 23/08/2019, [7]*

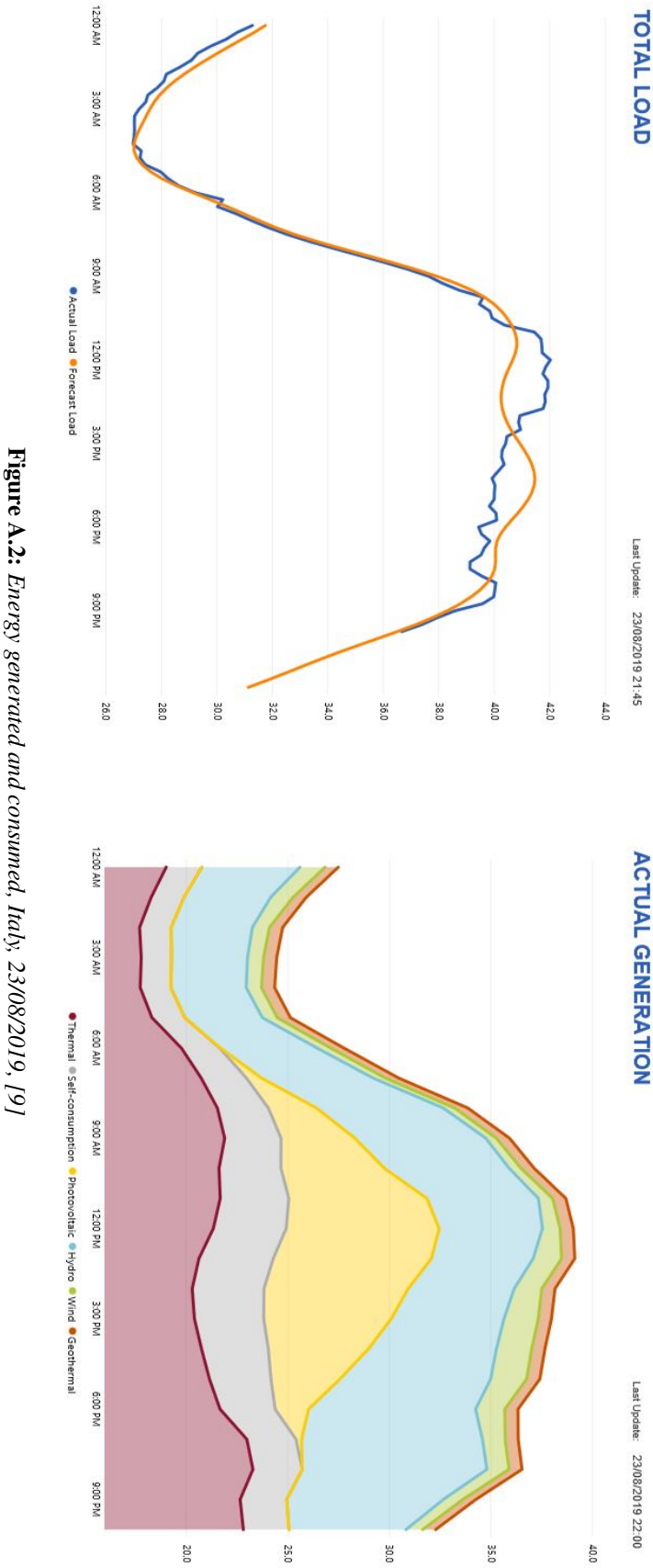

Figure A.2: *Energy generated and consumed, Italy, 23/08/2019, [9]*

APPENDIX B

Details of the ”Variance method”

This Appendix details the passage from Step 1 to Step 2 of the "Variance method" (presented in Section 4.2.2.2).

Recalling Equation (4.28) for convenience,

$$E_i(t)\angle\delta_i(t) = (jx_i)I_i(t)\angle\alpha_i(t) + V_i(t)\angle\theta_i(t) \tag{B.1}$$

The aim is to obtain $|\mathbf{E_i}|$ in terms of only measured (or calculable) quantities. For the sake of simplicity, for now on in this Appendix, the subscript i is not shown.

Expressing the right side of Equation (B.1) in rectangular coordinates,

$$E\angle\delta = xI[\cos(\alpha + \frac{\pi}{2}) + jsin(\alpha + \frac{\pi}{2})] + V[\cos(\theta) + j\sin(\theta)] \tag{B.2}$$

or alternatively

$$E\angle\delta = [xI\cos(\alpha + \frac{\pi}{2}) + V\cos(\theta)] + j[xI\sin(\alpha + \frac{\pi}{2}) + V\sin(\theta)] \tag{B.3}$$

Taking the magnitude of $E\angle\delta$, Equation (B.3) becomes

$$E = \sqrt{[xI\cos(\alpha + \frac{\pi}{2}) + V\cos(\theta)]^2 + [xI\sin(\alpha + \frac{\pi}{2}) + V\sin(\theta)]^2} \tag{B.4}$$

The explicit version of Equation (B.4) is

$$E = \sqrt{[x^2I^2\cos^2(\alpha+\frac{\pi}{2}) + V^2\cos^2(\theta) + 2xVI\cos(\alpha+\frac{\pi}{2})\cos(\theta)] + \overline{[x^2I^2\sin^2(\alpha+\frac{\pi}{2}) + V^2\sin^2(\theta) + 2xVI\sin(\alpha+\frac{\pi}{2})\sin(\theta)]}} \quad \text{(B.5)}$$

Using the relation $\sin^2(a) + \cos^2(a) = 1$, it is possible to simplify Equation (B.5), obtaining

$$E = \sqrt{x^2I^2 + V^2 + 2xVI[\cos(\alpha+\frac{\pi}{2})\cos(\theta) + \sin(\alpha+\frac{\pi}{2})\sin(\theta)]} \quad \text{(B.6)}$$

Using the relations $\cos(a+\frac{\pi}{2}) = -\sin(a)$ and $\sin(a+\frac{\pi}{2}) = \cos(a)$, Equation (B.6) becomes

$$E = \sqrt{x^2I^2 + V^2 + 2xVI[-sin(\alpha)\cos(\theta) + \cos(\alpha)\sin(\theta)]} \quad \text{(B.7)}$$

Using the relation $\sin(a-b) = \cos(b)\sin(a) - \cos(a)\sin(b)$, Equation (B.7) can be rewritten as

$$E = \sqrt{x^2I^2 + V^2 + 2xVI[-\sin(\alpha-\theta)]} \quad \text{(B.8)}$$

Making use of the property $\sin(-a) = -\sin(a)$, it is possible to obtain

$$E = \sqrt{x^2I^2 + V^2 + 2xVI[\sin(\theta-\alpha)]} \quad \text{(B.9)}$$

or, alternatively

$$E = \sqrt{x^2I^2 + V^2 + 2xQ} \quad \text{(B.10)}$$

where $Q = VI\sin(\theta-\alpha)$.

APPENDIX C

Additional details of the Dynamic matrix method

This Appendix provides additional details on the Dynamic matrix method, presented in Section 4.2.6.

C.1 System reduction

Figures C.1 and C.2 depict the procedure, considering a test-system of 9 buses as an example.

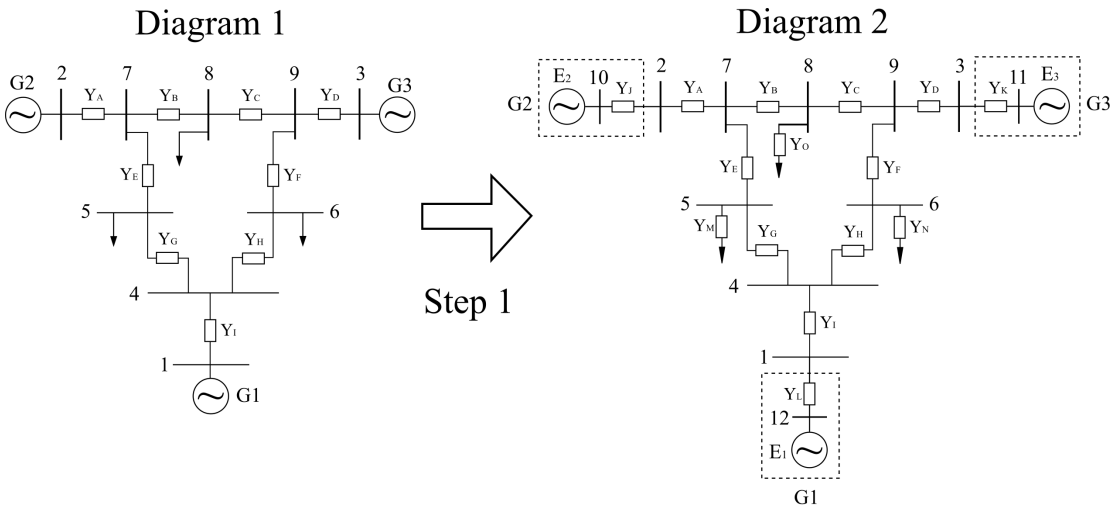

Figure C.1: *System reducing - Step 1*

Regarding Diagram 1, the Y_{bus} can be built in terms of the 9 admittances (Y_A to Y_I) related to the 9 transmission lines that connect the 9 buses of the system. The Step 1 consists in expanding the representation of the system to include the loads, here modelled as constant admittances (Y_M to Y_O) and the transient reactances (here represented by the admittances Y_J to Y_L). Note that three fictitious buses (buses 10 to 12) were added to represent the internal nodes of each generator. Consequently, the Y_{bus} related to Diagram 2 is (12×12).

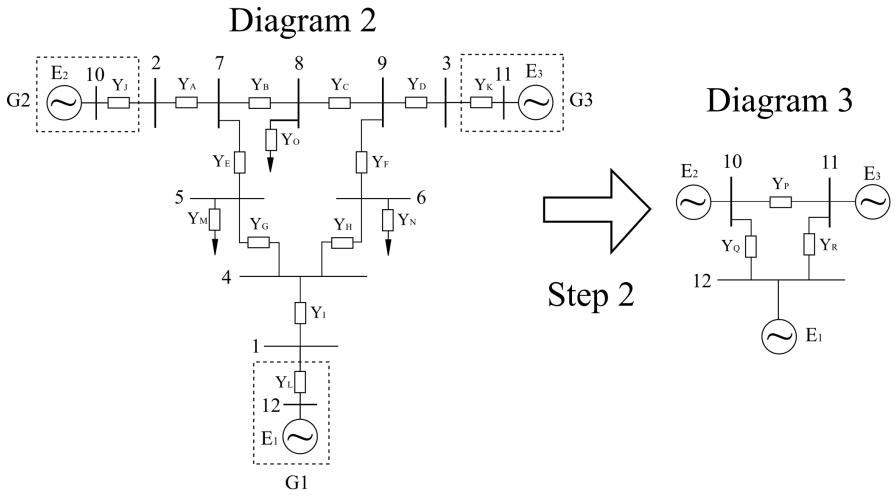

Figure C.2: *System reducing - Step 2*

Step 2 consists in using the Ward reduction method (as presented in Section 4.2.4) to reduce the system around the retained internal nodes of the generators (buses 10 to 12). The related Y_{bus} becomes (3×3). The interested reader may refer to [46].

C.2 From the infinite bus reference frame to the COI reference frame

The following deduction is based on [156].

A system with i synchronous machines represented with the classical model considering the infinite bus as reference for angle and speed can be represented by

$$\begin{cases} M_1\dot{\omega}_1 &= P_{m_1} - P_{e_1} - D_1\omega_1 \\ M_2\dot{\omega}_2 &= P_{m_2} - P_{e_2} - D_2\omega_2 \\ &\vdots \\ M_i\dot{\omega}_i &= P_{m_i} - P_{e_i} - D_i\omega_i \end{cases}$$

where $\dot{\omega}_i = \frac{d\omega_i(t)}{dt}$ and $M_i = 2H_i/\omega_0$. All the variables have been previously defined in Chapter 2.

Summing up all the i equations of the System (C.1), it is possible to obtain

$$\sum_{j=1}^{i} M_j\dot{\omega}_j = \sum_{j=1}^{i} P_{m_j} - P_{e_j} - D_j\omega_j \tag{C.1}$$

The left hand side of Equation C.1 can be expressed in terms of the COI. For that, Equation (2.18) is expressed here in terms of M and considering the same base power for each generator, for simplicity:

$$\omega_{COI} \triangleq \frac{\sum_{j=1}^{i} M_j \omega_j}{\sum_{j=1}^{i} M_j} \tag{C.2}$$

Calling $M_T = \sum_{j=1}^{i} M_j$, the term $\sum_{j=1}^{i} M_j \dot{\omega}_j$ can be exchanged for $M_T \dot{\omega}_{COI}$. Defining $P_{COI} = \sum_{j=1}^{i} P_{m_j} - P_{e_j}$, Equation (C.1) becomes

$$M_T \dot{\omega}_{COI} = P_{COI} - \sum_{j=1}^{i} D_j \omega_j \tag{C.3}$$

For the next step, the term $\sum_{j=1}^{i} D_j \omega_j$ is multiplied by M_j/M_j:

$$M_T \dot{\omega}_{COI} = P_{COI} - \sum_{j=1}^{i} D_j \omega_j \frac{M_j}{M_j} \tag{C.4}$$

Considering that the proportion in between inertia and damping of each single machine is the same of the proportion in between the total inertia and damping of the system [156], it is possible to write

$$\frac{D_j}{M_j} = \frac{D_T}{M_T} \tag{C.5}$$

where $D_T = \sum_{j=1}^{i} D_j$ and the other variables have been previously defined.

Substituting Equation (C.5) in Equation (C.4), it is possible to obtain

$$M_T \dot{\omega}_{COI} = P_{COI} - \sum_{j=1}^{i} \frac{D_T \omega_j M_j}{M_T} \tag{C.6}$$

The term $\sum_{j=1}^{i} \frac{D_T \omega_j M_j}{M_T}$ can be expressed in terms of ω_{COI} through Equation (C.2), such that the expression that represents the dynamics of the COI is

$$M_T \dot{\omega}_{COI} = P_{COI} - D_T \omega_{COI} \tag{C.7}$$

Alternatively,

$$\dot{\omega}_{COI} = \frac{P_{COI}}{M_T} - \frac{D_T \omega_{COI}}{M_T} \tag{C.8}$$

Each of the equations of the System (C.1) can then be referred to the COI. Considering $\tilde{\omega}_i = \omega_i - \omega_{COI}$, it is possible to obtain

$$\dot{\omega}_i - \dot{\omega}_{COI} = \frac{P_{m_i} - P_{e_i}}{M_i} - \frac{D_i \omega_i}{M_i} - \frac{P_{COI}}{M_T} + \frac{D_T \omega_{COI}}{M_T} \tag{C.9}$$

Making use of Equation (C.5), it is possible to rewrite Equation (C.9) as

$$M_i \dot{\tilde{\omega}}_i = P_{m_i} - P_{e_i} - \frac{M_i}{M_T} P_{COI} - D_i \tilde{\omega}_i \tag{C.10}$$

C.3 Expressing the motion of the n-th generator in function of the others

This section provides details of the deductions in between Equations (4.67) and (4.72).

The COI angle and the COI frequency (here repeated by convenience) can be obtained respectively with

$$\delta_{COI} \triangleq \frac{\sum_{i=1}^{n} S_{n_i} M_i \delta_i}{\sum_{i=1}^{i} S_{n_i} M_i} \quad rad \tag{C.11}$$

$$\omega_{COI} \triangleq \frac{\sum_{i=1}^{n} S_{n_i} M_i \omega_i}{\sum_{i=1}^{i} S_{n_i} M_i} \quad rad/s \tag{C.12}$$

All the rotor angles and speed of the system can be expressed by $\tilde{\delta}_i = \delta_i - \delta_{COI}$ and $\tilde{\omega}_i = \omega_i - \omega_{COI}$. Considering an example with three generators, from (C.11),

$$\delta_{COI} = \frac{S_{n_1} M_1 \delta_1 + S_{n_2} M_2 \delta_2 + S_{n_3} M_3 \delta_3}{S_{n_1} M_1 + S_{n_2} M_2 + S_{n_3} M_3} \tag{C.13}$$

Subsequently, it is possible to write

$$\delta_{COI}(S_{n_1} M_1 + S_{n_2} M_2 + S_{n_3} M_3) = S_{n_1} M_1 \delta_1 + S_{n_2} M_2 \delta_2 + S_{n_3} M_3 \delta_3 \tag{C.14}$$

Using the relation $\tilde{\delta}_i = \delta_i - \delta_{COI}$, it can be obtained

$$S_{n_1} M_1 \tilde{\delta_1} + S_{n_2} M_2 \tilde{\delta_2} + S_{n_3} M_3 \tilde{\delta_3} = 0 \tag{C.15}$$

From which it is possible to isolate $\tilde{\delta_3}$ and obtain

$$\tilde{\delta_3} = -\frac{S_{n_1} M_1 \tilde{\delta_1} + S_{n_2} M_2 \tilde{\delta_2}}{S_{n_3} M_3} \tag{C.16}$$

Making it general,

$$\tilde{\delta}_n = -\frac{\sum_{k=1}^{n-1} M_k \tilde{\delta}_k}{M_n} \tag{C.17}$$

The same procedure can be done for $\tilde{\omega}_n$, obtaining

$$\tilde{\omega}_n = -\frac{\sum_{k=1}^{n-1} M_k \tilde{\omega}_k}{M_n} \tag{C.18}$$

C.4 Derivatives of the linearized system

This section provides the deductions of the derivatives that appear in Equation (4.79). Recalling the expression,

$$(\frac{\partial \mathbf{P_e}}{\partial \tilde{\boldsymbol{\delta}}})_{COI} = (\frac{\partial \mathbf{P_e}}{\partial \tilde{\boldsymbol{\delta}}} + \mathbf{M}\frac{1}{M_T}\frac{\partial P_{COI}}{\partial \tilde{\boldsymbol{\delta}}}) \tag{C.19}$$

The variables involved are $\tilde{\boldsymbol{\delta}} = [\tilde{\delta}_1, ..., \tilde{\delta}_{n-1}]$, while $\tilde{\delta}_n$ is substituted in the expressions of P_e and P_{COI} according to Equation (4.71). Consequently, each one of the partial derivatives of $(\frac{\partial \mathbf{P_e}}{\partial \tilde{\boldsymbol{\delta}}})_{COI}$ can

be obtained by Equations (C.20) to (C.23), where $k, j = 1, ..., n-1$.

$$(\frac{\partial \mathbf{P_e}}{\partial \tilde{\boldsymbol{\delta}}})^{COI}_{kk} = \frac{\partial P_{e_k}}{\partial \tilde{\delta}_k} + \frac{M_k}{M_T}\sum_{i=1}^{n}\frac{\partial P_{e_i}}{\partial \tilde{\delta}_k} \tag{C.20}$$

$$(\frac{\partial \mathbf{P_e}}{\partial \tilde{\boldsymbol{\delta}}})^{COI}_{kj} = \frac{\partial P_{e_k}}{\partial \tilde{\delta}_j} + \frac{M_k}{M_T}\sum_{i=1}^{n}\frac{\partial P_{e_i}}{\partial \tilde{\delta}_j} \tag{C.21}$$

$$(\frac{\partial \mathbf{P_e}}{\partial \tilde{\boldsymbol{\delta}}})^{COI}_{jk} = \frac{\partial P_{e_j}}{\partial \tilde{\delta}_k} + \frac{M_j}{M_T}\sum_{i=1}^{n}\frac{\partial P_{e_i}}{\partial \tilde{\delta}_k} \tag{C.22}$$

$$(\frac{\partial \mathbf{P_e}}{\partial \tilde{\boldsymbol{\delta}}})^{COI}_{jj} = \frac{\partial P_{e_j}}{\partial \tilde{\delta}_j} + \frac{M_j}{M_T}\sum_{i=1}^{n}\frac{\partial P_{e_i}}{\partial \tilde{\delta}_j} \tag{C.23}$$

As P_{COI} is a function of P_{e_i} with $i = 1, ..., n$ as seen in Equation (4.70), the partial derivative of P_{e_n} is also needed. Hence, considering only the non-zero terms, each one of the terms $\frac{\partial P_{e_i}}{\partial \tilde{\delta}_j}$ can be calculated as

$$\frac{\partial P_{e_k}}{\partial \tilde{\delta}_k} = \sum_{j=1, j\neq i}^{n-1}\frac{\partial P_{kj}}{\partial \tilde{\delta}_k} + \frac{\partial P_{kn}}{\partial \tilde{\delta}_k} \tag{C.24}$$

$$\frac{\partial P_{e_j}}{\partial \tilde{\delta}_k} = \frac{\partial P_{jk}}{\partial \tilde{\delta}_k} + \frac{\partial P_{jn}}{\partial \tilde{\delta}_k} \tag{C.25}$$

$$\frac{\partial P_{e_n}}{\partial \tilde{\delta}_k} = \frac{\partial P_{nk}}{\partial \tilde{\delta}_k} + \sum_{j=1, j\neq i}^{n-1}\frac{\partial P_{nj}}{\partial \tilde{\delta}_k} \tag{C.26}$$

Explicitly,

$$\begin{aligned}\frac{\partial P_{e_k}}{\partial \tilde{\delta}_k} = &\sum_{j=1, j\neq i}^{n-1} E_k E_j (G_{kj}(-\sin(\tilde{\delta}_k - \tilde{\delta}_j)) + B_{kj} cos(\tilde{\delta}_k - \tilde{\delta}_j)) + \\ &E_k E_n (G_{kn}(-\sin(\tilde{\delta}_k + \frac{\sum_{l=1}^{n-1} M_l \tilde{\delta}_l}{M_n}))(1 + \frac{M_k}{M_n}) + B_{kn}\cos(\tilde{\delta}_k + \frac{\sum_{l=1}^{n-1} M_l \tilde{\delta}_l}{M_n})(1 + \frac{M_k}{M_n}))\end{aligned}$$

$$\begin{aligned}\frac{\partial P_{e_j}}{\partial \tilde{\delta}_k} = &E_j E_k (G_{jk}(+\sin(\tilde{\delta}_j - \tilde{\delta}_k)) - B_{kj} cos(\tilde{\delta}_j - \tilde{\delta}_k)) + \\ &E_j E_n (G_{jn}(-\sin(\tilde{\delta}_j + \frac{\sum_{l=1}^{n-1} M_l \tilde{\delta}_l}{M_n}))(\frac{M_k}{M_n}) + B_{jn}\cos(\tilde{\delta}_j + \frac{\sum_{l=1}^{n-1} M_l \tilde{\delta}_l}{M_n})(\frac{M_k}{M_n}))\end{aligned}$$

$$\begin{aligned}\frac{\partial P_{e_n}}{\partial \tilde{\delta}_k} = &[E_n E_k (G_{nk}(-\sin((-\frac{\sum_{l=1}^{n-1} M_l \tilde{\delta}_l}{M_n}) - \tilde{\delta}_k))(-\frac{M_k}{M_n} - 1) + \end{aligned}$$

$$B_{nk}\cos((-\frac{\sum_{l=1}^{n-1}M_l\tilde{\delta}_l}{M_n})-\tilde{\delta}_k)(-\frac{M_k}{M_n}-1))]+$$
$$[\sum_{i=1}^{n-1}E_nE_j(G_{nj}(-\sin((-\frac{\sum_{l=1}^{n-1}M_l\tilde{\delta}_l}{M_n})-\tilde{\delta}_j))(-\frac{M_k}{M_n})+$$
$$B_{nj}cos((-\frac{\sum_{l=1}^{n-1}M_l\tilde{\delta}_l}{M_n})-\tilde{\delta}_j)(-\frac{M_k}{M_n}))]$$

C.5 Application example - Calculation of the Jacobian

This section presents the calculation of the matrix $(\frac{\partial \mathbf{P_e}}{\partial \tilde{\boldsymbol{\delta}}})_{COI}$ for Study 13 (Subsection 5.5.2). Test-system D.5 is used.

C.5.1 Main parameters of the system

The full data of the system can be found in [46] and in `https://github.com/xiaozhew/Jacobian-Estimation`. The full admittance matrix can be found in [46].

The transient reactances of each generator are $x_1 = 0.0608p.u.$, $x_2 = 0.1198p.u.$, $x_3 = 0.1813p.u.$. The admittance matrix reduced around the three internal nodes of the generators (hence including x_1, x_2, and x_3) is

$$Y_{bus}^{red} = \begin{bmatrix} 0.8455 - 2.9883i & 0.2871 + 1.5129i & 0.2096 + 1.2256i \\ 0.2871 + 1.5129i & 0.4200 - 2.7239i & 0.2133 + 1.0879i \\ 0.2096 + 1.2256i & 0.2133 + 1.0879i & 0.2770 - 2.3681i \end{bmatrix}$$

The results of a performed power flow are $E_1 = 1.0566p.u.$, $E_2 = 1.0502p.u.$, $E_3 = 1.0170p.u.$, $\delta_1 = 0.0396rad$, $\delta_2 = 0.3444rad$, $\delta_3 = 0.2298rad$.

The inertias of the three generators considered in the referred study were $M_1 = 0.63s^2$, $M_2 = 0.34s^2$, $M_3 = 0.16s^2$, $M_T = M_1 + M_2 + M_3 = 1.13s^2$.

Applying Equation (C.11), $\delta_{COI} = 0.1582rad$. Hence, the relative angles are $\tilde{\delta}_1 = -0.1188rad$, $\tilde{\delta}_2 = 0.1859rad$, $\tilde{\delta}_3 = 0.0713rad$.

The rotor speed in steady state are $\omega_1 = \omega_2 = \omega_3 = 1rad/s$. Hence, applying Equation (C.12), $\omega_{COI} = 1$, and $\tilde{\omega}_1 = \tilde{\omega}_2 = \tilde{\omega}_3 = 0rad/s$.

C.5.2 Calculation of the partial Jacobian

As the system has three generators, the matrix $(\frac{\partial \mathbf{P_e}}{\partial \tilde{\boldsymbol{\delta}}})_{COI}$ is $(n-1 \times n-1) = 2x2$.

To obtain $(\frac{\partial \mathbf{P_e}}{\partial \tilde{\boldsymbol{\delta}}})_{11}^{COI}$, Equation (C.20) must be applied:

$$(\frac{\partial \mathbf{P_e}}{\partial \tilde{\boldsymbol{\delta}}})_{11}^{COI} = \frac{\partial P_{e_1}}{\partial \tilde{\delta}_1} - \frac{M_1}{M_T}(\frac{\partial P_{e_1}}{\partial \tilde{\delta}_1} + \frac{\partial P_{e_2}}{\partial \tilde{\delta}_1} + \frac{\partial P_{e_3}}{\partial \tilde{\delta}_1}) = 8.0627$$

where the results of the individual terms are: $\frac{\partial P_{e_1}}{\partial \tilde{\delta}_1} = 8.2924$, $\frac{\partial P_{e_2}}{\partial \tilde{\delta}_1} = 2.9387$ and $\frac{\partial P_{e_3}}{\partial \tilde{\delta}_1} = -10.8191$.

To obtain $(\frac{\partial \mathbf{P_e}}{\partial \tilde{\boldsymbol{\delta}}})_{12}^{COI}$, Equation (C.21) must be applied:

$$(\frac{\partial \mathbf{P_e}}{\partial \tilde{\boldsymbol{\delta}}})_{12}^{COI} = \frac{\partial P_{e_1}}{\partial \tilde{\delta}_2} - \frac{M_1}{M_T}(\frac{\partial P_{e_1}}{\partial \tilde{\delta}_2} + \frac{\partial P_{e_2}}{\partial \tilde{\delta}_2} + \frac{\partial P_{e_3}}{\partial \tilde{\delta}_2}) = 1.2361$$

where te results of the individual terms are $\frac{\partial P_{e_1}}{\partial \tilde{\delta}_2} = 1.1415$, $\frac{\partial P_{e_2}}{\partial \tilde{\delta}_2} = 5.0333$ and $\frac{\partial P_{e_3}}{\partial \tilde{\delta}_2} = -6.3445$.

To obtain $(\frac{\partial \mathbf{P_e}}{\partial \tilde{\boldsymbol{\delta}}})_{21}^{COI}$, Equation (C.22) must be applied:

$$(\frac{\partial \mathbf{P_e}}{\partial \tilde{\boldsymbol{\delta}}})_{21}^{COI} = \frac{\partial P_{e_2}}{\partial \tilde{\delta}_1} - \frac{M_2}{M_T}(\frac{\partial P_{e_1}}{\partial \tilde{\delta}_1} + \frac{\partial P_{e_2}}{\partial \tilde{\delta}_1} + \frac{\partial P_{e_3}}{\partial \tilde{\delta}_1}) = 2.8147$$

where all the individual terms have been previously calculated.

To obtain $(\frac{\partial \mathbf{P_e}}{\partial \tilde{\boldsymbol{\delta}}})_{22}^{COI}$, Equation (C.22) must be applied:

$$(\frac{\partial \mathbf{P_e}}{\partial \tilde{\boldsymbol{\delta}}})_{22}^{COI} = \frac{\partial P_{e_2}}{\partial \tilde{\delta}_2} - \frac{M_2}{M_T}(\frac{\partial P_{e_1}}{\partial \tilde{\delta}_2} + \frac{\partial P_{e_2}}{\partial \tilde{\delta}_2} + \frac{\partial P_{e_3}}{\partial \tilde{\delta}_2}) = 5.0844$$

where all the individual terms have been previously calculated.

Hence, the final matrix is

$$(\frac{\partial \mathbf{P_e}}{\partial \tilde{\boldsymbol{\delta}}})_{COI} = \begin{bmatrix} 8.063 & 1.236 \\ 2.815 & 5.084 \end{bmatrix}$$

APPENDIX D

Test Systems

D.1 Test-system A

Description: Radial 2-bus test-system, 2 generators, 1 load.

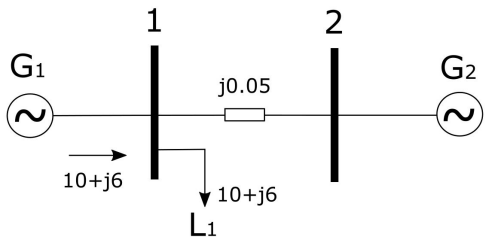

Figure D.1: *Test-system A*

D.2 Test-system B

Description: Radial 2-bus test-system.

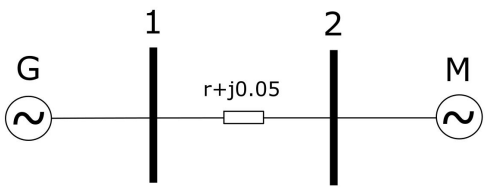

Figure D.2: *Test-system B*

D.3 Test-system C

Description: Original 11-bus test-system from [42]. The installed capacity is around 3250 MW.

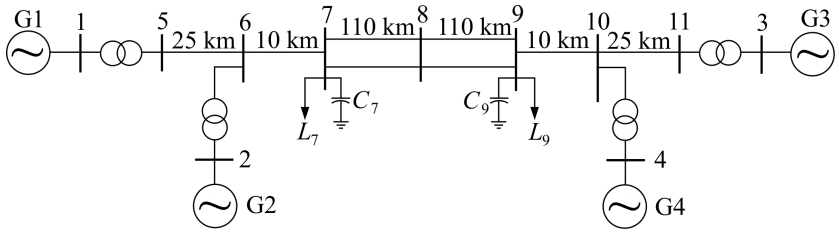

Figure D.3: *Test-system C*

Each transformer has an impedance of $j0.15$ p.u. on 900 MVA and 20/230 kV base. The parameters of the lines are $r = 0.0001$ p.u./km, $x_L = 0.001$ p.u./km and $b_C = 0.00175$ p.u./km, on 100 MVA, 230 kV base.

The loads are as follows:

Table D.1: *Test-system C - Loads, [42]*

	$\mathbf{P_L}$ [MW]	$\mathbf{Q_L}$ [Mvar]	$\mathbf{Q_c}$ [Mvar]
Bus 7	967	100	200
Bus 9	1767	100	350

The generator parameters are as follows:

Table D.2: *Test-system C - Machine parameters, [42]*

	$\mathbf{H}$ [s]	D	S [MVA]	$\cos(\phi)$
$\mathbf{G_1}$	6.5	0	900	0.9
$\mathbf{G_2}$	6.5	0	900	0.9
$\mathbf{G_3}$	6.175	0	900	0.9
$\mathbf{G_4}$	6.175	0	900	0.9

All the other parameters and original data can be found in [42].

D.4 Test-system D

Description: 66-bus test-system from [161].

The system consists on 66 buses, 16 generators and 51 transmission lines, divided in three meshed areas. The weak ties (due to long transmission lines interconnecting the areas) make the system useful for stability studies. It has been developed based on benchmark values of the European interconnected system. The installed capacity is around 15.93 GW and the total demand is 15.57 MW.

Table D.3: *Test-system D - Machine parameters*

Gen.	**H** [s]	**S** [MVA]	$\cos(\phi)$
A1ag	7,590002	1100	0,95
A1bG	7,590002	1100	0,95
A2aG	7,590002	1100	0,95
A2bG	7,590002	1100	0,95
A3G	3,036001	440	0,95
A6G	3,457999	494	0,98
B2aG	13,5975	1295	0,95
B2bG	13,5975	1295	0,95
B3G	24,4755	2331	0,95
B8G	6,915998	988	0,98
B10G	10,878	1036	0,95
C7G	10,374	1482	0,98
C2G	10,374	1482	0,98
C10G	6,915998	988	0,98
C12G	8,644997	1235	0,98
C14G	6,915998	988	0,98

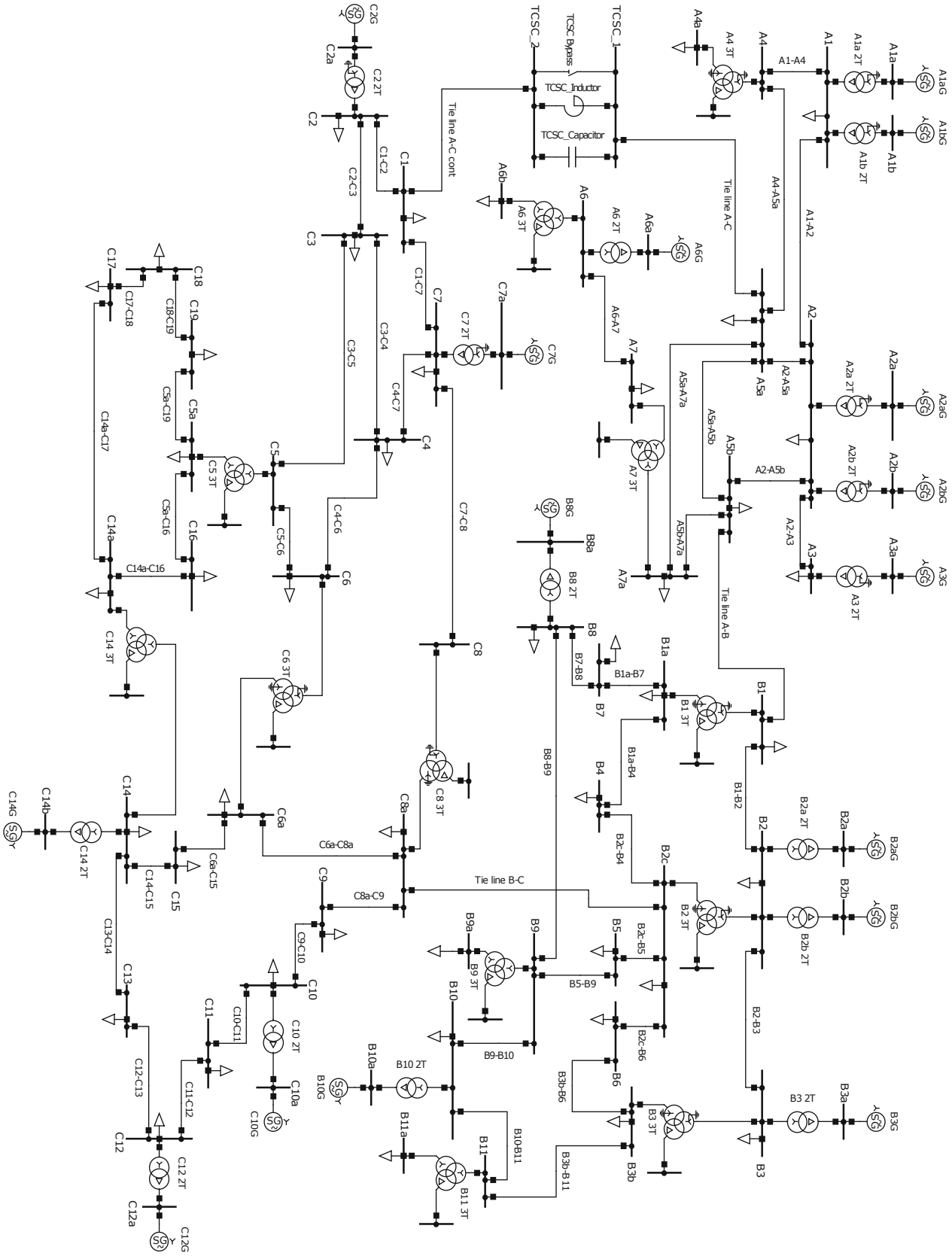

Figure D.4: *Test-system D*

D.5 Test-system E

Description: WSCC test-system, [46].

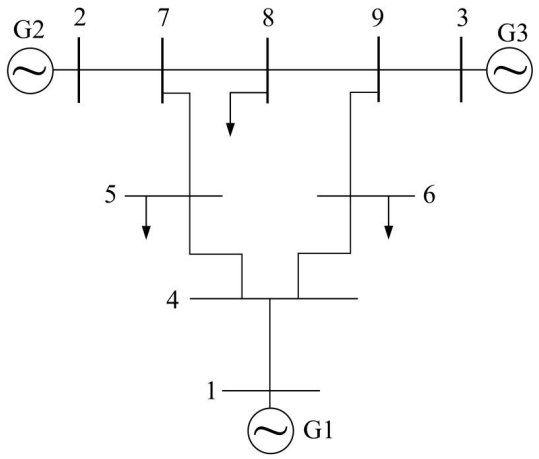

Figure D.5: *Test-system E*

Test-system E - Machine parameters

Gen.	$\mathbf{M}[\mathbf{s^2}]$	**D**	**S** [MVA]
$\mathbf{G_1}$	0.63	0.63	100
$\mathbf{G_2}$	0.34	0.34	100
$\mathbf{G_3}$	0.16	0.16	100

Test-system E - Load parameters

Bus	**S** [MVA]	**V** [kV]	$\mathbf{P_L}$ [p.u.]	$\mathbf{Q_L}$ [p.u.]
6	100	230	0.9	0.3
8	100	230	1	0.35
5	100	230	1.25	0.5

Table D.4: *Test-system E - Line parameters*

Line	**From**	**To**	**S** [MVA]	**V** [kV]	**r** [p.u.Ω/Km]	**x** [p.u. H/Km]	**b** [p.u. F/Km]
1	9	8	100	230	0.0119	0.1008	0.209
2	7	8	100	230	0.0085	0.072	0.149
3	9	6	100	230	0.039	0.17	0.358
4	7	5	100	230	0.032	0.161	0.306
5	5	4	100	230	0.01	0.085	0.176
6	6	4	100	230	0.017	0.092	0.158
7	2	7	100	18	0	0.0625	0
8	3	9	100	13.8	0	0.0586	0
9	1	4	100	16.5	0	0.0576	0

Additional details are available at: `https://github.com/xiaozhew/Jacobian-Estimation`. Accessed in 06/09/2019 at 16:17.

Bibliography

[1] IRENA, "Solutions to integrate high shares of variable renewable energy," International Renewable Energy Agency (IRENA), Tech. Rep., 2019 (cit. on pp. 1, 6).

[2] IRENA, "Renewable energy statistics 2019," International Renewable Energy Agency (IRENA), Tech. Rep., 2019 (cit. on pp. 1, 2).

[3] F. Appavou, A. Brown, B. Epp, A. Leidreiter, C. Lins, H. Murdock, E. Musolino, K. Petrichenko, T. C. Farrell, and T. T. Krader, "Renewables 2017 global status report," *Renewable Energy Policy Network for the 21st Century. Paris: REN21*, 2017 (cit. on p. 1).

[4] "Renewables 2018: Analysis and Forecasts to 2023," International Energy Agency (IEA), Tech. Rep., 2018 (cit. on p. 2).

[5] "Black System South Australia 28 Semptember 2016 - Preliminary report," Australian Energy Market Operator (AEMO), Tech. Rep., 2016 (cit. on pp. 2, 4).

[6] J. Berggreen, *Denmark Set New Wind Energy Record In 2017*, https://cleantechnica.com/2018/01/06/44-wind-denmark-smashed-already-huge-wind-energy-records-2017/, Accessed in 23/08/2019 at 21:35, 2019 (cit. on p. 2).

[7] EMD International A/S, *Elpriser og estimeret elproduktion og forbrug i vest-danmark (jylland/-fyn)*, https://www.emd.dk/el/, Accessed in 23/08/2019 at 21:30 (cit. on pp. 3, 151).

[8] *G.B. National Grid Status - Data courtesy of Elexon portal and Sheffield University*, www.gridwatch.templar.co.uk, Accesed in 23/08/2019 at 21:55, Aug. 2019 (cit. on p. 3).

[9] Terna S.p.A., *Transparency report*, https://www.terna.it/en/electric-system/transparency-report, Acessed in 23/08/2019 at 21:40 (cit. on pp. 5, 152).

[10] A. Ulbig, T. S. Borsche, and G. Andersson, "Impact of Low Rotational Inertia on Power System Stability and Operation," *IFAC Proceedings Volumes*, vol. 47, no. 3, pp. 7290 –7297, 2014, 19th IFAC World Congress, ISSN: 1474-6670. DOI: https://doi.org/10.3182/20140824-6-ZA-1003.02615. [Online]. Available: http://www.sciencedirect.com/science/article/pii/S1474667016427618 (cit. on pp. 4, 18).

[11] M. Rezkalla, M. Pertl, and M. Marinelli, "Electric power system inertia: Requirements, challenges and solutions," *Electrical Engineering*, vol. 100, no. 4, pp. 2677–2693, 2018, ISSN: 1432-0487. DOI: 10.1007/s00202-018-0739-z. [Online]. Available: https://doi.org/10.1007/s00202-018-0739-z (cit. on p. 4).

[12] "Inertia requirements methodology," Australian Energy Market Operator (AEMO), Tech. Rep., 2018 (cit. on p. 4).

[13] P. Tielens and D. V. Hertem, "The relevance of inertia in power systems," *Renewable and Sustainable Energy Reviews*, vol. 55, pp. 999–1009, 2016. DOI: 10.1016/j.rser.2015.11.016 (cit. on pp. 4, 18, 27, 28).

[14] O. P. Malik, "Evolution of Power Systems into Smarter Networks," *Journal of Control, Automation and Electrical Systems*, vol. 24, Apr. 2013. DOI: 10.1007/s40313-013-0005-6 (cit. on p. 5).

[15] A. G. Phadke and T. Bi, "Phasor measurement units, WAMS, and their applications in protection and control of power systems," *Journal of Modern Power Systems and Clean Energy*, vol. 6, no. 4, pp. 619–629, 2018, ISSN: 2196-5420. DOI: 10.1007/s40565-018-0423-3. [Online]. Available: https://doi.org/10.1007/s40565-018-0423-3 (cit. on pp. 6, 33, 34, 36, 43, 45, 46).

[16] J. H. Chow, A. Chakrabortty, L. Vanfretti, and M. Arcak, "Estimation of Radial Power System Transfer Path Dynamic Parameters Using Synchronized Phasor Data," *IEEE Transactions on Power Systems*, vol. 23, no. 2, pp. 564–571, May 2008, ISSN: 0885-8950. DOI: 10.1109/TPWRS.2008.919315 (cit. on pp. 6, 7, 44, 52, 60, 142).

[17] J. H. Chow, *Power system coherency and model reduction*. Springer, 2013 (cit. on pp. 6, 45, 52, 56–58, 87, 143).

[18] L. Fan, Z. Miao, and Y. Wehbe, "Application of Dynamic State and Parameter Estimation Techniques on Real-World Data," *IEEE Transactions on Smart Grid*, vol. 4, no. 2, pp. 1133–1141, Jun. 2013, ISSN: 1949-3053. DOI: 10.1109/TSG.2012.2230031 (cit. on pp. 6, 52, 64).

[19] P. Wall and V. Terzija, "Simultaneous Estimation of the Time of Disturbance and Inertia in Power Systems," *IEEE Transactions on Power Delivery*, vol. 29, no. 4, pp. 2018–2031, Aug. 2014, ISSN: 0885-8977. DOI: 10.1109/TPWRD.2014.2306062 (cit. on pp. 6, 44, 46, 51).

[20] P. M. Ashton, G. A. Taylor, A. M. Carter, M. E. Bradley, and W. Hung, "Application of phasor measurement units to estimate power system inertial frequency response," in *Proc. IEEE Power Energy Society General Meeting*, Jul. 2013, pp. 1–5. DOI: 10.1109/PESMG.2013.6672671 (cit. on pp. 6, 52).

[21] Z. Huang, P. Du, D. Kosterev, and B. Yang, "Application of extended Kalman filter techniques for dynamic model parameter calibration," in *Proc. IEEE Power Energy Society General Meeting*, Jul. 2009, pp. 1–8. DOI: 10.1109/PES.2009.5275423 (cit. on pp. 6, 44, 53).

[22] K. Kalsi, Y. Sun, Z. Huang, P. Du, R. Diao, K. K. Anderson, Y. Li, and B. Lee, "Calibrating multi-machine power system parameters with the extended Kalman filter," in *Proc. IEEE Power and Energy Society General Meeting*, Jul. 2011, pp. 1–8. DOI: 10.1109/PES.2011.6039224 (cit. on pp. 6, 44, 53, 63, 142).

[23] X. Cao, B. Stephen, I. F. Abdulhadi, C. D. Booth, and G. M. Burt, "Switching Markov Gaussian Models for Dynamic Power System Inertia Estimation," *IEEE Transactions on Power Systems*, vol. 31, no. 5, pp. 3394–3403, Sep. 2016, ISSN: 0885-8950. DOI: 10.1109/TPWRS.2015.2501458 (cit. on pp. 6, 52).

[24] N. Petra, C. G. Petra, Z. Zhang, E. M. Constantinescu, and M. Anitescu, "A Bayesian Approach for Parameter Estimation With Uncertainty for Dynamic Power Systems," *IEEE Transactions on Power Systems*, vol. 32, no. 4, pp. 2735–2743, Jul. 2017, ISSN: 0885-8950. DOI: 10.1109/TPWRS.2016.2625277 (cit. on pp. 6, 52).

[25] F. Milano, F. Dörfler, G. Hug, D. J. Hill, and G. Verbič, "Foundations and Challenges of Low-Inertia Systems (Invited Paper)," in *Proc. Power Systems Computation Conf. (PSCC)*, Jun. 2018, pp. 1–25. DOI: 10.23919/PSCC.2018.8450880 (cit. on pp. 6, 26).

[26] C. Wang, Z. Qin, Y. Hou, and J. Yan, "Multi-Area Dynamic State Estimation With PMU Measurements by an Equality Constrained Extended Kalman Filter," *IEEE Transactions on Smart Grid*, vol. 9, no. 2, pp. 900–910, Mar. 2018, ISSN: 1949-3053. DOI: 10.1109/TSG.2016.2570943 (cit. on pp. 6, 53).

[27] J. Schiffer, P. Aristidou, and R. Ortega, "Online Estimation of Power System Inertia Using Dynamic Regressor Extension and Mixing," *IEEE Transactions on Power Systems*, p. 1, 2019, ISSN: 0885-8950. DOI: 10.1109/TPWRS.2019.2915249 (cit. on pp. 6, 52).

[28] K. Tuttelberg, J. Kilter, D. Wilson, and K. Uhlen, "Estimation of Power System Inertia From Ambient Wide Area Measurements," *IEEE Transactions on Power Systems*, vol. 33, no. 6, pp. 7249–7257, Nov. 2018, ISSN: 0885-8950. DOI: 10.1109/TPWRS.2018.2843381 (cit. on pp. 6, 53).

[29] J. Zhao, Y. Tang, and V. Terzija, "Robust Online Estimation of Power System Center of Inertia Frequency," *IEEE Transactions on Power Systems*, vol. 34, no. 1, pp. 821–825, Jan. 2019, ISSN: 0885-8950. DOI: 10.1109/TPWRS.2018.2879782 (cit. on pp. 6, 53, 101).

[30] Smart Grid Investment Grant Program, "Factors affecting PMU installation costs," U.S. Department of Energy - Electricity Delivery & Energy Reliability, Tech. Rep., 2014. [Online]. Available: https://www.smartgrid.gov/files/PMU-cost-study-final-10162014_1.pdf (cit. on pp. 6, 45).

[31] T. Breithaupt et al., "Deliverable D1.1 - Report on systemic issues," MIGRATE – Massive InteGRATion of power Electronic devices, Tech. Rep., 2017 (cit. on pp. 6, 51).

[32] G. R. Moraes, A. Berizzi, V. Ilea, and G. D'Antona, "Inertia estimation of equivalent areas by a pmu-based approach following perturbations," in *18th IEEE EEEIC International Conference on Environment and Electrical Engineering*, 2018 (cit. on pp. 7, 8, 56, 57).

[33] G. R. Moraes, F. Pozzi, V. Ilea, A. Berizzi, E. M. Carlini, G. Giannuzzi, and R. Zaottini., "Measurement-based inertia estimation method considering system reduction strategies and dynamic equivalents," in *13th IEEE PES PowerTech*, 2019 (cit. on p. 7).

[34] Y. Wehbe, L. Fan, and Z. Miao, "Least squares based estimation of synchronous generator states and parameters with phasor measurement units," in *Proc. North American Power Symp. (NAPS)*, Sep. 2012, pp. 1–6. DOI: 10.1109/NAPS.2012.6336346 (cit. on pp. 7, 8, 52, 55, 60, 142).

[35] X. Wang, J. W. Bialek, and K. Turitsyn, "PMU-Based Estimation of Dynamic State Jacobian Matrix and Dynamic System State Matrix in Ambient Conditions," *IEEE Transaction on Power Systems*, 2018 (cit. on pp. 8, 72, 74, 76, 133, 143).

[36] J. Machowski, J. W. Bialek, and J. R. Bumby, *Power System Dynamics, Stability and Control*. Wiley, Jan. 2012 (cit. on pp. 10, 11, 13, 31, 65).

[37] P. Kundur et al., "Definition and classification of power system stability IEEE/CIGRE joint task force on stability terms and definitions," *IEEE Transactions on Power Systems*, vol. 19, no. 3, pp. 1387–1401, Aug. 2004, ISSN: 0885-8950. DOI: 10.1109/TPWRS.2004.825981 (cit. on pp. 10, 12, 13).

[38] J. G. Slootweg, "Wind Power Modelling and Impact on Power System Dynamics," PhD thesis, Delft Technological University, 2003 (cit. on pp. 11, 23).

[39] Arani and El-Saadany, "Implementing Virtual Inertia in DFIG-Based Wind Power Generation," *IEEE Transactions on Power Systems*, vol. 28, no. 2, pp. 1373–1384, 2013. DOI: 10.1109/tpwrs.2012.2207972 (cit. on pp. 11, 26).

[40] A. Bolzoni, C. Terlizzi, and R. Perini, "Analytical Design and Modelling of Power Converters Equipped with Synthetic Inertia Control," *2018 20th European Conference on Power Electronics and Applications (EPE'18 ECCE Europe)*, 2018 (cit. on pp. 11, 27).

[41] O. I. Elgerd, *Electric energy systems theory: an introduction*. McGraw-Hill Book Company, New York, NY, 1982 (cit. on pp. 13, 67, 82, 85, 87, 89, 97, 133).

[42] P. Kundur, N. J. Balu, and M. G. Lauby, *Power system stability and control*. McGraw-hill New York, 1994, vol. 7 (cit. on pp. 13–16, 30, 67, 72, 89, 91, 164).

[43] P. C. Krause, O. Wasynczuk, and S. D. Sudhoff, *Analysis of Electric Machinery and Drive Systems*, S. V. Kartalopoulos, Ed. IEEE Press, 2002 (cit. on pp. 13, 22).

[44] P. L. Dandeno, "Current Usage & Suggested Practices in Power System Stability Simulations for Synchronous Machines," *IEEE Transactions on Energy Conversion*, vol. EC-1, no. 1, pp. 77–93, 1986. DOI: 10.1109/tec.1986.4765673 (cit. on p. 14).

[45] "IEEE Guide for Synchronous Generator Modeling Practices and Applications in Power System Stability Analyses," *IEEE Std 1110-2002 (Revision of IEEE Std 1110-1991)*, pp. 1–72, 2003. DOI: 10.1109/IEEESTD.2003.94408 (cit. on pp. 14, 91, 98, 101, 107, 111, 115, 119, 124, 128).

[46] P. W. Sauer and A. Pai, *Power System Dynamics and Stability*. Prentice Hall, Jan. 1998 (cit. on pp. 16, 73, 156, 160, 167).

[47] P. M. Anderson and A. A. Fouad, *Power system control and stability*. John Wiley & Sons, 2008 (cit. on p. 18).

[48] H. Golpîra and A. R. Messina, "A Center-of-Gravity-Based Approach to Estimate Slow Power and Frequency Variations," *IEEE Transactions on Power Systems*, vol. 33, no. 1, pp. 1026–1035, Jan. 2018, ISSN: 0885-8950. DOI: 10.1109/TPWRS.2017.2710187 (cit. on p. 18).

[49] T. Ackermann, Ed., *Wind Power in Power Systems*. John Wiley & Sons, Ltd, 2012. DOI: 10.1002/9781119941842 (cit. on pp. 21–23).

[50] D. L. Contreras, J. M. Canedo, and D. P. Montoya, "A modified power flow algorithm in power systems with renewable energy sources," in *2017 North American Power Symposium (NAPS)*, IEEE, 2017. DOI: 10.1109/naps.2017.8107242 (cit. on p. 22).

[51] M. EL-Shimy and N. Ghaly, "Wind Energy Conversion Systems, Grid–Connected," in, S. Anwar, Ed. CRC Press, Jan. 2015, ch. 4, p. 21, ISBN: 9781466506732. DOI: 10.1081/E-EEE2-120051436 (cit. on p. 23).

[52] W. Xiao, *Photovoltaic Power System: Modelling, Design, and Control*. Wiley, 2017 (cit. on pp. 24, 25).

[53] Q. Alsafasfeh, O. Saraereh, I. Khan, and S. Kim, "Solar PV Grid Power Flow Analysis," *Sustainability*, vol. 11, pp. 1–25, Mar. 2019. DOI: 10.3390/su11061744 (cit. on p. 25).

[54] W. He, X. Yuan, and J. Hu, "Inertia Provision and Estimation of PLL-Based DFIG Wind Turbines," *IEEE Transactions on Power Systems*, vol. 32, no. 1, pp. 510–521, 2017. DOI: 10.1109/tpwrs.2016.2556721 (cit. on p. 26).

[55] M. R. B. Tavakoli, M. Power, L. Ruttledge, and D. Flynn, "Load Inertia Estimation Using White and Grey-Box Estimators for Power Systems with High Wind Penetration," *IFAC Proceedings Volumes*, vol. 45, no. 21, pp. 399–404, 2012. DOI: 10.3182/20120902-4-fr-2032.00071 (cit. on pp. 28, 29).

[56] "Load representation for dynamic performance analysis (of power systems)," *IEEE Transactions on Power Systems*, vol. 8, no. 2, pp. 472–482, 1993. DOI: 10.1109/59.260837 (cit. on p. 28).

[57] C. Concordia and S. Ihara, "Load Representation in Power System Stability Studies," *IEEE Transactions on Power Apparatus and Systems*, vol. PAS-101, no. 4, pp. 969–977, 1982. DOI: 10.1109/tpas.1982.317163 (cit. on p. 29).

[58] A. Sridharan and V. Sarkar, "A comparative study on phasor and frequency measurement techniques in power systems," in *Proc. National Power Systems Conf. (NPSC)*, Dec. 2016, pp. 1–6. DOI: 10.1109/NPSC.2016.7858890 (cit. on pp. 35, 44).

[59] "IEEE Standard for Synchrophasor Measurements for Power Systems," *IEEE Std C37.118.1-2011*, 2011 (cit. on pp. 35–37, 44).

[60] A. G. Phadke and J. S. Thorp, *Synchronized Phasor Measurements and Their Applications (Power Electronics and Power Systems)*. Springer, 2008, ISBN: 978-0-387-76535-8 (cit. on pp. 35–39, 42, 43, 45).

[61] "IEEE Draft Standard for Synchrophasor Data Transfer for Power Systems," *IEEE PC37.118.2/D3.2, May 2011*, pp. 1–54, 2011 (cit. on pp. 37, 44).

[62] H. Bentarzi, M. Tsebia, and A. Abdelmoumene, "PMU based SCADA enhancement in smart power grid," in *2018 IEEE 12th International Conference on Compatibility, Power Electronics and Power Engineering (CPE-POWERENG 2018)*, IEEE, 2018. DOI: 10.1109/cpe.2018.8372580 (cit. on pp. 37, 38).

[63] U.S. Energy Information Administration, *New technology can improve electric power system efficiency and reliability*, https://www.eia.gov/todayinenergy, Mar. 2012 (cit. on pp. 38, 45).

[64] A. Monti, C. Muscas, and F. Ponci, *Phasor Measurement Units and Wide Area Monitoring Systems: From the Sensors to the System*. Academic Press, Jun. 2016, pp. 1–286 (cit. on pp. 39, 40, 45).

[65] M. Vaiman and M. Vaiman, "Using Phase Angle for Steady-State Voltage Stability Assessment," in *In Proc. PACW Americas Conference*, Aug. 2017 (cit. on p. 39).

[66] R. Nebuloni, "The use of PCA for electromechanical oscillations identification," Master's thesis, Politecnico di Milano, 2018 (cit. on p. 41).

[67] F. Pozzi, "Synchrophasor-based inertia estimation methods in electric power systems," Master's thesis, Politecnico di Milano, 2018 (cit. on pp. 41, 42, 65).

[68] S. Skok and I. Ivankovic, *WAMPAC seduces SCADA in a control room*, Special session at PowerTech Milano 2019, Available at `https://attend.ieee.org/powertech-2019/wp-content/uploads/sites/107/2019/07/ss04-5.pdf`, Jun. 2019 (cit. on p. 43).

[69] F. Aminifar, M. Fotuhi-Firuzabad, A. Safdarian, A. Davoudi, and M. Shahidehpour, "Synchrophasor Measurement Technology in Power Systems: Panorama and State-of-the-Art," *IEEE Access*, vol. 2, pp. 1607–1628, 2014. DOI: `10.1109/access.2015.2389659` (cit. on p. 44).

[70] A. G. Phadke, J. S. Thorp, and M. G. Adamiak, "A New Measurement Technique for Tracking Voltage Phasors, Local System Frequency, and Rate of Change of Frequency," *IEEE Transactions on Power Apparatus and Systems*, vol. PAS-102, no. 5, pp. 1025–1038, May 1983, ISSN: 0018-9510. DOI: `10.1109/TPAS.1983.318043` (cit. on p. 44).

[71] M. M. Begovic, P. M. Djuric, S. Dunlap, and A. G. Phadke, "Frequency tracking in power networks in the presence of harmonics," *IEEE Transactions on Power Delivery*, vol. 8, no. 2, pp. 480–486, 1993 (cit. on p. 44).

[72] T. Lobos and J. Rezmer, "Real-time determination of power system frequency," *IEEE Transactions on Instrumentation and measurement*, vol. 46, no. 4, pp. 877–881, 1997 (cit. on p. 44).

[73] P. Romano and M. Paolone, "Enhanced interpolated-DFT for synchrophasor estimation in FPGAs: Theory, implementation, and validation of a PMU prototype," *IEEE Transactions on Instrumentation and Measurement*, vol. 63, no. 12, pp. 2824–2836, 2014 (cit. on p. 44).

[74] P. R. Bedse and N. N. Jangle, "Review on PMU using Recursive DFT Algorithm," in *2018 International Conference on Computing, Power and Communication Technologies (GUCON)*, IEEE, 2018. DOI: `10.1109/gucon.2018.8675049` (cit. on p. 44).

[75] "IEEE Standard for Synchrophasors for Power Systems," *IEEE Std 1344-1995(R2001)*, pp. 1–36, Nov. 1994. DOI: `10.1109/IEEESTD.1994.8684605` (cit. on p. 44).

[76] J. Bertsch, M. Zima, A. Suranyi, C. Carnal, and C. Rehtanz, "Experiences with and perspectives of the system for wide area monitoring of power systems," in *Proc. CIGRE/PES 2003. CIGRE/IEEE PES Int. Symp. Quality and Security of Electric Power Delivery Systems*, Oct. 2003, pp. 5–9. DOI: `10.1109/QSEPDS.2003.159787` (cit. on p. 44).

[77] Y. Xue, "Some viewpoints and experiences on wide area measurement systems and wide area control systems," in *Proc. IEEE Power and Energy Society General Meeting - Conversion and Delivery of Electrical Energy in the 21st Century*, Jul. 2008, pp. 1–6. DOI: `10.1109/PES.2008.4596251` (cit. on p. 44).

[78] S. M. Brahma and A. A. Girgis, "Fault location on a transmission line using synchronized Voltage measurements," *IEEE Transactions on Power Delivery*, vol. 19, no. 4, pp. 1619–1622, Oct. 2004, ISSN: 0885-8977. DOI: 10.1109/TPWRD.2003.822532 (cit. on p. 44).

[79] A. Salehi-Dobakhshari and A. M. Ranjbar, "Application of synchronised phasor measurements to wide-area fault diagnosis and location," *Transmission Distribution IET Generation*, vol. 8, no. 4, pp. 716–729, Apr. 2014, ISSN: 1751-8687. DOI: 10.1049/iet-gtd.2013.0033 (cit. on p. 44).

[80] N. Shams, P. Wall, and V. Terzija, "Active Power Imbalance Detection, Size and Location Estimation Using Limited PMU Measurements," *IEEE Transactions on Power Systems*, vol. 34, no. 2, pp. 1362–1372, 2019. DOI: 10.1109/tpwrs.2018.2872868 (cit. on pp. 44, 46).

[81] R. B. Leandro, A. S. Silva, I. C. Decker, and M. N. Agostini, "Identification of the Oscillation Modes of a Large Power System Using Ambient Data," *Journal of Control, Automation and Electrical Systems*, vol. 26, no. 4, pp. 441–453, 2015 (cit. on p. 44).

[82] X. Wang and I. Zenelis, "Estimating Participation Factors and Mode Shapes for Electromechanical Oscillations in Ambient Conditions," in *IEEE Canadian Conference on Electrical & Computer Engineering (CCECE)*, 2018 (cit. on p. 44).

[83] L. Fan and Y. Wehbe, "Extended Kalman filtering based real-time dynamic state and parameter estimation using PMU data," *Electric Power Systems Research*, vol. 103, pp. 168–177, 2013 (cit. on pp. 44, 53, 100).

[84] B. Ahmadzadeh-Shooshtari, R. Torkzadeh, M. Kordi, H. Marzooghi, and F. Eghtedarnia, "SG parameters estimation based on synchrophasor data," *Transmission Distribution IET Generation*, vol. 12, no. 12, pp. 2958–2967, 2018, ISSN: 1751-8687. DOI: 10.1049/iet-gtd.2017.1989 (cit. on pp. 44, 52, 101).

[85] S. Rovnyak, S. Kretsinger, J. Thorp, and D. Brown, "Decision trees for real-time transient stability prediction," *IEEE Transactions on Power Systems*, vol. 9, no. 3, pp. 1417–1426, Aug. 1994, ISSN: 0885-8950. DOI: 10.1109/59.336122 (cit. on p. 44).

[86] C.-. Liu and J. Thorp, "Application of synchronised phasor measurements to real-time transient stability prediction," *Transmission and Distribution IEE Proceedings-Generation*, vol. 142, no. 4, pp. 355–360, Jul. 1995, ISSN: 1350-2360. DOI: 10.1049/ip-gtd:19951975 (cit. on p. 44).

[87] R. Diao, V. Vittal, and N. Logic, "Design of a Real-Time Security Assessment Tool for Situational Awareness Enhancement in Modern Power Systems," *IEEE Transactions on Power Systems*, vol. 25, no. 2, pp. 957–965, May 2010, ISSN: 0885-8950. DOI: 10.1109/TPWRS.2009.2035507 (cit. on p. 44).

[88] G. Valverde, S. Chakrabarti, E. Kyriakides, and V. Terzija, "A Constrained Formulation for Hybrid State Estimation," *IEEE Transactions on Power Systems*, vol. 26, no. 3, pp. 1102–1109, Aug. 2011, ISSN: 0885-8950. DOI: 10.1109/TPWRS.2010.2079960 (cit. on p. 44).

[89] E. Andreoli, A. S. Costa, and K. A. Clements, "Topology validation via simultaneous state amp; topology estimation with phasor data processing capability," in *Proc. Power Systems Computation Conf*, Aug. 2014, pp. 1–7. DOI: 10.1109/PSCC.2014.7038474 (cit. on pp. 44, 65).

[90] Y. Chakhchoukh, V. Vittal, and G. T. Heydt, "PMU Based State Estimation by Integrating Correlation," *IEEE Transactions on Power Systems*, vol. 29, no. 2, pp. 617–626, Mar. 2014, ISSN: 0885-8950. DOI: 10.1109/TPWRS.2013.2284560 (cit. on p. 44).

[91] V. Freitas and A. S. Costa, "Integrated State and topology estimation based on a priori topology information," in *Proc. IEEE Eindhoven PowerTech*, Jun. 2015, pp. 1–6. DOI: 10.1109/PTC.2015.7232440 (cit. on pp. 44, 65).

[92] M. Göl and A. Abur, "Observability and Criticality Analyses for Power Systems Measured by Phasor Measurements," *IEEE Transactions on Power Systems*, vol. 28, no. 3, pp. 3319–3326, Aug. 2013, ISSN: 0885-8950. DOI: 10.1109/TPWRS.2012.2236367 (cit. on p. 44).

[93] N. H. Abbasy and H. M. Ismail, "A Unified Approach for the Optimal PMU Location for Power System State Estimation," *IEEE Transactions on Power Systems*, vol. 24, no. 2, pp. 806–813, May 2009, ISSN: 0885-8950. DOI: 10.1109/TPWRS.2009.2016596 (cit. on p. 44).

[94] B. Gou and R. G. Kavasseri, "Unified PMU Placement for Observability and Bad Data Detection in State Estimation," *IEEE Transactions on Power Systems*, vol. 29, no. 6, pp. 2573–2580, Nov. 2014, ISSN: 0885-8950. DOI: 10.1109/TPWRS.2014.2307577 (cit. on pp. 44, 92).

[95] E. Caro, R. Singh, B. C. Pal, A. J. Conejo, and R. A. Jabr, "Participation factor approach for phasor measurement unit placement in power system state estimation," *Transmission Distribution IET Generation*, vol. 6, no. 9, pp. 922–929, Sep. 2012, ISSN: 1751-8687. DOI: 10.1049/iet-gtd.2011.0705 (cit. on p. 44).

[96] F. Aminifar, A. Khodaei, M. Fotuhi-Firuzabad, and M. Shahidehpour, "Contingency-Constrained PMU Placement in Power Networks," *IEEE Transactions on Power Systems*, vol. 25, no. 1, pp. 516–523, Feb. 2010, ISSN: 0885-8950. DOI: 10.1109/TPWRS.2009.2036470 (cit. on p. 44).

[97] N. M. Manousakis and G. N. Korres, "A Weighted Least Squares Algorithm for Optimal PMU Placement," *IEEE Transactions on Power Systems*, vol. 28, no. 3, pp. 3499–3500, Aug. 2013, ISSN: 0885-8950. DOI: 10.1109/TPWRS.2013.2242698 (cit. on pp. 44, 92).

[98] L. Huang, Y. Sun, J. Xu, W. Gao, J. Zhang, and Z. Wu, "Optimal PMU Placement Considering Controlled Islanding of Power System," *IEEE Transactions on Power Systems*, vol. 29, no. 2, pp. 742–755, Mar. 2014, ISSN: 0885-8950. DOI: 10.1109/TPWRS.2013.2285578 (cit. on pp. 44, 92).

[99] A. Chakrabortty and C. F. Martin, "Optimal Measurement Allocation Algorithms for Parametric Model Identification of Power Systems," *IEEE Transactions on Control Systems Technology*, vol. 22, no. 5, pp. 1801–1812, Sep. 2014, ISSN: 1063-6536. DOI: 10.1109/TCST.2014.2299437 (cit. on p. 44).

[100] J. S. Thorp, A. G. Phadke, S. H. Horowitz, and M. M. Begovic, "Some applications of phasor measurements to adaptive protection," *IEEE Transactions on Power Systems*, vol. 3, no. 2, pp. 791–798, May 1988, ISSN: 0885-8950. DOI: 10.1109/59.192936 (cit. on p. 44).

[101] V. Centeno, J. de la Ree, A. G. Phadke, G. Michel, R. J. Murphy, and R. O. Burnett, "Adaptive out-of-step relaying using phasor measurement techniques," *IEEE Computer Applications in Power*, vol. 6, no. 4, pp. 12–17, Oct. 1993, ISSN: 0895-0156. DOI: 10.1109/67.238199 (cit. on p. 44).

[102] J. Bertsch, C. Carnal, D. Karlson, J. McDaniel, and Khoi Vu, "Wide-Area Protection and Power System Utilization," *Proceedings of the IEEE*, vol. 93, no. 5, pp. 997–1003, May 2005, ISSN: 0018-9219. DOI: 10.1109/JPROC.2005.847266 (cit. on p. 44).

[103] E. E. Bernabeu, J. S. Thorp, and V. Centeno, "Methodology for a Security/Dependability Adaptive Protection Scheme Based on Data Mining," *IEEE Transactions on Power Delivery*, vol. 27, no. 1, pp. 104–111, Jan. 2012, ISSN: 0885-8977. DOI: 10.1109/TPWRD.2011.2168831 (cit. on p. 44).

[104] K. Seethalekshmi, S. N. Singh, and S. C. Srivastava, "Synchrophasor Assisted Adaptive Reach Setting of Distance Relays in Presence of UPFC," *IEEE Systems Journal*, vol. 5, no. 3, pp. 396–405, Sep. 2011, ISSN: 1932-8184. DOI: 10.1109/JSYST.2011.2158694 (cit. on p. 44).

[105] G. C. Zweigle and V. Venkatasubramanian, "Wide-Area Optimal Control of Electric Power Systems With Application to Transient Stability for Higher Order Contingencies," *IEEE Transactions on Power Systems*, vol. 28, no. 3, pp. 2313–2320, Aug. 2013, ISSN: 0885-8950. DOI: 10.1109/TPWRS.2012.2233764 (cit. on p. 44).

[106] C. Liu, K. Sun, Z. H. Rather, Z. Chen, C. L. Bak, P. Thøgersen, and P. Lund, "A Systematic Approach for Dynamic Security Assessment and the Corresponding Preventive Control Scheme Based on Decision Trees," *IEEE Transactions on Power Systems*, vol. 29, no. 2, pp. 717–730, Mar. 2014, ISSN: 0885-8950. DOI: 10.1109/TPWRS.2013.2283064 (cit. on p. 44).

[107] I. Kamwa, R. Grondin, and Y. Hebert, "Wide-area measurement based stabilizing control of large power systems-a decentralized/hierarchical approach," *IEEE Transactions on Power Systems*, vol. 16, no. 1, pp. 136–153, Feb. 2001, ISSN: 0885-8950. DOI: 10.1109/59.910791 (cit. on p. 44).

[108] A. Chakrabortty, "Wide-Area Damping Control of Power Systems Using Dynamic Clustering and TCSC-Based Redesigns," *IEEE Transactions on Smart Grid*, vol. 3, no. 3, pp. 1503–1514, Sep. 2012, ISSN: 1949-3053. DOI: 10.1109/TSG.2012.2197029 (cit. on p. 44).

[109] J. He, C. Lu, X. Wu, P. Li, and J. Wu, "Design and experiment of wide area HVDC supplementary damping controller considering time delay in China southern power grid," *Transmission Distribution IET Generation*, vol. 3, no. 1, pp. 17–25, Jan. 2009, ISSN: 1751-8687. DOI: 10.1049/iet-gtd:20080129 (cit. on p. 44).

[110] J. Ma, T. Wang, S. Wang, X. Gao, X. Zhu, Z. Wang, and J. S. Thorp, "Application of Dual Youla Parameterization Based Adaptive Wide-Area Damping Control for Power System Oscillations," *IEEE Transactions on Power Systems*, vol. 29, no. 4, pp. 1602–1610, Jul. 2014, ISSN: 0885-8950. DOI: 10.1109/TPWRS.2013.2296940 (cit. on p. 44).

[111] D. Molina, G. K. Venayagamoorthy, J. Liang, and R. G. Harley, "Intelligent Local Area Signals Based Damping of Power System Oscillations Using Virtual Generators and Approximate Dynamic Programming," *IEEE Transactions on Smart Grid*, vol. 4, no. 1, pp. 498–508, Mar. 2013, ISSN: 1949-3053. DOI: 10.1109/TSG.2012.2233224 (cit. on p. 44).

[112] R. Garcia-Valle, G.-Y. Yang, K. E. Martin, A. H. Nielsen, and J. Ostergaard, "DTU PMU laboratory development - Testing and validation," in *2010 IEEE PES Innovative Smart Grid Technologies Conference Europe (ISGT Europe)*, IEEE, 2010. DOI: 10.1109/isgteurope.2010.5638883 (cit. on p. 44).

[113] A. Angioni, G. Lipari, M. Pau, F. Ponci, and A. Monti, "A Low Cost PMU to Monitor Distribution Grids," in *2017 IEEE International Workshop on Applied Measurements for Power Systems (AMPS)*, IEEE, 2017. DOI: 10.1109/amps.2017.8078337 (cit. on p. 44).

[114] D. M. Laverty, L. Vanfretti, I. A. Khatib, V. K. Applegreen, R. J. Best, and D. J. Morrow, "The OpenPMU Project: Challenges and perspectives," in *2013 IEEE Power & Energy Society General Meeting*, IEEE, 2013. DOI: 10.1109/pesmg.2013.6672390 (cit. on p. 44).

[115] D. Schofield, F. Gonzalez-Longatt, and D. Bogdanov, "Design and Implementation of a Low-Cost Phasor Measurement Unit: A Comprehensive Review," in *2018 Seventh Balkan Conference on Lighting (BalkanLight)*, IEEE, 2018. DOI: 10.1109/balkanlight.2018.8546936 (cit. on p. 45).

[116] Zobaa and Vaccaro, Eds., *Wide area monitoring, protection and control systems: the enabler for smarter grids*. Institution of Engineering and Technology, 2016. DOI: 10.1049/pbpo073e (cit. on p. 45).

[117] M. Kezunovic, S. Meliopoulos, V. Venkatasubramanian, and V. Vittal, *Application of Time-Synchronized Measurements in Power System Transmission Networks*. Springer International Publishing, 2014. DOI: 10.1007/978-3-319-06218-1 (cit. on p. 45).

[118] P. W. Sauer, A. Pai, and J. H. Chow, *Power System Dynamics and Stability with Synchrophasor Measurement and Power System Toolbox*. Wiley-Blackwell, 2017, 374 pp., ISBN: 111935577X. [Online]. Available: https://www.ebook.de/de/product/29865714/peter_w_sauer_power_system_dynamics_and_stability.html (cit. on p. 45).

[119] A. Chakrabortty and M. D. Ilić, Eds., *Control and Optimization Methods for Electric Smart Grids*. Springer New York, 2012. DOI: 10.1007/978-1-4614-1605-0 (cit. on p. 45).

[120] *North American SynchroPhasor Initiative (NASPI)*, http://gnssconsortium.org, Acessed in 29/08/2019 at 19:22. (cit. on p. 45).

[121] *Global Network for Synchrophasor Solutions*, https://www.naspi.org/, Acessed in 29/08/2019 at 19:23. (cit. on p. 45).

[122] D. Dotta, J. H. Chow, and D. B. Bertagnolli, "A teaching tool for phasor measurement estimation," *IEEE Transactions on Power Systems*, vol. 29, no. 4, pp. 1981–1988, 2014 (cit. on p. 45).

[123] I. C. Decker, M. N. Agostini, A. S. Silva, and D. Dotta, "Monitoring of a large scale event in the Brazilian Power System by WAMS," in *2010 IREP Symposium Bulk Power System Dynamics and Control - VIII (IREP)*, IEEE, 2010. DOI: 10.1109/irep.2010.5563249 (cit. on p. 45).

[124] *Proyeto MedFasee - Monitoreo del sistema eléctrico en tiempo real*, http://www.medfasee.ufsc.br/conosur/, Accessed in 30/08/2019 at 16:35. (cit. on p. 46).

[125] *Projeto MedFasee - Medição do SIN em tempo real*, http://www.medfasee.ufsc.br/temporeal/, Accessed in 30/08/2019 at 16:30. (cit. on p. 46).

[126] *Protótipo MedFasee Ibérico - Observatório da Dinâmica do Sistema Eléctrico Ibérico*, http://medfasee.ufsc.br/portugal/, Accessed in 30/08/2019 at 16:37. (cit. on p. 46).

[127] C. Energia, *ONS e GE firmam contrato para sistema de monitoramento do SIN*, http://canalenergia.com.br/noticias/42701219/ons-e-ge-firmam-contrato-para-sistema-de-monitoramento-do-sin, Acessed in 30/08/2019 at 16:41, 2017 (cit. on p. 46).

[128] P. Wall, F. Gonzalez-Longatt, and V. Terzija, "Estimation of generator inertia available during a disturbance," in *Proc. IEEE Power and Energy Society General Meeting*, Jul. 2012, pp. 1–8. DOI: 10.1109/PESGM.2012.6344755 (cit. on pp. 46, 51).

[129] E. Grebe, J. Kabouris, S. L. Barba, W. Sattinger, and W. Winter, "Low frequency oscillations in the interconnected system of Continental Europe," in *IEEE PES General Meeting*, IEEE, 2010. DOI: 10.1109/pes.2010.5589932 (cit. on p. 47).

[130] G. Giannuzzi, D. Lauria, C. Pisani, and D. Villacci, "Real-time tracking of electromechanical oscillations in ENTSO-e Continental European Synchronous Area," *International Journal of Electrical Power & Energy Systems*, vol. 64, pp. 1147–1158, 2015. DOI: 10.1016/j.ijepes.2014.09.016 (cit. on p. 46).

[131] Y. Matsukawa, J. Terashi, M. Watanabe, and Y. Mitani, "Power systems inertia evaluation associated with PV installation by frequency analysis of inter-area oscillation based on phasor measurements," *Journal of International Council on Electrical Engineering*, vol. 7, no. 1, pp. 153–158, 2017. DOI: 10.1080/22348972.2017.1345368 (cit. on p. 46).

[132] G. Ledwich, D. Geddey, and P. O'Shea, "Phasor Measurement Units for system diagnosis and load identification in Australia," in *2008 IEEE Power and Energy Society General Meeting - Conversion and Delivery of Electrical Energy in the 21st Century*, IEEE, 2008. DOI: 10.1109/pes.2008.4596347 (cit. on p. 46).

[133] J. C. H. Peng, R. Sherry, and N. K. C Nair, "Phasor measurement network and its applications in the New Zealand grid: Overview and experiences," in *2011 IEEE Power and Energy Society General Meeting*, IEEE, 2011. DOI: 10.1109/pes.2011.6039284 (cit. on p. 46).

[134] D. Brnobic, *UMEME 24/7: Synchrophasor measurements in Kenya*, http://www.wamster.net/w2/news/kenya-umeme-24-7-wamster-installation, Acessed in 31/08/2019 at 18:37., 2012 (cit. on p. 46).

[135] D. H. Wilson, R. A. Folkes, A. Edwards, B. Berry Eskom, N. Mbuli, and B. van Rensburg, *Phasor-based wide area monitoring in the South African power system*, https://www.ee.co.za/magazines/energize/energize-back-issues, Jun. 2011 (cit. on p. 46).

[136] T. Inoue, H. Taniguchi, Y. Ikeguchi, and K. Yoshida, "Estimation of power system inertia constant and capacity of spinning-reserve support generators using measured frequency transients," *IEEE Transactions on Power Systems*, vol. 12, no. 1, pp. 136–143, 1997. DOI: 10.1109/59.574933 (cit. on p. 51).

[137] A. Chakrabortty and J. H. Chow, "Interarea model estimation for radial power system transfer paths with voltage support using synchronized phasor measurements," in *2008 IEEE Power and Energy Society General Meeting - Conversion and Delivery of Electrical Energy in the 21st Century*, IEEE, 2008. DOI: 10.1109/pes.2008.4596292 (cit. on p. 52).

[138] A. Chakrabortty and J. H. Chow and A. Salazar, "Interarea Model Estimation for Radial Power System Transfer Paths With Intermediate Voltage Control Using Synchronized Phasor Measurements," *IEEE Transactions on Power Systems*, vol. 24, no. 3, pp. 1318–1326, 2009. DOI: 10.1109/tpwrs.2009.2022995 (cit. on p. 52).

[139] A. Chakrabortty, J. H. Chow, and A. Salazar, "A Measurement-Based Framework for Dynamic Equivalencing of Large Power Systems Using Wide-Area Phasor Measurements," *IEEE Transactions on Smart Grid*, vol. 2, no. 1, pp. 68–81, 2011. DOI: 10.1109/tsg.2010.2093586 (cit. on p. 52).

[140] Y. Wehbe and L. Fan, "PMU-based system identification for a modified classic generator model," in *Proc. North American Power Symp. (NAPS)*, Oct. 2015, pp. 1–6. DOI: 10.1109/NAPS.2015.7335120 (cit. on p. 52).

[141] J. Zhang and H. Xu, "Online Identification of Power System Equivalent Inertia Constant," *IEEE Transactions on Industrial Electronics*, vol. 64, no. 10, pp. 8098–8107, 2017. DOI: 10.1109/tie.2017.2698414 (cit. on p. 52).

[142] S. Guo and J. Bialek, "Synchronous machine inertia constants updating using Wide Area Measurements," in *Proc. 3rd IEEE PES Innovative Smart Grid Technologies Europe (ISGT Europe)*, Oct. 2012, pp. 1–7. DOI: 10.1109/ISGTEurope.2012.6465659 (cit. on p. 52).

[143] G. Bishop, G. Welch, *et al.*, "An introduction to the Kalman filter," *Proc of SIGGRAPH, Course*, vol. 8, no. 27599-3175, p. 59, 2001 (cit. on pp. 53, 62, 63).

[144] H. G. Aghamolki, Z. Miao, L. Fan, W. Jiang, and D. Manjure, "Identification of synchronous generator model with frequency control using unscented Kalman filter," *Electric Power Systems Research*, vol. 126, pp. 45–55, 2015 (cit. on pp. 53, 100).

[145] M. Kezunovic, "Monitoring of Power System Topology in Real-Time," in *Proc. 39th Annual Hawaii Int. Conf. System Sciences (HICSS'06)*, vol. 10, Jan. 2006, 244b. DOI: 10.1109/HICSS.2006.355 (cit. on p. 65).

[146] U. Rudez and R. Mihalic, "Analysis of underfrequency load shedding using a frequency gradient," *IEEE transactions on power delivery*, vol. 26, no. 2, pp. 565–575, 2009 (cit. on p. 68).

[147] H. Marzooghi et al., "Solutions to monitor in real-time and forecast KPIs enabling TSOs to assess the impact of PE penetration. Deliverable D2.2," MIGRATE – Massive InteGRATion of power Electronic devices, Tech. Rep., 2017 (cit. on p. 68).

[148] M. Kuivaniemi, M. Laasonen, K. Elkington, A. Danell, N. Modig, A. Bruseth, E. A. Jansson, and E. Orum, "Estimation of System Inertia in the Nordic Power System Using Measured Frequency Disturbances," in *Cigre Conference*, 2015, pp. 27–28 (cit. on pp. 69, 128).

[149] P. Regulski, P. Wall, Z. Rusidovic, and V. Terzija, "Estimation of load model parameters from PMU measurements," in *IEEE PES Innovative Smart Grid Technologies, Europe*, IEEE, 2014, pp. 1–6 (cit. on p. 69).

[150] B. Alinejad, M. Akbari, and H. Kazemi, "PMU-based distribution network load modelling using Harmony Search Algorithm," in *2012 Proceedings of 17th Conference on Electrical Power Distribution*, IEEE, 2012, pp. 1–6 (cit. on p. 69).

[151] E. Polykarpou, M. Asprou, and E. Kyriakides, "Dynamic load modelling using real time estimated states," in *2017 IEEE Manchester PowerTech*, IEEE, 2017, pp. 1–6 (cit. on p. 69).

[152] D. Zografos and M. Ghandhari, "Power system inertia estimation by approaching load power change after a disturbance," in *2017 IEEE Power & Energy Society General Meeting*, IEEE, 2017, pp. 1–5 (cit. on pp. 69, 70, 124).

[153] D. Bliznyuk, A. Berdin, and I. Romanov, "PMU data analysis for load characteristics estimation," in *2016 57th International Scientific Conference on Power and Electrical Engineering of Riga Technical University (RTUCON)*, IEEE, 2016, pp. 1–5 (cit. on pp. 69, 144).

[154] V. Vignesh, S. Chakrabarti, and S. C. Srivastava, "Power system load modelling under large and small disturbances using phasor measurement units data," *IET Generation, Transmission & Distribution*, vol. 9, no. 12, pp. 1316–1323, 2015 (cit. on pp. 69, 128, 144).

[155] G. Ghanavati, P. D. H. Hines, and T. I. Lakoba, "Identifying Useful Statistical Indicators of Proximity to Instability in Stochastic Power Systems," *IEEE Transactions on Power Systems*, vol. 31, no. 2, pp. 1360–1368, 2016. DOI: 10.1109/tpwrs.2015.2412115 (cit. on pp. 72, 143).

[156] A. A. Fouad and V. Vittal, *Power System Transient Stability Analysis Using the Transient Energy Function Method*. Prentice Hall, 1991 (cit. on pp. 73, 156, 157).

[157] T. Odun-Ayo and M. L. Crow, "An analysis of power system transient stability using stochastic energy functions," *International Transactions on Electrical Energy Systems*, vol. 23, no. 2, pp. 151–165, 2011. DOI: 10.1002/etep.646 (cit. on p. 74).

[158] C. W. Gardiner, *Handbook of Stochastic Methods*. Springer Berlin Heidelberg, 2004. DOI: 10.1007/978-3-662-05389-8 (cit. on p. 75).

[159] "IEEE Guide for Synchronous Generator Modeling Practices in Stability Analyses," *IEEE Std 1110-1991*, 1991. DOI: 10.1109/IEEESTD.1991.101073 (cit. on p. 99).

[160] D. del Giudice, "Real-time inertia estimation methods in electric power systems," Master's thesis, Politecnico di Milano, 2017 (cit. on pp. 99, 100).

[161] F. M. Gonzalez-Longatt and J. L. Rueda, Eds., *PowerFactory Applications for Power System Analysis*. Springer International Publishing, 2014. DOI: 10.1007/978-3-319-12958-7 (cit. on pp. 101, 102, 165).

[162] H.-D. Chiang, *Direct Methods for Stability Analysis of Electric Power Systems*. John Wiley & Sons, Inc., 2010. DOI: 10.1002/9780470872130 (cit. on p. 133).